JAAVSO

Volume 43
Number 2
2015

The Journal of the American Association of Variable Star Observers

Changing Periods of ST Puppis

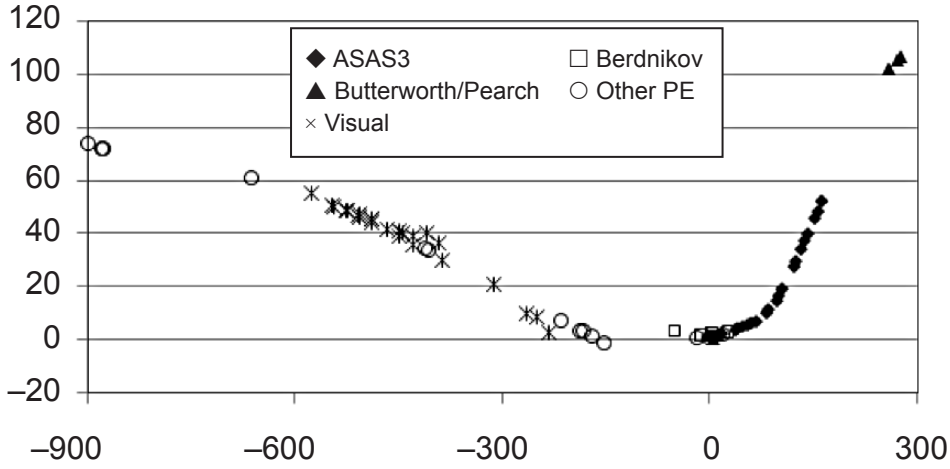

The O–C diagram of ST Puppis since 1955. The vertical scale shows days late (+) or early (–) as compared to the given ephemeris. The value of the visual measures from the AAVSO International Database is quite clear, although the accuracy of those epochs is probably ± 2 days at best.

Also in this issue...

Complete table of contents inside...

The American Association of Variable Star Observers
49 Bay State Road, Cambridge, MA 02138, USA

The Journal of the American Association of Variable Star Observers

The Council of the American Association of Variable Star Observers 2014–2015

ISSN 0271-9053 (print)
ISSN 2380-3606 (online)

JAAVSO

The Journal of
The American Association
of Variable Star Observers

Volume 43
Number 2
2015

ISSN 0271-9053 (print)
ISSN 2380-3606 (online)

AAVSO
49 Bay State Road
Cambridge, MA 02138
USA

Publication Schedule

The Journal of the American Association of Variable Star Observers is published twice a year, June 15 (Number 1 of the volume) and December 15 (Number 2 of the volume). The submission window for inclusion in the next issue of JAAVSO closes six weeks before the publication date. A manuscript will be added to the table of contents for an issue when it has been fully accepted for publication upon successful completion of the referee process; these articles will be available online prior to the publication date. An author may not specify in which issue of JAAVSO a manuscript is to be published; accepted manuscripts will be published in the next available issue, except under extraordinary circumstances.

Page Charges

Page charges are waived for Members of the AAVSO. Publication of unsolicited manuscripts in JAAVSO requires a page charge of US $100/page for the final printed manuscript. Page charge waivers may be provided under certain circumstances.

Publication in *JAAVSO*

With the exception of abstracts of papers presented at AAVSO meetings, papers submitted to JAAVSO are peer-reviewed by individuals knowledgable about the topic being discussed. We cannot guarantee that all submissions to JAAVSO will be published, but we encourage authors of all experience levels and in all fields related to variable star astronomy and the AAVSO to submit manuscripts. We especially encourage students and other mentees of researchers affiliated with the AAVSO to submit results of their completed research.

Subscriptions

Institutions and Libraries may subscribe to JAAVSO as part of the Complete Publications Package or as an individual subscription. Individuals may purchase printed copies of recent JAAVSO issues via Createspace. Paper copies of JAAVSO issues prior to volume 36 are available in limited quantities directly from AAVSO Headquarters; please contact the AAVSO for available issues.

Instructions for Submissions

The *Journal of the AAVSO* welcomes papers from all persons concerned with the study of variable stars and topics specifically related to variability. All manuscripts should be written in a style designed to provide clear expositions of the topic. Contributors are encouraged to submit digitized text in MS WORD, LATEX+POSTSCRIPT, or plain-text format. Manuscripts should be submitted through the online submission portal (https://www.aavso.org/apps/jaavso/); submission instructions and information for authors and referees can be found there as well.

Manuscripts must be submitted according to the following guidelines, or they will be returned to the author for correction:

Manuscripts must be:
1) original, unpublished material;
2) written in English;
3) accompanied by an abstract of no more than 100 words.
4) not more than 2,500–3,000 words in length (10–12 pages double-spaced).

Figures for publication must:
1) be camera-ready or in a high-contrast, high-resolution, standard digitized image format;
2) have all coordinates labeled with division marks on all four sides;
3) be accompanied by a caption that clearly explains all symbols and significance, so that the reader can understand the figure without reference to the text.

Maximum published figure space is 4.5" by 7". When submitting original figures, be sure to allow for reduction in size by making all symbols, letters, and division marks sufficiently large.

Photographs and halftone images will be considered for publication if they directly illustrate the text.

Tables should be:
1) provided separate from the main body of the text;
2) numbered sequentially and referred to by Arabic number in the text, e.g., Table 1.

References:
1) References should relate directly to the text.
2) References should be keyed into the text with the author's last name and the year of publication, e.g., (Smith 1974; Jones 1974) or Smith (1974) and Jones (1974).
3) In the case of three or more joint authors, the text reference should be written as follows: (Smith et al. 1976).
4) All references must be listed at the end of the text in alphabetical order by the author's last name and the year of publication, according to the following format: Brown, J., and Green, E. B. 1974, *Astrophys. J.*, **200**, 765.
Thomas, K. 1982, *Phys. Rep.*, **33**, 96.
5) Abbreviations used in references should be based on recent issues of the *Journal* or the listing provided at the beginning of *Astronomy and Astrophysics Abstracts* (Springer-Verlag).

Miscellaneous:
1) Equations should be written on a separate line and given a sequential Arabic number in parentheses near the right-hand margin. Equations should be referred to in the text as, e.g., equation (1).
2) Magnitude will be assumed to be visual unless otherwise specified.
3) Manuscripts may be submitted to referees for review without obligation of publication.

Online Access

Articles published in JAAVSO, and information for authors and referees may be found online at: https://www.aavso.org/apps/jaavso/

The American Association of Variable Star Observers, 49 Bay State Road, Cambridge, MA 02138, USA journal@aavso.org

The Journal of the American Association of Variable Star Observers
Volume 43, Number 2, 2015

Editorial

Variable star analysis

Table of Contents continued on following pages

Table of Contents continued on following pages

Abstracts of Papers and Posters Presented at the 104th Spring Meeting of the AAVSO, Held in Muncie, Indiana, June 4–6, 2015

Table of Contents continued on next page

Editorial

Variable Stars and Science and Math Education

John R. Percy
Editor-in-Chief, *Journal of the AAVSO*

Department of Astronomy and Astrophysics and Dunlap Institute for Astronomy and Astrophysics, University of Toronto, 50 St. George Street, Toronto, ON M5S 3H4, Canada; john.percy@utoronto.ca

Received November 23, 2015

Observation, analysis, and interpretation of variable stars can be a powerful tool for effective science and math education. That was the motivation behind the AAVSO's *Hands-On Astrophysics* project (Percy and Mattei 1998), which subsequently evolved and expanded into the on-line *Variable Star Astronomy* (https://www.aavso.org/education/vsa), thanks especially to the work of Donna Young. Students can develop and integrate their science, math, and computing skills, motivated by the excitement of doing real science with real data. Project components may include background reading and planning; research judgment, strategy, and problem-solving; careful observation and measurement; recognizing and dealing with random and systematic errors; computer programming, and data processing and management; construction, analysis, and interpretation of graphs; concepts of regularity and prediction; and curve-fitting, time-series analysis, and other statistical and numerical procedures. At the conclusion of their project, students can communicate their results through a paper, poster, presentation, or informal discussion with their classmates.

JAAVSO already welcomes papers based on student projects. They are reviewed in the normal way, to ensure that their content is accurate and significant. My students and I have published many papers in these pages, most based on AAVSO data. Good science is done. The students benefit. AAVSO members and observers learn how their observations contribute to science and education. It's a win-win-win situation.

I believe that the AAVSO and *JAAVSO* can go even further in contributing to science and math education. AAVSO Director Stella Kafka's hopes for *JAAVSO* include having more papers which connect variable star astronomy and STEM (science, technology, mathematics, engineering) education. Does that just mean more papers with students as co-authors? Yes and no. Such papers are already frequent, and always welcome. There is even more that the AAVSO could do.

(1) Undergraduate research experiences are highly valued in college and university education, but instructors are not always aware of how students can do projects which are original but manageable. We could therefore collect ideas—both general and specific—for student projects, and disseminate them to science and math educators, both through *JAAVSO* and through other widely-read and respected sources. These ideas should be accompanied by brief, user-friendly instructions on how to get started. This project could perhaps be supported by a small grant, or otherwise carried out on a voluntary basis, by a small team (I would be happy to participate).

Variable Star Astronomy is a good starting point for high school students, and it includes many activities. The next step would be a guide to original *projects*. What science is doable, and worth doing? What sources of un-analyzed data are available, in addition to the AAVSO International Database? How can they be accessed, and data downloaded? How can AAVSO analysis tools such as VSTAR be used to analyze the data? What are the challenges in analyzing variable star data? What constitutes a good final project report, written or oral? Much of this information already exists on-line, and could be linked to. The document could conclude with an annotated list of published student projects—preferably ones which were exemplary or innovative in some way.

The AAVSO has already carried out a useful "step one" by setting up a new Education and Outreach forum, promoting outreach to students and educators. It solicits help in finding suitable projects, invites success stories and advice on what worked and what didn't, and encourages sharing of resources and materials. Many AAVSO members and observers are formal or informal educators. They have experience in both variable stars and in education. Let's use the forum, and think about how we could proceed further. At one time, the AAVSO had an Education Committee. It seems to be dormant. Why not revive it?

(2) We should also encourage project supervisors/mentors to use best educational practices, and encourage and actively solicit education papers which reflect and convey these—perhaps even new and improved practices. This would be helpful to other students and educators. To me, any effective educational activity or project should have four components: (1) the educational *objectives* for the student (not just for the project); (2) educational *content* such as the development of STEM knowledge, skills, and attitudes; (3) an effective *process* for achieving the objectives and educational content, such as by inquiry-based learning; and (4) *assessment and improvement* at every step in the process, both as the project proceeds, and at the end. For instance: is the purpose of the project to provide the student with an engaging and beneficial educational experience? Or just to get the project done? Does the student have any say in what project, or part of a project to do, and how to do it? Is there scope for inquiry-based learning? Is the student encouraged to be curious and creative? Does the student meet regularly with their supervisor/mentor? Is there a constant emphasis on the student's intellectual growth?

(3) For those with some background in education research, there might even be opportunities for research on students'

understanding of stars and their evolution; see Percy (2015) for a brief guide to education research. Much research has been done on students' understanding of earth-moon-sun relations. Much *less* has been done on students' understanding of stars, galaxies, and the universe (Lelliot and Rollnick 2010). Warning: remember that education research in a school or other institutional setting may require the approval of an ethics committee.

I encourage you to discuss these ideas on the new "promoting outreach to students and educators" forum: https://www.aavso.org/forums/variable-star-observing/variable-stars-education

References

Lelliott, A., and Rollnick, M. 2010, *Int. J. Sci. Education*, **32**, 1771.

Percy, J. R., and Mattei, J. A. 1998, *J. Roy. Astron. Soc. Canada*, **92**, 322.

Percy, J. R. 2015, *J. Roy. Astron. Soc. Canada*, **109**, 88.

A Photometric Study of the Misclassified Variable AK Ursae Minoris

Horace A. Dale III
Lauren A. Sgro
Emory University Department of Physics, 400 Dowman Drive, Atlanta, GA 30322; hdale@emory.edu

Received September 9, 2013; revised June 22, 2015; accepted July 9, 2015

Abstract The star AK UMi [GSC 4656-0461] was originally misidentified as an RRc-Lyrae pulsating variable by analyzing undersampled survey data. We used greater time resolved differential photometry to positively identify this variable as a W UMa overcontact (subtype A) binary system. The secondary minimum is a total eclipse, which enabled us to approximate the model for this system using some well-known characteristics of overcontact binaries. Our model solution parameters were found to be: i = 90°, q = 0.21 (M_2/M_1), and T_1 = 6750K, which indicated that the primary should be an F4.

1. Introduction

Recent variable star surveys, such as the Northern Sky Variability Survey (NSVS; Wozniak *et al.* 2004) and the All-Sky Automated Survey (ASAS; Pojmański *et al.* 2013), have provided the astronomical community with a wealth of variable star discoveries. The availability of the data has led to independent groups using data mining techniques in an attempt to extract more variable star discoveries. Unfortunately, sampling rates from many of the surveys lack the time resolution to properly identify the nature of the variability of systems with P < 1 day. This can lead to some confusion between light curves of similar profiles, especially those systems that exhibit symmetry. Distinguishing between RRc-Lyrae stars and contact binaries (both A and W subtypes) can be difficult when the sampling rate is inadequate. W Ursae Majoris binaries are further subdivided into two subtypes: the W-type and the A-type. In the W-type, the primary star is the smaller and more compact component. These systems are less massive with short periods, between 0.2 and 0.4 day, with spectral types from G to K. The A-type systems have a smaller and less massive secondary component. In these larger-mass systems the spectral types are A to F with longer periods ranging from 0.4 to 0.8 day (Binnendijk 1965).

GSC 4656-0461 (R.A. $19^h\ 40^m\ 41.5^s$, Dec. +86° 21' 10.4" (J2000.0)), also recently named AK UMi (Kazarovets *et al.* 2013), was identified as an RRc-Lyrae type variable by Otero (2007) using data from the NSVS imported into a period analyzing software, known as AVE (Analysis of Stellar Variability) (Bareberá 1996), that utilizes a user-defined period range along with an algorithm to search for the best possible solution. More recently, Hoffman *et al.* (2009) used Fourier coefficients which resulted in their conclusion that AK UMi may be a W UMa eclipsing binary. However, the light curve generated by the NSVS data used by Otero (2007) to support their claim was compiled using only 104 NSVS observations that were made over a 260-day time span, equivalent to an average sampling rate of 0.4 obs/day. The symmetrical shape of the light curve from the original discovery paper has led to this photometric campaign to definitively identify the type of variability. We were able to gather much more data than available in the original discovery paper and therefore come to a more conclusive, and very different, supposition about the nature of the variability of AK UMi.

2. Observations

Differential photometry was performed on AK UMi using the 0.6-m Cassegrain telescope atop the Math and Science Center at Emory University. Data were collected on the evenings of December 2, 13, and 22, 2012, using an Apogee Alta U47 at f/8. To achieve the best time resolution possible and the highest SNRs, we chose to image through a Johnson R filter for the entire observing campaign. Since AK UMi is circumpolar, we were able to acquire images for each entire night through air masses that ranged only between 1.16 and 1.26, and a total of 1,537 high-quality images were taken over the three nights. Figure 1 shows the field of view. The designations for the comparison stars that were used are listed in Table 1, along with their (J2000.0) coordinates provided by SKY6 Planetarium Software (Software Bisque 2015).

All of the images were calibrated through MAXIMDL (Diffraction Limited 2012) using biases, darks, and flats.

Table 1. Comparison stars used for AK UMi.

Star	*Catalog Number*	*R.A. (J2000.0) h m s*	*Dec. (J2000.0) ° ′ ″*
Reference 1	GSC 4656-0288	19 40 45	+86 22 27
Check 1	GSC 4656-0453	19 45 08	+86 16 15
Check 2	GSC 4656-0260	19 46 19	+86 17 08

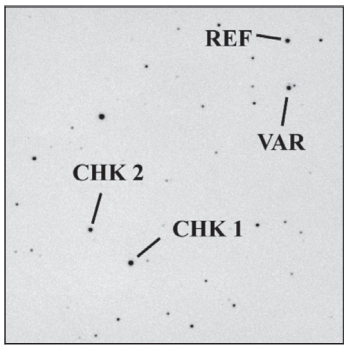

Figure 1. Field of View 9.5' × 9.5'. VAR is the target star, AK UMi. One potential third light component can be seen close on the right of VAR.

The two check stars showed no short-term variability during our observations with standard deviations averaging 0.007 magnitude over all three nights. Figure 1 shows the target star with another star nearby that could potentially contaminate the photometry, so a photometric aperture was chosen in an attempt to exclude this source but still allow for accurate measurements. Note that there is a second nearby star that does not show in Figure 1.

3. Light curves and analysis

The light curves from the nights of December 2, 13, and 22 were imported into the period analysis software PERANSO (Vanmunster 2013) and HJD corrected with times of minimum (shown in Table 2) extracted using the extremum tool (Kwee and van Woerden 1956). The final phased light curve is shown in Figure 2. The period found for this variable was 0.536608 day (±0.000154) with an overall Δm of 0.3R. The minimum timing for what appeared to be a primary eclipse was used to establish the following ephemeris (Equation 1).

$$T_{pri}\,(HJD) = 2456275.765569 + 0.536608 \times E \qquad (1)$$

This phased light curve shows the distinctive characteristics of a W UMa-type eclipsing binary of subtype A, as evidenced by the distinct total eclipse that occurs at the secondary minimum. The period-color relation established by Eggen (1961), and more recently by Wang (1994) and Gazeas and Stępień (2008) (Equation 2), was used to estimate the temperature of the system for modeling purposes.

$$(B–V)_0 = 0.062 – 1.31 \log_{10} P \qquad (2)$$

The orbital period of 0.536608±0.000154 day yields a $(B–V)_0$ value of +0.416, which was used to interpolate an effective temperature from the standard tables found in *Allen's Astrophysical Quantities* (Drilling and Landolt 2000). The implied effective temperature of 6750K corresponds to a spectral type of approximately F4. The masses were estimated using the period-mass equations (Equations 3 and 4) derived by Gazeas and Stępień (2008). This allowed the masses to be constrained to a smaller range of values for purposes of modeling.

Table 2. Minimum timings of AK UMi.

2450000 + HJD	*Error (10^{-4} days)*	*Eclipse*
6264.766666	±0.66	Secondary
6275.765539	±1.28	Primary
6284.617772	±1.12	Secondary

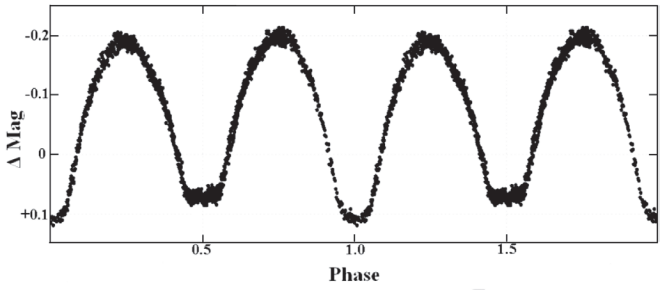

Figure 2. AK UMi phased light curve. The Δ Magnitude shown is the Johnson R magnitude difference from the reference star.

$$\log M_1 = (0.755 \pm 0.059) \log P + (0.416 \pm 0.024) \qquad (3)$$

$$\log M_2 = (0.352 \pm 0.166) \log P – (0.262 \pm 0.067) \qquad (4)$$

Using the established period and the limits given in Equations 3 and 4, we determined that the initial range of values for the mass ratio (M_2/M_1) should be $0.19 < q < 0.38$.

4. Modeling

Once a suitable range for the mass ratio (q) and temperature was determined, BINARY MAKER (Bradstreet and Steelman 2004) was employed to solve a first order approximation by adjusting the system parameters until a minimum residual value was obtained. Since the temperature of the system was estimated to be less than 7200K, the gravity brightening coefficients were set to the standard value of 0.32, which is commonly used for stars with convective envelopes (Lucy 1967; Rucinski 1973). Gravity brightening refers to a phenomenon in which the poles of a star are brightened due to a higher surface gravity, and, therefore, higher effective temperature, which results from rapid rotation that causes the star to be oblate in shape. BINARY MAKER uses this coefficient in its calculation of local temperature, as the local emergent flux of a star is directly proportional to its local gravity and, therefore, the gravity coefficient (Bradstreet 2005). The primary star was set to the interpolated value of 6750K, and the secondary star was adjusted to achieve the correct ratio that fit the data. Since the secondary eclipse here is in totality, the inclination of the system will be kept at a value of 90°. Limb darkening coefficients were derived from Van Hamme (1993). Limb darkening, an optical effect in which an observer witnesses a diminishment in brightness of a star when looking toward the edge of its disk as opposed to its center, is a function of the gravity coefficient. BINARY MAKER uses the linear limb darkening law (Bradstreet 2005). We set the reflection coefficient to 0.5, as suggested by Rucinski (1969) for binary systems with convective envelopes. The reflection coefficient, also referred to as the "bolometric albedo," represents the percentage of radiation from one member that is absorbed and re-emitted by the companion star (Bradstreet 2005).

The very first attempts for solving the mass ratio made it obvious that a third light component was needed for any reasonable fit to the data. The third light component is a background star that is not part of the AK UMi system and contributes a source of light that cannot be accounted for by examining either member of the binary. The third light parameter in BINARY MAKER is a function of flux (Bradstreet 2005). After a considerable amount of trial and error, a value of $L_3 = 0.36$ was determined to be the best solution. Comparing the residual calculations for mass ratios $0.19 < q < 0.38$, the mass ratio was found to be approximately $q = 0.21$, meaning the primary star is approximately 5 times more massive than the secondary. Further improvements to the residuals were made by adjusting the fillout factors, measurements of the degree of contact between the stars, which were initially set to 0.15.

Table 3. Solution Parameters for AK UMi.

Parameter	*Symbol*	*Value*
Period (days)	P	0.536608
Mass Ratio	M_0/M_1	0.21
Third Light	L_3	0.36
Gravity Coefficient 1, 2	$g_{1,2}$	0.32
Limb Darkening 1, 2	$l_{1,2}$	0.478
Reflection 1, 2	$R_{1,2}$	0.5
Inclination (°)	i	~90
Temperature 1 (K)	T_1	6750
Temperature 2 (K)	T_2	6650
Fillout 1, 2	f	0.6

For an overcontact system in Binary Maker, the fillout factor ($0 < f < 1$) represents the percentage that the surface potential of the binary lies from the inner critical surface compared to the outer one (Bradstreet 2005). The parameters of the best-fit model from Binary Maker can be found in Table 3.

The relative depths of the eclipses are indicative of overcontact binaries in which the two components are nearly in thermal equilibrium with only a 100K difference. BINARY MAKER only allows for modeling the mean surface effective temperatures of the independent members of the binary and disregards any temperature gradient in their shared convective envelope (Bradstreet 2005). The discovery of the total secondary eclipse has provided a means of computing reasonable first order approximations for the system parameters that would have been otherwise difficult without obtaining radial velocity measurements. The brightness maximums at $\phi = 0.25$ and $\phi = 0.75$ differ slightly in magnitude, where one is brighter than the other. The observation of uneven heights in the two maxima that occur outside of eclipse, known as the O'Connell effect, is likely caused by spot activity in this case (Milone 1968). It would, therefore, also be possible to obtain a slightly better fit to the shoulders of the light curve by the addition of a spot or two. However, since the O'Connell effect is more prevalent at shorter wavelengths and less obvious through an R filter, a full BVR observing campaign would be needed before attempting any valid spot modeling.

5. Conclusion

The variable AK UMi has been positively identified by this campaign as a W UMa overcontact binary system of subtype A and not an RRc-Lyrae star. The use of adequate sampling rates has allowed for more details to emerge that would not have been detected by other surveys such as the NSVS and ASAS.

References

Barberá, R. 1996, Introducing AVS (http://www.astrogea.org/soft/ave/aveint.htm).

Binnendijk, L. 1965, *Veröeff. Remeis Sternw. Bamberg*, No. 40, 36.

Bradstreet, D. H. 2005, in *The Society for Astronomical Sciences 24th Annual Symposium on Telescope Science, held May 24–26*, 2005, Society for Astronomical Sciences, Ontario, CA, 23.

Bradstreet, D. H., and Steelman, D. P. 2004, BINARY MAKER 3, Contact Software (http://www.binarymaker.com).

Diffraction Limited. 2012, MAXIMDL image processing software (http://www.cyanogen.com).

Drilling, J. S., and Landolt, A. U. 2000, *Allen's Astrophysical Quantities* (4th ed.) Springer, New York), 388.

Eggen, O. J. 1961, *Roy. Obs. Bull.*, Series E, No. 31, 107.

Gazeas, K., and Stępień, K. 2008, *Mon. Not. Roy. Astron. Soc.*, **390**, 1577.

Hoffman, D. I., Harrison, T. E., and McNamara, B. J. 2009, *Astron. J.*, **138**, 466.

Kazarovets, E. V., Samus, N. N., Durlevich, O. V., Kireeva, N. N., and Pastukhova, E. N. 2013, *Inf. Bull. Var. Stars*, No. 6052, 1.

Kwee, K. K., and van Woerden, H. 1956, *Bull. Astron. Inst. Netherlands*, **12**, 327.

Lucy, L. B. 1967, *Z. Astrophys.*, **65**, 89.

Milone, E. F. 1968, *Astron. J.*, **73**, 708.

Otero, S. A. 2007, *Open Eur. J. Var. Stars*, **59**, 1.

Pojmański, G., Szczygiel, D., and Pilecki, B. 2013, The All-Sky Automated Survey Catalogues (ASAS3; http://www.astrouw.edu.pl/asas/?page=catalogues).

Rucinski, S. M. 1969, *Acta Astron.*, **19**, 245.

Rucinski, S. M. 1973, *Acta Astron.*, **23**, 79.

Software Bisque. 2015, SKYX Planetarium Software (http://www.bisque.com/sc/pages/TheSkyX-Editions.aspx).

Van Hamme, W. 1993, *Astron. J.*, **106**, 2096.

Vanmunster, T. 2013, Light Curve and Period Analysis Software, PERANSO v.2.50 (http://www.peranso.com/).

Wang, J. M. 1994, *Astrophys. J.*, **434**, 277.

Wozniak, P. R., *et al.* 2004, *Astron. J.*, **127**, 2436.

Pulsation Properties of Carbon and Oxygen Red Giants

John R. Percy
Danping Joanna Huang
Department of Astronomy and Astrophysics and Dunlap Institute for Astronomy and Astrophysics, University of Toronto, 50 St. George Street, Toronto, ON M5S 3H4, Canada; john.percy@utoronto.ca

Received May 12, 2015; revised June 18, 2015; accepted July 16, 2015

Abstract We have used up to 12 decades of AAVSO visual observations, and the AAVSO VSTAR software package to determine new and/or improved periods of 5 pulsating biperiodic carbon (C-type) red giants, and 12 pulsating biperiodic oxygen (M-type) red giants. We have also determined improved periods for 43 additional C-type red giants, in part to search for more biperiodic C-type stars, and also for 46 M-type red giants. For a small sample of the biperiodic C-type and M-type stars, we have used wavelet analysis to determine the time scales of the cycles of amplitude increase and decrease. The C-type and M-type stars do not differ significantly in their period ratios (first overtone to fundamental). There is a marginal difference in the lengths of their amplitude cycles. The most important result of this study is that, because of the semiregularity of these stars, and the presence of alias, harmonic, and spurious periods, the periods which we and others derive for these stars—especially the smaller-amplitude ones—must be determined and interpreted with great care and caution. For instance: spurious periods of a year can produce an apparent excess of stars, at that period, in the period distribution.

1. Introduction

Red giants are unstable to radial pulsation. In general: the larger, cooler, and more luminous the star, the longer the period, and the greater the amplitude. Smaller red giants tend to pulsate in higher overtones, larger ones in lower overtones—the fundamental or first overtone. A few stars pulsate in two (or more) modes, and this is particularly useful since it provides twice as much precise information.

Percy and Abachi (2013) showed that the amplitudes of almost all pulsating red giants change significantly—by factors of up to 10—on time scales of a few tens of pulsation periods. Percy and Khatu (2014) showed that the same was true of pulsating red supergiants, and Percy and Kim (2014) found the same behavior in many pulsating yellow giants and supergiants. Percy and Yook (2014) investigated whether these changes in amplitude resulted in small changes in period, due to non-linear effects in the pulsation. Indeed, they did—*but only in carbon (C-type) red giants*. That led us, in the present study, to investigate whether there were any other differences in the pulsation properties of C red giants and normal oxygen (M) red giants. Since period ratios are a sensitive probe of stellar structure, we made a special effort to find biperiodic C-type stars, and to check the periods of "known" biperiodic C stars. In the course of doing this, we examined the periods and amplitudes of many C red giants, and were able to refine these and, in some cases, identify literature periods which were actually alias, harmonic, or spurious periods (see section 2). We also analyzed some M red giants, to check and refine their periods. Almost all of the stars in our sample had ranges in visual magnitude which were less than 2.5, so they would be classified as semiregular (SR) rather than Mira. See Mattei *et al.* (1997) for a discussion of the classification of red variables. To emphasize: our initial aim was to look for possible differences between the pulsational behavior of C and M stars. This led to the second aim: to look more critically at the periods which we and others derived for these stars.

Multiperiodicity provides one very precise way of analyzing pulsating stars, and looking for differences between subgroups of those stars—such as between C and M red giants—and comparing observed periods with those predicted by theory. Petersen (1973) was a pioneer in such work. He plotted the ratio of periods, such as the ratio of the first overtone period to the fundamental period (P1/P0), against the fundamental period (P0). Such a plot is now called a Petersen diagram.

The most extensive study of multiperiodicity in pulsating red giants is by Kiss *et al.* (1999), hereafter KSCM; see also Mattei *et al.* (1997). We reanalyzed many of their stars, especially those which were C stars, and a selection of M stars for comparison with the C stars. Our database is, of course, up to 15 years longer than theirs.

Many pulsating red giants also have a "long secondary period" (LSP) of unknown origin. Based on our previous studies, and especially on massive photometric surveys such as MACHO and OGLE, these LSPs are known to be about 10 times the fundamental pulsation period. In the present study, we are not immediately concerned with these.

2. Data and analysis

We used visual observations, and for a few stars V observations, from the AAVSO International Database (AID; Henden 2014, Kafka 2015), of the stars listed in the tables. For determination of the average period and amplitude of the star during the time of the observations, we used the Fourier routine (DC-DFT) in the AAVSO software package VSTAR (Benn 2013). Our approach was somewhat different than that of KSCM, who used and merged three different sources of visual data, and first binned them in 10-day bins.

The red giants in our sample generally have pulsation periods in the range of 100–500 days. Because of seasonal gaps in the data, they can show *alias* periods which differ in frequency from the true periods by N cycles per year, where N is usually ±1, but are lower in amplitude. They are identified

by the fact that they differ in frequency from the strongest frequency by ±N/365.25 cycles per day, where N is usually 1.

Because of a physiological effect called the Ceraski effect (Ceraski was an eminent Russian photometrist of a century ago; see Sharonov (1933) for an experimental investigation of this effect), visual observations can also have *spurious* periods of about one year. Although the Ceraski effect is generally thought to be physiological in nature, it is possible that some or all of it may be due to aliasing of very long-term, low-frequency variability in the star (Percy 2015, in preparation). Any period of about one year is therefore suspect. These spurious periods generally have amplitudes less than 0.1 magnitude. Both alias and spurious periods are a special problem for stars, such as red giants, which have one or more true periods of a few hundred days. They are even more of a problem if the star is multiperiodic. There is an additional problem: if the light curve is non-sinusoidal, there are harmonic periods in the Fourier spectrum and, in the case of fundamental-mode pulsators, the P/2 harmonic is very close to possible first-overtone periods which are 0.4–0.6 times the fundamental period. Harmonic periods are not true periods; they are a mathematical result of representing a non-sinusoidal light curve by a sum of sinusoids.

Figure 1 shows the DC-DFT power spectrum for V Boo, a simple monoperiodic pulsator. The 258-day period is flanked by two alias periods with much lower amplitude. Figure 2 shows the DC-DFT power spectrum for RR Her, an example of a biperiodic pulsator. The 237-day period is flanked by two alias periods, but there is an additional period of 124 days which we assume to be a real first-overtone period.

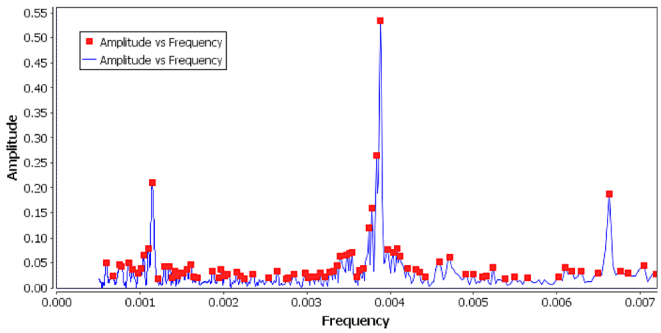

Figure 1. The DC-DFT power spectrum of V Boo, an example of a monoperiodic pulsator. The 258-day period is flanked by two alias periods, whose frequencies differ from the true frequency by ±1 cycle per year. In this and Figure 2, the red symbols are the "top hits"—the peaks of the spectrum. The continuous line is the spectrum itself.

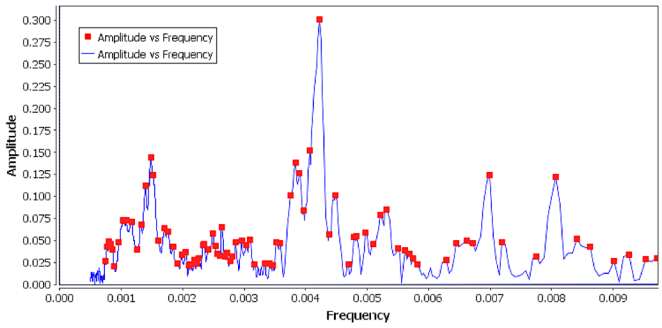

Figure 2. The DC-DFT power spectrum of RR Her, an example of a biperiodic pulsator. The 237-day period is flanked by two alias periods, but there is an additional period of 124 days which we assume to be a true period.

3. Results

3.1. Double-mode pulsators

Table 1 lists the results for five C red giants which we believe to have two radial periods which are not alias, spurious, or harmonic periods, and a selection of twelve M red giants which are also biperiodic, for comparison. The columns give the name of the star, the spectral type (from SIMBAD), the periods in days, the amplitudes, the ratio P1/P0, the dominant period DP (P0 or P1), and notes about each star. The uncertainties in the periods, as estimated from the half-width at half-height in the Fourier spectrum, are 1–2 percent, unless otherwise indicated in the notes. The amplitudes in Tables 1, 2, and 3 are average

Table 1. Double-mode Carbon and Oxygen Red Giants.

Star	*SpT*	*P1(d)*	*A1*	*P0(d)*	*A0*	*P1/P0*	*DP*	*Notes**
RU And	M5-6e	146.8:	0.16	234.3	0.29	0.532	P0	3
SV Cas	M6.5	239.9	0.32	455.6	0.56	0.498	P0	1,3,8
RU Cyg	M6-8e	233.9	0.31	443.0	0.14	0.527	P1	1,3,8
RZ Cyg	M7.0-8.2e	275.9	0.72	537.6	0.54	0.513	—	1,3,8
AH Dra	M7	105.9	0.18	190.0	0.26	0.557	P0	1,3,8
AY Dra	M7:	130.5:	1.51	262.8	2.83	0.497	P0	3,6
BQ Ori	M5-8IIIe	125.8:	0.10	246.5	0.14	0.510	P0	1,3,8
DP Ori	M6.5	146.9	0.12	245.8	0.23	0.515	P0	—
W Tau	M4-6.5	127.5	0.09	240.8	0.20	0.529	P0	1,3,3,7
Z UMa	M5III	98.8	0.14	189.2	0.30	0.522	P0	1,3,8
EP Vel	M6	258.9	0.57	513.6	0.55	0.504	P1	—
RU Vul	M3-4e	154.7	0.18	368.2	0.28	0.420	P0	1,3,8
S Cep	C7,4e (N8e)	208.3	0.20	486.1	0.95	0.496	P0	3
V Cyg	C5,3-7.4e (Npe)	195.6	0.33	420.9	1.43	0.497	P0	3,6
RS Cyg	C8,2e (N0pe)	195.1	0.17	419.0	0.49	0.504	P0	3
RR Her	C5,7-8,1e (N0e)	124.2	0.12	236.7	0.31	0.525	P0	3,5
SY Per	C6,4e (N3e)	231.5	0.18	479.2	0.82	0.483	P0	3

**The amplitudes are average values over the dataset. Also see notes to individual stars in section 3.5. (1) also analyzed by KSCM; (2) low amplitude; (3) see note in section 3.5; (4) extremely low amplitude (less than 0.10 mag.); (5) there is a gap in the data; (6) the data are sparse; (7) monoperiodic according to KSCM; (8) biperiodic according to KSCM (these periods refer to pulsation periods, not LSPs).*

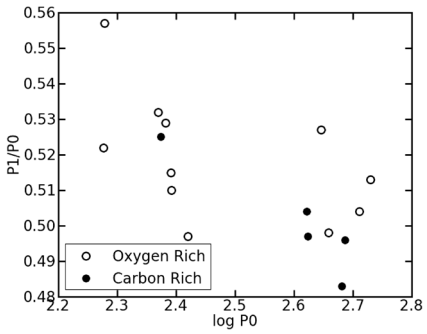

Figure 3. The Petersen diagram for the biperiodic stars in Table 1; it plots the ratio of P1/P0 against logP0. The filled circles are carbon stars; the open circles are normal (oxygen) stars.

values over the dataset; the amplitudes of pulsating red giants vary significantly on timescales of dozens of pulsation periods (Percy and Abachi 2013).

Figure 3 shows the Petersen diagram for the stars in Table 1. It plots P1/P0 against the logarithm of P0, in days. The filled circles are C stars; the open circles are M stars. For longer periods, the period ratios of the C stars are marginally lower than those of the M stars, but not significantly so. The trend and levels in this diagram are consistent with the theoretical models of Xiong and Deng (2007), though the observed period ratios are slightly larger than the theoretical ones for the longer-period stars. There is some scatter in the graph. This may be observational in nature, or it may be due to actual differences between the stars. For instance: Wood (2015) has presented convincing evidence for mass differences among pulsating red giants in the Large Magellanic Cloud.

3.2. Carbon-rich stars

Table 2 lists the results for monoperiodic C red giants. The columns give the name of the star, the spectral type (from SIMBAD), the period in days, the average amplitude, and notes about the star. Tables 2 and 3 include a few stars which we studied but were unable to find periods for.

3.3. Oxygen-rich stars

Table 3 lists the results for some monoperiodic M red giants. The columns give the name of the star, the spectral type (from SIMBAD), the period in days, the average amplitude, and notes about each star.

3.4. Amplitude variations

Because of our recent studies of the pulsational amplitude variations in red giants (e.g. Percy and Abachi 2013), we used the wavelet (WWZ) routine in VSTAR to study the cyclic variations in the pulsation amplitudes of some of the biperiodic stars in Table 1, using the same methodology as Percy and Abachi (2013). We also analyzed GY Aql, W Ori, and RZ Peg, which were initially thought to be biperiodic. We determined the number of cycles of amplitude increase and decrease N and the average length L of the cycles, and expressed them in units of the pulsation period P. The results are given in Table 4; the first few stars are M type, and the last few stars are C type. The columns give, for the fundamental and first overtone mode, the period P, the number of amplitude cycles N, and the ratio of L to P, and the initial JD. For the biperiodic M stars, we obtained L/P = 43 ± 16 (standard deviation) or ±4 (standard error of the mean). For the biperiodic C stars, we obtained L/P = 31 ± 18 (standard deviation) or ±6 (standard error of the mean). The median values were 42 and 32, respectively. The difference between the two values of L/P is suggestive but not statistically significant. See Percy and Abachi (2013) for many examples of amplitude-versus-time graphs, and for a discussion of the determination of L, and the uncertainties therein.

Table 2. Periods and amplitudes of monoperiodic Carbon Red Giants.

Star	*SpT*	*P(d)*	*A*	*Notes**
ST And	C4,3-6,4e	338.2	0.50	1,3,8
VX And	C4,5J(N7)	367.0	0.29	1,3,6,8
VY And	C3,5J-4,4-5(R8)	445.1:	0.13	2
AQ And	C5,4(Nb)	336.1	0.13	1,2,3,8
BI And	S8,8	—	—	3,6
V Aqr	M6e	241.2	0.22	1,3,7
V Aql	C5,4-6,4(N6)	381.9:	0.09	1,3,4,6,8
S Aur	C4-5,4-5(N3)	367.7:	0.61	1,3,7
V Aur	C6,2e(N3e)	352.6	1.24	—
S Cam	C7,3(R8e)	327.7	0.79	1,3,7
U Cam	C3,9-6,4e(N5)	219.4	0.08	1,3,4,5,8
ST Cam	C5,4(N5)	365.6:	0.11	1,2,3,6,8
T Cnc	C3,8-5,5(R6-N6)	486.8	0.35	1,5,7
X Cnc	C5,4(N3)	370.7:	0.08	1,3,4,8
Y CVn	C5,4J(N3)	358.2:	0.06	1,3,4,8
RT Cap	C6,4(N3)	407.9	0.25	1,3,5,6,7
WZ Cas	C9,2JLi(N1p)	370.8	0.15	1,2,3,8
V CrB	C6,2e(N2e)	357.6	1.49	—
U Cyg	C7,2-9,2e(Npe)	465.3	1.25	—
RV Cyg	C6,4e(N5)	362.6:	0.13	2,3
SV Cyg	C5,5-7,4(N3)	369.9:	0.09	3,4,5
TT Cyg	C5,4e(N3e)	373.1:	0.03	1,3,4,5,8
WX Cyg	C8,2JLi(N3e)	409.4	1.12	—
AW Cyg	C4,5(N3)	357.5:	0.07	1,3,4,8
V460 Cyg	C6,4(N)	164.8	0.06	1,3,4,7
T Dra	C6,2-8,3e(N0e)	422.3	1.27	—
RY Dra	C4,5J(N4p)8	276.8:	0.06	1,3,4,7
UX Dra	C7,3(N0)	364.1:	0.06	1,3,4,8
R For	C4,3e(Ne)	388.5	1.24	3
U Hya	C6.5,3(N2)(Tc)	369.8:	0.08	1,3,4,7
V Hya	C6,3-7,5e(N6e)	—	—	1,3,7
Y Hya	C5,4(N3p)	363.3:	0.14	2,3,6
RY Hya	C6,4e(Nb)	—	—	3
T Lyr	C6,5(R6)	596.0:	0.09	2,3,5,6
V Oph	C5,2-7,4e(N3e)	297.7	1.10	—
W Ori	C5,4(N5)	210.5:	0.13	1,3,7
GP Ori	C8,0J:(SC)ea	183.3	0.29	6
RX Peg	C4,4J(N3)	637.9	0.14	2,3,5,6
RZ Peg	C9,1e(Ne)(Tc)	437.2	1.83	3
Y Per	C4,3e(R4e)	252.9	0.42	1,3,8
TX Psc	C7,2(N0)(Tc)	852.0:	0.08	3,4
FK Pup	C6,3e(N)	252::	0.39	3,6
S Sct	C6,4(N3)	268.4:	0.07	1,3,4,5,8
Y Tau	C6.5,4e(N3)	244.1:	0.12	1,2,3,8
VY UMa	C6,3(N0)	121.8	0.03	3,4
RU Vir	C8,1e(R3ep)	436.5	1.27	3
SS Vir	C6,3e(Ne)	359.7	0.77	1,7

**The amplitudes are average values over the dataset. Also see notes to individual stars in section 3.5. (1) also analyzed by KSCM; (2) low amplitude; (3) see note in section 3.5; (4) extremely low amplitude (less than 0.10 mag.); (5) there is a gap in the data; (6) the data are sparse; (7) monoperiodic according to KSCM; (8) biperiodic according to KSCM (these periods refer to pulsation periods, not LSPs).*

3.5. Notes on individual stars

This section contains notes on individual stars in Tables 1, 2, and 3, in a single list in alphabetical order of constellation name, and in order of variable star name within each constellation.

RU And The results are somewhat uncertain because of the higher-than-average noise level.

ST And KSCM obtained periods of 181 and 338 days, but these are aliases of each other.

VX And KSCM obtained periods of 375 and 904 days; we do not find the latter period. Data after JD2441000 were used.

AQ And The period is close to a year, the amplitude is low, the data are noisy, but the result agrees with that of KSCM. We note, however, that the periods that they obtain—169 and 346 days—are close to being aliases of each other.

BI And The data were sparse and noisy.

V Aqr There is a possible 123-day period. The 689-day period reported by KSCM is an alias of the 241-day period.

S Aql There is a 245-day period whose amplitude is almost as high as that of the 147-day period. The latter is highest in the V data.

V Aql KSCM obtained periods of 400 and 215 days. We also find the latter, but there are also other peaks of comparable amplitude. There is a long time scale of about 6000 days, and the period in the table is close to an alias of this. Data after JD 2425000 were used.

GY Aql There is a 204.6-day alias, and a 230.7-day harmonic. This star does not appear to be biperiodic.

S Aur There are periods of about 368 and 590 days, with comparable amplitudes; these periods are present in the V observations also; the latter period agrees with that (590 days) of KSCM; the shorter one may be a secondary period, though the ratio 368/590 is not close to the expected ratio of about 0.5. The light curve is dominated by large, slow changes in brightness.

V Boo The amplitude is slowly decreasing. There is a possible 137-day period, as reported by KSCM.

RV Boo The 144-day period reported by KSCM is one of several low-amplitude (≤ 0.06) peaks.

S Cam Our period agrees with that of KSCM.

U Cam KSCM obtained periods of 220 and 400 days. The latter is weakly present in our results, but the strongest peak is a long secondary period of 3001 days.

RR Cam Possible 124 and 220-day periods, both reported by KSCM, with small amplitudes.

RS Cam The 160-day period reported by KSCM is one of several comparable peaks in the power spectrum. There is also a long secondary period.

ST Cam Observations after JD 2442897 were used. Results agree with those of KSCM but data are sparse, amplitude is low, and period is close to one year; it is probably spurious.

X Cnc KSCM obtained periods of 193 and 350 days, but these are close to being aliases; the amplitudes are low; and the strongest period is dangerously close to a year. V data, however, support a period of about a year.

RT Cnc Possible 700-day period, but with small amplitude.

Y CVn KSCM obtained periods of 160 and 273 days; we do not find these in our results. The amplitudes of all the peaks are low; the period in the table may be spurious.

RT Cap Because of a gap in the data, only observations after JD2434000 were analyzed; our results agree with those of KSCM.

Table 3. Periods and amplitudes of monoperiodic Oxygen Red Giants.

Star	*SpT*	*P(d)*	*A*	*Notes**
RV And	M4e	171.2	0.22	1,7
V Aqr	M6e	241.2	0.22	1,3,8
S Aql	M3-5.5e	146:	0.75	1,3,5
GY Aql	M6-8IIIe	463.4	2.05	1,3,6,7
T Ari	M6-8e	320.5	0.80	1,5,7
RS Aur	M4-6e	172.3	0.29	1,7
U Boo	M4e	201.7	0.62	1,5,7
V Boo	M6e	257.7	0.56	1,3,8
RV Boo	M5-7e	—	—	3
RR Cam	M6	—	—	3
RS Cam	M4III	90.5	0.20	1,3,6,8
RY Cam	M3III	135.2	0.19	1,7
RT Cnc	M5III	370.0:	0.11	2,3
V CVn	M4-6IIIea:	192.3	0.29	1,5,7
AA Cas	M6III	80.0	0.04	3,4
SS Cep	M5III	101.1:	0.06	1,3,4,8
DM Cep	M4	363.0:	0.05	1,4,7
RS CrB	M7	330.9	0.24	1,6,7
W Cyg	M4-6IIIe(Tc:)	132.2	0.14	1,2,3,8
TZ Cyg	M6	567.4	0.06	1,3,4,8
AB Cyg	M4IIIe	—	—	3
AF Cyg	M5-7e	94.0	0.13	1,2,3,8
AI Cyg	M6-7	—	—	1,3,7
U Del	M4-6II-III	1161	0.21	1,2,3,8
CT Del	M7	358.7:	0.12	2
CZ Del	M5	0.05	—	4
EU Del	M6.4III	62.5	0.06	1,4,7
S Dra	M7	180.1	0.10	1,2,3,5,8
RS Dra	M5e	273.6	0.40	5,6
TX Dra	M4-5e	712.0	0.14	1,8
Y Gem	M6-7e	0.10	—	2,3
SW Gem	M5III	238.4	0.08	1,3,4,7
X Her	M6e	176.9	0.06	1,3,4,8
ST Her	M6-7IIIaS	256.6	0.11	1,2,3,8
UW Her	M5e	106.8	0.10	1,2,3,8
g Her	M6III	880.0	0.06	1,3,4,7
RY Leo	M2e	159.9	0.34	1,3,7
U LMi	M6e	273.3	0.40	1,3,8
RX Lep	M6.2III	572.2	0.06	3,4,7
SV Lyn	M5III	368.2	0.07	3
SZ Lyr	M6	143.7	0.15	2,3
X Mon	M1-6IIIep	155.7	0.52	1,7
SW Mon	M4-6III	193.6	0.14	2,3
UZ Per	M5II-III	893.4	0.27	1,7
V UMa	M5-6III	197.8	0.12	1,2,3,7
Y UMa	M7II-III:	325.0	0.11	1,2,3,8
RY UMa	M2-3IIIe	287.9	0.14	1,2,3,7
RZ UMa	M5-6	260 ± 5	0.11	2
ST UMa	M4-5III	625.1	0.07	1,3,4,7
R UMi	M7IIIe	324.5	0.43	1,3,8
V UMi	M5IIIab:	72.9	0.11	1,2,3,8
SW Vir	M7III	155.4	0.20	1,3,7

**The amplitudes are average values over the dataset. Also see notes to individual stars in section 3.5. (1) also analyzed by KSCM; (2) low amplitude; (3) see note in section 3.5; (4) extremely low amplitude (less than 0.10 mag.); (5) there is a gap in the data; (6) the data are sparse; (7) monoperiodic according to KSCM; (8) biperiodic according to KSCM (these periods refer to pulsation periods, not LSPs).*

SV Cas Only data after JD2435000 were analyzed. KSCM obtained periods of 262 and 460 days. A 227-day harmonic is present. Our error in P1 is slightly large.

WZ Cas KSCM obtained periods of 187 and 373 days, but these are close to being aliases of each other. Although the period in the table is close to a year, the amplitude suggests that it is real.

AA Cas Amplitudes are very small, but the peak stands out.

S Cep There is a 243-day harmonic.

SS Cep We do not find the 340-day period reported by KSCM. The strongest peak is a long secondary period.

V Cyg There is a 209.1-day harmonic.

W Cyg There is also a 250-day period, comparable with KSCM's 240-day period, with $\Delta v = 0.07$. This period is less secure in the power spectrum of the V data.

RS Cyg There is a 211.2-day harmonic.

RU Cyg Our results are consistent with those of KSCM.

RV Cyg The amplitudes are low; the period may be spurious.

RZ Cyg Our results are consistent with those of KSCM.

SV Cyg Large gap in the data, amplitude is low, and period is close to one year. V data suggest a period of about 418 days.

TT Cyg KSCM obtained periods of 188 and 390 days, but the amplitudes of these and our periods (which include ones close to KSCM's) are less than 0.03!

TZ Cyg KSCM reported periods of 79 and 138 days. We find the second, but not the first. All peaks have $\Delta v \leq 0.06$.

AB Cyg KSCM reported periods of 429 and 513 days. We find a peak near the second, but not the first.

AF Cyg KSCM reported periods of 93 and 163 days. We find the first, and a second period of 173 ± 10 days.

AI Cyg KSCM reported a period of 146 days. We find several peaks, of comparable height, including 1864, 273, and 144 days.

AW Cyg The data are sparse, and the amplitude is small.

V460 Cyg The amplitude of the 165-day period is small, but our result agrees with that of KSCM and with an analysis of the V data.

U Del KSCM found this star to be biperiodic, with periods 110 and 580 days. The latter is an alias of the long secondary period of 1161 days, as is the period of 278 days.

S Dra KSCM reported periods of 172 and 311 days. We find periods near these, but the strongest period is actually a long secondary period.

RY Dra Observations after JD2433000 used; data are noisy, and peaks are of low amplitude. Our quoted period may be an alias of a long secondary period.

UX Dra Our highest peak is at 364.07 days, with a small amplitude, but this may be spurious. KSCM list periods of 176 and 317 days. We find periods close to these, with small amplitudes.

AH Dra Our results are consistent with those of KSCM.

AY Dra The data are sparse, but the amplitudes are high. The 130-day period may actually be a harmonic; there is a weaker 149-day period which may be the overtone.

R For The amplitude is low.

Y Gem Results highly uncertain.

SW Gem KSCM reported a period of 700 days. Our strongest peak is at 685 days, but there are also alias periods of 238 and 783 days, and a probably-spurious period of 365 days.

X Her KSCM obtained periods of 178 and 102 days; we find the shorter period in our results, but with small amplitude (≤ 0.05). The highest peaks are at periods of 650–800 days.

RR Her The shorter period is uncertain; KSCM did not list it. There is a 143.5-day alias. There is a large gap in the dataset.

ST Her KSCM obtained periods of 149 and 263 days, but these are aliases of each other, and have comparable amplitudes. The longer period produces a slightly more satisfactory alias pattern.

UW Her KSCM obtained periods of 172 and 107 days; the 107-day period is one of several with comparable small amplitude.

g Her The (low-amplitude) pulsation period is about 90 days; the 880-day period is a long secondary period. KSCM obtained periods of 887 and 90 days.

U Hya KSCM obtained a period of 791 days; we find a peak at this period, but it does not stand out; its amplitude is somewhat smaller than that of the 370-day period.

V Hya This famous star shows deep minima with a period of 6300 days; there are periods of 345 and 387 days which are aliases of this. KSCM obtained a period of 531 days which, in our results, is the highest peak which is not an alias.

Y Hya The amplitude suggests that the 363-day period may be real.

RY Hya Insufficient data for analysis.

RY Leo The power spectrum is complex. KSCM obtained close periods of 145 and 160 days.

U LMi KSCM obtained periods of 272 and 144 days; we also find the latter period; it has a much smaller amplitude than the longer period.

RX Lep The power spectrum is complex.

SV Lyn The period is probably spurious.

T Lyr There is a 340-day period which is an alias of a long secondary period; 596 days is a *possible* pulsation period.

SZ Lyr The 144-day period is supported by the V data.

SW Mon 194 days is one of several comparable peaks in the power spectrum.

W Ori KSCM listed a 208-day period, and a long secondary period of 2300 days. There are alias periods of the latter: 432 and possibly 210 days.

BQ Ori our results are consistent with those of KSCM, but are uncertain.

RX Peg Possible secondary period at 388.7 days, with an amplitude of 0.14, but this peak is noisy. Also: the strongest peak is a long secondary period. The 638-day period is supported by the V data.

RZ Peg There is a 199.0-day alias, and a 218-day harmonic. This star does not appear to be biperiodic.

Y Per KSCM obtained periods of 127 and 245 days. The former period does not stand out in our results.

SY Per Only data after JD 2447000 were analyzed. KSCM listed only a 477-day period; our 231-day period is marginally significant, but the power spectrum is noisy. There is a 207.2-day alias.

TX Psc There is a slightly weaker 255-day period which is an alias of the 852-day period, and could possibly be the true one.

FK Pup The data are sparse, but periods of about 250 and 500 days appear in both the visual and V observations.

S Sct Observations after JD 2432000 were used. The data are sparse and noisy, and the amplitudes of the peaks are small (less than 0.07), so the results are highly uncertain. KSCM obtained periods of 269 and 149 days; the latter is present in our results.

W Tau KSCM found this star to be biperiodic, with periods 265 and 243 days; we find a reasonably significant period of 127.5 days. The amplitude is low.

Y Tau KSCM obtained periods of 242 and 461 days; the latter period is present in our results, but does not stand out. The V data suggest a possible period of 320–330 days. There is also a long secondary period.

V UMa there is also a possible 107-day period.

Y UMa the power spectrum is complex. KSCM obtained periods of 164, 315 and 324 days. We also find a period of 167 ± 1 days.

Z UMa Our results are consistent with those of KSCM.

RY UMa KSCM obtained close periods of 287 and 305 days.

ST UMa The results are highly unncertain, due to small amplitude, but the 625-day period stands out.

VY UMa The 122-day period is of low amplitude, but stands out in the power spectrum; it is one of three possible periods in the V data.

R UMi KSCM obtained periods of 170 and 325 days, but these are aliases of each other.

V UMi KSCM obtained periods of 73 and 126 days. We find a broad peak at the latter period, but with amplitude less than 0.03. There is also a 770-day long secondary period.

RU Vir there is a clear period at 436 days, and a possible one at 220 days, but the latter peak is noisy. There are slow changes in mean magnitude.

SW Vir Result confirmed by V data. KSCM obtained close periods of 154 and 164 days.

RU Vul There is a large change in amplitude, half-way through the dataset. Templeton *et al.* (2005) noted that the period of this star decreased from 155 to 110 days over 65 years. The period spectrum in the first half of the data is understandably different from that in the second half. KSCM found average periods of 369 and 136 days; we find average periods of 155 and 368 days. Given the change in period and the abrupt change in amplitude, neither pair is meaningful.

4. Discussion

This study is limited by the nature and timing of the observations. As noted above, there are both alias periods (because of the yearly spacing of the observations) and possible low-amplitude spurious periods because of the Ceraski effect. These are compounded by the fact that the stars undergo only semi-regular variability, which causes the power spectrum to be more complex. If the stars are large-amplitude stars with non-sinusoidal light curves, the power spectra are also complicated by harmonics. The P/2 harmonic can masquerade as an overtone, since P1/P0 is close to 0.5 in these stars. The presence of a long secondary period (and its aliases) in about a third of the stars can also be a complication. The intrinsic variations in most of the stars are small to begin with, especially in the C stars. The C stars are also more difficult to observe, because they are very red; it is difficult to find suitable comparison stars, and different observers' eyes respond differently to red light. Furthermore: because these stars vary, on long time scales, in period, amplitude, mean magnitude, and sometimes light curve shape, our results in the tables provide only an average picture over the interval of observation.

The C stars behaved marginally differently from the M stars in terms of the relation between changing amplitude and changing period (Percy and Yook 2014). They do not behave significantly differently in terms of period ratio (Figure 3). They behave slightly differently in terms of the length of cycles of amplitude variation (Table 4), but the differences are not statistically significant. Differences might be expected, given the differences in chemical composition, and therefore of opacity and structure, in the envelopes of the stars. KSCM also looked for differences between the C and M stars, but "the photometric parameters did not allow to determine such a discrimination."

Table 4. Amplitude variations in Oxygen (top group) and Carbon (bottom group) Red Giants.

Star	*P0(d)*	*N(0)*	*L/P(0)*	*P1(d)*	*N(1)*	*L/P(1)*	*JD range*
GY Aql	463.4	1	22	—	—	—	JD 2447065+
SV Cas	455.6	1	49	239.9	3	32	JD 2435000+
RU Cyg	443.0	1.6	61	233.9	3	57	JD 2416783+
RZ Cyg	537.6	3	25	275.9	4.5	32	JD 2416792+
AH Dra	190.0	2	42	105.9	3.5	43	JD 2441000+
BQ Ori	246.5	3	34	125.8	5	39	JD 2432294+
Z UMa	189.2	2	78	98.9	5	60	JD 2427525+
S Cep	486.1	3	32	208.3	6:	32:	JD 2411073+
V Cyg	420.9	4	22	195.6	8:	22:	JD 2419700+
RS Cyg	419.0	1.5	72	195.1	4:	54:	JD 2411686+
RR Her	236.7	1.5	62	124.2	—	—	JD 2435000+
W Ori	432.4	1.5	38	210.5	3.5	34	JD 2432151+
RZ Peg	437.2	2.5	31	—	—	—	JD 2423200+
SY Per	479.2	1	23	231.5	2	24	JD 2446039+

The number of periods in the tables—especially of the C stars—which are close to one year is concerning; there is a distinct excess of stars which have periods in the range 350–380 days. Specifically: there are 11–12 C stars, and 3 M stars, whose periods are between 350 and 380 days, and which we are unsure of. The same effect is noted in KSCM, Figure 10, in which there is a pronounced peak, for the C stars, at a period of one year. Some of these periods may be spurious periods, caused by the Ceraski effect, especially if the amplitude is 0.1 magnitude or less. Reduction of the above-mentioned peak would reduce the apparent difference between the period distributions of the C and M stars in KSCM's Figure 10.

We have shown that there is still some useful science contained in the decades of visual observations of pulsating red giants in the AAVSO International Database. We have also shown the many challenges to extracting that science. The new frontier of pulsating-red-giant research is massive photometric surveys such as MACHO and OGLE. Peter Wood's (2015) paper on pulsation modes, masses, and evolution of luminous red giants is an exemplary illustration of that frontier.

5. Conclusions

Using AAVSO visual observations, and the AAVSO VSTAR time-series analysis software, we have determined improved periods for 5 biperiodic C red giants, 43 monoperiodic C red giants, 12 biperiodic M red giants, and 46 monoperiodic M red giants. We have compared the period ratios in the two biperiodic groups; they are marginally but not significantly different. We have also used VSTAR wavelet analysis to study

the cyclic pulsation amplitude variations in some stars in the two groups; they are marginally different. Our main conclusion is that, because of the small amplitudes in many of these stars, and because of the presence of alias, harmonic, and spurious periods, this kind of study requires great care and caution. In particular, spurious periods, caused by the Ceraski effect, can produce an artificial peak in the period distribution, at a period of about a year.

6. Acknowledgements

We thank the AAVSO observers who made the observations on which this project is based, the AAVSO staff who archived them and made them publicly available, and the developers of the VSTAR package which we used for analysis. We acknowledge and thank the University of Toronto Work-Study Program for financial support. We also thank the anonymous referee for many helpful suggestions. JRP thanks DJH, a biophysics major with no formal background in astronomy, for organizing and carrying out this project in such a professional way. This project made use of the SIMBAD database, maintained in Strasbourg, France.

References

Benn, D. 2013, VSTAR data analysis software (http://www.aavso.org/vsta9r-overview).

Henden, A. A. 2014, observations from the AAVSO International Database (http://www.aavso.org).

Kafka, S. 2015, observations from the AAVSO International Database (http://www.aavso.org).

Kiss, L. L., Szatmary, K., Cadmus, R. R. Jr., and Mattei, J. A. 1999, *Astron. Astrophys.*, **346**, 542.

Mattei, J. A., Foster, G., Hurwitz, L. A., Malatesta, K. H., Willson, L. A., and Mennessier, M. O. 1997, in *Proceedings of the ESA Symposium "Hipparcos-Venice '97"*, 13–16 May, Venice, Italy, ed. B. Battrick, ESA SP-402, ESA Publications Division, Noordwijk, The Netherlands, 269.

Percy, J. R. 2015, in preparation.

Percy, J. R., and Abachi, R., 2013, *J. Amer. Assoc. Var. Star Obs.*, **41**, 193.

Percy, J. R., and Khatu, V. 2014, *J. Amer. Assoc. Var. Star Obs.*, **42**, 1.

Percy, J. R., and Kim, R. 2014, *J. Amer. Assoc. Var. Star Obs.*, **42**, 267.

Percy, J. R, and Yook, J. Y. 2014, *J. Amer. Assoc. Var. Star Obs.*, **42**, 245.

Petersen, J. O. 1973, *Astron. Astrophys.*, **27**, 89.

Sharonov, V. V. 1933, *Bull. Tashkent Obs.*, **1**, 4 (in Russian, with an English summary).

Templeton, M. R., Mattei, J. A., and Willson, L. A. 2005, *Astron. J.*, **130**, 776.

Wood, P. R. 2015, *Mon. Not. Roy. Astron. Soc.*, **448**, 3829.

Xiong, D. R., and Deng, L. 2007, *Mon. Not. Roy. Astron. Soc.*, **378**, 1270.

Observations and Analysis of Three Field RR Lyrae Stars Selected using Single-epoch SDSS Data

W. Lee Powell Jr.
Stephanie N. Jameson
University of Nebraska Kearney, Department of Physics, Bruner Hall of Science, 2401 11th Avenue, Kearney, NE 68849;address email correcpondence to W. L. Powell, Jr., powellwl@unk.edu

Nathan De Lee
Northern Kentucky University, Department of Physics and Geology, Natural Science Center 204H, Nunn Drive, Highland Heights, KY 41099; and Vanderbilt University, Department of Physics and Astronomy, Nashville, TN 37235

Ronald J. Wilhelm
University of Kentucky, Department of Physics and Astronomy, 177 Chemistry-Physics Building, 505 Rose Street, Lexington, KY 40506

Received September 16 2014; revised August 18, 2015; accepted August 28, 2015

Abstract We present the results of our Johnson B and V observations of three RR Lyrae candidate stars that we identified as likely variable stars using SDSS data. The stars were selected based upon a single epoch of photometry and spectroscopy. The stars were observed at McDonald Observatory to obtain full light curves. We present full light curves, measured periods, and amplitudes, as well as the results of our Fourier analysis of the light curves.

1. Introduction

In an effort to obtain as much useful information as possible out of large survey datasets, we derived a means of using a single epoch of photometry and spectroscopy data to identify RR Lyrae variable stars. Our method takes advantage of correlated changes in observed colors versus effective width of lines in the spectrum to find stars that have different surface temperatures at the two pulsation states. We found a large disparity between the (g–r) color and the strength of the Hydrogen Balmer lines when two observations were made at random phase, which we exploit to identify RR Lyrae pulsating variable stars. As a result of that effort we identified over 1,000 candidate RR Lyrae stars in the halo of the Milky Way ranging from around g = 14 to g = 20 using Sloan Digital Sky Survey data (York *et al.* 2000). This dataset is not complete since it will only identify stars that were at different points of their pulsation cycle when the photometry and spectroscopy observations were made (Wilhelm *et al.* 2007; Powell *et al.* 2010). Testing the method using the known variables identified in the SDSS Stripe 82 (Sesar *et al.* 2007) shows that our method is ~85% accurate in predicting variability. This accuracy has been confirmed by previous work by the authors (Powell *et al.* 2010). For that paper an assortment of candidate stars was observed sparely to confirm their variability. Since RR Lyrae stars have such large amplitudes they are easily identified even using sparse data. Our previous work combined with on-going work agrees well with the results determined using Stripe 82, with 15 stars confirmed as variable, three stars that appear to be variable but not RR Lyrae stars, and two stars that appear to not be variable, out of 20 stars observed between 2009 and 2014. Undergraduate students have made the vast majority of the photometry observations described in this paper. The three stars described in this paper appear to be previously unknown variables.

2. Observations and calibration

2.1. General observation information

All photometry observations described in this paper were made at McDonald Observatory using the 0.8-m telescope and the f/3.0 prime focus corrector (PFC). The PFC uses a Loral-Fairchild nitrogen-cooled 2048 × 2048 pixel CCD chip. The Johnson B and V filters were used for all observations. The readout time for this chip is quite long and the field of view is larger than needed so only the central portion of the chip was used. Using a 750 × 750 pixel region resulted in a field of view of around 15 arcminutes and a readout time of just over 70 seconds. This allowed us to achieve a faster cadence and more complete light curves. Dark current is negligible for this LN2-cooled instrument. Dome flat field frames and bias frames were taken nightly for all observing runs.

Table 1: Details of observations.

Star	*SDSS ID*	*R. A. (2000) h*	*Dec. (2000) °*	*Dates*	*Observers*
RR 444	4828-301-5-116-0447	266.368714	+26.141512	May 27–30, 2011	Powell, Hans Amende, Caleb Bahr
				July 5–8, 2011	Powell, Hans Amende, Caleb Bahr
RR 143	4512-301-3-0275-0084	240.399352	+23.467972	June 6–12, 2013	Powell, Stephanie Smith
RR 397	3705-301-2-0292-0054	245.745375	+36.573442	June 6–12, 2013	Powell, Stephanie Smith

Table 2. Comparison stars.

Variable	*APASS Comparison*	*R. A. (2000) h*	*Dec. (2000) °*	*Number of Observations*	*APASS Magnitudes V*	*V error*	*B*	*B error*	*B–V*
RR 143	C1	240.40006	23.50305	4	15.65	0.00	16.38	–0.06	0.73
	C3	240.51872	23.41518	2	15.96	0.00	16.69	–0.07	0.73
	C5	240.36162	23.45008	4	15.20	0.04	15.99	0.20	0.79
	C6	240.37839	23.43636	4	12.78	0.10	15.59	0.20	0.81
	C7	240.44765	23.46511	4	15.50	0.02	15.91	0.12	0.86
RR 397	C1	245.71351	36.560951	2	15.39	0.01	15.82	0.09	0.42
	C2	245.81440	36.558467	2	14.69	0.01	15.27	0.03	0.58
	C5	245.77940	36.556515	2	14.74	0.01	15.41	0.01	0.67
RR 444	C1	266.40591	26.235944	2	14.72	0.07	15.29	0.06	0.57
	C2	266.44629	26.141434	2	15.81	0.00	16.09	–0.05	0.29
	C4	266.33562	26.136753	2	15.65	0.03	16.20	0.10	0.54
	C5	266.31716	26.162361	2	15.35	0.07	15.93	0.02	0.58

2.2. Observing runs

Results for three stars are presented in this paper. The full SDSS names, coordinates, and observing run dates for these stars are listed in Table 1. Star RR 444 was observed for a total of seven nights, four in May 2011 and three in July 2011. The two stars RR 143 and RR 397 were both observed during our seven night June 2013 observing run.

2.3. Data processing

All data were processed using the CCDPROC routine in IRAF. A master bias frame was made by median combining the bias frames from each observing run. An ovserscan correction was also made. Flat field images from the McDonald 0.8-m require additional processing to remove a gradient introduced by the geometry of the telescope, screen, and lighting system. The IRAF routine IMSURFIT was used to remove the geometry-induced gradient. The corrected flat field images were median combined to create a master flat field image for each night. The process CCDPROC was used to bias- and flat-correct the science frames, and was also used to correct bad pixels in an automated fashion. The final processed images from each night were then registered and aligned to make the photometry process simpler.

2.4. Comparison stars and photometry measurements

2.4.1. Comparison stars

All comparison stars used for this project were found in the AAVSO Photometric All-Sky Survey (APASS; Henden *et al.* 2014). The AAVSO APASS online search tool was used to search the area around each variable star, within the field of view of the images. The final comparison stars were chosen based on their proximity to each variable star, as well as their similarity in color. By choosing comparison stars that are very similar in color to the variable star, we minimized error induced by differential affects of the atmosphere on each star's light due to its color. The comparison stars used are detailed in Table 2. None of the comparison stars used exhibited any noticeable variability more than the scatter one would expect from the errors in the photometry.

2.4.2. Photometry measurements with MIRA

Since the intention of this project, in part, was to introduce undergraduate students to photometry, the use of a commercial photometry package was useful to speed the learning process. MIRA Pro Ultimate Edition (Mirametrics 2010) provides a tool for doing calibrated differential photometry. While identifying stars in each frame, the tool allows the appropriate magnitude to be entered for each standard star. The software then calculates a plate solution that returns a calibrated magnitude for each star in the image. The argument is that since all stars in the image are recorded at the same airmass and time, and since the color of the standards is approximately the same as that of the variable, then the magnitudes returned should be at the very least approximately on the standard system. The advantage with this approach when working with undergraduate students is that the math is automatically performed by the software, and the graphical interface is very user-friendly. The obvious disadvantage is that it is not immediately obvious that the resulting magnitudes are truly standard. This approach was used to extract magnitudes for the standards and variable star for all of the science images.

2.4.3. Determination of extinction coefficients

To test that it is indeed the case that the resulting magnitudes are truly standard, the photometry was performed using a traditional approach for one night per variable star. This will provide evidence both that the standard stars chosen are consistent in their behavior, and that the MIRA approach yields the same answers as are obtained by calculating the magnitudes from instrumental magnitudes and extinction coefficients calculated for each night.

The approach used to determine the extinction coefficients follows closely the approach advocated by Peter Stetson (Stetson 1992). A full solution would follow this form:

$$v = V + a_0 + a_1(B–V) + a_2(B–V)^2 + a_3(B–V)^3 + a_4(X–1.25) + a_5(X–1.25)(B–V) + a_6 t \quad (1)$$

where v is the instrumental magnitude, V is the standard magnitude, B–V is the color index, X is the airmass, and t is the Universal Time of the observation. Rather than using just X, the equation uses (X – 1.25) to avoid ringing in the numerical solution. The coefficients, **A**, that result from solving the system of simultaneous equations for all standard star observations,

Table 3. Extinction coefficients.

Coefficient	*RR 143 V*	*Night 1 B*	*RR 397 V*	*Night 7 B*	*RR 444 V*	*Night 2 B*
a_0	–21.55160	–21.1404	–21.6222	–21.189	–21.5376	–21.0956
a_1	0.45330	0.7428	0.1365	0.3615	0.195	0.3358
a_2	0.02700	0.0223	0.0041	–0.0046	0.0073	0.0149

can then be used to solve for the measured magnitude on the standard system from the measured instrumental magnitude and instrumental color. Care must be taken to determine the instrumental magnitude, which usually means solving an abbreviated version (Equation 2) of the above equation to find preliminary coefficients that can be used to get an improved estimate of the instrumental color index for input into the longer equation for use in determining the full set of coefficients.

$$v = V + a_0 + a_1 (X - 1.25) + a_2 t \quad (2)$$

For this paper, the abbreviated form was used exclusively since the color indices were all quite similar. Since the numerical sampling in B–V is small, the resulting coefficients are unreliable and prone to ringing. The approach to solving this problem for this paper thus involved measuring the instrumental magnitude for the variable star and the standard stars, and recording X and t for each observation. Two matrices were then formed from the observations. The first matrix, **M**, has one row for each observation with column entries of the form:

$$1 \qquad (X - 1.25) \qquad t \quad (3)$$

A second column matrix, **m**, was created with each row formed from the corresponding number that results from subtracting the published standard magnitude from the instrumental magnitude for each observation, that is (v–V). Using tools from linear algebra we can solve for the coefficients using these matrices using the following equation:

$$\mathbf{A} = (\mathbf{M^T} \cdot \mathbf{M})^{-1} \cdot \mathbf{M^T} \cdot \mathbf{m} \quad (4)$$

which takes inverse of the matrix that results from taking the transpose of **M** times itself, multiplying that times the transpose of **M**, then multiplying that times the column matrix **m**. The result is a column matrix **A** with coefficients a_0, a_1, and a_2, where a_0 is the zero point and a_1 and a_2 are the slope terms for airmass and time. These matrix operations can be complete in a number of ways. For this paper we used the commercial package MATLAB (MathWorks 2014). This process was used to determine the coefficients for the V filter for one night per variable star, and repeated to find the coefficients for the B filter. The coefficients that were found are detailed in Table 3. The resulting coefficients were used to calculate the magnitudes of the stars in both V and B for comparison with the magnitudes that resulted from the use of MIRA.

2.4.4. Comparing the photometry results

For each variable star, the results of the two methods of photometry were compared for one night. The photometry results were compared to the published magnitude, and to each other. An average difference in magnitude was calculated, as was the standard deviation in the magnitude difference. The typical estimated error in the photometry, calculated by MIRA during the aperture photometry process using the signal-to-noise ratio, ranges from an average of around 0.005 to 0.03. As a preface to examining the differences between the two methods we note that the standard magnitudes for the RR 143 field are larger than those for the other fields, particularly in the B filter where the estimated APASS magnitude error grows to around 0.1. This seems to be echoed in our results. Table 4 summarizes the various comparisons between the two approaches.

We calculated the magnitude using two methods to confirm that the McDonald 0.8-m telescope data were transforming to the standard system reliably, and to explore whether using MIRA was introducing any systematic errors. The answer to the first question is yes. The result of both methods closely matched the standard system to the level of the error present in our photometry and the APASS photometry. No systematic problems were evident in our data. The answer to the question of whether using MIRA to calibrate the magnitude introduces systematic errors is shown to be no. The standard deviation in the magnitude difference of the MIRA photometry and the APASS standard magnitude was found to be smaller for both filters for all three nights than what we found doing an extinction calculation. Considering the errors in the photometry and the errors provided for the APASS data, any differences between the two methods are indistinguishable. Particularly reassuring is the fact that the average difference in all cases is very much smaller than the errors in the photometry. Considering all of the results we assert that the MIRA standard star correction seems to give reliable results, at least for the case of standard stars that are chosen to be similar in color to the variable star. Since this occurred for all three stars we chose not to perform the longer calculation for every night. The results of the MIRA photometry were used for the light curve fitting.

Table 4. Comparison of magnitudes found using MIRA and the extinction method.

Star	*MIRA vs APASS*		*Calculation vs APASS*		*MIRA vs Calculation*	
	Average Difference	*Standard Deviation*	*Average Difference*	*Standard Deviation*	*Average Difference*	*Standard Deviation*
RR 143V	0.000002564	0.05146	–0.00354653	0.053817	–0.003549	0.01062
RR 143B	–0.00000303	0.1102	0.0001996	0.11158	0.00002613	0.01546
RR 397V	–0.0000029	0.0009005	–0.00018	0.01371	–0.00077	0.010201
RR 397B	0.000958	0.0280009	0.00179	0.03145	–0.00145	0.012158
RR 444V	–0.007921	0.025381	–0.00008135	0.02556	–0.00784	0.009358
RR 444B	–0.0000016	0.034901	0.000221	0.03686	–0.00022	0.011602

3. Light curves and Fourier analysis

3.1. Period finding

The photometric analysis begins by identifying the correct period for each of the RR Lyrae stars. Given the sampling rate of this data set, there are a number of programs which can do this. For this work, SUPERSMOOTHER (Reimann 1994) was used. SUPERSMOOTHER uses a variable-span linear smoother that calculates a short, medium, and long smooth and then uses the best fit to the data. The period is determined by whichever frequency gives the best sum of absolute residuals. SUPERSMOOTHER has the benefit of being entirely automatic, and does not make assumptions about the shape of the light curve. SUPERSMOOTHER generates a list of the 15 most probable periods in order of likelihood.

3.2. Spline fitting

In order to determine the amplitudes, epochs of maximum, and weighted mean magnitudes of our stars it is useful to have a model of the light curve that is complete at all phases and can use information for each epoch in the light curve. There are several ways this could be achieved (fitting Fourier series, using previously defined templates, and so on), but in this paper we have chosen to use a smoothed spline. Normal splines weight each data point equally. A smoothed spline combines a spline and a chi square test to allow the error of each point to be taken into account. For this paper we use the smoothed spline algorighm described in Chapter 11 of Pollock (1999). The smoothed spline follows the actual shape of the data better than a template fit, and it is less prone to ringing than a Fourier series fit. The light curve properties for each star are given in Table 5.

3.3. Detemining metallicity

Due to the variable nature of RR Lyrae stars it is often difficult to get spectroscopic metallicities. As a result, a number of photometric methods have been developed to achieve such a measurement. Since the pulsation in RR Lyrae stars is driven by opacity changes in the atmosphere (the κ-mechanism (King and Cox 1968)), it is not surprising that metallicity would have an impact on the light curve shape. There are two techniques that take advantage of this fact, the Φ_{31}-Period-metallicity (Jurcsik and Kovacs 1996) and Period-Amplitude-Metallicity (Sandage 2004) relations. Both are primarily used with type RRab stars, which have more variation in their light curve shape. Although progress has been made on the Fourier method with RRc stars in (Morgan *et al.* 2006), there are theoretical reasons to believe that the Period-Amplitude-Metallicity relation may not be as useful for RRc stars (Bono *et al.* 2007). For that reason, in this work both of these methods will be restricted to the RRab star.

3.4. Fourier metallicities

Fitting a Fourier sine series to a light curve provides a way to quantify the shape of the curve. In the Fourier sine series equation (Equation 5), A_i is the amplitude of each order, φ_i is the frequency offset, t is the HJD, and ω is the frequency. Once the sine series is fit to data, the adopted convention is to create a parameter $R_{ij} = A_i / A_j$ to relate the amplitudes and to relate the phases. For this work we fit an 11th-order sine series. We used the Φ_{31}-period-metallicity relationship (Jurcsik and Kovacs 1996, shown in Equation 6) to determine the metallicity from the measured Φ_{31} and period.

$$V = A_0 + \sum_{i=1}^{n} A_i \sin [i\omega (t - t_0) + \varphi_i] \quad (5)$$

$$J_{[Fe/H]} = -5.038 - 5.39P + 1.345\ \Phi_{31} \quad (6)$$

In order to use Fourier sine fitting, a light curve must have relatively complete phase coverage, or else ringing will be induced in the fit. For those light curves that are too incomplete to use Fourier sine fitting we can use an amplitude-period-metallicity relationship. Sandage (2004) found a relationship among the amplitude in the Johnson V filter, the period, and the metallicity of an RRab star. His relationship is shown in equation (7).

$$[Fe/H] = -1.453\,(\pm 0.027)\,A_v - 7.990\,(\pm 0.091) \log P - 2.145 \pm 0.025 \quad (7)$$

In general the period-amplitude relation for determining metallicity has much more scatter in it relative to the Fourier method. This only makes sense given that it uses amplitude, which is much less sensitive to light curve shape than Φ_{31} (Bono *et al.* 2007). On the other hand, amplitude is a much easier quantity to measure and can be used on relatively incomplete light curves. Figure 7 shows RR 143 with the Fourier-fit to the V data. Table 5 details the parameters derived from our analysis of the light curves. The table lists for both V and B the amplitude and minimum magnitude of the light curve, the average magnitude derived from a magnitude-weighted and intensity-weighted average, the period of pulsation, the template that resulted in the best fit, the HJD of maximum magnitude, and the derived metallicities.

Table 5. Light curve derived parameters.

Variable	*V Amplitude*	*B Amplitude*	*Minimum V Mag.*	*Minimum B Mag.*	*V Mag. Weighted Average Mag.*	*V Intensity Weighted Average Mag.*	*B Mag.Weighted Average Mag.*	*B Intensity Weighted Average Mag.*
RR 143	1.30	1.57	15.73	16.20	15.32	15.25	15.72	15.60
RR 397	0.48	0.61	15.58	15.89	15.34	15.33	15.58	15.56
RR 444	0.51	0.66	16.20	16.48	15.95	15.93	16.16	16.13

Variable	*Period V*	*Period B*	*HJD Max V*	*HJD Max B*	*[Fe/H]_J*	*[Fe/H]_S*
RR 143	0.45543213	0.45543213	2456454.357537	2456454.35952526	–1.46	–1.32
RR 397	0.36811239	0.37180909	2456456.889431	2456456.89763209	NA	NA
RR 444	0.34790353	0.34790809	2455712.855586	2455712.850264	NA	NA

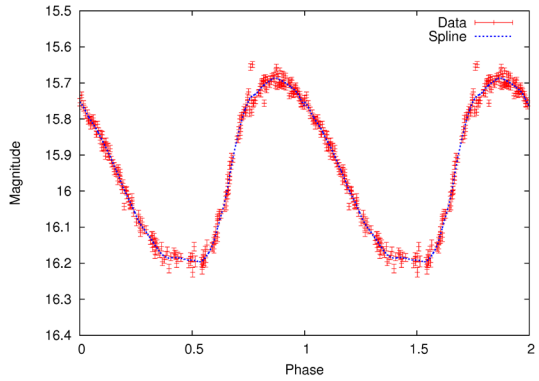

Figure 1. RR 444 Smoothed Spline-fit light curve in V.

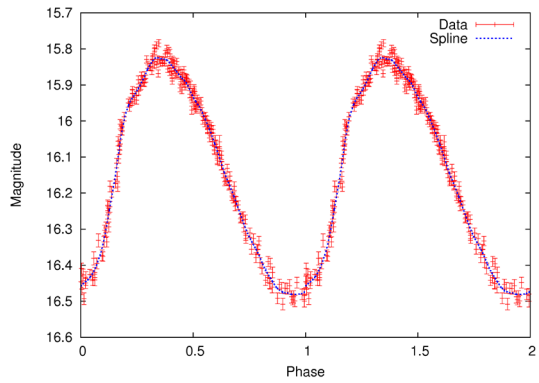

Figure 2. RR 444 Smoothed Spline-fit light curve in B.

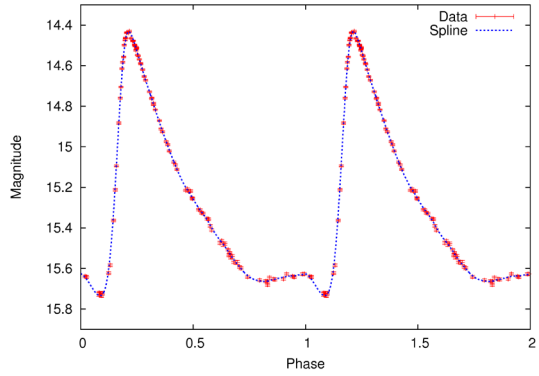

Figure 3. RR 143 Smoothed Spline-fit light curve in V.

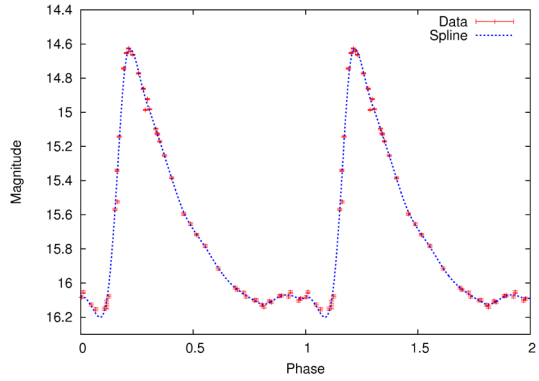

Figure 4. RR 143 Smoothed Spline-fit light curve in B.

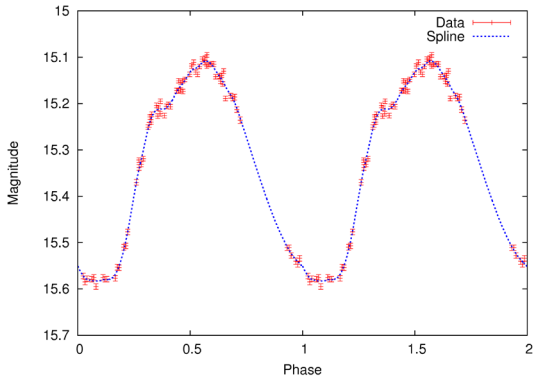

Figure 5. RR 397 Smoothed Spline-fit light curve in V.

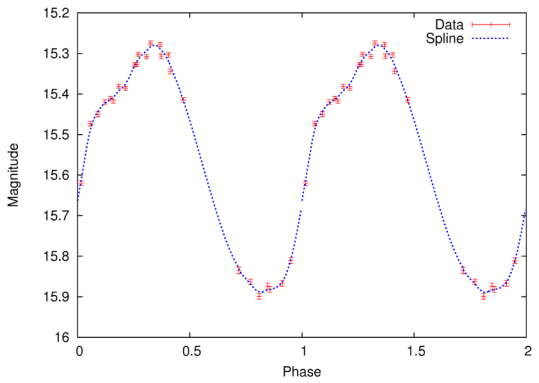

Figure 6. RR 397 Smoothed Spline-fit light curve in B.

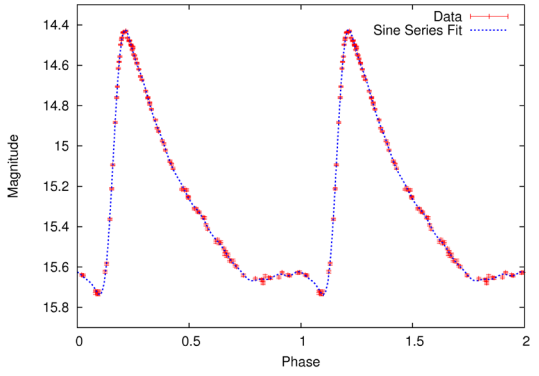

Figure 7: RR 143 Fourier-fit light curve in V.

4. Results

Figures 1 through 6 present results for three RR Lyrae stars. These figures show the light curves of each star for both B and V, including the observational data with error bars and the smoothed spline-fit results. RR 444 and RR 397 are RRc's. RR 143 is a RRab. The parameters derived from our analysis are presented in Table 5. The amplitudes for all three stars are typical for their types. As previously mentioned, only the metallicity derived from the Fourier analysis of the V data for RRab stars has meaning. That measurement yields for RR 143 a [Fe / H] value of –1.49 ± 0.054 derived from the Jurcsik and Kovacs method, and –1.37 ± 0.26 using Sandage's method. Both of these agree well with what might be expected for a halo field

star. For details on this calculation and the estimated errors, see Jurcsik and Kovacs (1996) and Sandage (2004).

The results presented are for three previously unknown variables. It is important to note that these were identified from the SDSS using only a single epoch of photometry and a single epoch of spectroscopy. This again serves as confirmation of our method of identifying RR Lyrae stars with single observations in large surveys.

This served as an excellent project to introduce undergraduate students to observational astronomy in general, and photometry specifically.

5. Future and on-going work

We are continuing to observe a large sample (N > 1,000) of suspected variables. We ultimately plan to continue working to confirm variability for much of the set. We have at this point confirmed variability for several more stars and are working on obtaining complete light curves for these confirmed variables. The area surrounding our RR Lyrae stars that is within the field of view of the images is being searched for additional new variable stars. All of this work is very accessible to undergraduate students and they will continue to be heavily involved in this project. AAVSO members interested in observing a sub-sample of these stars to help with either the confirmation of variability for the candidate stars or with the effort to obtain complete light curves may contact Dr. Powell to request more information on how to help.

6. Acknowledgements

The authors would like to thank McDonald Observatory for generous allocations of observing time to Dr. Powell and his students on the 0.8-m telescope. Dr. Powell would like to thank Nebraska EPSCoR for support of his student, Mrs. Jameson, in her research with a Summer Research at Undergraduate Institutions grant. Dr. Powell would also like to thank two undergraduate students that worked on the early stages of this project: Caleb Bahr and Hans Amende.

IRAF is distributed by the National Optical Astronomy Observatory, which is operated by the Association of Universities for Research in Astronomy (AURA) under cooperative agreement with the National Science Foundation.

This research was made possible through the use of the AAVSO Photometric All-Sky Survey (APASS), funded by the Robert Martin Ayers Sciences Fund.

This paper includes data taken at The McDonald Observatory of the University of Texas at Austin.

This paper was supported in part by NASA through the American Astronomical Society's Small Research Grant Program.

References

Bono, G., Caputo, F., and di Criscienzo, M. 2007, *Astron. Astrophys.*, **476**, 779.

Henden, A. A., *et al.* 2014, AAVSO Photometric All-Sky Survey, data release 8 (http://www.aavso.org/apass).

Jurcsik, J., and Kovacs, G. 1996, *Astron. Astrophys.*, **312**, 111.

King, D. S., and Cox, J. P. 1968, *Publ. Astron. Soc. Pacific*, **80**, 365.

The Mathworks Inc. 2014, MATLAB version 8.3.0.532, Natick, MA (http://www.mathworks.com/).

Mirametrics Inc. 2010, MIRA Pro 7 Ultimate Edition (http://www.mirametrics.com/).

Morgan, S., Wahl, J., and Wieckhorst, R. 2006, *Mem. Soc. Astron. Italiana*, **77**, 178.

Pollock, D. S. G. 1999, *A Handbook of Time-Series Analysis, Signal Processing and Dynamics*, Cambridge Univ. Press, Cambridge.

Powell, W. L., Muehlbrad, T., Wilhelm, R. J., Ginn, D., and Jastram, A. 2010, in *New Horizons in Astronomy: Frank N. Bash Symposium 2009*, eds. L. M. Stanford, J. D. Green, L. Hai, and Y. Mao, Astronomical Society of the Pacific, San Francisco, 235.

Reimann, J. 1994, Ph.D. Thesis, University of California, Berkeley.

Sandage, A. 2004, *Astron. J.*, **128**, 858.

Sesar, B., *et al.* 2007, *Astron. J.*, **134**, 2236.

Stetson, P. B. 1992, *J. Roy. Astron. Soc. Canada*, **86**, 71.

Wilhelm, R. J., *et al.* 2007, arXiv:astro-ph/0712.0776v1.

York, D. G., *et al.* 2000, *Astron. J.*, **120**, 1579.

Investigation of Structure in the Light Curves of a Sample of Newly Discovered Long Period Variable Stars

Eric R. Craine
Western Research Company, Inc. and GNAT, Inc., 3275 W. Ina Road, Suite 217, Tucson, AZ 85741; send email correspondence to ercraine@wrc-inc.com

Roger B. Culver
Department of Physics, Colorado State University, Fort Collins, CO 80523, and GNAT, Inc.

Richard Eykholt
Department of Physics, Colorado State University, Fort Collins, CO 80523

K. M. Flurchick
Department of Physics, North Carolina Agriculture and Technology University, 1601 E. Market Street, Greensboro, NC, 27411, and GNAT, Inc.

Adam L. Kraus
Department of Astronomy, University of Texas, 2515 Speedway, Stop C1400, Austin, TX 78712, and GNAT, Inc.

Roy A. Tucker
Goodricke-Pigott Observatory, 5500 West Nebraska Street, Tucson, Arizona 85757, and GNAT, Inc.

Douglas K. Walker
Department of Physics and Astronomy, University of Canterbury, New Zealand and GNAT, Inc.

Received February 25, 2015; revised June 30, 2015 and August 24, 2015; accepted September 1, 2015

Abstract Long period variable stars exhibit hump structures, and possibly flares, in their light curves. While the existence of humps is not controversial, the presence of flaring activity is less clear. Mining of a sky survey database of new variable star discoveries (the first MOTESS-GNAT Variable Star Catalog (MG1-VSC)) has led to identification of 47 such stars for which there are sufficient data to explore the presence of anomalous light curve features. We find a number of hump structures, and see one possible flare, suggesting that they are rare events. We present light curves and measured parameters for these stars, and a population statistical analysis.

1. Introduction

Long Period Variable stars (LPVs) have been reported to show anomalous structure in their light curves, in the form of "humps" or shorter duration flares. The nature of these features, and even the reality of the flares, has been a subject of discussion (see, for example, Mais *et al.* 2006). A statistical evaluation of these features is undertaken.

1.1. Long Period Variable stars

Red giant stars that show fairly regular cyclical light curves with periods in the range of 80 to 1,000 days are known as long period variables. Light curve amplitudes are typically > 2.5-magnitude in V, with a smaller change in unfiltered or near infrared bands. Periods can vary between cycles by as much as 10 to 15%. Light curve amplitudes can likewise vary from cycle to cycle. Spectral types are M, S, or C, often exhibiting emission lines resulting from pulsation-driven shock waves interacting with the extended atmospheres.

Several types of light curve activity in LPVs have been recognized and broadly characterized as humps, flares, or micro-variability.

Humps are described (see, for example, Lockwood and Wing 1971), as anomalous increases in brightness of duration typically several tens of days with amplitudes on order 0.1 magnitude or greater at I (1.04), and are fairly common. They are reported by Lockwood and Wing to occur only on the ascending leg of the light curve. The Lockwood and Wing data are sparse and the light curves were sketched by hand, however the existence of the features is convincing. Analysis of Hipparcos data by Melikian (1999) suggest that about 37% of Mira stars in their sample show post-minima humps.

Flares are characterized as short-duration (hours to a day or two) increases in brightness of a few hundredths to many tenths of a magnitude. Schaefer (1991) made a list of 14 candidates, some of which were single observations, and all of which were recognized to be potentially dubious. At best such flares appear to be very rare. Among the most intriguing of the flare mechanisms is one described by Willson and Struck (2001) in which the flare is presumed to be a consequence of interaction between the material outflows of the star and a planet that is being engulfed by the host star.

Micro-variability is discussed in several papers (see, for example, de Laverny *et al.* 1998), and is taken to be short term

(on order 0.1 to 1 day) variation, both positive and negative variations, in excess of Hp ~ .25–1.2 magnitude, predominantly near light curve minimum. The data of de Laverny *et al.* were taken from Hipparcos observations, and in some cases "features" were represented by a single observation. Subsequent studies (Wozniak *et al.* 2004), using the OGLE-II light curves, with less sparse data and photometric accuracy much better than 0.2 magnitude, were unable to confirm the Hipparcos results.

1.2. MG1-VSC

The Global Network of Astronomical Telescopes (GNAT) in collaboration with the Moving Object and Transient Event Search System (MOTESS), is creating new catalogs of variable stars along and within about +12° of the celestial equator. The MOTESS system consists of an array of three conventional Newtonian reflectors with 35-centimeter aperture, f/5 primaries. Imaging is accomplished with thermoelectrically-cooled CCD cameras that are operated in continuous time-delay integration mode. In normal MOTESS operation, the three telescopes are aimed at the same declination but spread in Right Ascension at intervals of 15 to 60 minutes to produce a data stream of image triplets separated in time that reveal moving and time-varying objects; see Tucker (2007).

The time-delay integration (scan mode) imaging allows the telescopes to remain fixed in altitude and azimuth, while the rotation of the Earth continuously scans the established declination band. The telescopes operate each clear night (excepting very bright moon time) from twilight to twilight, yielding an observing cadence of three images per clear night per observing season for each field. The net result is an observing season of four months on and eight months off, with three seasons of data for a 2.5 year survey.

GNAT has also implemented a comprehensive data pipeline for extracting photometric measurements for all of the stars observed in each of the discrete declination bands observed with the scan-mode system. For the first declination band (designated the MG1 Survey), 48 arcminutes wide and centered at $+03^{d}$ 18^{m}, this has resulted in 2.5-year photometric light curves for 2.07 million stars with $-3 < R–B < 5$ and R brighter than 19 magnitude. From these observations a new catalog of variable stars (the *MG1 Variable Star Catalog* (MG1-VSC)) was created. Variable stars numbering 26,042, of which 5,271 are periodic at the 99% confidence level, were found (Kraus *et al.* 2007). Only 59 of these stars were previously known to be variable and appeared as entries in the *General Catalogue of Variable Stars* (GCVS; Kholopov *et al.* 1985).

The MG1 survey is compared with several other photometric sky surveys as shown in Figure 1. The figure shows the survey surface area as a function of limiting magnitude. The surveys are identified for each locus along with a number in parentheses representing the typical number of observations of each field in the survey.

Small, low-cost telescopes can be dedicated to high frequency observations of small areas of sky, such as the Trans-Atlantic Exoplanet Survey (TReS) (Alonso *et al.* 2004), or they can make small numbers of observations of large areas of sky, such as the All-Sky Automated Survey (ASAS) (Pojmański *et al.* 2005). In either case, these surveys have modest magnitude limits because of the small telescope size. Larger aperture telescope surveys can reach much fainter limiting magnitudes, but usually at the expense of less frequent observation or coverage of much smaller areas of the sky, as, for example, the Sloan Digital Sky Survey (SDSS) (York *et al.* 2000) and the Optical Gravitational Lensing Experiment II (OGLE2) (Udalski *et al.* 1997).

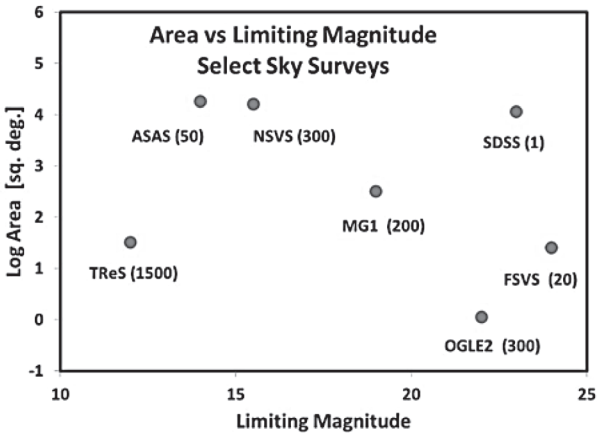

Figure 1. Comparison of coverage area and limiting magnitude for a selection of digital sky surveys including: Sloan Digital Sky Survey (York *et al.* 2000), ASAS (Pojmański *et al.* 2005), Faint Sky Variability Survey (Groot *et al.* 2003), Northern Sky Variability Survey (Wozniak *et al.* 2004), Optical Gravitational Lensing Experiment II (Udalski *et al.* 1997), TReS (Alonso *et al.* 2004), and the MOTESS-GNAT 1 Survey (Kraus *et al.* 2007). The numbers in parentheses are the typical number of times each survey visits a given field.

Examination of the parameter space of Figure 1 indicates that the MG1 survey, better than the other surveys represented, occupies a unique intermediate position in terms of area, limiting magnitude, and observing cadence that is advantageous for stellar variability studies in the field. Other surveys in Figure 1 are more constrained either by limiting magnitude (TReS, ASAS, and NSVS), spatial area (TReS, FSVS, and OGLE2), or by cadence (SDSS).

2. Observational data

The observational data available in the MG1-VSC include a basic data and statistics summary, a file of reduced photometric observations, a light curve plot, and a trial phased light curve. The summary file includes the following: R. A., Dec., light curve amplitude, mean brightness, standard deviation about the mean, photometric error, skew of the observed data points, number of observations, log P (period), and log PFA (period false alarm probability). The brightness measures derived from the MG1 data are an MG1 R magnitude (RMG), as defined in Kraus *et al.* (2007). This magnitude is obtained thorough open channel images yielding the silicon spectral response of the camera. For the long period variable stars discussed in this paper, the photometric errors for each observation typically range from 0.01 to 0.05 mag. Note that for the MG1-VSC compilation, only the A and C MOTESS telescope images were reduced. The B telescope images are also available in the archive. In the event that a potential flare, or other interesting anomalous event, is observed, the B telescope image can also be measured for added clarification.

The period, P, is specified in days and is determined using the Lomb-Scargle method (Lomb 1976; Scargle 1982) as described in Press *et al.* (1992). Because of the telescope spacing, and the interval between nightly observations, short period systems are subject to aliasing. Fortunately, this problem does not impact the LPVs of current interest. The scan mode observations yield an observing season of approximately 4 months' duration, separated by 8-month intervals. A periodogram analysis on a season-by-season basis is then performed. The result is that there can be aliasing for periods of approximately one year as a result of this seasonal cadence. This can lead to confusion in the periods of some LPVs of interest. It is important to recognize that that values of P, and the associated false alarm probability, serve primarily as guides and must be used with extreme caution. For this reason, a new, comprehensive periodogram analysis is computed for all MG1-VSC stars for which we engage in follow-up observation and analysis.

In addition to the MG1-VSC data, United States Naval Observatory (USNO) B magnitude (Monet *et al.* 2003), and J, H, and K magnitudes have been extracted where possible for each of the MG1-VSC stars. The J, H, and K data were taken from 2MASS observations (Skrutskie *et al.* 2006).

3. Data reduction methods

A series of data reduction steps, consisting of manual and automated techniques, were applied to the data set to search for potential flare events, as well as hump-type structures. Steps include visual search for LPV candidates, period determination, and detailed inspection of the resulting suspected flare events.

3.1. LPV identification

The MG1-VSC catalog was initially culled for stars with P > 80 d. This list was then sorted by amplitude and truncated. Rather than truncating the list at 2.5 mag, only very low amplitude variables were deleted. The rationale for this procedure is two-fold: 1) since the MG1 images were unfiltered, the smallest LPV amplitudes are smaller than the 2.5 mag cutoff in V, and 2) to compare this list visually with the corresponding light curves. Visual examination of the remaining light curves was rendered fairly straightforward, since the LPV candidates have very distinctive light curves. The LPV identification process yielded a final list of 47 LPV candidates, for which raw and phased light curves appear in Appendix A.

3.2. Period determination

The MG1-VSC photometric data files for each of the candidate LPVs were then analysed using the ANOVA protocol of the PERANSO period analysis software package (Vanamuster 2014). Systems with periods close to one year (or multiples of one year) were subject to aliasing effects as described above. In these cases, graphical representations of possible phased light curves were constructed, using MATHEMATICA (Wolfram Research, Inc. 2015), to attempt a fit of those peaks in the graphs to computed peak frequencies produced by PERANSO. In most instances a satisfactory period could be distinguished.

In a small number of cases true periodicity is not observable, in the sense that fewer than two complete cycles were observed. This is noted in the data where it occurs. In each instance, the light curve is so distinctively similar to the other LPVs that these stars are also classified as LPVs.

The epoch of maximum brightness for each light curve was obtained either by a direct observation of the maximum brightness epoch or by an estimation of such an epoch. In those cases where the actual maximum epoch could not be directly observed, the epoch Julian date was estimated either by assuming it was located a half period away from the Julian date of an observed minimum light position for a given star or by an interpolation of the star's ascending and descending light curve data.

3.3. Light curve reduction

Selected segments of the datasets, where suspected flaring events were identified, were analyzed as follows:

- A visual inspection was performed on the individual light curves identifying possible flare events.

- The subset of data points surrounding the area of interest was isolated into a separate file.

- A least-square fit to the data points was obtained in order to form a reference line with respect to which distances to individual data points were measured.

- The local slope of the light curve data was "de-trended." This process was performed by generating a perpendicular segment from each data point to the reference line, which yielded the distance of each point off the reference line. The reference line was then redrawn with a slope of zero, with the data points at the appropriate distance from the de-trended line.

- The arithmetic mean of all points in the segment was generated along with standard deviations off the mean. Significant events were indicated by data points lying outside of +2 standard deviations from the mean.

To gain some insights into the limits on the resolution obtainable from the MG1 light curves for possible flares or humps, a series of artificial events was introduced into the light curve data. The flares were set up to have total maximum outbursts of 0.2, 0.1, 0.02, and 0.05 magnitude, with each flare occurring over a total of three days. The flare data were introduced into several light curve regions for which a relatively continuous data stream was available. These segments were tested at all phases of the light curves. The data for each region were de-trended into a horizontal data set, and these de-trended data points were then averaged and the 2-sigma error lines were drawn. From the results of this exercise, it appeared that light curve events having amplitudes of about 0.1 magnitude or larger fall within the limits of detectability, while those with amplitudes equal to or smaller than 0.05 magnitude are not detectable in these light curve data.

When a potential feature is identified, it was characterized as follows. The duration total of each hump feature, in Julian days, was calculated from the value of $t_e - t_b$, where t_e is the

Julian date of the end of a given hump's appearance and t_b is the Julian date of the beginning of the hump's appearance. The Julian date, t_c , of the center of the hump feature was then calculated from $t_c = t_b + 0.5\ t_{total}$. The phase of the center of the event was calculated with respect to the epoch of maximum determined for each light curve.

Because LPVs are well known to have basic periodic light curves for which amplitudes and periods themselves can change by several percent from cycle to cycle, it was important that the above discussed analysis be performed on the raw light curves and not the phased curves. Visual perusal of phased light curves can often "reveal" hump-like features that are not intrinsic humps in the sense used here, but rather artifacts of cycle-to-cycle variations in basic light curve parameters. Hump features reported here are isolated by consistent, objective, statistical considerations applied only to the raw light curves. As such, this method consistently allows detection of more subtle features than visual examination alone, and may lead to higher rates of detection than has otherwise been the case, in part because of increased sensitivity of the approach.

4. Results

Table 1 provides the basic data for the 47 LPV stars under study from the MG1-VSC. The table columns comprise the MG1-serial number (LPV star name), epoch 2000.0 Right Ascension and Declination, the number of observations in the MG1-VSC, the MG1-VSC red magnitude, the period in days, and the Julian date of the epoch of maximum.

Some of the LPV stars in Table 1 were also observed in the 2MASS survey, and J, H, K photometry was obtained. The resulting data are tabulated in Table 2.

Seven clear hump features were identified from the light curve analysis discussed in section 3.3. There are some other light curve segments that are suggestive of the presence of humps, but the data were sufficiently sparse that we have elected not to pursue those features as definitively real. The seven humps identified are shown in Appendix B. These are the de-trended light curve segments, so the magnitude scale for each should be interpreted as a differential magnitude relative to an arbitrary underlying "continuum" mean. Each light curve segment is fit with a high order polynomial to help define the shape of the hump. In two or three cases the hump appears open-ended because it occurred before or after a lapse in observations. The parameters of these features are summarized in Table 3, which lists the star name, the approximate epoch of the hump, the duration of the feature in days, the phase and phase quadrant of the hump event, and the mean magnitude of the event.

A single potential flare event was observed in MG1-1440964 on 5 July 2003, as shown in Figure 2. These data are re-measurements of the MG1 survey images, using all three telescopes. In this case, five sequential nights were measured; the flare event occurred on one night only. Regrettably, this event occurred on the final night of the observing run. This was the only candidate flare that was observed in all three telescopes on the same night, a rigorous criterion we implemented for identifying a real candidate flare.

Table 1. Newly discovered MG1-VSC long period variable stars.

MG1-	*R. A. (2000)*			*Dec. (2000)*			N_{obs}	*R_MG1*	*P*	*Epoch Max.*
	h	*m*	*s*	°	′	″			*(days)*	*JD 2450000+*
1098444	18	02	32	03	05	11	225	14.36	250.0	2594
1117392	18	05	23.8	02	56	36	177	13.65	189.0	2667
1155788	18	10	46.5	02	57	10	218	14.41	181.2	2483
1248064	18	23	34.3	03	24	40	168	13.79	271.0	2370
1258871	18	25	14.7	03	40	25	153	13.51	243.5	2758
1270097	18	26	54.7	02	54	38	168	13.70	232.9	2785
1270289	18	26	56.6	03	13	16	149	13.62	152.8	2455
1287551	18	29	35	03	28	14	128	13.53	424.8	2632
1291327	18	30	10.4	03	23	30	129	13.40	238.8	2818
1315064	18	35	21.7	03	38	18	103	13.32	292.9	2665
1326286	18	37	45	03	39	23	208	14.62	297.6	2623
1334111	18	39	19.7	03	03	04	194	14.38	294.9	2629
1334664	18	39	26.7	03	16	42	151	14.23	292.9	2642
1336304	18	39	47.9	03	05	19	204	13.96	348.0	2357
1339600	18	40	33.7	03	25	50	205	15.29	331.7	2553
1341934	18	41	14.6	03	20	06	188	14.21	232.3	2750
1344747	18	42	03.5	03	05	54	207	14.31	190.3	2455
1372707	19	04	25.4	03	25	17	153	15.51	343.6	2573
1375418	19	04	51.9	02	54	16	198	15.12	541.6:	2518
1376419	19	05	01.1	03	10	19	133	15.22	320.0	2604
1379672	19	05	30.1	03	33	20	147	13.49	151.1	2788
1388413	19	06	41.4	03	02	17	109	13.36	234.0	2569
1388633	19	06	43.1	03	17	12	145	13.65	188.2	2790
1391053	19	06	58.5	02	59	14	185	14.11	432.0	2676
1393846	19	07	16	02	57	34	173	13.67	365.5	2817
1406788	19	09	17.3	02	54	52	132	13.49	296.5	2648
1410394	19	09	48	03	34	30	170	13.73	176.7	2794
1410977	19	09	53	02	54	21	169	13.40	344.7	2699
1413873	19	10	16.1	03	01	58	199	14.76	347.5	2348
1414532	19	10	21.2	02	58	05	151	13.39	306.5	2794
1428501	19	12	07.2	03	03	11	118	13.55	215.7	2497
1440964	19	13	59.4	03	07	44	165	13.70	427.1	2697
1444065	19	14	26.9	03	11	18	125	13.89	258.7	2434
1448319	19	15	03.2	02	55	05	186	13.64	210.8	2797
1457857	19	16	17.3	03	37	02	149	13.07	271.3	2463
1466778	19	17	31.5	03	23	08	127	13.65	298.2	2642
1468465	19	17	45.7	02	55	39	166	14.80	167.3	2579
1477416	19	19	00.1	03	30	46	121	13.37	137.8	2427
1478012	19	19	05.2	03	24	33	185	16.44	353.2	2760
1492532	19	21	09.3	03	32	06	183	14.14	204.2	2775
1496600	19	21	50.1	03	31	04	78	13.32	272.8	2439
1518640	19	24	49.1	03	37	21	81	13.06	226.0	2640
1523972	19	25	30.5	03	18	32	159	13.86	265.3	2636
1540903	19	27	36.9	03	23	11	137	13.69	266.6	2430
1545107	19	28	08.1	03	00	26	189	14.65	520.8	2460
1653368	19	42	25.2	03	32	01	137	13.60	228.0	2430
1877036	20	28	46.8	02	59	06	169	14.15	171.2	2520

Table 2. 2MASS infrared photometry.

MG1-	*J*	*J–H*	*H–K*	*MG1-*	*J*	*J–H*	*H–K*
1248064	14.287	0.454	0.292	1440964	9.563	1.247	0.834
1258871	9.644	0.931	0.646	1444065	8.827	1.079	0.634
1270289	8.851	0.931	0.552	1457857	12.486	0.463	0.104
1287551	7.082	1.313	1.06	1466778	9.461	1.166	0.789
1291327	9.623	0.964	0.562	1477416	10.686	0.888	0.686
1315064	9.369	1.094	0.724	1492532	13.647	0.755	0.228
1326286	9.071	1.209	0.624	1496600	9.176	1.004	0.674
1334664	13.938	1.037	0.324	1518640	7.997	0.974	0.568
1339600	14.9	0.82	0.454	1523972	10.011	0.881	0.552
1341934	9.679	1.246	0.626	1540903	9.791	0.894	0.538
1372707	9.888	1.524	0.925	1545107	9.826	1.643	1.277
1379672	9.619	1.13	0.504	1653368	10.126	0.885	0.576
1388633	10.165	1.062	0.562	1877036	11.449	0.842	0.409
1410394	9.569	1.092	0.612				

Table 3. LPV hump statistics.

MG1-	*Approximate Hump Center JD 2450000+*	*Approximate Duration (days)*	*Phase (del t)/P*	*Phase Segment**	*Amplitude (magnitude)*
1098444	2458	15	0.46	3	0.1
1258871	2785	46	0.11	1	0.2
1291327	2460	>20	0.50	3	0.1
1334111	2455	20	0.41	3	0.1
1339600	2775	86	0.67	4	0.4
1341934	2438	45	0.66	4	0.1
1414532	2390	>40	0.68	4	0.1

**Phase quadrants: 1, maximum; 2, descending; 3, minimum; and 4, ascending.*

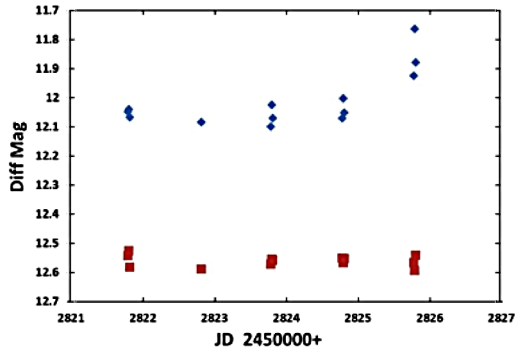

Figure 2. A possible flare event in MG1-1440964 (diamonds); compared with a field check star (squares). The differential magnitudes have been arbitrarily scaled to magnitude 12.0 for the check star. The flare event lies entirely outside the 2-sigma limits around the mean magnitude of the star.

5. Discussion

In this section, the probability for observing a flare in a set of observations is derived. For long period variable stars, the observations can have large observing gaps, so a statistical analysis for the probability of observing a flare is derived. This normalized probability is a function of the average time for a flare to occur, and the observing time.

To begin, define the finite probability, P(Δt), for a flare to occur in a short time, Δt, as:

$$P(\Delta t) = \alpha\, \Delta t \tag{1}$$

where α is the probability per unit time for a flare to occur. In the limit, as Δt goes to zero, Equation 1 becomes exact.

The probability for a flare not occurring in a short time, Δt, is simply:

$$\tilde{P}(\Delta t) = 1 - P(\Delta t) \cong 1 - \alpha\, \Delta t \tag{2}$$

Then, for a long time (that is, a large number of finite time intervals t = N Δt), the probability that a flare does not occur is given by:

$$\tilde{P}(t) \cong [\tilde{P}(\Delta t)]^N \cong (1 - \alpha\, \Delta t)^N \cong (1 - \frac{\alpha t}{N})^N \tag{3}$$

and the exact probability that a flare does not occur during a time t is:

$$\tilde{P}(t) = \lim_{n\to\infty} (1 - \frac{\alpha t}{N})^N = e^{-\alpha t} \tag{4}$$

Now, the exact probability for a flare not to occur until time t, but to occur during the next time interval dt, is the product of the probability of the flare not occurring during the time t and the flare occurring in the infinitesimal time step dt:

$$\mathcal{P}(t) = \tilde{P}(t)\, P(dt) = e^{-\alpha t}\, \alpha dt \tag{5}$$

Therefore, the average time for a flare to occur, T_0, is simply:

$$T_0 = \int_0^\infty \mathcal{P}(t)\, t\, dt = \alpha \int_0^\infty t\, e^{-\alpha t}\, dt = \alpha^{-1} \tag{6}$$

which gives $\alpha = 1/T_0$, and, finally, the exact probability for a flare not to occur during an observing time t is:

$$\tilde{P}(t) = e^{-t/T_0} \tag{7}$$

If the duration of a flare is τ_0, then observing for a time τ will rule out a flare starting during an observation time interval $\tau + \tau_0$. This is the observation gap time. Thus, observation gaps need to be reduced by τ_0, but not become less than zero. The total observation time biased by the occurrence of a flare, can be found as follows:

1. Find the total observing time. Subtract the start time of the first observation from the end time of the final observation (the observing time).

2. Subtract the reduced gap time from Eqn. 1 and add τ_0.

3. Combine these results for all stars, denoted as the total observation time t.

The total observation time, biased by the reduced gap time, gives the probability of not seeing flares in these observations. This can be expressed as in Equation 7. Using this approach, we can hypothesize detectible flare intervals and flare durations for each star in our sample, as shown in Table 4, and calculate the probability that in each case we would not observe at least one flare event in the ensemble.

The one possible flare event observed was at the end of the observing cycle, and so cannot be confirmed as a flare. This leaves us in an ambiguous position with regard to flare events, and supports the conclusion that such features are likely quite rare.

Table 4. Probabilities of observing no flares for the LPV observations.

Flare Interval (years)	*Flare Duration (days)*			
	0.25	0.5	1	2
	Probability			
0.5	0.00174	1.20E-06	3.10E-12	1.20E-15
1	0.0292	0.0011	1.80E-06	3.50E-08
2	0.171	0.0328	0.0013	1.90E-04
3	0.3079	0.1025	0.0121	0.0033
5	0.4934	0.2549	0.0708	0.0323

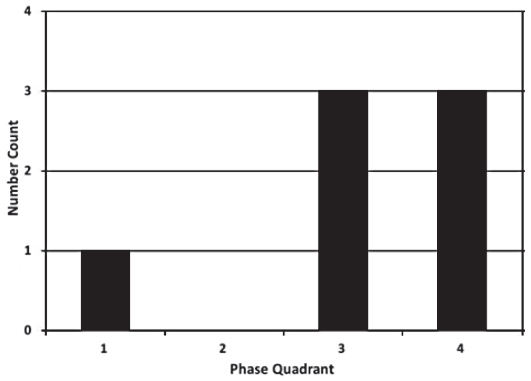

Figure 3. Frequency count of hump features as a function of phase segment; segment 1 is centered at maximum, 2 is the descending leg, 3 is centered at minimum; and 4 is the ascending leg.

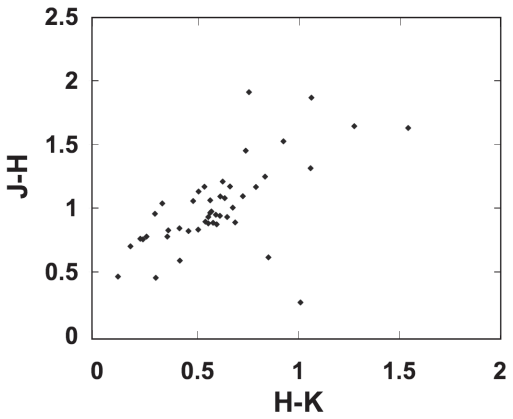

Figure 4. This is the (J–H) vs (H–K) color-color diagram for the LPV candidates that were extracted from the MG1-VSC.

The hump feature distributions as a function of light curve phase can be evaluated, as shown in Figure 3. They predominate at minimum and on the ascending leg, though these are statistics of small numbers.

The (J–H) and (H–K) colors of these stars are plotted in Figure 4. The locus of these observations is consistent with the interpretation that these stars are of spectral types M, S, or C (Cox 2000).

6. Conclusions

The conclusions of this program may be summarized as follows:

• The MG1-VSC catalog is a productive source of LPV discoveries and yields additional data on anomalous light curve features.

• The cadence of MG1-VSC observations allows good definition of hump features and is equivalent to, or superior to, the hump sensitivity in most other reports of such features.

• Unlike visual examination of LPV light curves for hump features used in the literature cited earlier, this paper presents an objective mathematical algorithm for detecting and characterizing the hump features.

• Hump structures are relatively common, and appear to be somewhat preferentially distributed across specific phases of variability. Unlike reports of Lockwood and Wing (1971) and others, we see hump features across a broader range of light curve phase, including not only ascending legs but also during minima and maxima. We saw no hump features on descending legs.

• High temporal resolution allowed reasonably accurate constraints on the range of durations of hump features. In the data reported here hump durations ranged from about 15 to 90 days. This is an average of 0.14P with a standard deviation of 0.04P, where P is the mean variable period in days.

• Based on these stars from the MG1-VSC, short period flares appear to be rare at best, but there is an indication that some may exist in the collective MG surveys. A rigorous statistical analysis is presented to set limits on flare detection using the MG1-VSC data.

Future work includes mining other MG-VSC catalogs, with follow-on observations of some of the current candidate stars.

7. Acknowledgements

This research has made use of the SIMBAD database, operated at CDS, Strasbourg, France. We appreciate a grant from Dr. Janice Nerger, Dean of the College of Natural Sciences, Colorado State University, Fort Collins, Colorado, for computer resources to apply to GNAT research projects.

References

Alonso, R., *et al.* 2004, *Astrophys. J.*, **613**, L153.

Cox, A. N. 2000, *Allen's Astrophysical Quantities*, 4th ed., Springer, New York.

de Laverny, P., Mennessier, M., Mignard, F., and Mattei, J. 1998, *Astron. Astrophys.*, **330**, 169.

Groot, P. J., *et al.* 2003, *Mon. Not. Roy. Astron. Soc.*, **339**, 427.

Kholopov, P. N., *et al.* 1985, *General Catalogue of Variable Stars*, 4th ed., Moscow.

Kraus, A. L., Craine, E. R., Giampapa, M. S., Scharlach, W. W. G., and Tucker, R. A. 2007, *Astron. J.*, **134**, 1488.

Lockwood, G. W., and Wing, R. F. 1971, *Astrophys, J.*, **169**, 63.

Lomb, N. R. 1976, *Astrophys. Space Sci.*, **39**, 447.

Mais, D. E., Richards, D., and Stencel, R. E. 2006, *The Society for Astronomical Sciences 25th Annual Symposium on Telescope Science* (May 23–25, 2006), Society for Astronomical Sciences, Rancho Cucamonga, CA, 31.

Melikian, N. 1999, *Astrophys.*, **42**, 408.

Monet, D., *et al.* 2003, USNO-B V2.0 Catalog, *Astron. J.*, **125**, 984.

Pojmański, G., Pilecki, B., and Szczygiel, D. 2005, *Acta Astron.*, **55**, 275.

Press, W. H., Teukolsky, S. A., Vetterling, W. T., and Flannery, B. P. 1992, *Numerical Recipes in FORTRAN*, Cambridge Univ. Press, Cambridge.

Scargle, J. D. 1982, *Astrophys. J.*, **263**, 835.

Schaefer, B. 1991, *Astrophys. J.*, **366**, L39.
Skrutskie, M. F., *et al.* 2006, The Two Micron All Sky Survey, *Astron. J.*, **131**, 1163.
Tucker, R. A. 2007, *Astron. J.*, **134**, 1483.
Udalski, A., Kubiak, M., and Szymanski, M. 1997, *Acta Astron.*, **47**, 319.
Vanmunster, T. 2014, Light Curve and Period Analysis Software, PERANSO v.2.50 (http://www.peranso.com/).
Willson, L. A., and Struck, C. 2001, *J. Amer. Assoc. Var. Star Obs.*, **30**, 23.
Wolfram Research, Inc. 2015, MATHEMATICA software (http://www.wolfram.com/mathematica/).
Wozniak, P. R., *et al.* 2004, *Astron. J.*, **127**, 2436.
York, D. G., *et al.* 2000, *Astron. J.*, **120**, 1579.

Appendix A. Raw and phased light curves for MG1-VSC LPVs

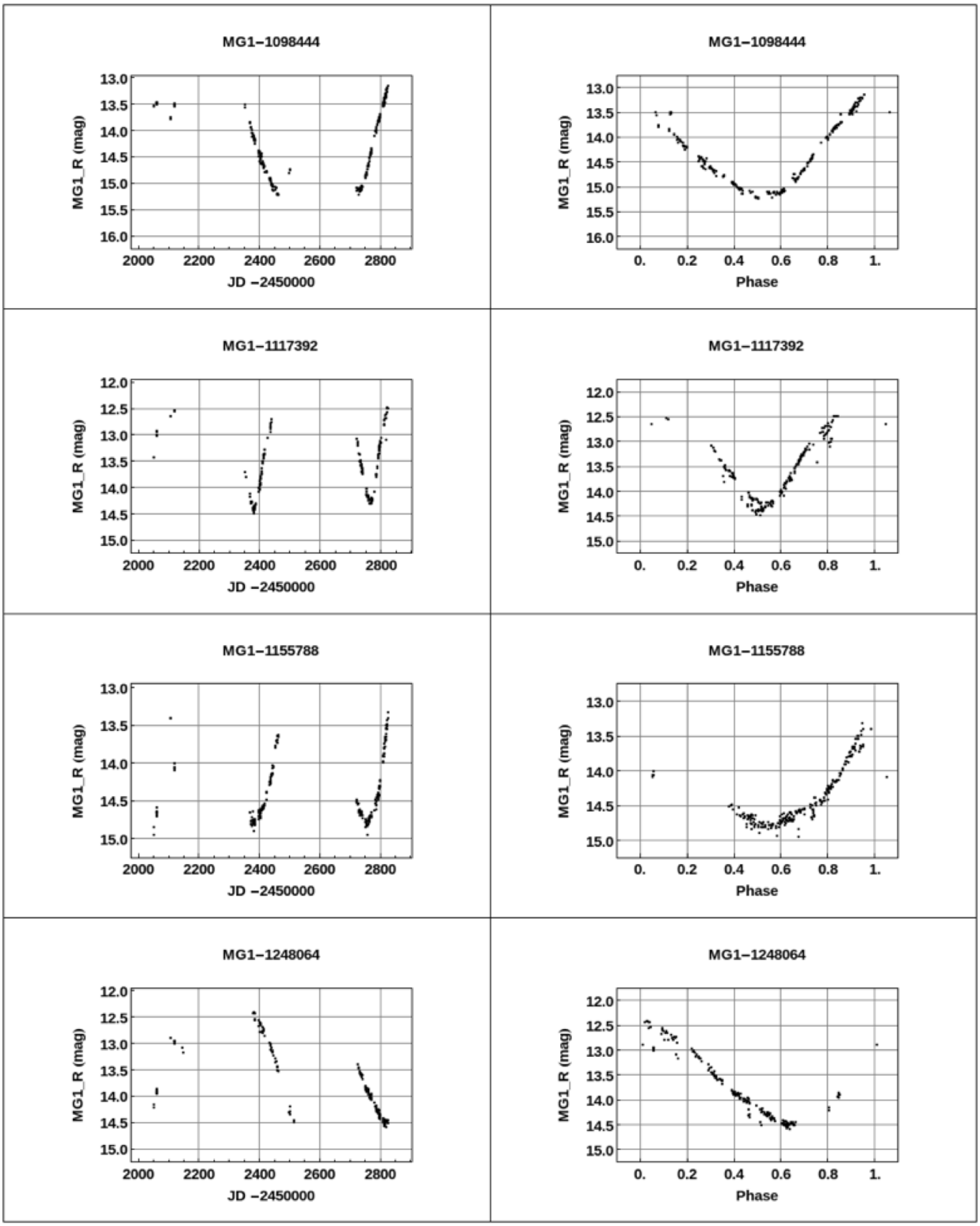

Figure 5. Raw and phased light curves for MGI-VSC LPVs (figure continued on following pages).

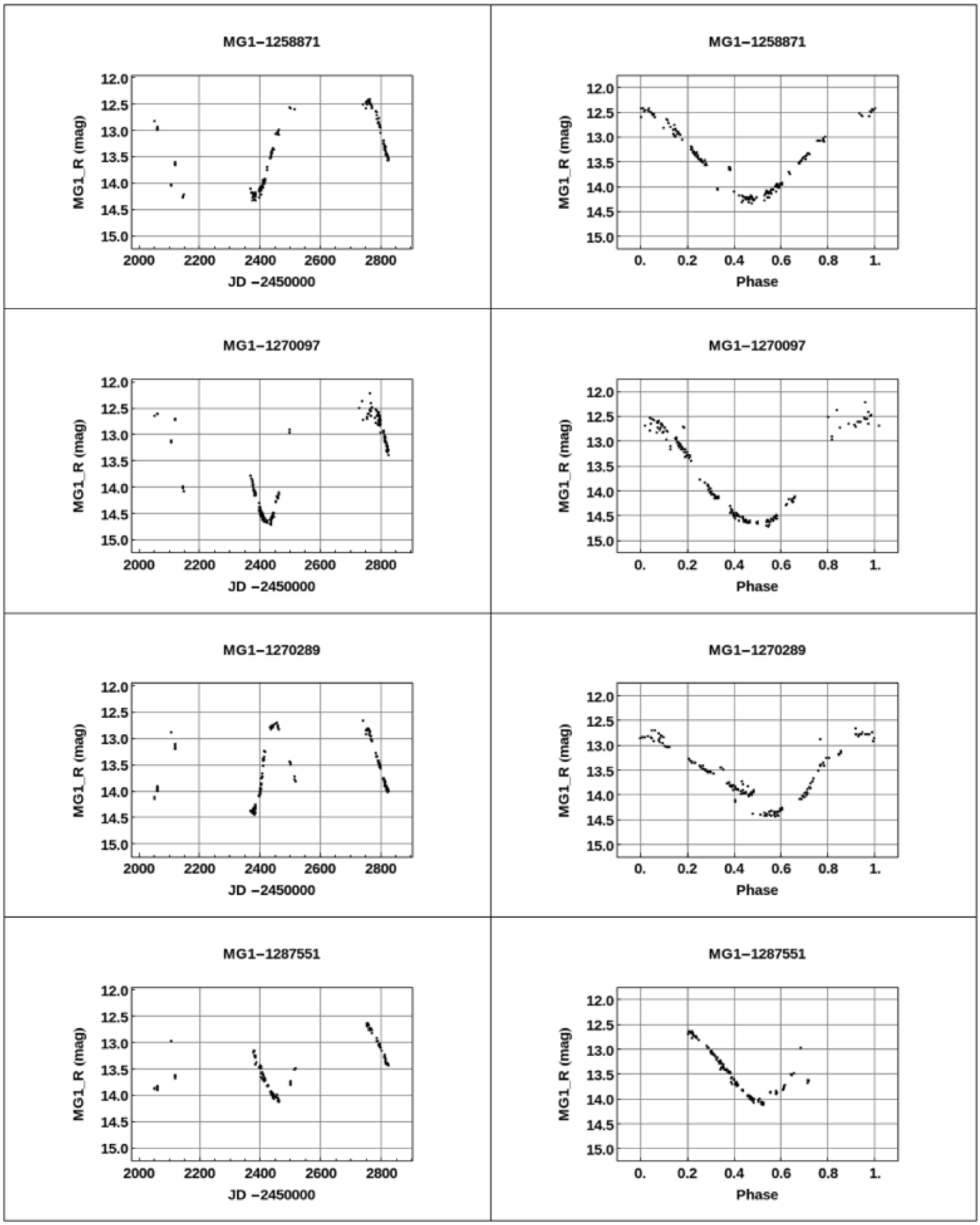

Figure 5. Raw and phased light curves for MGI-VSC LPVs, continued.

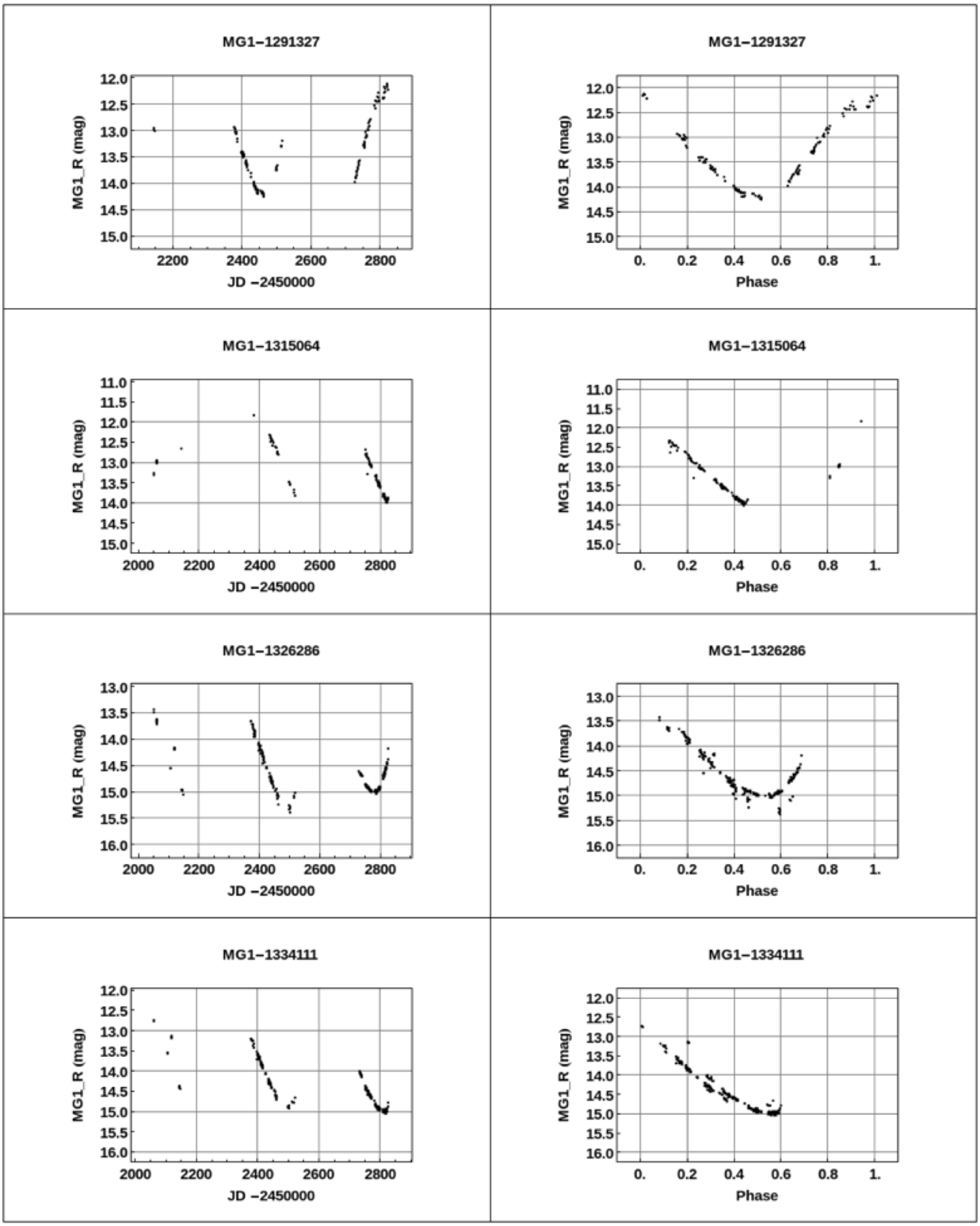

Figure 5. Raw and phased light curves for MGI-VSC LPVs, continued.

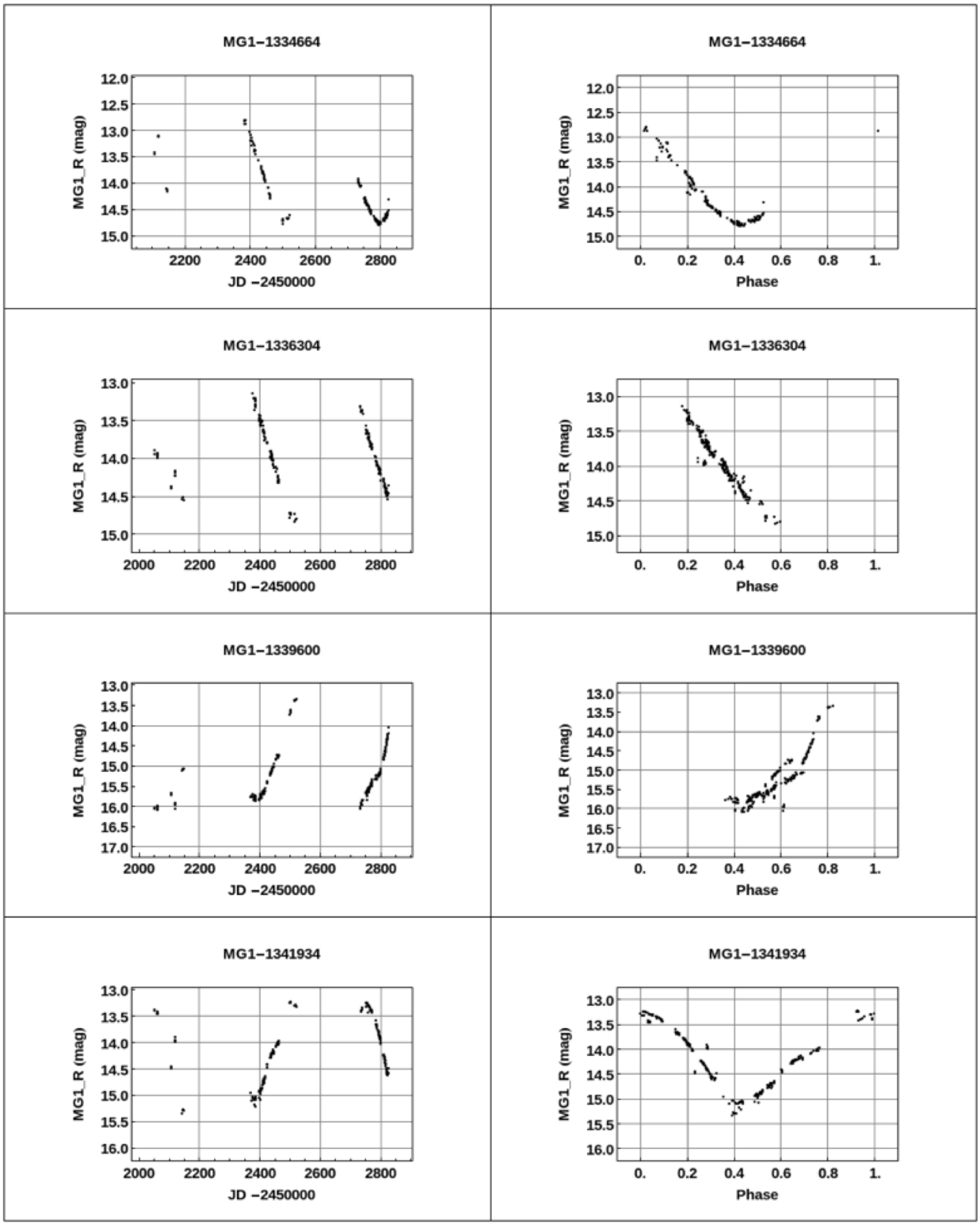

Figure 5. Raw and phased light curves for MGI-VSC LPVs, continued.

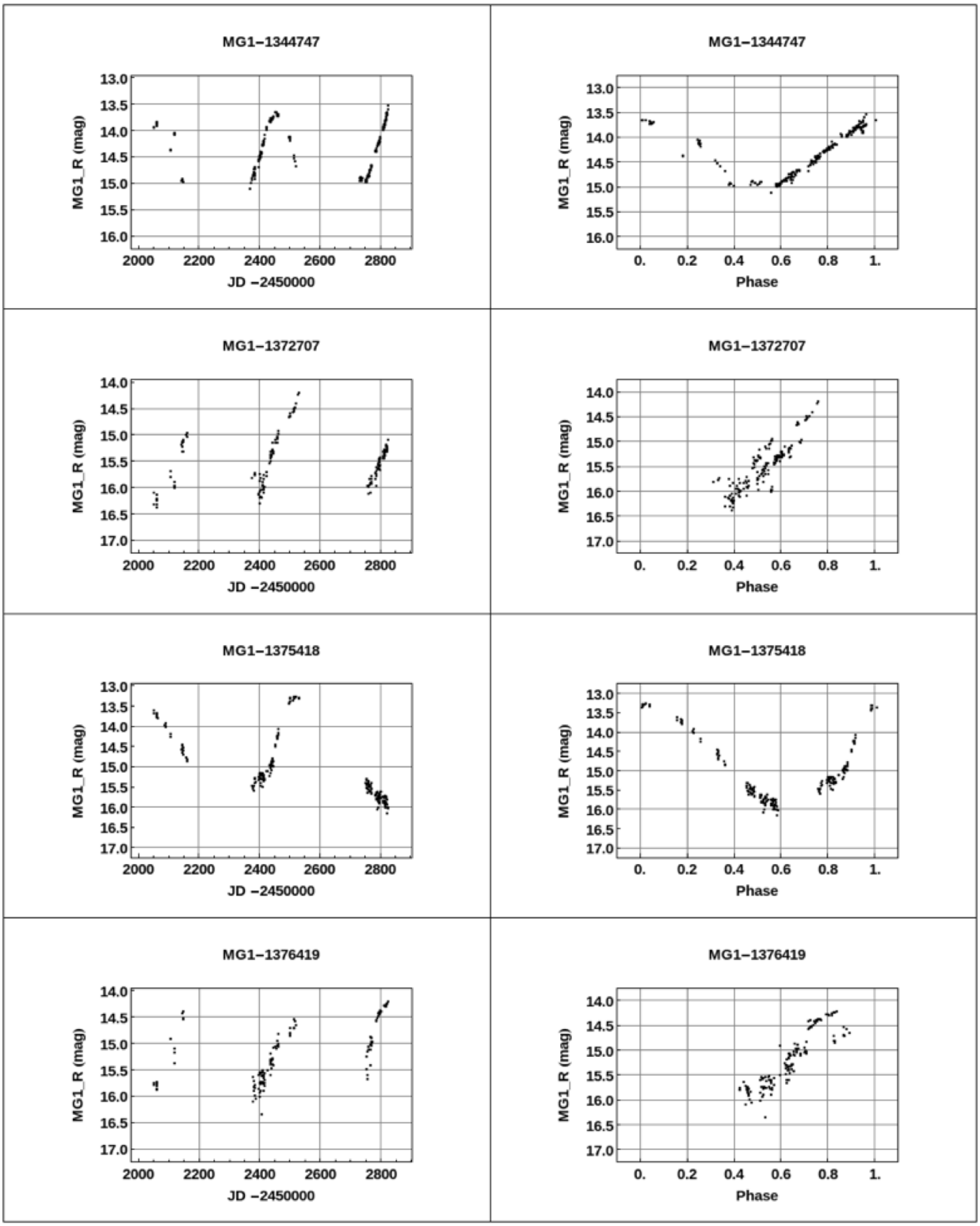

Figure 5. Raw and phased light curves for MGI-VSC LPVs, continued.

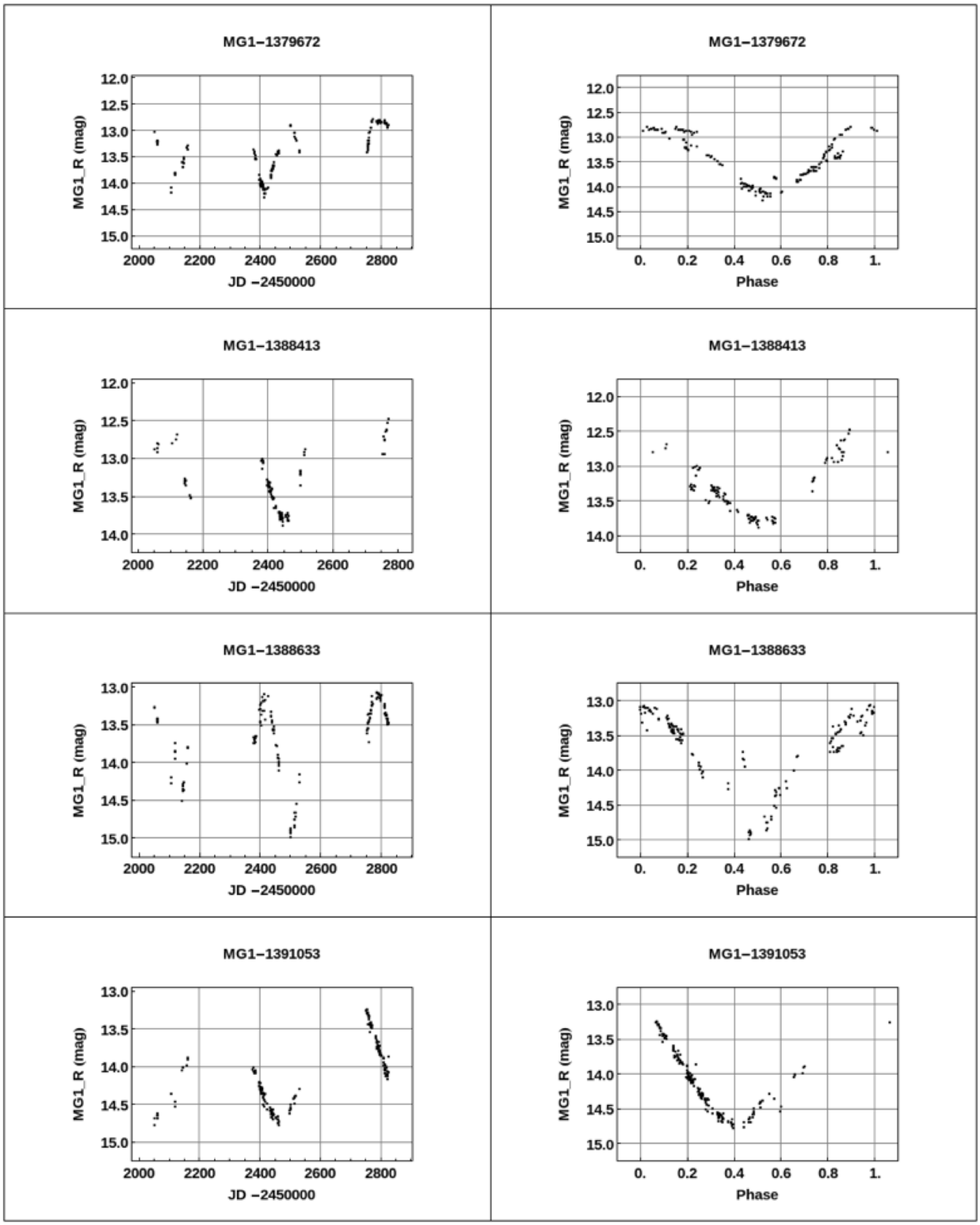

Figure 5. Raw and phased light curves for MGI-VSC LPVs, continued.

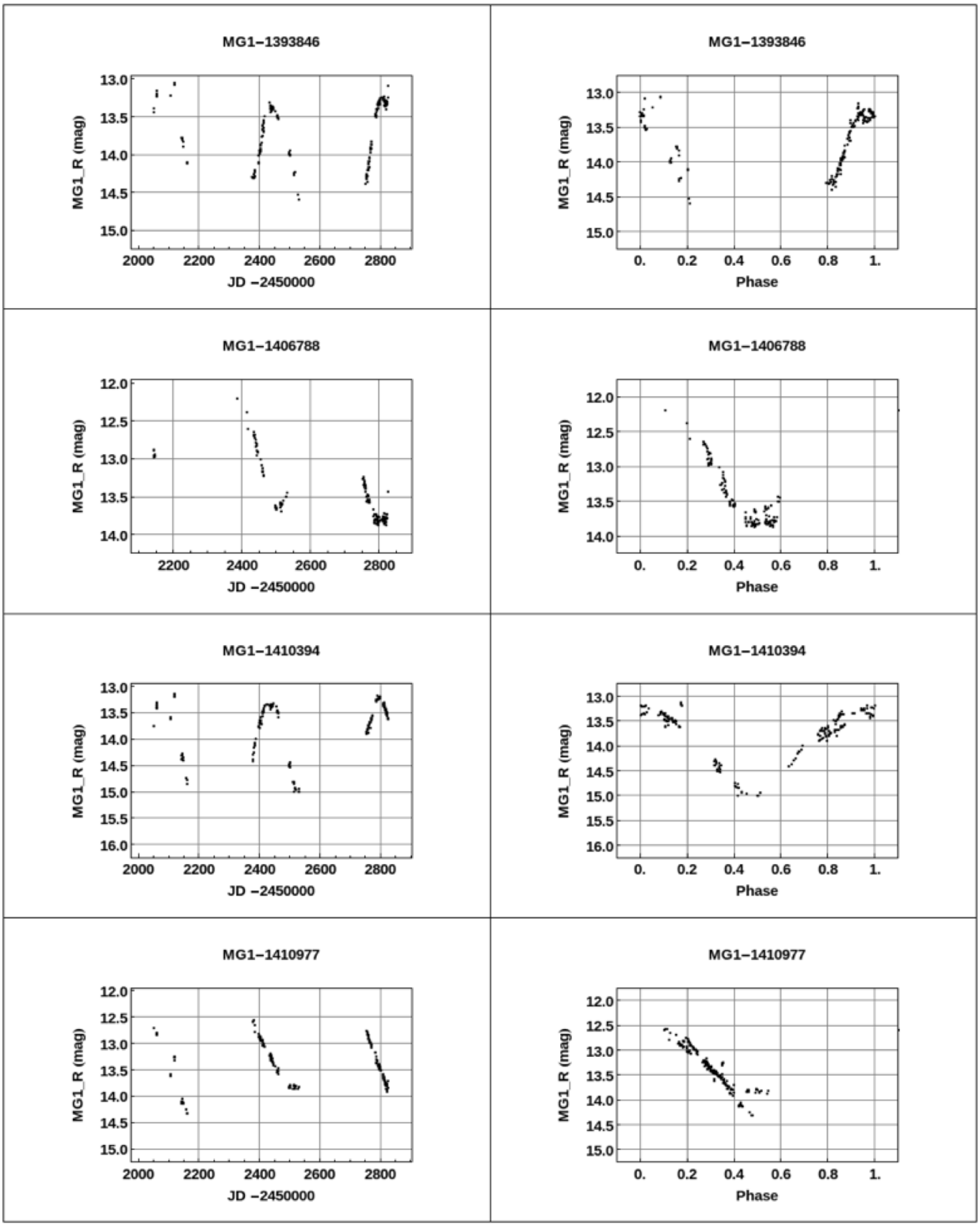

Figure 5. Raw and phased light curves for MGI-VSC LPVs, continued.

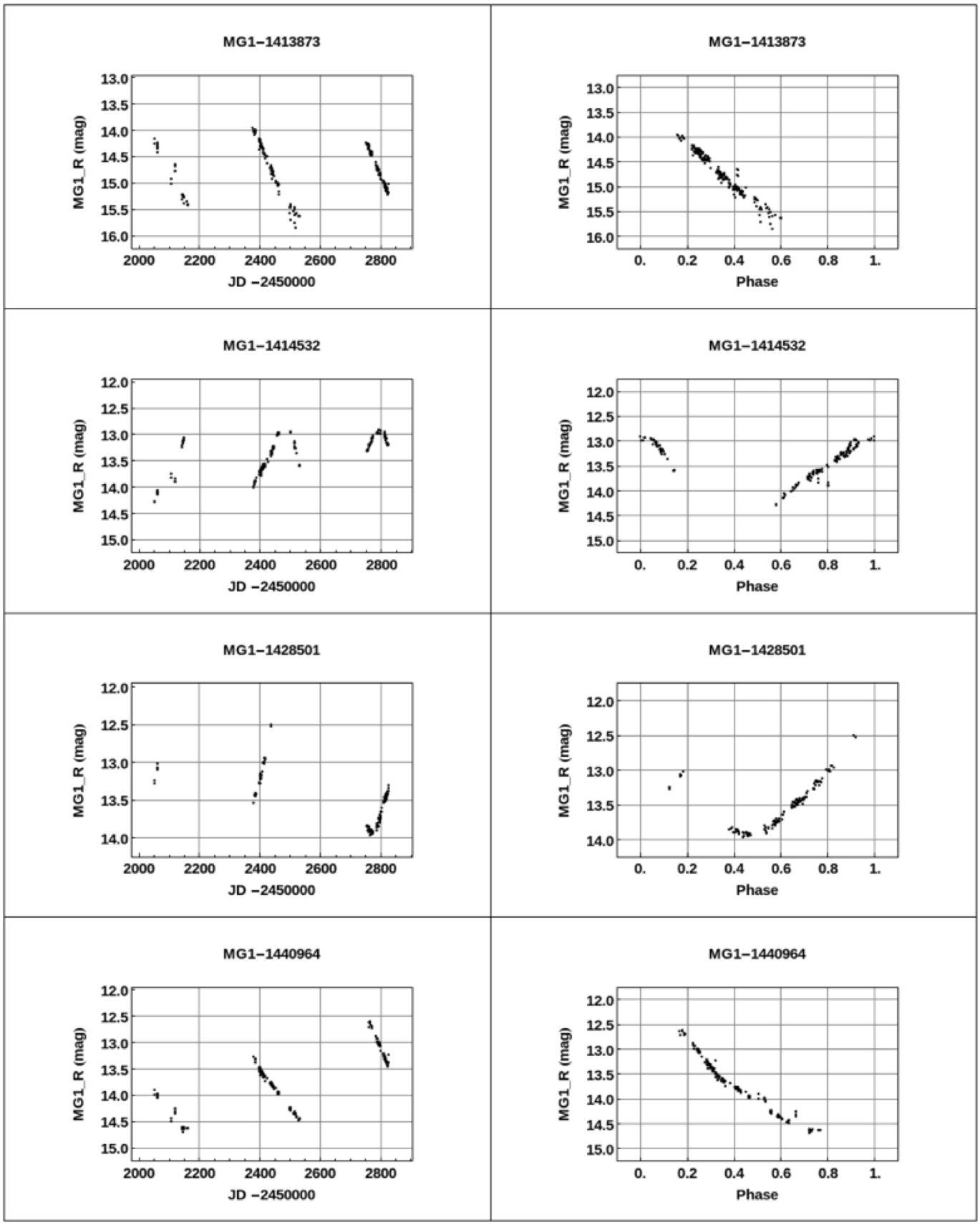

Figure 5. Raw and phased light curves for MGI-VSC LPVs, continued.

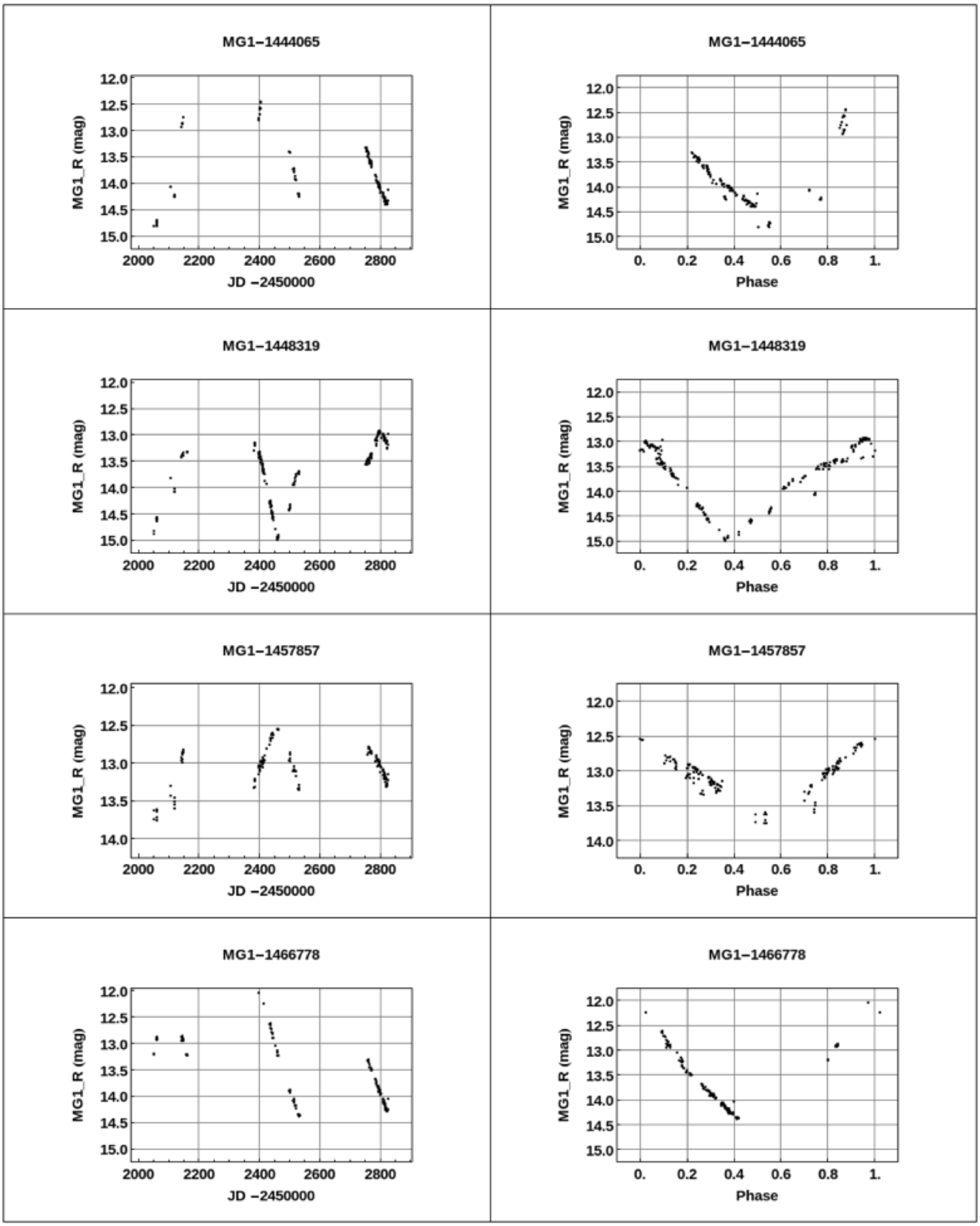

Figure 5. Raw and phased light curves for MGI-VSC LPVs, continued.

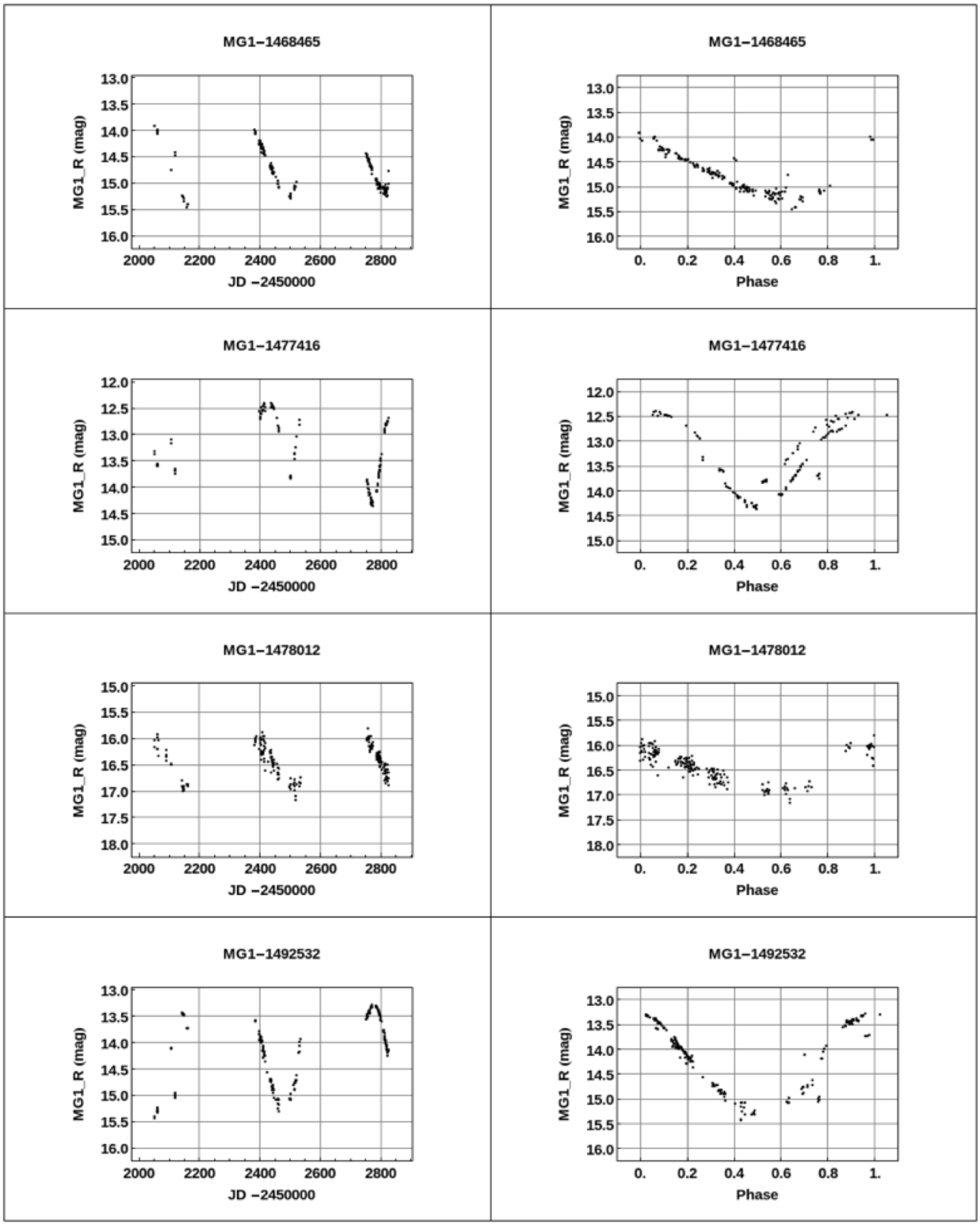

Figure 5. Raw and phased light curves for MGI-VSC LPVs, continued.

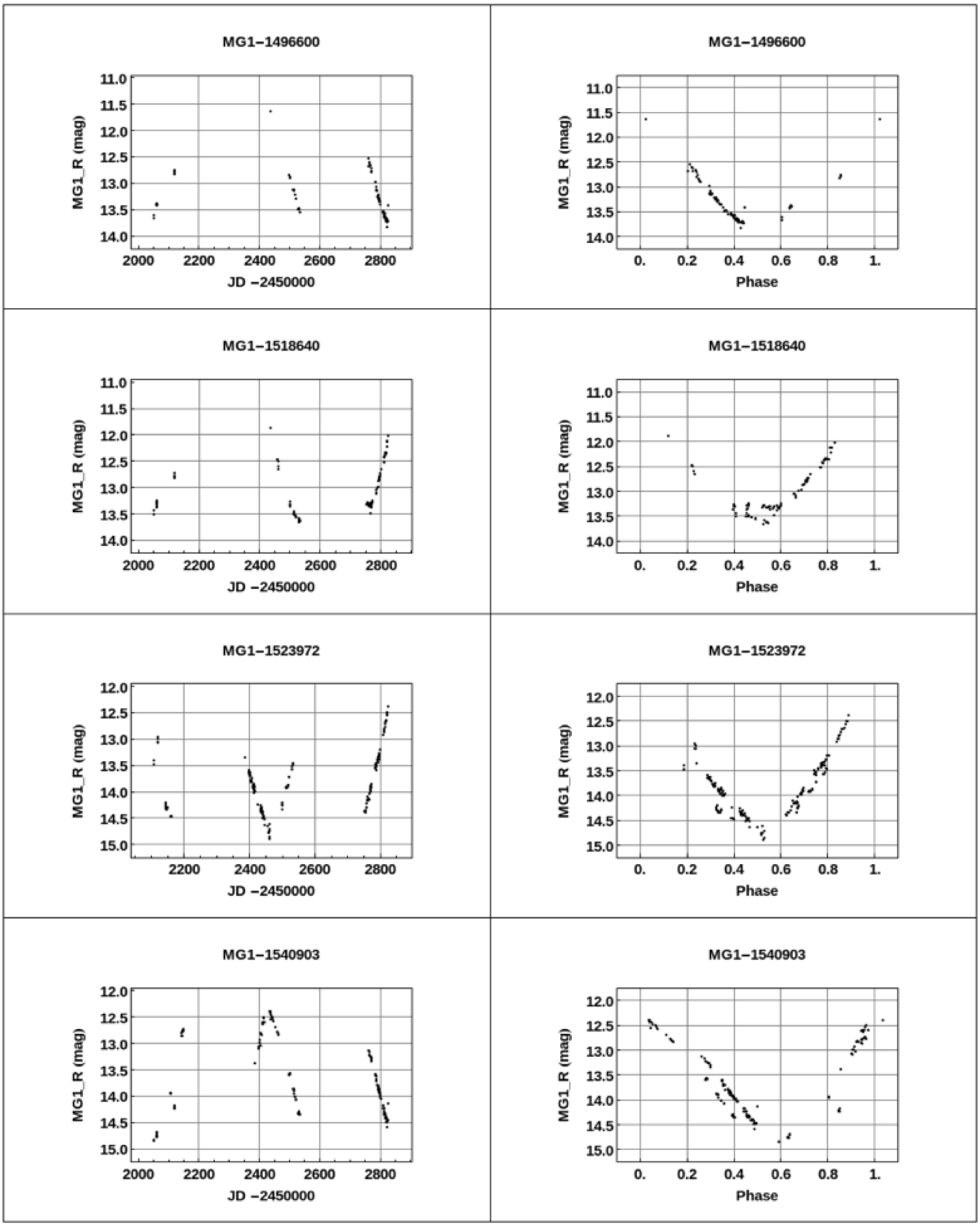

Figure 5. Raw and phased light curves for MGI-VSC LPVs, continued.

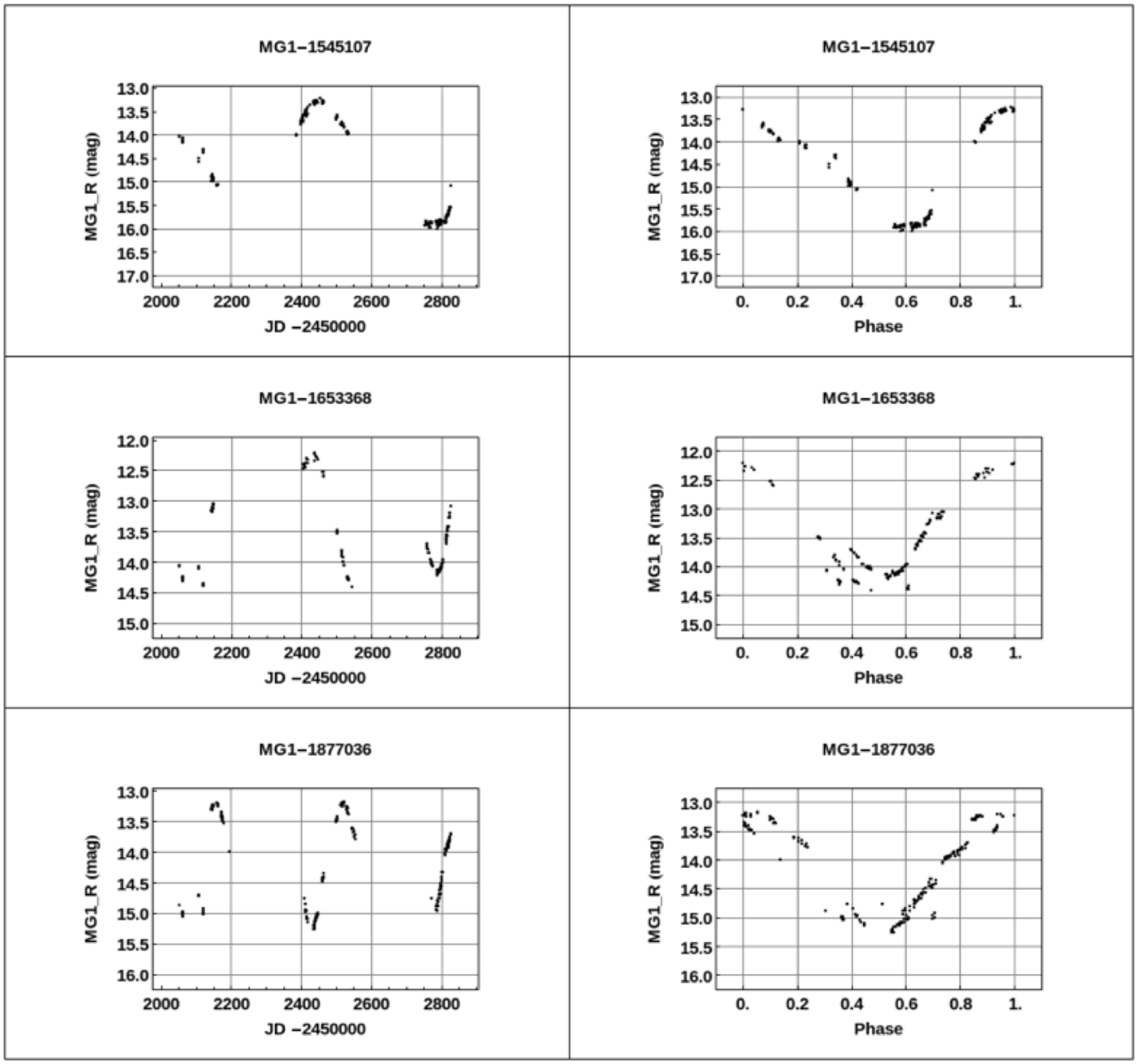

Figure 5. Raw and phased light curves for MGI-VSC LPVs, continued.

Appendix B. Hump features in light curves of MG1-VSC LPVs

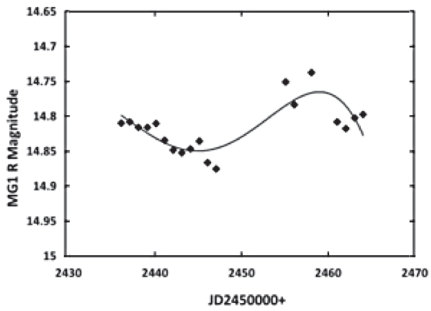

Figure 6a. Hump features in light curve of MG1-1098444.

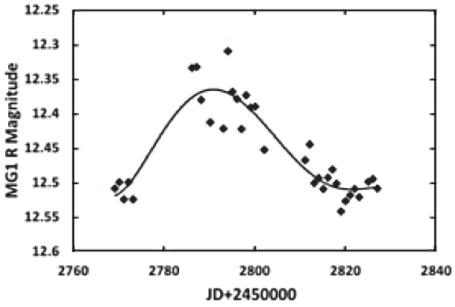

Figure 6b. Hump features in light curve of MG1-1258871.

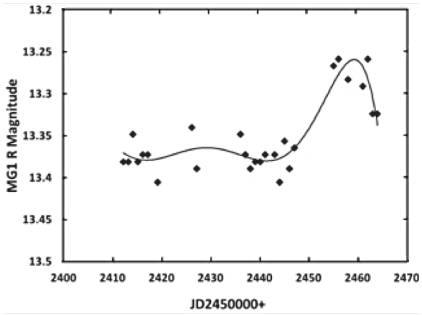

Figure 6c. Hump features in light curve of MG1-1291327.

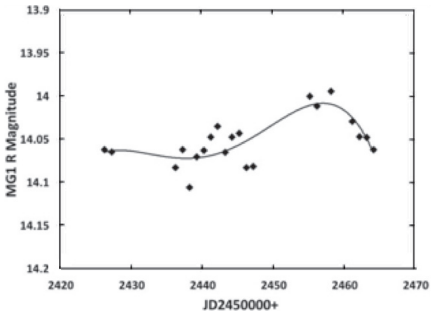

Figure 6d. Hump features in light curve of MG1-1334111.

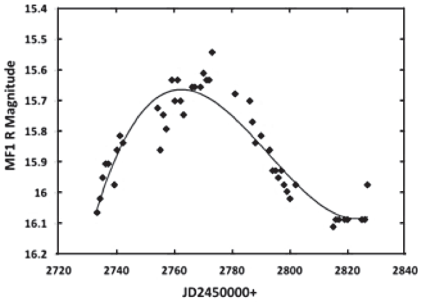

Figure 6e. Hump features in light curve of MG1-1339600.

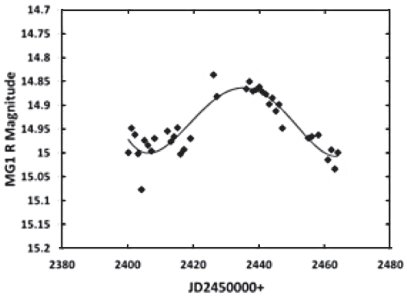

Figure 6f. Hump features in light curve of MG1-1341934.

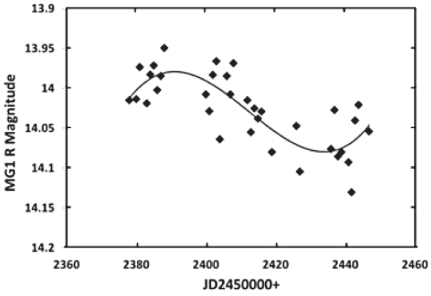

Figure 6g. Hump features in light curve of MG1-1414532.

Period Analysis, Photometry, and Astrophysical Models of the Eclipsing Binary TW Crucis

David J. W. Moriarty
315 Main Road, Wellington Point, Qld. 4160, Australia and School of Mathematics and Physics, The University of Queensland, Qld 4072, Australia; djwmoriarty@bigpond.com

Received July 27, 2015; revised August 20, 2015; accepted September 1, 2015

Abstract TW Crucis is a W-type W UMa contact eclipsing binary that has not been studied in detail since discovery in 1926. During 5 seasons from 2011 to 2015, photometric CCD observations were obtained mostly in the V passband, but also some in B and I passbands. The period was found to be 0.3881444 ± 0.0000006 day, which is not substantially different from the original period of 0.3881358 day. There were slight variations in the period from cycle to cycle and year to year, which are most likely due to asymmetry in the light curves caused by star spots. A preliminary model of the light curves indicates the mass ratio may be about 0.67, inclination 70.8°, and fillout factor 0.11. As no spectra are available, the range in B–V and V–I color indices of 0.8–0.87 and 0.87–0.92, respectively, were used to estimate the effective temperatures for the modelling, based on the spectral types of K0–K2. The spectral type may be earlier, if the color indices are affected by interstellar reddening. Star spots, which changed over short period cycles and were required to obtain good fits of the models to the light curves, indicate the stars are magnetically active.

1. Introduction

The formation and evolution of short period contact binary stars is not well understood. Pribulla and Rucinski (2006) comment that those with periods of less than 1 day should not exist, and suggest they may have formed in triple or larger multiple systems. They applied several methods to examine whether contact eclipsing binary systems brighter than Vmax = 10 might have a third component and commented their statistical analysis was limited by the paucity of data from the southern hemisphere as well as for fainter systems generally. A third component would be apparent from cyclic or sinusoidal variations in the period, which would be detected by comparing observed times of minimum with times calculated from an ephemeris. Small apparent cycle-to-cycle variations in the period of eclipsing binaries have been discussed recently by Mohajerani and Percy (2015), who offered several explanations, including the effect of star spots and the presence of a third star. The W Ursae Majoris contact eclipsing binaries have been divided into two classes: the A type, in which the more massive and brighter component is the hotter star, and the W type, in which the more massive and brighter component is the cooler star (Binnendijk 1970). Thus the primary eclipse in A-type systems is a transit, whereas in W-type systems, the primary eclipse is an occultation of the smaller, hotter star.

TW Crucis is a W-type W UMa-type contact eclipsing binary that was discovered in 1926 by Bruna (1930), who determined a period of 0.3881358 ± 0.000002 day. It has not been studied in detail since then other than as part of the All Sky Automated Survey (ASAS), which has provided data to update the period to 0.388149 day (Pojmański 2002). A similar period of 0.38814626 day was reported by Kreiner (2004). In the work reported here, the aims were to check times of minima to determine whether there were any changes in the period and to develop a preliminary model of the system with photometric data from full light curves in B, V, and I passbands.

2. Methods, observations, and analysis

The instruments used for photometry were a 280-mm Celestron Schmidt-Cassegrain with a SBIG ST8 charge-coupled device (CCD) camera with Johnson B and V and Ic filters, on a German Equatorial mount at Wellington Point, a coastal site. In 2014, a new observatory was established at Glen Aplin, a dark sky site at 750-m altitude, with a 356-mm Celestron Edge HD 1400 aplanatic Schmidt Cassegrain telescope on a Mathis Instruments fork mount and a Moravian G3-6303 CCD camera with Johnson B and V and Bessel I filters. As the initial aim was to determine whether there were period changes, the V filter only was used between 2011 and 2014. For a better understanding of the TW Cru system and to obtain color index values, the B and I filters were also used in 2015. However, as exposure times of 3 minutes were required for the B passband, cadences were lower than optimum for determining accurate times of minimum, and as cloudy weather intervened, the light curves in the B band were not of high quality.

The images were reduced using aperture photometry with MAXIMDL (Diffraction Limited 2012). Magnitudes were calibrated against the standard stars in the LSE 259, WD 1153-484, and MCT 2019-4339 sequences at about –50° declination (Landolt 2007). The instrumental magnitudes in two or three passbands were transformed to the standard system with spreadsheets in MICROSOFT EXCEL (Richards 2013, 2015). The computer clock was synchronized at 15-to-20 minute intervals with an NTP time server using DIMENSION 4 (Thinking Man Software 1992–2014).

The comparison star chosen for this work was GSC 08978-00019 (UCAC4: 136-071292), as it was close to the variable and had a similar magnitude and color indices (Table 1). The check star was TYC 8978 1844-1. The positions are marked on a portion of the AAVSO-VSP chart (Figure 1).

The times of minima and the magnitudes at minimum (phases 0 and 0.5) and maximum light (phases 0.25 and

Table 1. Magnitude and color indices of TW Cru, comparison, and check stars used in this work.

Star	*R. A. (2000)* *h m s*	*Dec. (2000)* *° m s*	*B*	*V*	*Ic*	*B–V*	*V–Ic*
GSC 08978-00019	12 03 00.14	–62 55 41.8	13.351	12.598	11.715	0.753	0.888
error			0.035	0.006	0.073	0.041	0.079
TYC 8978 1844-1	12 02 43.22	–62 52 30.3	12.448	11.98	11.362	0.468	0.618
error			—*	0.006	0.025	—	0.031
TW Cru	12 03 16.15	–62 56 15.6	13.22	12.452	11.538	0.768	0.914
error			0.028	0.006	0.032	0.034	0.038

**Error for B not available. Source: APASS DR7: Henden et al. (2013). The Ic magnitudes were calculated from the Sloan g and i values with the formula* $Ic = i - 0.3645 - 0.0743 \times (g - i) + 0.0037 \times (g - i)^2$ *(Munari et al. 2014).*

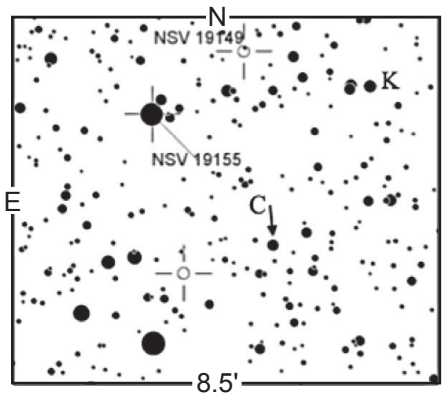

Figure 1. The central portion of the finder chart for TW Cru showing the comparison (C) indicated with the arrow and check (K) stars (https://www.aavso.org/apps/vsp/chart/X15281GC.png).

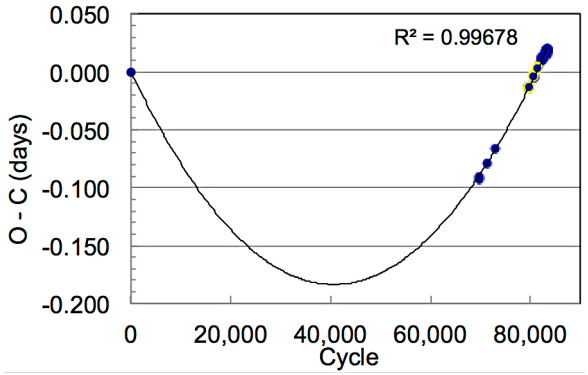

Figure 2. TW Cru (O–C) diagram for the period between 1926 and 2015, based on the original period and epoch. See Table 2 for details of epochs.

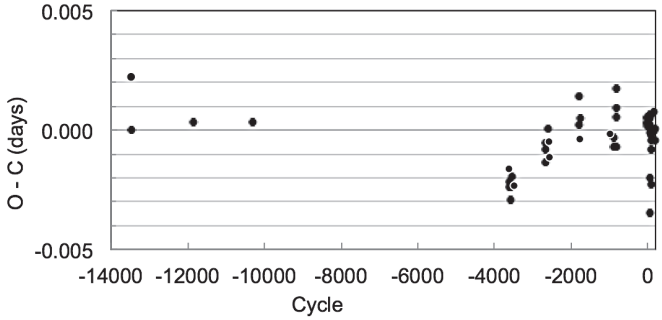

Figure 3. Variations in O–C values for primary and secondary minima between 2000 and 2015.

0.75) were determined using a 7-order polynomial fit in PERANSO (Vanmunster 2013). Phase-magnitude light curves were produced in PERANSO and exported for modelling. The procedures described in the BINARY MAKER 3 manual (Bradstreet and Steelman 2002) and by Bradstreet (2005) were used to determine models of the TW Cru system.

3. Results

3.1. Period analysis

In the 5 years between 2011 and 2015, 45 times of minimum were recorded (Table 2). A new ephemeris was determined from these data with a least squares linear regression (Equation 1). The epoch for this work was calculated from 96 data points around the primary minimum of HJD 2457101.1430, which was a night with good seeing; the total data set for that night, which included the secondary minimum, was 423 observations in the V passband.

$$\text{HJD (Min I)} = 2457101.1433\ (0.0002) + 0.3881444\ (0.0000006) \times E \quad (1)$$

A parabola can be fitted to the graph of the observed minus calculated epochs (O–C) between the original epoch determined by Bruna (1930) and cycle 83,463, the most recent in 2015 (Figure 2).

$$y = 1 \times 10^{-10}\, x^2 - 9 \times 10^{-6}\, x - 9 \times 10^{-5} \quad (2)$$

The coefficient of 1×10^{-10} in Equation 2 indicates that the period determined originally was about 0.7 second shorter than that determined in this work. The difference between the original period determined by Bruna (1930) and that determined from my data with a linear regression is also 0.7 second.

An (O–C) diagram for the years 2000 to 2015, based on the ephemeris in Equation 1, shows variations, although the differences are small and within the range of the average error of 0.016 day (Figure 2). However, there was an apparent sinusoidal trend in the O–C values from 2011 (epoch –3625) to 2015 (Figure 3). In 2015, the two very low O–C values of –0.002 and –0.0035 were due to minima in the I band and the other very low value of –0.002 was in the V band, yet the O–C values in other bands on those dates were not different from other sets in 2015.

There were variations in the magnitudes of the primary and secondary eclipse minima (Table 2) and in the amplitudes of the

Table 2. TW Cru times of minimum, observed minus calculated (O–C) differences in epochs, and photometric data.

*Year**	*Cycle*	*Epoch HJD*	*Error**	*O–C*	*Error*	*Band*	*Magnitude*	*Error*
1926[a]	–83281	2424776.15740		0.0353	0.0050			
2000[b]	–13476.5	2451870.32000		0.0000	0.0013	V		
2002[c]	–11853.5	2452500.27800		0.0003		V		
2004[d]	–10291	2453106.75300		0.0003		V		
2011	–3625.5	2455693.92413	0.00141	–0.0024	0.0014	V	12.80	0.006
2011	–3623	2455694.89528	0.00113	–0.0016	0.0012	V	12.85	0.006
2011	–3594.5	2455705.95682	0.00125	–0.0022	0.0013	V	12.80	0.007
2011	–3587	2455708.86768	0.00112	–0.0024	0.0012	V	12.85	0.007
2011	–3586.5	2455709.06123	0.00115	–0.0029	0.0012	V	12.81	0.007
2011	–3540.5	2455726.91681	0.00105	–0.0019	0.0011	V	12.78	0.009
2011	–3489	2455746.90585	0.00112	–0.0023	0.0012	V	12.86	0.005
2012	–2677	2456062.07976	0.00104	–0.0013	0.0011	V	12.86	0.005
2012	–2662	2456067.90247	0.00113	–0.0008	0.0012	V	12.87	0.005
2012	–2661.5	2456068.09679	0.00130	–0.0005	0.0013	V	12.84	0.005
2012	–2595	2456093.90897	0.00093	0.0001	0.0010	V	12.88	0.006
2012	–2579.5	2456099.92465	0.00118	–0.0005	0.0012	V	12.82	0.004
2012	–2551	2456110.98609	0.00122	–0.0012	0.0012	V	12.86	0.005
2013	–1788.5	2456406.94846	0.00146	0.0014	0.0015	V	12.81	0.007
2013	–1788	2456407.14136	0.00130	0.0002	0.0013	V	12.89	0.007
2013	–1775.5	2456411.99343	0.00155	0.0005	0.0016	V	12.80	0.009
2013	–1775	2456412.18664	0.00139	–0.0004	0.0014	V	12.89	0.009
2014	–974	2456723.09018	0.00045	–0.0002	0.0005	V	12.84	0.013
2014	–902	2456751.03599	0.00125	–0.0007	0.0013	V	12.86	0.009
2014	–897	2456752.97711	0.00124	–0.0003	0.0013	V	12.86	0.006
2014	–825	2456780.92308	0.00019	–0.0007	0.0003	V	12.85	0.015
2014	–824.5	2456781.11878	0.00190	0.0009	0.0019	V	12.80	0.014
2014	–822.5	2456781.89589	0.00150	0.0017	0.0015	V	12.80	0.014
2014	–822	2456782.08876	0.00140	0.0005	0.0014	V	12.82	0.011
2015	–13	2457096.09706	0.00104	0.0003	0.0011	V	12.89	0.004
2015	–13	2457096.09727	0.00137	0.0005	0.0014	I	11.86	0.006
2015	–0.5	2457100.94868	0.00122	0.0002	0.0012	V	12.83	0.004
2015	0	2457101.14310	0.00102	0.0005	0.0010	V	12.88	0.004
2015	2	2457101.91918	0.00120	0.0003	0.0012	I	11.97	0.006
2015	53.5	2457121.90481	0.00140	–0.0035	0.0014	I	11.80	0.006
2015	53.5	2457121.90820	0.00196	–0.0001	0.0020	V	12.80	0.006
2015	53.5	2457121.90880	0.00316	0.0005	0.0032	B	13.63	0.012
2015	54	2457122.10039	0.00302	–0.0020	0.0030	I	11.86	0.006
2015	54	2457122.10256	0.00179	0.0002	0.0018	B	13.71	0.012
2015	54	2457122.10302	0.00192	0.0007	0.0019	V	12.86	0.006
2015	95	2457138.01397	0.00160	–0.0023	0.0016	V	12.89	0.004
2015	95	2457138.01585	0.00173	–0.0004	0.0017	B	13.74	0.008
2015	100	2457139.95675	0.00275	–0.0002	0.0028	V	12.88	0.005
2015	100	2457139.95691	0.00179	–0.0001	0.0018	I	11.87	0.006
2015	100.5	2457140.15026	0.00175	–0.0008	0.0018	V	12.80	0.005
2015	100.5	2457140.15171	0.00189	0.0006	0.0019	I	11.80	0.006
2015	146.5	2457158.00564	0.00564	0.0000	0.0056	V	12.83	0.003
2015	146.5	2457158.00646	0.00224	0.0008	0.0022	B	13.67	0.007
2015	180	2457171.00805	0.00163	–0.0005	0.0016	I	11.96	0.009
2015	180	2457171.00856	0.00171	0.0001	0.0017	V	12.88	0.01

**Notes. Source: (a) Bruna 1930; (b) Pojmański 2002; (c) Kreiner 2004; (d) Dvorak 2004. Errors for epoch, O–C, and magnitudes, respectively, are shown for the present work.*

Table 3. Color indices and estimated spectral types and temperatures of the TW Cru component stars.

Parameter	*B–V*	*V–I*	*Spectral type*	*Teff (K)*
Maximum light	0.82 ± 0.01	0.87 ± 0.01	K0V	5280
Primary minimum	0.87 ± 0.01	0.92 ± 0.01	K2V	5040
Secondary minimum	0.86 ± 0.01	0.90 ± 0.02	K1V	5170

Table 4. Light curve model data used for the models shown in Figures 6 through 10. The convention used in BINARY MAKER 3 for W-type UMa systems, where the more massive star is the cooler component, is to invert the mass ratio.

Parameter	*General*	*Star 1*	*Star 2*
Mass ratio	1.5		
Fillout	0.11		
Inclination	70.8°		
Temperature (K)		5000	5170
Gravity coefficient		0.32	0.32
Limb darkening (V)		0.70	0.66
Limb darkening (I)		0.48	0.44
Limb darkening (B)		0.87	0.84

Table 5. Star spot parameters for the TW Cru light curve solutions in Figures 6 through 8. The Johnson V band fluxes were modeled, with an example of the solution in the I band for 2015-04-27. In each case, star 1 is the larger, cooler component.

Date and Passband	*Star*	*Co-Latitude*	*Longitude*	*Radius*	*Temperature factor*
2013-04-29 (V)	1	84	3	20	1.10
"	1	80	260	17	0.90
"	2	90	65	12	0.92
2015-03-19 (V)	1	70	135	18	0.93
"	2	60	200	22	0.96
2015-04-09 (V)	1	70	90	20	0.96
"	2	30	110	14	0.96
2015-04-09 (B)	1	70	90	20	0.96
"	2	30	110	14	0.96
2015-04-09 (I)	1	70	90	20	0.96
"	2	30	110	10	0.98
2015-04-27 (V)	1	80	112	20	0.86
"	1	70	200	24	0.96
"	2	55	112	24	0.86
2015-04-27 (I)	1	80	112	20	0.86
"	1	70	200	24	0.96
"	2	55	112	24	0.86

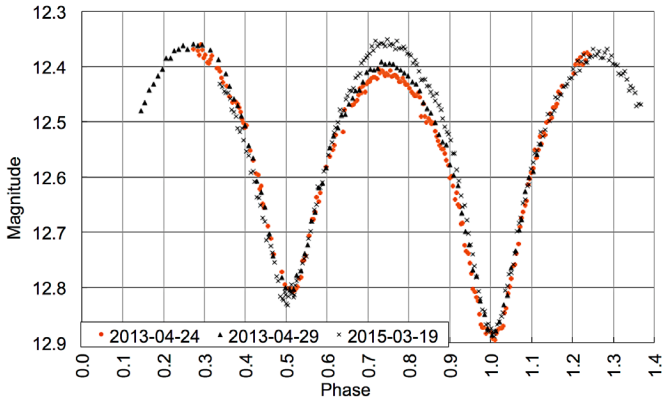

Figure 4. Phased light curves in the V passband demonstrating variations in eclipse amplitudes. The maximum magnitude was brighter after the primary minimum than after the secondary on 2013-04-24 and 2013-04-29. The maximum magnitude was brighter after the secondary minimum on 2015-03-19.

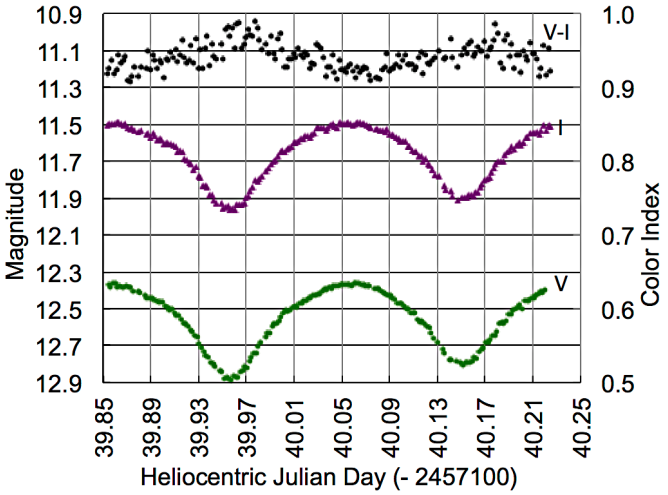

Figure 5. Light curves of TW Cru in V and I passbands (left Y axis) and the variation in color index (right Y axis) on 2015-04-27. The maximum magnitudes were similar after both the primary and secondary minima.

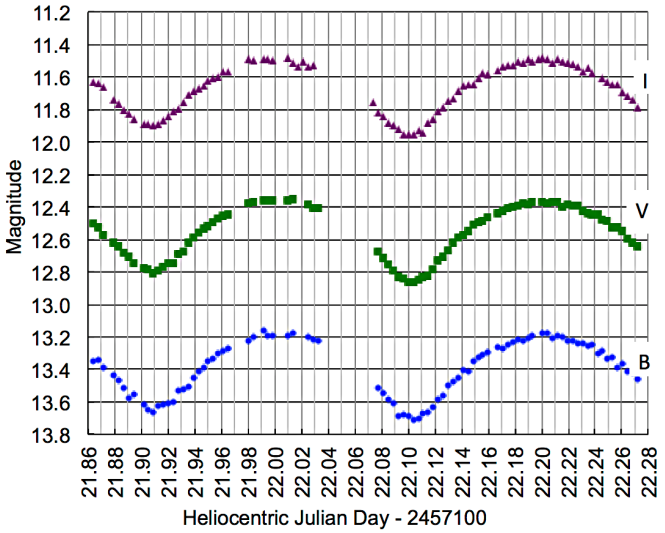

Figure 6. Light curves of TW Cru in B, V and I for 2015-04-09. The maximum magnitudes were similar after both the primary and secondary minima. The seeing was affected by a humid air mass and some cloud, which prevented the determination of accurate color indices.

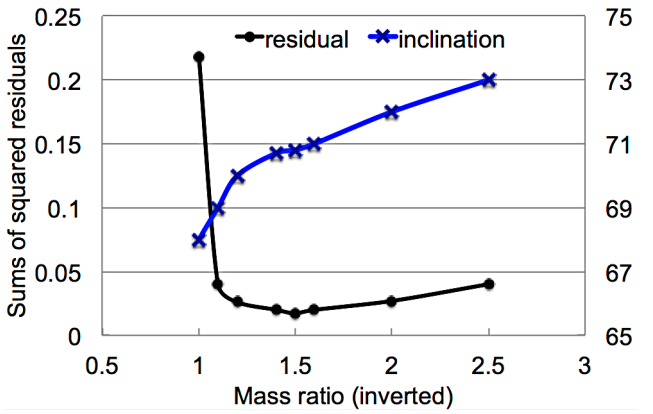

Figure 7. Selection of probable mass ratio with the q method: plot of the sum of squared residuals of the light curve fit (left axis) against a range of mass ratios. The inclination that gave the lowest residual value for each mass ratio is also shown (right axis).

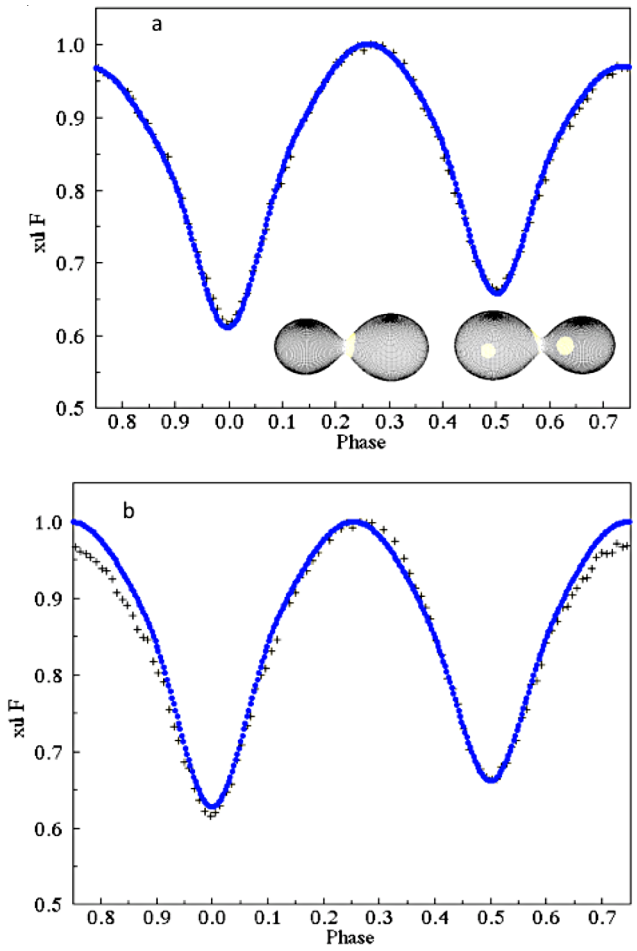

Figure 8. (a) Light curve (crosses) and best fit (blue line) of the V pass band for 2013-04-29. The average of residuals for the light curve fit was 0.006. Inset: the binary model at phases 0.25 (left) with a hot spot on star 1 at the point of contact and the positions of 2 cool spots at phase 0.75. Star 1 is the larger star, on the right at phase 0.25. (b) Light curve (crosses) and model (blue line) with the same parameters as in (a), but without spots.

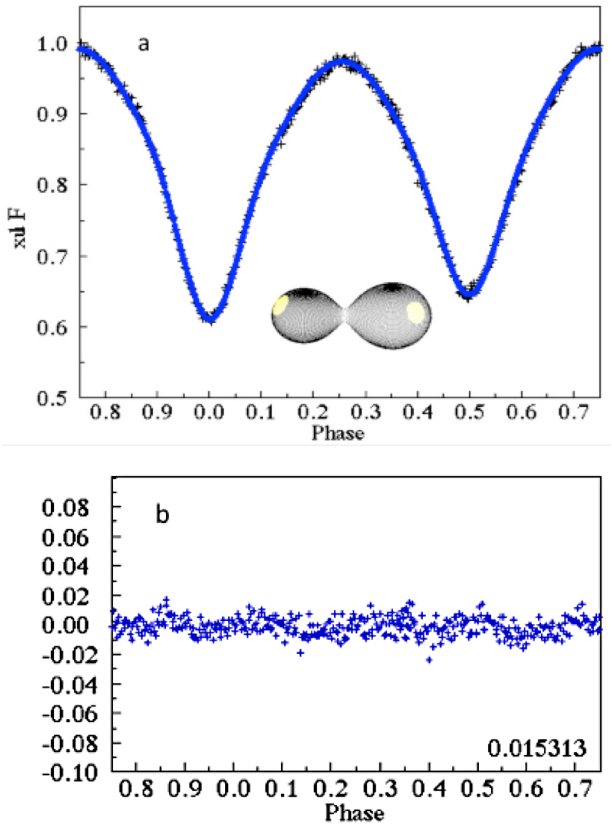

Figure 9. (a) Light curve (crosses) and best fit (blue line) of the V pass band for 2013-03-19 (epoch HJD 2457101.14310). The inset shows the spot positions on the binary at phase 0.25. (b) Residuals for the light curve plot (mean: 0.015).

eclipses. For example, the magnitude at maximum brightness between eclipses (phases 0.25 and 0.75) was brighter after the primary eclipses on some occasions, on 2013-04-24 (HJD 2456407.14136) and on 2013-04-29 (HJD 2456412.18664), for example, and it was brighter after the secondary eclipses at other times, on 2015-03-19 (HJD 2457100.94868), for example (Figure 4). In April 2015, the magnitudes at maximum brightness after both primary and secondary minima were similar (Figures 5 and 6). The color index was redder after the primary minimum than after the secondary and bluer at maximum light Figure 5).

3.2. Light curve modelling

As there are no spectral data available for TW Cru, the effective temperatures for modelling the light curves were estimated from the observed B–V and V–I color indices, which indicate the spectral types to be about K0 to K2 if there were no interstellar reddening (Table 3). The B–V value in the APASS database is 0.768, which indicates the spectral type may be G9 (Table 1). A range of values for the mass ratio, inclination, and fillout factor was tried and those that gave the best fit to the light curves, with the lowest sums of squared residuals of 0.006 for the light curve on 2013-04-29, are shown in Table 4. The "q method" was used to select a probable mass ratio (Figure 7). Star spots had to be included before good fits to the observed light curves were obtained; compare Figures 8a and 8b. Examples showing the variation in spot positions, size, and relative temperature are shown in Figures 8, 9, 10, and 11. The spot parameters are given in Table 5.

For a good fit, the astrophysical model of the light curve obtained in 2013-04-29 required the addition of a cool spot on each star and a hot "spot" at the zone of contact on the larger component (Figure 8a and Table 5). Two cool spots, one on each star, provided a good fit for modelling the light curve obtained on 2015-03-19 (Figure 9a and Table 5). An example of the graph of the residuals in the light curve model plot is shown in Figure 9b.

A comparison of the fitting of the model in the V bandpass to the light curves in the B and I bands is shown in Figure 10. Although there were some gaps in the light curve due to cloud, and poor seeing affected the signal to noise ratio, especially in the B band, the fit was good. Only a small adjustment was made to the spot size and temperature on star 2 in the I band. On 2015-04-27, three cool spots were required to provide a good fit, with two spots on the larger star and one on the smaller, hotter component (Figure 11a and Table 5). The model of the light curve in the I passband did not require a change in the relative temperatures of the spots (Figure 10c and Table 5).

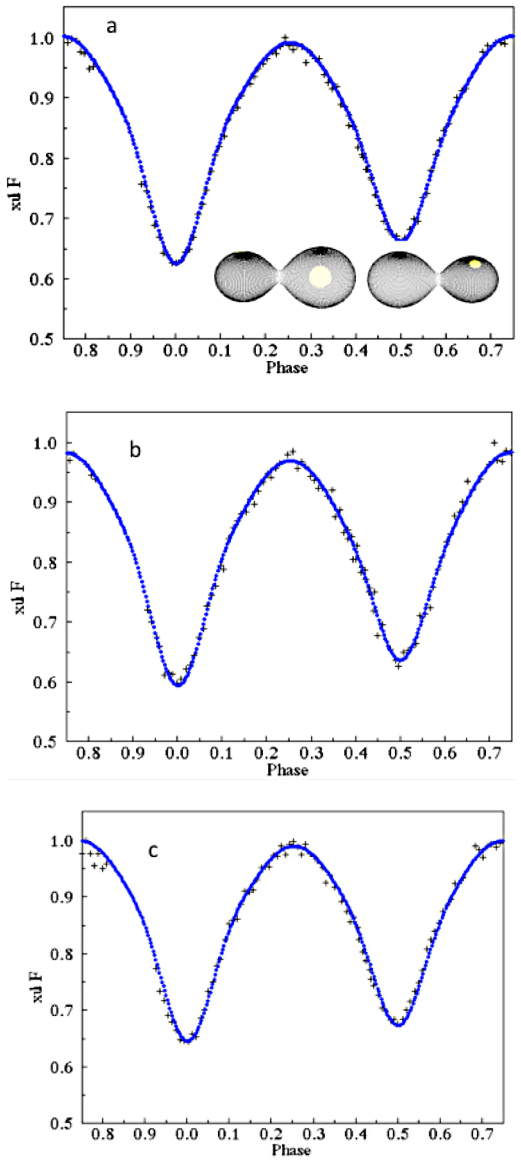

Figure 10. (a) Light curve (crosses) and best fit (blue line) of the V pass band for 2015-04-09; the mean of the residuals was 0.007. Inset: spot positions on the binary model at phases 0.25 and 0.75. (b) Light curve and best fit for the B pass band; mean of the residuals was 0.012. (c) Light curve and best fit for the I pass band; the mean of the residuals was 0.012.

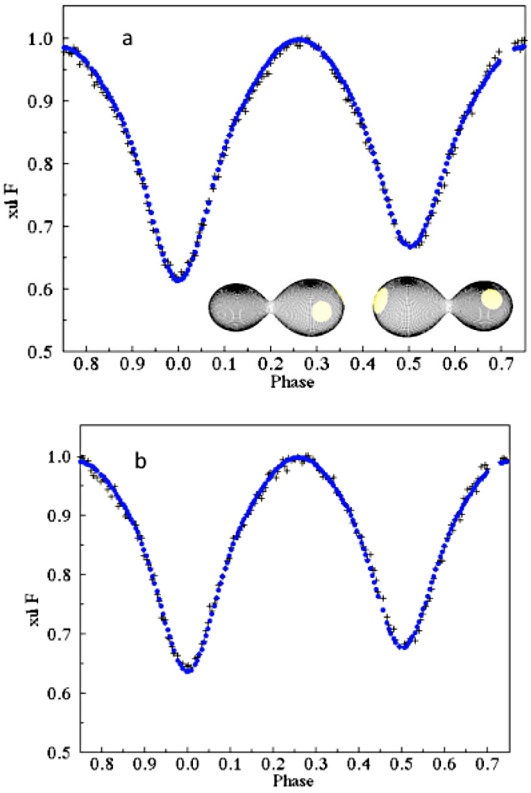

Figure 11. (a) Light curve (crosses) and best fit (blue line) of the V pass band for 2015-04-27. The mean of the light curve residuals was 0.014. Inset: spot positions on the binary model at phases 0.25 and 0.75. (b) Light curve (crosses) and best fit (blue line) of the I pass band. The mean of the light curve residuals was 0.012. Spot parameters were not changed (see Table 5).

4. Discussion

The period determined here is similar to that determined by Kreiner (2004) and differs by 0.7 second from the period derived originally by Bruna (1930). Note that the first epoch shown in Table 2 differs from that given in the *General Catalogue of Variable Stars* (GCVS; Kholopov, *et al.* 1985); the latter is in fact the epoch at phase 0.378 shown in Table 1 of Bruna (1930). As there are no data for times of minimum between 1926 and 2000, it is possible that the error stated for the original period was larger than that published and so there may not be any difference in the period.

The variability in times of minimum is probably due to asymmetry in the light curves; in particular, the rise from the minima to maximum light was slower than the decrease to minima on several occasions. Kwee (1958), in his study of eclipsing binaries using photoelectric photometry, concluded that very short term variations in the periods were due to asymmetry in the light curves, and not the effect of mass exchange. Some of the variability in the times of minimum could also be variability in the light curves due to poor seeing conditions, which was often the case in southeast Queensland where the wet season extends from January to April, the prime season for Crux.

As a quadratic equation could be fitted to the O–C curve for the 2011–2015 data, it is possible that the some of the year-to-year variation in the O–C values might be caused by the presence of a third component. However, a longer time series of observations is required to determine if that is the case. A more likely explanation for the apparent differences in O–C values over the 5-year period from 2011 to 2015 is that the formation and movement of star spots varies not only between cycles on a short term basis—over about 100 cycles—but also on a much longer term like the sunspot cycle on the Sun. Variations in the magnitudes and exact times of the maxima and minima of the light curves are probably caused by the movement of cool spots on the stars.

The spectral type may be earlier due to interstellar reddening, but as the distance of TW Cru is not known, the effect of reddening on color index cannot be determined. If it were severe, then the B–V value would indicate a spectral class a little later than that given by the V–I value, but in fact both

values agree with recent tabulated values for K0 and K2 dwarf stars (Pecaut and Mamajek 2013). However, these values are only a guide; the spectral types of the TW Cru stars could be earlier. Until spectral types and the mass ratio are determined spectroscopically, the models shown here are provisional. Their main value is in indicating that the short term variability in the light curves is probably due to cool star spots, which is what would be expected from magnetic activity in G or K type stars with very rapid rotation rates (Hilditch 2001). Hilditch (2001) discussed the problems in modelling contact binary stars with asymmetric light curves and commented that the placement of cool star spots over the surfaces can lead to ambiguous results; Doppler imaging and detailed eclipse mapping, together with photometry in several band passes and high resolution spectroscopy, are needed to improve our understanding of these systems.

Although the cool spots were sufficient to explain most variations in the light curves, a hot zone on the cooler star around the contact region gave the best fit to the model for 2013-04-29 (Table 5). The variation in color index from reddest (coolest) during the eclipses, particularly the primary eclipse, and bluer (hotter) at phases 0.25 and 0.75 suggests that the contact zone was, in general, hotter than other regions of the binary (Figure 5). There may be other solutions to the light curve with the incorporation of a hot contact zone, but until the mass ratio and spectral types are determined spectroscopically, further work on model parameters is not warranted.

5. Conclusions

There has been no substantial change in the period of TW Cru since its discovery in 1926. Small variations apparent in the times of minimum and asymmetry in the light curves are most likely due to the effect of cool star spots. Star spots were required to produce good fits to the light curves in preliminary astrophysical models prepared in BINARY MAKER 3. These indicate that the component stars are very active magnetically. Spectroscopic studies are needed for determining the spectral types and mass ratio of TW Cru.

6. Acknowledgements

I am grateful to Dr. Tom Richards for introducing me to the study of eclipsing binary stars and for his guidance and encouragement in photometry. I thank the referee, whose comments improved the presentation of this work. Some of the equipment was purchased with the aid of grants from the Edward Corbould Research Fund of the Astronomical Association of Queensland. This research made use of the VizieR catalogue access tool, the SIMBAD database, operated at CDS, Strasbourg, France, and the AAVSO Photometric All-Sky Survey (APASS), funded by the Robert Martin Ayers Sciences Fund.

References

Binnendijk, L. 1970, *Vistas Astron.*, **12**, 217.

Bradstreet, D. H. 2005, in *The Society for Astronomical Sciences 24th Annual Symposium on Telescope Science* (May 24–26, 2005), Society for Astronomical Sciences, Rancho Cucamonga, CA, 23.

Bradstreet, D. H., and Steelman, D. P. 2002, *Bull. Amer. Astron. Soc.*, **34**, 1224.

Bruna, P. P. 1930, *Bull. Astron. Inst. Netherlands*, **6**, 45.

Diffraction Limited. 2012, MAXIMDL image processing software (http://www.cyanogen.com).

Dvorak, S. W. 2004, *Inf. Bull. Var. Stars*, No. 5542, 1.

Henden, A. A., *et al.* 2013, AAVSO Photometric All-Sky Survey, data release 7 (http://www.aavso.org/apass).

Hilditch, R. W. 2001, *An Introduction to Close Binary Stars*, Cambridge Univ. Press, Cambridge.

Kholopov, P. N., *et al.* 1985, *General Catalogue of Variable Stars*, 4th ed., Moscow.

Kreiner, J. M. 2004, *Acta Astron.*, **54**, 207.

Kwee, K. K. 1958, *Bull. Astron. Inst. Netherlands*, **14**, 131.

Landolt, A. U. 2007, *Astron. J.*, **133**, 2502.

Mohajerani, S., and Percy, J. R. 2015, *J. Amer. Assoc. Var. Star Obs.*, **39**, 80.

Munari, U., Henden, A. A., Frigo, A., and Dallaporta, S. 2014, *J. Astron. Data*, **20**, 4.

Pecaut, M. J., and Mamajek, E. E. 2013, *Astrophys. J., Suppl. Ser.*, **208**, 9.

Pojmański, G. 2002, *Acta Astron.*, **52**, 397.

Pribulla, T., and Rucinski, S. M. 2006, *Astron. J.*, **131**, 2986.

Richards, T. 2013, Southern Eclipsing Binaries Programme of the Variable Stars South group (http://www.variablestarssouth.org/index.php/research/eclipsing-binaries).

Richards, T. 2015, private communication.

Thinking Man Software. 1992–2014, DIMENSION 4 software (http://www.thinkman.com/dimension4/).

Vanmunster, T. 2013, Light Curve and Period Analysis Software, PERANSO v.2.50 (http://www.peranso.com/).

Validation of "Sloan Magnitudes for the Brightest Stars" and Suggestions for Observing with Small Telescopes

Anthony Mallama
14012 Lancaster Lane, Bowie, MD 20715; anthony.mallama@gmail.com

Bruce Krobusek
5950 King Hill Drive, Farmington, NY 14425; bkrobusek@gmail.com

Received August 5, 2015; revised September 4, 2015; accepted September 18, 2015

Abstract Synthetic magnitudes derived from published spectral fluxes and photometric magnitudes from CCD observations are compared to those values listed in the catalogue "Sloan Magnitudes for the Brightest Stars." The RMS differences for synthetic and observed magnitudes generally agree with the transformation-based catalogue values within the uncertainties quoted therein. These quoted values are 0.03 magnitude for the g', r', i', and z' bands, and 0.08 magnitude for the u' band. When separated according to stellar color the RMS values of the red stars are generally smaller than those of the blue stars.

1. Introduction

The catalogue "Sloan Magnitudes for the Brightest Stars" (Mallama 2014) contains 3,969 stellar objects brighter than r' ~ 7. The magnitudes of these objects, which are referred to herein as catalogue stars, were derived by transforming Johnson system magnitudes (Johnson *et al.* 1966) to the Sloan system. In this study we compare two newly determined sets of Sloan magnitudes with those of a sample of catalogue stars. One set was derived synthetically from radiometrically calibrated spectral fluxes while the other was determined by direct photometry with Sloan filters. Statistics of the differences are computed for the purpose of validating the catalogue.

We describe how synthetic magnitudes were derived from the Hubble Space Telescope library of spectral energy distributions (SEDs) and then compare the synthetic and catalogue values in section 2. The method of photometric observation and the resulting dataset are presented in section 3, and those resulting magnitudes are compared to catalogue magnitudes. Section 4 discusses the combined synthetic and photometric comparison and summarizes our conclusions. Section 5 offers a few suggestions for using the catalogue in astronomical research.

2. Synthetic magnitudes

SEDs from the Space Telescope Imaging Spectrograph (STIS) instrument on-board Hubble are considered to be the best such data available. The STIS fluxes of the CalSpec database (Bohlin *et al.* 2014) are accurate to 1% (0.01 magnitude) according to a comparison with Johnson-Cousins B, V, R, and I magnitudes of eleven stars (Bohlin and Landolt 2015). The central wavelengths of those bands range from 440 to 900 nm. Additionally, Mallama (2015) compared STIS/CalSpec fluxes to the magnitudes of six Sloan standard stars listed by Smith *et al.* (2002) in all five Sloan bands (u', g', r', i' and z') which extended the range of wavelengths down to 355 nm in the near-UV. The agreement was, again, about 0.01 magnitude. Therefore, the STIS/CalSpec data are judged to be a reliable source for validating the Sloan magnitudes in the catalogue.

Stars were chosen for the synthetic comparison by matching the catalogue objects with those in the CalSpec library. FITS files of CalSpec data were retrieved from http://www.stsci.edu/hst/observatory/crds/calspec.html. The header of each file was checked to verify that SEDs extending over all Sloan band-passes were obtained from the STIS instrument, thus insuring that only the most accurate SEDs were used. For HD 172167 STIS data extended to only 535 nm. However, this star is the fundamental standard, α Lyr (Vega), and the fluxes beyond 535 nm are from a carefully derived model which is considered to be highly accurate. For HD 14943 and HD 38666, the catalogue lists only the g' and r' magnitudes, so the other bands were excluded from the analysis for these stars. The seven matching stars are listed in Table 1 and it is notable that they are all hot bluish stars. This selection effect is compensated by a broader range of colors for the photometric comparison, as discussed in the next section.

Table 1. Catalogue and CalSpec stars

Catalog Name	*CalSpec Name*	*Spectral Type**	*Color g'-r'***
HD 14943	HD 14943	A5V	–0.45
HD 15318	ξ² Cet	B9III	–0.27
HD 34816	λ Lep	B0.5IV	–0.45
HD 38666	μ Col	0.95V	–0.50
HD 48915	α CMa (Sirius)	A1V	–0.22
HD 172167	α Lyr (Vega)	A0V	–0.23
HD 214680	10 Lac	O9V	–0.41

** from Bohlin et al. (2014)*
*** from the catalogue*

The synthetic magnitudes were derived from SEDs by integrating the product of spectral energy multiplied by system response over each Sloan band-pass. Equation 1 (Smith *et al.* 2002; Fukugita *et al.* 1996) indicates the relationship among magnitude, flux, and system response.

$$m = -2.5 \frac{\int d(\log \nu) f_\nu S_\nu}{\int d(\log \nu) S_\nu} \quad (1)$$

where m is magnitude, f is flux, S is the system response, and ν is frequency. The units are ergs per square centimeter per Hertz per second. The five system response functions referenced by Smith *et al.* (2002) were retrieved from http://www-star.fnal.gov/ugriz/Filters/response.html . After solving for m, a constant of –48.60 was added to place Sloan magnitudes on the absolute AB system (Oke and Gunn 1983; Fukugita *et al.* 1996).

The synthetic magnitudes of the seven matching stars are listed in Table 2. The differences, in the sense "catalogue minus synthetic" magnitude, are listed in Table 3. The mean and the root-mean-square (RMS) of the differences in Table 3 are summarized in Table 4. These statistics will be discussed in section 4 along with those from the photometric comparison, which is described next.

Table 2. Synthetic magnitudes.

Star	*u′*	*g′*	*r′*	*i′*	*z′*
HD 14943	n/a	5.906	5.948	n/a	n/a
HD 15318	5.037	4.128	4.421	4.673	4.829
HD 34816	3.741	4.016	4.492	4.858	5.153
HD 38666	n/a	4.881	5.378	n/a	n/a
HD 48915	–0.583	–1.575	–1.310	–1.068	–0.908
HD 172167	0.987	–0.090	0.153	0.378	0.521
HD 214680	4.351	4.642	5.063	5.396	5.675

Table 3. Catalogue magnitudes minus synthetic magnitudes.

Star	*u′*	*g′*	*r′*	*i′*	*z′*
HD 14943	n/a	0.044	–0.018	n/a	n/a
HD 15318	0.103	0.032	0.009	0.007	0.031
HD 34816	0.079	0.044	0.018	0.062	0.047
HD 38666	n/a	0.039	0.042	n/a	n/a
HD 48915	0.093	0.025	–0.020	–0.022	–0.002
HD 172167	0.073	0.030	0.017	0.012	0.049
HD 214680	0.029	0.028	0.017	0.014	–0.025

Table 4. Statistics of the differences between catalogue and synthetic magnitudes.

	u′	*g′*	*r′*	*i′*	*z′*
Mean	+0.075	+0.035	+0.009	+0.015	+0.020
RMS	0.080	0.035	0.022	0.031	0.035

3. Photometric magnitudes

Nine catalogue stars were observed a total of 16 times by author BK. The magnitudes of Sloan standard stars used for reference were reported by Smith *et al.* (2002) and they are also available on-line at http://www-star.fnal.gov/ugriz/tab08.dat. The raw data were recorded using a 20-cm aperture Schmidt-Cassegrain telescope, an SBIG CCD camera containing a cooled Kodak KAF-0400 sensor, and a set of five Generation 2 Astrodon Sloan filters.

The observations from Farmington, New York, were scheduled so that they occurred when the catalogue and standard stars were within 0.15 air mass of zenith, with the average distance being 0.07. Furthermore, the delta air mass of the two stars was never greater than 0.05, with the average being 0.03. These precautions minimized uncertainties due to atmospheric extinction. Tables 7 and 8 list the air masses and delta air masses in the columns AM and ΔAM, respectively. Additionally, each catalogue star was matched with a standard star of approximately the same color to minimize transformation uncertainties.

The procedure for acquiring image data for a single Sloan magnitude in a single filter was to record two separate series of three images of the catalogue star interleaved with two such series for the standard star. The resulting magnitude for that filter represents the average of six values derived from six pairs of catalogue-and-standard CCD images. Thus, each set of five u', g', r', i', z' magnitudes derives from 60 separate images. The average exposure durations in seconds were u', 256; g', 6; r', 6; i', 14; and z', 39. Additional flat field and dark frames for image reduction were recorded at all observing sessions.

The flat field images were obtained with a light box specially constructed by author BK. A mylar sheet and a piece of milk plastic diffused the light. A Philips three-way "Reveal" bulb installed on a 10-inch reflector was used as illumination for the g', r', i', and z' filters. A blacklight was used for the u' filter and the milk plastic was removed. Flat field images obtained with the telescope aimed at the device gave practically identical results as images obtained using the twilight sky as illumination. There was almost no vignetting across the field of view and only minimal variation due to dust spots.

Early in the program we compared three different computer applications for extracting instrumental magnitudes from the CCD images. These three were AIP4WIN (Berry and Burnell 2011), the Aperture Photometry Tool (APT; California Institute of Technology 2015), and our own program called EXTRACT which we have developed over the past 25 years. EXTRACT was found to provide the best combination of accuracy and ease of use for our purposes, so we employed it for all our data reduction.

Instrumental magnitudes derived from the images were corrected for extinction and transformed to standard Sloan magnitudes. The methods originally developed by Hardie (1962) for the UBV system were adapted for the five-color Sloan system. The procedures for characterizing the color response of the hardware and of the atmospheric extinction at the observing site are also adapted from those outlined by Hardie. Color transformation coefficients were derived from observations of the primary standard stars taken at small air masses on four different nights. Atmospheric extinction coefficients were determined from time-series observations of catalogue stars as they traversed a range of about one air mass on three nights. About one hour is required for extinction stars to travel between 20 degrees elevation (2.9 air masses) and 30 degrees elevation (2.0 air masses). Figure 1 illustrates the extinction observations. The resulting coefficients are listed in Table 5.

The sixteen sets of photometric magnitudes for the nine stars listed in Table 6 are reported in Table 7. The differences, in the sense "catalogue minus photometric" magnitude, are listed in

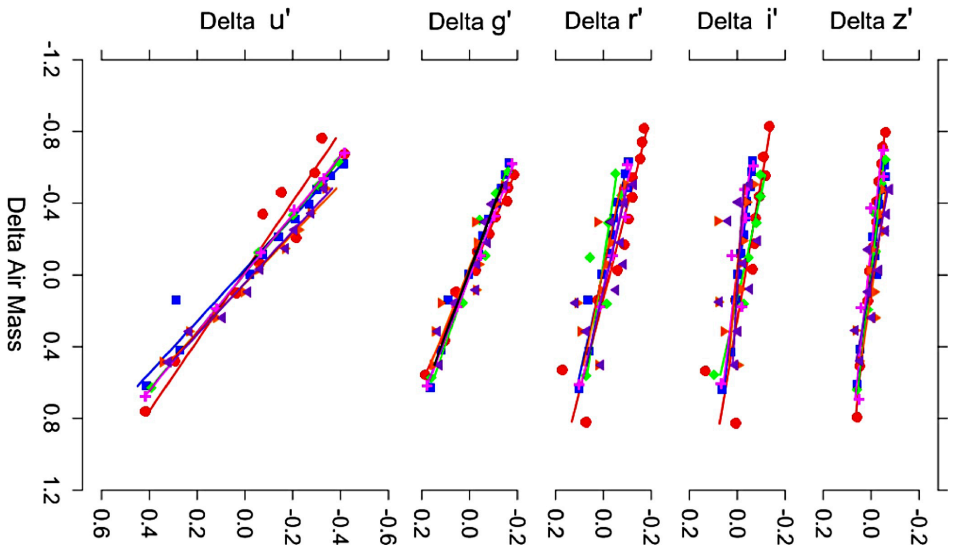

Figure 1. Magnitude changes are plotted as a function of the change in air mass. Six stars observed on three nights determined the five extinction coefficients.

Table 5. Sloan photometric calibration coefficients.

Band	*Extinction**	*Transformation***
u'	0.69	+0.102
g'	0.31	+0.064
r'	0.17	+0.019
i'	0.10	–0.072
z'	0.08	–0.017

** Magnitudes per air mass. Second order extinction was taken to be –0.02 for u′ and g′, and zero otherwise.*
*** Color indices corresponding to the transformation coefficients are as follows: u′–g′(u'), g′–r′ (g'), g′–r′ (r'), r′–i′ (i'), and r′–z′ (z').*

Table 6. Catalogue and photometric stars.

HD	*Spectral Type**	*Color g′-r′***
120818	A5IV	-0.11
125642	A2V	-0.17
186408	G1.5Vb	+0.42
186427	G3V	+0.42
195593	F5Ib	+0.82
206538	A2V	-0.14
207198	08.5II	+0.11
208501	B8Ib	+0.54
210702	K1III	+0.74

** from Centre de Données Astronomiques de Strasbourg*
*** from the catalogue*

Table 7. Photometric magnitudes.

HD	*JD**	*u′*	*g′*	*r′*	*i′*	*z′*	*AM*	*ΔAM*
120818	6808.65	7.770	6.598	6.700	6.869	7.008	1.06	0.02
120818	6816.64	7.836	6.662	6.727	6.900	7.016	1.07	0.02
125642	6808.63	7.360	6.247	6.401	6.590	6.733	1.04	0.05
125642	6816.63	7.399	6.288	6.420	6.613	6.756	1.04	0.04
186408	6899.63	7.589	6.246	5.798	5.675	5.657	1.05	0.04
186408	6904.61	7.640	6.234	5.787	5.675	5.641	1.05	0.05
186427	6899.63	7.879	6.512	6.048	5.926	5.885	1.05	0.04
186427	6904.61	7.871	6.507	6.041	5.919	5.882	1.05	0.05
195593	6943.58	8.707	6.690	5.834	5.436	5.177	1.08	0.02
206538	6917.59	7.068	6.015	6.156	6.327	6.439	1.04	0.05
207198	6928.54	6.305	6.080	5.898	5.909	5.998	1.08	0.02
207198	6933.54	6.332	6.005	5.880	5.889	5.976	1.07	0.01
208501	6926.59	7.191	6.143	5.547	5.263	5.089	1.05	0.03
208501	6927.55	7.182	6.143	5.559	5.247	5.078	1.06	0.01
210702	6926.66	8.584	6.346	5.643	5.382	5.310	1.15	0.00
210702	6927.63	8.586	6.344	5.658	5.414	5.321	1.12	0.01

** Add 2450000.00*

Table 8. Catalogue magnitudes minus photometric magnitudes.

HD	*JD**	*u′*	*g′*	*r′*	*i′*	*z′*	*AM*	*ΔAM*
120818	6808.65	0.080	0.022	0.030	0.041	0.052	1.06	0.02
120818	6816.64	0.014	-0.042	0.003	0.010	0.044	1.07	0.02
125642	6808.63	0.100	0.013	0.029	0.070	0.107	1.04	0.05
125642	6816.63	0.061	-0.028	0.010	0.047	0.084	1.04	0.04
186408	6899.63	0.021	-0.036	0.002	0.015	-0.007	1.05	0.04
186408	6904.61	-0.030	-0.024	0.013	0.015	0.009	1.05	0.05
186427	6899.63	0.001	-0.042	0.002	0.014	0.015	1.05	0.04
186427	6904.61	0.009	-0.037	0.009	0.021	0.018	1.05	0.05
195593	6943.58	0.063	-0.050	-0.014	-0.016	0.013	1.08	0.02
206538	6917.59	0.222	0.035	0.034	0.023	0.041	1.04	0.05
207198	6928.54	-0.025	-0.060	0.012	0.021	-0.018	1.08	0.02
207198	6933.54	-0.052	0.015	0.030	0.041	0.004	1.07	0.01
208501	6926.59	0.009	-0.043	0.013	0.017	0.041	1.05	0.03
208501	6927.55	0.018	-0.043	0.001	0.033	0.052	1.06	0.01
210702	6926.66	-0.084	0.034	-0.003	0.038	0.000	1.15	0.00
210702	6927.63	-0.086	0.036	-0.018	0.006	-0.011	1.12	0.01

** Add 2450000.00*

Table 9. Statistics of the differences between catalogue and photometric magnitudes.

	u'	*g'*	*r'*	*i'*	*z'*
Mean	+0.020	-0.016	+0.010	+0.025	+0.028
RMS	0.076	0.037	0.018	0.031	0.044

Table 10. Photometric statistics for red stars (g'-r' > 0).

	u'	*g'*	*r'*	*i'*	*z'*
Mean	-0.014	-0.023	+0.004	+0.019	+0.011
RMS	0.046	0.040	0.013	0.024	0.023

Table 11. Photometric statistics for blue stars (g'-r' < 0).

	u'	*g'*	*r'*	*i'*	*z'*
Mean	+0.095	0.000	+0.021	+0.038	+0.066
RMS	0.118	0.030	0.025	0.043	0.070

Table 12. Combined synthetic and photometric statistics for blue stars.

	u'	*g'*	*r'*	*i'*	*z'*
Mean	+0.085	+0.018	+0.015	+0.026	+0.043
RMS	0.099	+0.032	+0.024	0.037	0.052

Table 8. The mean and the RMS of the differences in Table 8 are summarized in Table 9. These statistics will be discussed in the next section along with those from the synthetic magnitude comparison.

4. Discussion and conclusions

Tables 4 and 9 listed the mean and RMS differences of catalogue minus synthetic magnitudes and of catalogue minus photometric magnitudes, respectively. The RMS values (which are necessarily larger than the means) are generally consistent with the uncertainties quoted in the catalogue, that is, 0.03 magnitude in the g', r', i', and z' band, and 0.08 in the u' band. To be more specific, the values for u' and r' are within the quoted uncertainties, the i' values come close, and those for g' and z' are somewhat greater. In the context of error estimation this level of validation is satisfactory.

The largest mean and RMS differences are those of the u' band for the synthetic magnitude comparison, 0.075 and 0.080, respectively. The similarity of their sizes implies that the most of the RMS difference is due to the mean. Such a finding is not surprising as Chonis and Gaskell (2008) and others have reported similar difficulties with the u' bandpass.

Since the stars selected for the synthetic comparison were all blue (g'–r' < 0), it is informative to separate the blue stars from the red in the photometric comparison. The red star results are shown in Table 10 while the blue results are in Table 11. Now it is apparent that the means for the u' filter of the blue photometric stars from Table 11 and those of the blue-by-default synthetic stars in Table 4 are similar at +0.095 and +0.075, respectively. Given the findings for the u' band, it is reasonable to separate the statistical results by color. Thus, the RMS values of the u', r', i' and z' bands for red photometric stars in Table 10 are all found to be within the quoted uncertainties while g' is slightly high (0.040 statistically as compared to 0.03 quoted). The synthetic and photometric results for all blue stars are averaged in Table 12. The RMS values for the g', r' and i' bands (+0.032, +0.024 and +0.037) approximate the 0.03 quoted uncertainties, while those for u' and z' (+0.099 and +0.052) both exceed the quoted values by about 0.02 magnitude.

Finally, the results for red and blue stars are plotted along with the uncertainties from the catalogue in Figure 2. The quoted uncertainties are seen to be generally consistent with the RMS values derived by comparing catalogue magnitudes with synthetic and photometric values.

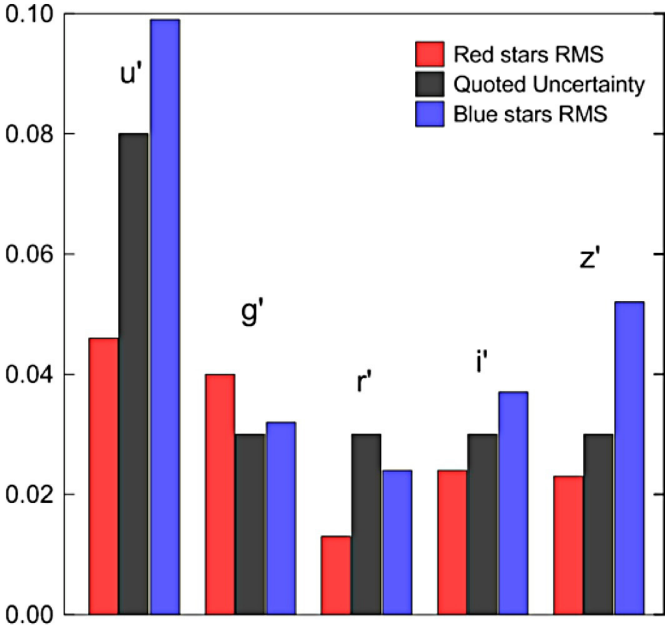

Figure 2. RMS differences for red and blue stars compared with uncertainties quoted in the catalogue.

5. Suggestions for observing with small telescopes

The measured accuracy of the catalogue "Sloan Magnitudes for the Brightest Stars" has been shown to approximate the values quoted in that paper. The uncertainties of the g', r', i', and z' magnitudes are precise enough for many useful investigations of bright objects as described later in this section. Ultraviolet (u') observations are always difficult to measure due to high atmospheric extinction and weak signals at those wavelengths, so their rather large uncertainty is not surprising. Chonis and Gaskell (2008) have commented on this. An alternative to using the u' (and other) catalogue magnitudes is to tie additional bright stars to the Sloan system by direct photometry.

Bright objects would saturate the detectors in most large observatory instrument being used today. However, the strong signals and (in some cases) the nearness of these stars to the Earth allow better spatial, photometric, and spectroscopic resolution than is possible for more distant stars. Therefore bright stars are important and the catalogue is especially well suited as a photometric reference.

One example where bright Sloan reference stars could be useful concerns novae. The magnitudes of bright novae can be accurately measured for a longer period of time than can those of faint ones. An uncertainty of 0.03 for the magnitude of the reference star is relatively small in comparison to the brightness variations of novae which may exceed 10 magnitudes. The same is true of other bright variable stars having large amplitudes.

The planets, which are all brighter than r' ~ +8, are also well suited for observing with reference stars from the catalogue. The authors of this paper, along with several other observers, have recorded and studied the brightness variations of the planets on the Johnson-Cousins system for many years. These analyses have revealed characteristics of the surface of Mercury (Mallama *et al.* 2002) and led to the detection of sulfuric acid droplets at very high altitudes in the atmosphere of Venus (Mallama *et al.* 2006), among other findings. We are now recording planetary magnitudes on the Sloan system.

Photometry of the bright satellites of Jupiter and Saturn as well as those of the large asteroids could also be pursued with small telescopes using reference magnitudes from the catalogue. Sloan magnitudes for the satellites and asteroids have not yet been determined as far as we know.

Sloan filters are now commercially available for CCD cameras and photometers. So, amateur observers can make important contributions to astronomical research by recording observations on this photometric system. The capability to report Sloan magnitudes will become more critical over time in order to maintain compatibility with the professional community. Sloan filters are being installed in most new photometric instruments being developed for large observatories and for spacecraft.

6. Acknowledgement

The authors wish to thank the anonymous reviewer whose knowledgeable comments led to significant improvements in the manuscript.

References

Berry, R., and Burnell, J. 2011, "Astronomical Image Processing for Windows," version 2.4.0, provided with *The Handbook of Astronomical Image Processing*, Willmann-Bell, Richmond, VA.

Bohlin, R. C., Gordon, K. D., and Tremblay, P.-E. 2014, *Publ. Astron. Soc. Pacific*, **126**, 711 (DOI 10.1086/677655).

Bohlin, R. C., and Landolt, A. U. 2015, *Astron. J.*, **149**, 122 (DOI 10.1088/0004-6256/149/4/122).

California Institute of Technology. 2015, Apeture Photometry Tool (APT; http://www.aperturephotometry.org/).

Chonis, T. S., and Gaskell, C. M. 2008, *Astron. J.*, **135**, 264 (DOI 10.1088/0004-6256/135/1/264).

Fukugita, M., Ichikawa, T., Gunn, J. E., Doi, M., Shimasuka, K., and Schneider, D. P. 1996, *Astron. J.*, **111**, 1748 (DOI 10.1086/117915).

Hardie, R. H. 1962, in *Astronomical Techniques*, ed. W. A. Hiltner, University of Chicago Press, Chicago, 178.

Johnson, H. L., Mitchell, R. I., Iriarte, B., and Wisniewski, W. Z. 1966, *Commun. Lunar Planet. Lab.*, **4**, 99.

Mallama, A. 2014, *J. Amer. Assoc. Var. Star Obs.*, **42**, 443.

Mallama, A. 2015, *J. Amer. Assoc. Var. Star Obs.*, **43**, 64.

Mallama, A., Wang, D., and Russell, R. A. 2002, *Icarus*, **155**, 253 (http://dx.doi.org/10.1006/icar.2001.6723).

Mallama, A., Wang, D., and Russell, R. A. 2006, *Icarus*, **182**, 10 (http://dx.doi.org/10.1016/j.icarus.2005.12.014).

Oke, J. B., and Gunn, J. E. 1983, *Astrophys. J.*, **266**, 713 (DOI 10.1086/160817).

Smith, J. A., *et al.* 2002, *Astron. J.*, **123**, 2121 (DOI 10.1086/339311).

Discovery of an "Eclipse" in the WC9d-Type Wolf-Rayet Star, WR 53

Rod Stubbings
Tetoora Road Observatory, 2643 Warragul-Korumburra Road, Tetoora Road 3821, Victoria, Australia; stubbo@sympac.com.au

Received August 26, 2015; revised September 9, 2015; accepted September 18, 2015

Abstract The WC9d- type Wolf-Rayet star WR 53 was observed visually entering into an "eclipse" with a depth of 1.2 magnitude Subsequent visual and CCD data showed a steady linear rise over 10 days to recover and return to its normal brightness level. This is the first-ever recorded "eclipse" of this star which has previously shown no photometric variability.

1. Introduction

Wolf-Rayet stars (WR-stars) are massive, luminous stars with unusual spectra showing prominent broad emission lines of helium, nitrogen, or carbon. Some Wolf–Rayet stars of the carbon sequence ("WC"), especially those belonging to the latest types, are noticeable due to their production of dust. They have lost or burnt almost all of their hydrogen and are now fusing helium in their cores, or heavier elements for a very brief period at the end of their lives.

Infrared (IR) excess due to the existence of dust in the winds of WC late-type stars was identified by Allen *et al.* (1972), Gehrz and Hackwell (1974), and Cohen *et al.* (1975). The dust shells are being restored as the dust is swept away by the stellar wind. With new dust being formed continuously in some WC stars, this suggested their designation as persistent dust makers by Williams and van der Hucht (2000). The classification introduced by van der Hucht (2001) was WCd, with "d" indicating a persistent dust maker.

A totally different manifestation of dust formation by WR stars is eclipsing of the visual light by line-of-sight dust clumps that are not caused by the companion, or variability of the star itself. This model was developed by Veen *et al.* (1998), who suggest occasional "eclipses" shown by other dusty WC stars (like WR 103, WR 113, and WR 121) are obscurations by clouds in the line of sight. Another significant observation was the color changes during the "eclipses" of WR 103 and WR 121. It shows the star becomes redder, caused by short term condensing dust clouds Veen *et al.* (1998).

The presence of dust shells around WC late- type stars was also investigated by Williams *et al.* (1987) using infrared photometry, who found WR 53 to be a dust maker from its IR emission. The spectrum of WR 53 has since been reclassified from WC8d to WC9d by Crowther *et al.* (1998).

General information on WR stars can be found in the catalogue by Crowther (2007).

The discovery and a well-defined "eclipse" of WR 53 is presented in this paper.

2. History

The discovery of a probable HI interstellar bubble associated with the Wolf-Rayet star WR 53 was found by Martin *et al.* (2007).

Photometric V- and I-band variability in WR 53 was not detected in a 20-day run by Fahed *et al.* (2009).

Photometry from ASAS-3 V-band data during the years 2001–2010 showed no eclipse or fading events (Pojmański 1997; Williams 2014).

All the surveys (ASAS-3, HIPPARCOS (Perryman *et al.* 1997), and APASS) have recorded WR 53 having V ~ 10.53 over the past decades.

3. Observations

Visual observations of WR 53 first started in 2005 by Albert Jones who noted some slight variations. The author (RS) monitored WR 53 from 2011, also showing variations. These variations have yet to be proved as past photometric data on WR 53 have shown the star to be constant.

On July 15, 2015, a visual observation of WR 53 showed it to be fainter than normal at magnitude 10.7. The previous estimate on July 7 was recorded at 10.5. The next observation was on July 19, and the star had notably faded further to magnitude 11.0. The following night a further drop in brightness to 11.5 was observed and this was clearly an "eclipse" event in progress. A request was sent privately that night to Peter Nelson to take an image of WR 53, which showed the star at V = 11.66. An alert request was then sent to observers for follow-up CCD time series observations, which were commenced the next night, along with visual observations during this event until the star returned to its normal quiescence level of V = 10.53.

The "eclipse" was first noticed on July 15, and from this point showed a fading trend of 5 days to minimum, with a depth of 1.2 magnitude. A steady linear rise of 10 days followed. The light curve is presented in Figure 1.

A spectrum was obtained after the "eclipse" event at the El Leoncito Astronomical Complex CASLEO (Argentina) which was similar to ones published in 2001 and 2012 (Gamen 2015).

Data from the AAVSO Photometric All-Sky Survey (APASS; Henden *et al.* 2014) taken a month earlier on JD 2457163.2416 (May 20, 2015) showed a (B–V) of 0.45. Both V and B bands were observed during the egress of this "eclipse." From the AAVSO database (Kafka 2015) on JD 2457225.4733 (July 21) the (B–V) was 0.52 just after minimum. On JD 2457236.4693 (August 1), at the end of the "eclipse," the (B–V) was 0.45. This shows a slight reddening during minimum. The light curve is presented in Figure 2.

4. Summary

WR 53 has been constantly monitored visually by the

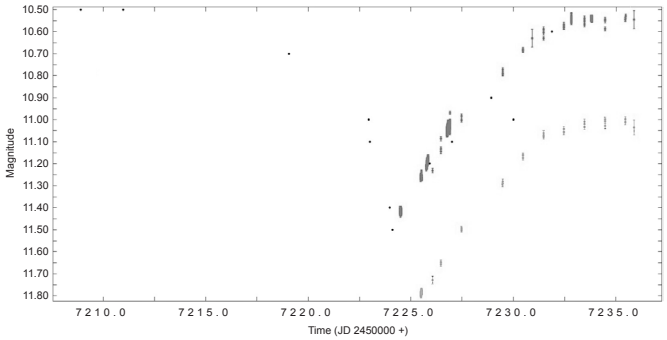

Figure 1. Light curve of WR 53. AAVSO data from JD 2457208 through JD 2457236 (July 4, 2015–August 1, 2015) showing the first ever "eclipse" of the Wolf-Rayet star WR 53. Black dots (no error bars) are visual data, dark gray (mid-plot) are Johnson V, and light gray (lower right) are Johnson B.

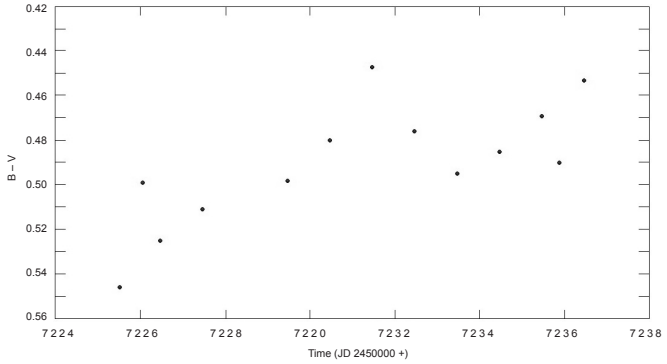

Figure 2. Light curve of WR 53 (B–V). AAVSO data from JD 2457225.4733 through JD 2457236.4693 (July 21, 2015–August 1, 2015) showing a slight reddening at minimum and the rising trend.

author since 2011 with no sign of deep fading episodes. ASAS3 V-band data during the years 2001–2010 showed no eclipse or fading events (Williams 2014). There was a dip in 2003 around magnitude 10.8 but the data showed no faint observations either side of this. Another dip in the data in 2008, again around 10.8, showed no observations a few days before and up to a week later. Given that the discovered "eclipse" activity lasted for over 15 days and at a depth of 1.2 magnitude, the dip also seems unlikely. Of course, there are the usual seasonal gaps in the observing where shallow "eclipses" could have been missed.

WR 53 is one of only a few of the late-type WC stars that has shown a deep "eclipse"; WR 104 (2.7 mag.) and WR 103 (1.3 mag.) are others. Typically, their durations can last up to several weeks as shown by Veen *et al.* (1998). Apart from WR 104 and WR 106, which show frequent "eclipses" of varying depths, other WC8 and WC9 stars have only shown shallow "eclipses" after years of monitoring (Williams 2014). What becomes apparent is how rare these "eclipse" events are in WC late-type stars.

An intensive monitoring program of WR 53 is needed to find more "eclipse" events in the hope that spectra and photometric multi-color monitoring can be taken when this occurs.

The present discovery of this "eclipse" event in WR 53 has established its variability and has now been included as a variable star in the International Variable Star Index (VSX) (Watson *et al.* 2015).

5. Acknowledgements

It is a pleasure to thank P. M. Williams for his comments. This research has made use of the International Variable Star Index (VSX) database, operated at AAVSO, Cambridge, Massachusetts, USA, and through the use of the AAVSO Photometric All-Sky Survey (APASS), funded by the Robert Martin Ayers Sciences Fund. I would like to thank Peter Nelson for providing a V- band image when faint, Josch Hambsch and Rolf Carstens for follow-up CCD observations. I would also like to thank the anonymous referee whose comments and suggestions were very helpful.

References

Allen D. A., Harvey P. M., and Swings, J. P. 1972, *Astron. Astrophys.*, **20**, 333.

Benn, D. 2012, *J. Amer. Assoc. Var. Star Obs.*, **40**, 852.

Cohen, M., Barlow, M. J., and Kuhi, L.V. 1975, *Astron. Asstrophys.*, **40**, 291.

Crowther, P. A. 2007, *Ann. Rev. Astron. Astrophys.*, **45**, 177.

Crowther, P. A., De Marco, O., and Barlow, M. J. 1998, *Mon. Not. Roy. Astron. Soc.*, **296**, 367.

Fahed, R., Moffat, A. F. J., and Bonanos, A. Z. 2009, *Mon. Not. Roy. Astron. Soc.*, **392**, 376.

Gamen, R. 2015, private communication.

Gehrz, R. D., and Hackwell, J. A. 1974, *Astrophys. J.*, **194**, 619.

Henden, A. A., *et al.* 2014, AAVSO Photometric All-Sky Survey, data release 8 (http://www.aavso.org/apass).

Kafka, S. 2015, observations from the AAVSO International Database (http://www.aavso.org).

Martin, M. C., Cappa, C. E., and Testori, J. C. 2007, *Rev. Mex. Astron. Astrofis.*, **43**, 243.

Perryman, M. A. C., European Space Agency Space Science Department, and the Hipparcos Science Team. 1997, The Hipparcos and Tycho Catalogues, ESA SP-1200 (VizieR On-line Data Catalog: I/239), ESA Publications Division, Noordwijk, The Netherlands.

Pojmański, G. 1997, *Acta Astron.*, **47**, 467.

van der Hucht, K. A. 2001, *New Astron. Rev.*, **45**, 135.

Veen, P. M., van Genderen, A. M., van der Hucht, K. A., Li, A., Sterken, C., and Dominik, C. 1998, *Astron. Astrophys.*, **329**, 199.

Watson, C., Henden, A. A., and Price, C. A. 2015, AAVSO International Variable Star Index VSX (Watson+, 2006–2015; http://www.aavso.org/vsx).

Williams, P. M. 2014, *Mon. Not. Roy. Astron. Soc.*, **445**, 1253.

Williams, P. M., and van der Hucht, K. A. 2000, *Mon. Not. Roy. Astron. Soc.*, **314**, 23 .

Williams, P. M., van der Hucht, K. A., and Thé, P. S. 1987, *Astron. Astrophys.*, **182**, 91.

A Photometric Study of the Eclipsing Variable Star NSVS 3068865

Robert C. Berrington
Ball State University, Department of Physics and Astronomy, Muncie, IN 47306; rberring@bsu.edu

Erin M. Tuhey
Ball State University, Department of Physics and Astronomy, Muncie, IN 47306; emtuhey@bsu.edu

Received May 22, 2014; revised August 13, 2014 and October 26, 2015; accepted November 12, 2015

Abstract We present new multi-band differential aperture photometry of the eclipsing variable star NSVS 3068865. The light curves are analyzed with the Wilson-Devinney model to determine best-fit stellar models. Our models show that NSVS 3068865 is consistent with a W Ursae Majoris eclipsing variable star near thermal contact with similarities to the aforementioned proto-type.

1. Introduction

The star NSVS 3068865 [= TYC 3929-1500-1, R. A. = 19^h 21^m 4.43^s, Dec. = +56º 19' 41.1", J2000.0] was designated [GGM2006] 3068864 by Gettel *et al.* (2006) and found to be an eclipsing variable star by using the photometric data from the Northern Sky Variability Survey (NSVS; Woźniak 2004) with a period of P = 0.334292 day. Later, the automated classification system developed by Hoffman *et al.* (2009) classified the star as a W Ursae Majoris contact eclipsing binary and reported a photometric period of P = 0.33428 day. The NSVS is a search for variability in the stars observed with the Robotic Optical Transient Search Experiment (ROTSE-1; Woźniak 2004). The primary goal of the NSVS is to search for optical transients associated with quick response to Gamma-Ray Burst (GRB) events reported from satellites to measure optical light curves of GRB counterparts. When no GRB events were available, ROSTE-I was devoted to a systematic sky patrol of the sky northward of declination δ = –38º.

In this paper we present a new extensive photometric study of this system. The paper is organized as follows. Observational data acquisition and reduction methods are presented in section 2. Time analysis of the photometric light curve and Wilson-Devinney models are presented in section 3. Discussion of the results and conclusions are presented in section 4.

2. Observational data

We present new three-filter photometry of the eclipsing variable star NSVS 3068865. The data were taken by the Meade 0.4-meter Schmidt Cassegrain telescope within the Ball State University observatory located atop the Cooper science complex. All exposures were acquired by a Santa Barbara Instruments Group (SBIG) STL-6303e camera through the Johnson-Cousins B, V, and R (R_C) filters on the nights of July 12, 13, 14, 16, and 18, 2013. All images were bias and dark current subtracted, and flat field corrected using the CCDRED reduction package found in the Image Reduction and Analysis Facility (IRAF) version 2.16 (IRAF is distributed by the National Optical Astronomy Observatories, http://iraf.net/). All photometry presented is differential aperture photometry and was performed on the target eclipsing candidate and two comparison standards by the AIP4WIN (v2.2.0) photometry package (Berry and Burnell 2005). Over the three nights a total of 482 images were taken in B, 486 images in V, and 510 images in R_C. Figure 1 shows a representative exposure with the eclipsing star candidate and the two comparison stars marked. We have chosen the Tycho catalog star (Høg *et al.* 2000) TYC 3929-1375-1 as the primary comparison star (C1). The folded light curves (see section 3.1) for the instrumental differential B, V, and R_C magnitudes are shown in Figure 2, and are defined as the variable star magnitude minus C1 (Variable – C1). Also shown (bottom panel) in Figure 2 is the differential V magnitude of C1 minus the second comparison star (C2, TYC 3929-1366-1), or the check star. The comparison light curve was inspected for variability. None was found.

Measured instrumental B and V differential magnitudes were reduced onto Johnson B and V magnitudes by comparison with known calibrated magnitudes for C1. The star C1 has measured Johnson B and V magnitudes of 11.37 ± 0.07 and 10.66 ± 0.05, respectively Høg *et al.* (2000). The calibrated

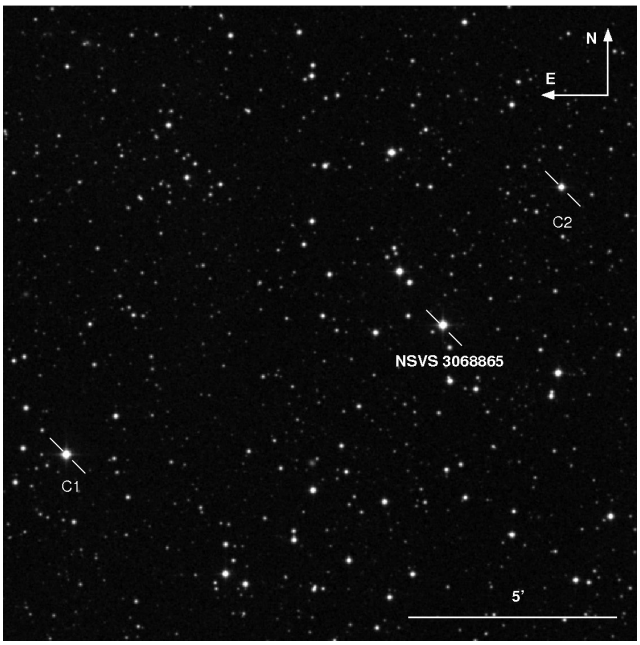

Figure 1. Star field containing the variable star NSVS 3068865. The location of the variable star is shown along with the comparison (C1) star TYC 3929-1375-1 and the check (C2) star TYC 3929-1366-1used to calculate the differential magnitudes reported in Figure 2.

V light curve with the (B–V) color index versus orbital phase is shown in Figure 3 with error bars removed for clarity. The orbital phase (Φ) is defined as:

$$\Phi = \frac{T - T_0}{P} - \text{Int}\left(\frac{T - T_0}{P}\right), \quad (1)$$

where T_0 is the ephemeris epoch and is the time of minimum of a primary eclipse. Throughout this paper we will use the value of 2456487.66872 for T_0. The variable T is the time of observation, and P is the period of the orbit. The value of Φ ranges from a minimum of 0 to a maximum of 1.0. All light curve figures will plot phase values (–0.6,0.6) where the negative values are given by Φ – 1. Simultaneous B and V magnitudes are used to determine (B–V) colors by linear interpolating between measured B magnitudes to a similar time for measured V magnitudes.

3. Analysis

3.1. Period analysis and ephemerides

Heliocentric Julian dates (HJD) for the observed times of minimum were calculated for each of the B, V, and R_C band light curves shown in Figure 2 for all observed primary and secondary minima. A total of three primary eclipses and three secondary eclipses were observed for each band. The times of minimum are determined by the algorithm described by Kwee and van Woerden (1956). Similar times of minimum from differing band passes were compared and no significant offsets or wavelength-dependent trends were observed. Similar times of minimum from each of the band passes were averaged together and reported in Table 1 along with 1σ error bars.

Light curves were inspected by the PERANSO (v2.5) software (CBA Belgium Observatory 2011) to determine the orbital period by applying the analysis of variance (ANOVA) statistic, which uses periodic orthogonal polynomials to fit observed light curves (Schwarzenberg-Czerny 1996). Our best-fit orbital period was found to be 0.33440 ± 0.00037 day and is consistent (<1σ) with the orbital period reported by Hoffman *et al.* (2009), which uses the photometric data reported by the NSV survey (Woźniak 2004). The resulting linear ephemeris becomes

$$T_{min} = 2456487.66872(26) + 0.33440(37)E \quad (2)$$

where the variable E represents the epoch number, and is a count of orbital periods from the epoch T_0 = 2456487.66872. Figure 2 shows the folded differential magnitudes versus orbital phase for NSVS 3068865 for the B, V, and R_C Johnson-Cousins bands folded over the period determined by the current photometric study.

The observed minus calculated residual times of minimum (O–C) were determined from Equation 2 and are given in Table 1 along with 1σ error bars. The best-fit linear line determined by a linear regression to the (O–C) residual values is shown in Figure 11, and indicates the times of minima are well described by an orbital period of 0.33438 ± 0.00040 day, and is consistent with our previously determined value from

Table 1. Calculated heliocentric Julian dates (HJD) for the observed times of minimum for NSVS 3068865.

T_{min}	Eclipse	E	(O–C)
2456487.66872 ± 0.00026	p	0	0
2456487.83712 ± 0.00019	s	0.5	0.00112 ± 0.00030
2456489.67456 ± 0.00019	p	6	0.00056 ± 0.00029
2456489.84345 ± 0.00017	s	6.5	0.00113 ± 0.00029
2456491.68105 ± 0.00014	p	12	-0.00047 ± 0.00046
2456491.84843 ± 0.00033	s	12.5	-0.00029 ± 0.00056

Notes: Calculated heliocentric Julian dates (HJD) for the observed times of minimum (column 1) with the type of minima (column 2). Observed minus Calculated (O–C) residual (column 4) values are given for the linear ephemeris given in Equation 2. All reported times are averaged from the individual B-, V-, and R-band times of minimum determined by the algorithm described by Kwee and van Woerden (1956). All (O–C) values are given in units of days with primary eclipse values determined from integral epoch numbers, and secondary eclipse values determined from half integral epoch numbers (column 3).

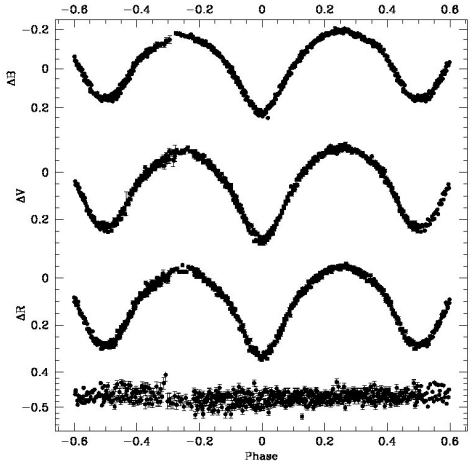

Figure 2. Folded light curves for differential aperture Johnson-Cousins B-, V-, and R_C-band magnitudes. Phase values are defined by Equation 1. Top three panels show the folded light curves for Johnson B (top panel), Johnson V (middle panel), and Cousins R_C (bottom panel) magnitudes. Bottom panel shows differential Johnson V-band magnitudes for the comparison minus the check star. All error bars are 1σ error bars. Repeated points do not show error bars (points outside the phase range of (–0.5,0.5)).

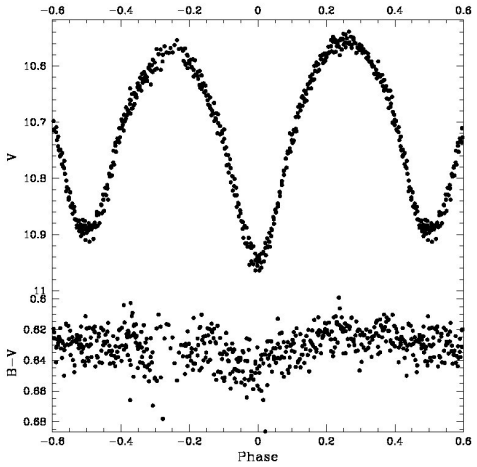

Figure 3. Folded light curve for differential aperture Johnson V-band magnitudes (top panel) and (B–V) color (bottom panel) versus orbital phase. Phase values are defined by Equation 1. Error bars are not shown for clarity. All (B–V) colors are calculated by subtracting linearly interpolated B magnitudes from measured V magnitudes.

PERANSO at 1σ deviation. For all subsequent fitting the orbital period of 0.33440 ± 0.00037 day will be assumed, and does not change any of the results of this study.

Effective temperature and spectral type are estimated from the (B–V) color index values measured at orbital quadrature (Φ = ±0.25) with a value of (B–V) = 0.63 ± 0.03. Interstellar extinction estimates following (Schlafly and Finkbeiner 2011) at the galactic coordinates for the object are E(B–V) = 0.084. The resulting intrinsic color becomes $(B–V)_0$ = 0.54 ± 0.03. Effective temperatures and errors were estimated by Table 3 from Flower (1996) to be T_{eff} = 6118 ± 120K. The corresponding stellar spectral type is a F8 (Fitzgerald 1970) with an estimated stellar mass $M_\star = 1.20^{+0.04}_{-0.03} M_\odot$ derived from Equation 4 of Harmanec (1988). It should be noted that these masses are for normal main sequence stars, and may be suspect. We include them in the analysis as an estimate on the stellar mass only. Furthermore, the 2MASS All Sky Survey (Skrutskie *et al.* 2006) reports a (J–H) = 0.29 ± 0.04 for NSVS 3068865 which corresponds to a spectral type of F8 (Ducati *et al.* 2001) after correcting for interstellar extinction ($(J–H)_0$ = 0.27 ± 0.04) following Schlafly and Finkbeiner 2011), and supports our prior claim despite the unknown orbital phase at which the 2MASS magnitudes were obtained. The semi-major axis (a) is determined by Kepler's third law.

3.2. Light curve analysis

All observations taken during this study were analyzed using the Physics of Eclipsing Binaries (PHOEBE) software package (v0.31a) (Prša and Zwitter 2005). The PHOEBE software package is a modeling package that provides a convenient, intuitive graphical user interface (GUI) to the Wilson-Devinney (WD) code (Wilson and Devinney 1971). Table 2 summarizes the authors' analysis for NSVS 3068865.

All three Johnson-Cousins B, V, and R_C bands were fit simultaneously by the following procedure. Initial fits were performed assuming a common convective envelope in direct thermal contact resulting in a common surface temperature of T_{eff} = 6118K determined by the procedure discussed in section 3.1. Orbital period was set to the value of 0.33440 ± 0.00037 day. Surface temperatures imply that the outer envelopes are convective so the gravity brightening coefficients β_1 and β_2, defined by the flux dependency $F \propto g^\beta$, were initially set at the common value consistent with a convective envelope of 0.32 (Lucy 1967). The more recent studies of Alencar and Vaz (1997) and Alencar *et al.* (1999) predict values for $\beta \approx 0.4$. These values were also used but had no effect on the resulting best-fit model. We adopted the standard stellar bolometric albedo $A_1 = A_2 = 0.5$ as suggested by Ruciński 1969) with two possible reflections.

The fitting procedure was used to determine the best-fit stellar models and orbital parameters from the observed light curves shown in Figure 2. Initial fits were performed assuming a common convective envelope in thermal contact which assumes similar surface temperatures for both after normalization of the stellar luminosity, the light curve was crudely fit by altering the stellar shape by fitting the Kopal (Ω) parameter. The Kopal parameter describes the equipotential surface that the stars fill.

Table 2. Model parameters for NSVS 3068865 determined by the best-fit WD model.

Parameter	*Symbol*	*Value*	
		Stellar spots not allowed	*Stellar Spots allowed*
Period	P_0 [days]	0.33440 ± 0.00037	0.33440 ± 0.00037
Epoch	T_0 [HJD]	2456487.66872 ± 0.00026	2456487.66872 ± 0.00026
Inclination	i [º]	66.26 ± 0.29	66.00 ± 0.29
Semimajor Axis[a]	a [$R_\odot$]	2.72 ± 0.20	2.72 ± 0.20
Surface Temp.	$T_{eff,1}$ [K]	6118. ± 120	6118. ± 120
	$T_{eff,2}$ [K]	6066. ± 120	6122. ± 120
Surface Potential	$\Omega_{1,2}$ [—]	3.624 ± 0.043	3.570 ± 0.043
Mass Ratio	q [—]	0.95 ± 0.02	0.92 ± 0.02
Luminosity	$[L_1/(L_1 + L_2)]_B$	0.573 ± 0.005	0.571 ± 0.004
	$[L_1/(L_1 + L_2)]_V$	0.559 ± 0.006	0.560 ± 0.005
	$[L_1/(L_1 + L_2)]_{R_C}$	0.550 ± 0.008	0.552 ± 0.006
Stellar Mass[a]	M_1 [$M_\odot$]	1.24 ± 0.24	1.26 ± 0.24
	M_2 [$M_\odot$]	1.17 ± 0.24	1.15 ± 0.24
Limb Darkening	$x_{bol,1,2}$	0.644	0.644
	$y_{bol,1,2}$	0.225	0.225
	$x_{B,1,2}$	0.823	0.823
	$y_{B,1,2}$	0.197	0.197
	$x_{V,1,2}$	0.736	0.736
	$y_{V,1,2}$	0.262	0.263
	$x_{R,1,2}$	0.644	0.644
	$y_{R,1,2}$	0.271	0.271
Spot Colatitude	ϕ_1 [º]	—	90
Spot Longitude	λ_1 [º]	—	0
Spot Radius	ϱ_1 [º]	—	45
Temperature Factor	τ_1 [—]	—	0.95

Notes: Values for the best fit stellar model not allowing for the presence of stellar spots (column 3) as well as best fit values for models allowing for the presence of stellar spots (column 4). Some parameters can be further specified by a the numerical value 1 for the primary stellar component, or 2 for the secondary stellar component. Fitting procedure is described in sections 3.2 and 3.3. Surface potentials for both stars for contact/overcontact binaries is defined to be of equal value for both stars. Errors for surface temperatures (T_{eff}) were estimated from color values in Figure 3. Please note that the parameters L_1 and L_2 refer to the luminosities of primary and secondary components, respectively. All remaining errors are 1σ errors. a) See section 3.1 for discussion.

For overcontact binaries, this has the effect of determining the shape of the stars, and has a strong effect on the the global morphology of the light curve.

After the fit could no longer be improved, we started to consider the other parameters to fit the light curve. These additional parameters were also allowed to vary with the previous parameters and included the effective temperature of the secondary star $T_{eff,2}$, the mass ratio $q = M_2 / M_1$ and the orbital inclination i. The mass ratio (q) was further refined after a standard q-search method was applied. In this method the mass ratio is fixed and all other parameters are allowed to converge to a best-fit model. The χ^2 values (sum of the squares of the residuals) are recorded for each fixed value of the mass ratio. The reported mass ratio is the minimum in the resulting curve. Minor improvement of the of the best-fit model could be achieved by decoupling stellar luminosities from T_{eff}. We interpreted this as the possibility that the stars are in poor thermal contact and therefore could have differing surface temperatures. All further model fits were performed assuming the primary and secondary components are in poor thermal contact.

All model fits were performed with a limb darkening correction. PHOEBE allows for differing functional forms to be specified by the user. Late-type stars (T_{eff} < 9000K) are best described by the logarithmic law that was first suggested by Klinglesmith and Sobieski (1970), and later supported by the more recent studies of Diaz-Cordoves and Gimenez (1992) and van Hamme (1993). The values for the linear (x_λ) and non-linear (y_λ) coefficients were determined at each fitting iteration by the van Hamme (1993) interpolation tables.

Figures 4 through 6 show the folded Johnson B, Johnson V, and Cousins R_C band light curves along with the synthetic light curve calculated by the best-fit model, respectively. The best-fit models were determined by the aforementioned fitting procedure. Note how the synthetic light curve consistently over-predicts the observed light curve for phases in the interval (–0.3,0.1), and under-predicts for phases in the interval (0.3,0.5). The parameters along with 1σ error bars describing this best-fit model are given in column 3 of Table 2.

The filling factor is defined by the inner and outer critical equipotential surfaces that pass through the L_1 and L_2 Lagrangian points of the system, and is given by the following equation:

$$\mathcal{F} = \frac{\Omega(L_1) - \Omega}{\Omega(L_1) - \Omega(L_2)} \quad (3)$$

where Ω is the equipotential surface describing the stellar surface, and $\Omega(L_1)$ and $\Omega(L_2)$ are the equipotential surfaces that pass through the Lagrangian points L_1 and L_2, respectively. For our system the these equipotential surfaces are $\Omega(L_1) = 3.669$ and $\Omega(L_2) = 3.149$. The best-fit model is consistent with an overcontact binary described by a filling factor $\mathcal{F} = 0.09 \pm 0.04$.

3.3. Spot model

It is apparent from Figures 4 through 6 that the previous model is unable to reproduce accurately the observed light curve. To improve the fit, a single spot was necessary. Unfortunately, all we have at our disposal are the observed light curves, and differing spot models may be degenerate to the observed light curve.

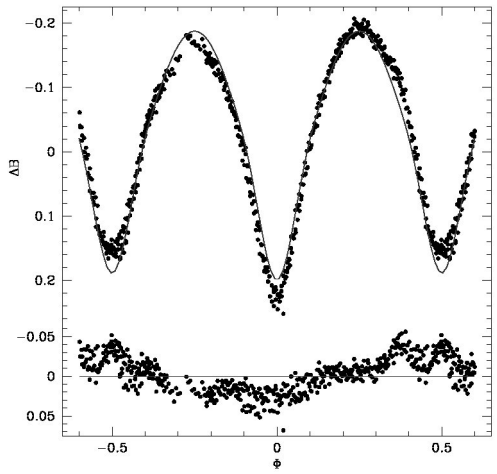

Figure 4. Best-fit WD model fit without spots (solid curve) to the folded light curve for differential Johnson B band magnitudes (top panel). The best-fit orbital parameters used to determine the light curve model are given in Table 2. The bottom panel shows residuals from the best-fit model (solid curve). Error bars are omitted from the points for clarity.

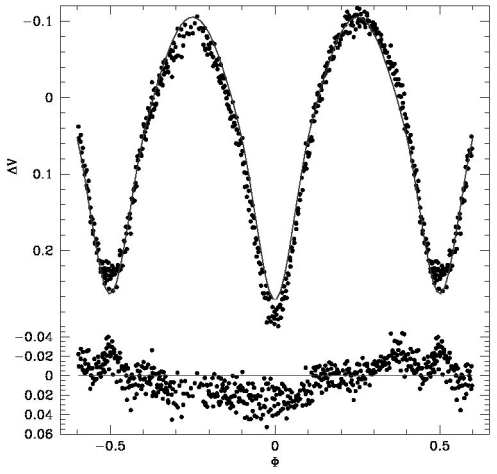

Figure 5. Best-fit WD model fit without spots (solid curve) to the folded light curve for differential Johnson V band magnitudes (top panel). The best-fit orbital parameters used to determine the light curve model are given in Table 2. The bottom panel shows residuals from the best-fit model (solid curve). Error bars are omitted from the points for clarity.

The best-fit model with a single cool spot on the primary star is given in Table 2. Spot parameters given by the WD model are the longitude θ, colatitude ϕ, radius ϱ, and temperature factor ($\tau = T_{spot} / T_{eff}$). The spot longitude is measured counterclockwise (CCW) from the L_1 Lagrangian point. Spot colatitude is measured from stellar rotation axis with the equator represented by $\phi = 90^o$. Light curves were found to be minimally dependent on the spot's colatitude and therefore difficult to converge when allowed to vary. All spot models restricted spots to be located on the equator ($\phi = 90^o$).

Initial models started from the model without spots determined in section 3.2. We were unsuccessful with simultaneous convergence of the parameters. The spot longitude eluded successful convergence, and forced a manual procedure. But both the spot radius and the spot temperature factor did

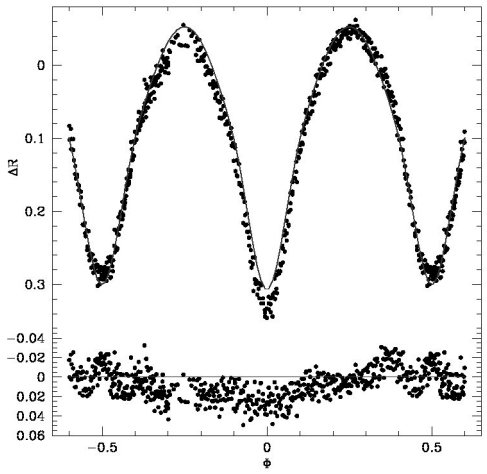

Figure 6. Best-fit WD model fit without spots (solid curve) to the folded light curve for differential R_C band magnitudes (top panel). The best-fit orbital parameters used to determine the light curve model are given in Table 2. The bottom panel shows residuals from the best-fit model (solid curve). Error bars are omitted from the points for clarity.

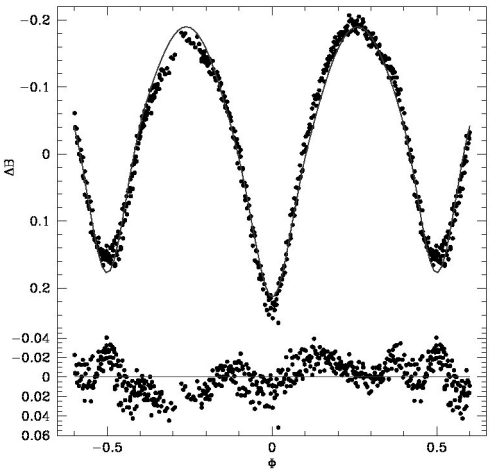

Figure 7. Best-fit WD model fit with a single spot (solid curve) to the folded light curve for differential Johnson B band magnitudes (top panel). The best-fit orbital parameters used to determine the light curve model are given in Table 2. The bottom panel shows residuals from the best-fit model (solid curve). Error bars are omitted from the points for clarity.

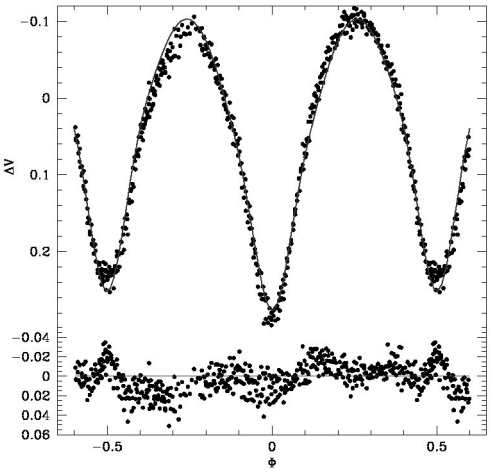

Figure 8. Best-fit WD model fit with a single spot (solid curve) to the folded light curve for differential Johnson V band magnitudes (top panel). The best-fit orbital parameters used to determine the light curve model are given in Table 2. The bottom panel shows residuals from the best-fit model (solid curve). Error bars are omitted from the points for clarity.

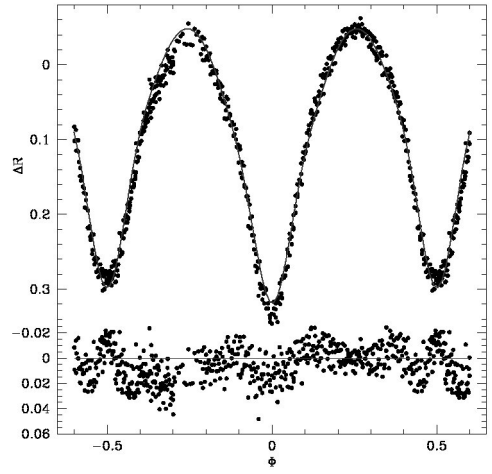

Figure 9. Best-fit WD model fit with a single spot (solid curve) to the folded light curve for differential R_C band magnitudes (top panel). The best-fit orbital parameters used to determine the light curve model are given in Table 2. The bottom panel shows residuals from the best-fit model (solid curve). Error bars are omitted from the points for clarity.

converge individually, but not conjointly. The best-fit spot model was determined by alternating between convergence of the spot radius and the spot temperature factor. Once a satisfactory convergence was determined, the spot parameters were then held fixed and the stellar parameters were then allowed to converge to the final model. Figures 7 through 9 show the final best-fit stellar model. Graphical representations for the best-fit spot WD model are shown in Figure 12.

Our best-fit spot model does fit the observed data well, but as noted above may be degenerate to alternate possible explanations for the observed deviations shown in Figures 4 through 6. The spot determined by the spot fitting procedure described above covers the majority of the hemisphere facing the stellar juncture (L_1) with a weak temperature factor $\tau \approx 1$.

4. Discussion and conclusions

Figure 10 shows a comparison of the NSVS light curve with the light curve measured during this study. It is immediately apparent that both the NSVS light curve and the light curve measured during this study show similar heights for max I ($\phi = 0.25$) and max II $\phi = -0.25$). Differing heights between max I and max II is known as the O'Connell effect (O'Connell 1951) and is not uncommon in overcontact binaries. Temporal variance of this effect has also been observed, but evidence for the O'Connell effect in NSVS 3068865 is minimal.

Recent studies have shown that degeneracies exist between the orbital inclination (i), mass ratio (q), and filling factor ($\mathcal{F}(\Omega)$) for partially eclipsing overcontact binaries (Terrell and Wilson 2005; Hambálek and Pribulla 2013). To investigate these degeneracies, we generated ten groups of B, V, R_C synthetic light curves from the observed light curve by the following procedure. Prior studies have shown that partially eclipsing overcontact binaries are accurately (rms residuals ~0.0002) represented by a Fourier series of 10th order (Rucinski 1993; Hambálek and Pribulla 2013). A mean light curve was first generated by fitting the observed light curve with a Fourier

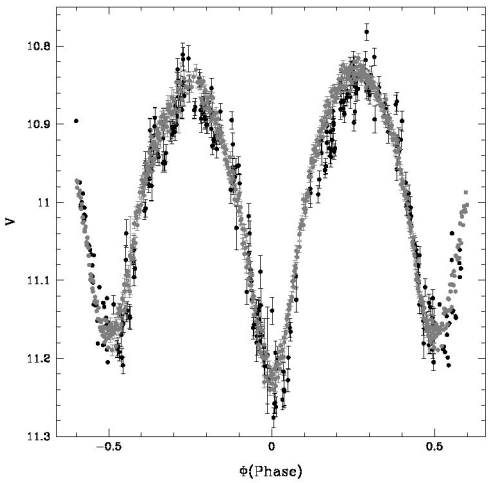

Figure 10. Folded light curve for Johnson V magnitudes. Grey points are measured magnitudes from the Ball State University 0.4m telescope. Measured values from the NSV Survey (Woźniak *et al.* 2004) are shown by the black points. Any systematic offsets resulting from the calibration of the unfiltered CCD magnitudes of the NSV survey (see text) are removed for comparison of light curves. All error bars are 1σ error bars. Repeated points do not show error bars.

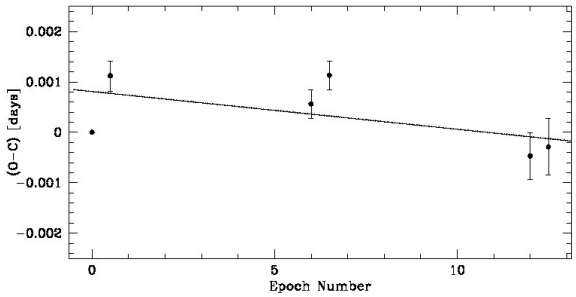

Figure 11. Observed minus calculated residual times of minimum (O–C) versus orbital epoch number. All point values are given in Table 1. Secondary times of minimum are plotted at half integer values, and all error bars are 1σ error bars. Solid curve shows the best-fit linear line determined by a linear regression fit to the (O–C) residual values.

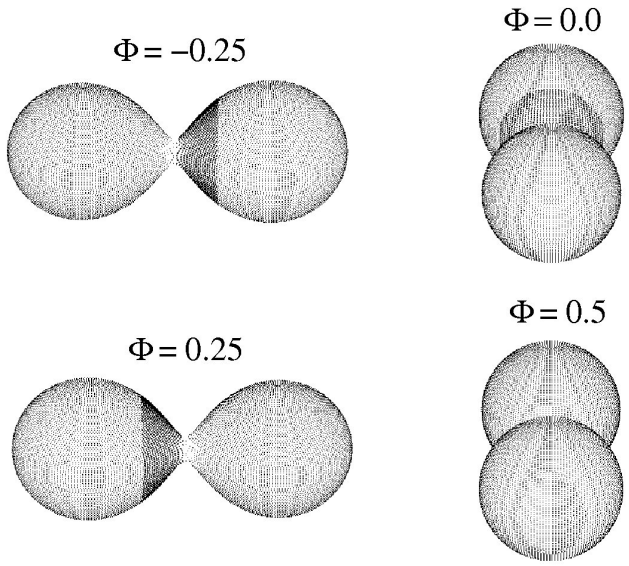

Figure 12. Graphical representation for the best-fit single spot WD model. The best-fit orbital parameters used to determine the light curve model are given in Table 2 Corresponding orbital phase is given in each panel.

series of 10th order. The synthetic light curve is then generated by adding a Gaussian deviate of standard deviation equal to the photometric error of the observed data point to the mean value generated by the Fourier representation at a similar phase determined by Equation 2. Solutions were obtained from three randomly selected starting points in the [i,q,Ω] parameter space for each of the ten synthetic light curve groups. All fits were run without any user input or guidance. We found our solution for the light curves to be remarkably robust. The errors reported for the best-fit parameters in Table 2 reflect the standard deviation of the range of values resulting for the synthetic light curve solutions. It is possible that degeneracies still exist in the [i,q,Ω] parameter space, but will require spectroscopic followup of NSVS 3068865 to break these degeneracies.

Given the best-fit model parameters in Table 2, we can estimate the distance to NSVS 3068865. (Rucinski and Duerbeck 1997) determined that the absolute visual magnitude is given by

$$M_V = -4.44 \log_{10}(P) + 3.02(B-V)_0 + 0.12 \qquad (4)$$

to within an accuracy of ±0.1. The distance modulus of the system (m – M) = 6.44. After accounting for the extinction (A_V = 0.26) determined from color excess given in section 3.1, we determined the distance to the system is 194 ± 10 pc, Distance errors do not account for possible errors in the extinction maps of Schlafly and Finkbeiner (2011).

This study has confirmed that NSVS 3068865 is a W UMa contact binary in or near thermal contact. Our measured light curve does not show conclusive evidence of the O'Connell effect, and was fairly well described by the stellar orbital parameters alone. The star NSVS 3068865 appears be consistent with a slightly larger primary component eclipsed during the primary minimum. A spot model with a single spot did improve the best-fit model. However, deviations from the light curve determined by the orbital parameters alone could not account for all the observed variation. We favored a single spot model with a weak temperature factor covering the hemisphere centered on the stellar juncture. This system shows similarities to the prototype W Ursae Majoris. Both systems are members of the W-subclass with similar orbital periods (Linnell 1991). While W UMa has shown to have an unpredictable O'Connell effect (Linnell 1991), NSVS 3068865, with a comparison to the previously measured NSVS data (Woźniak 2004), appears to have stable maxima of comparable brightness (see Figure 10). Further spectroscopic follow up will be necessary to place further constraints and to validate the stellar masses and orbital parameters to further improve our knowledge of the system.

5. Acknowledgements

We wish to thank both the referee and Edward Devinney for their detailed and constructive comments.

References

Alencar, S. H. P., and Vaz, L. P. R. 1997, *Astron. Astrophys.*, **326**, 257.

Alencar, S. H. P., Vaz, L. P. R., and Nordlund, Å. 1999, *Astron. Astrophys.*, **346**, 556.
Berry, R., and Burnell, J. 2005, *Handbook of Astronomical Image Processing*, Willmann-Bell, Richmond.
CBA Belgium Observatory. 2011, PERANSO (v2.51) software, Flanders, Belgium (http://www.cbabelgium.com/).
Diaz-Cordoves, J., and Gimenez, A. 1992, *Astron. Astrophys.*, **259**, 227.
Ducati, J. R., Bevilacqua, C. M., Rembold, S. B., and Ribeiro, D. 2001, *Astrophys. J.*, **558**, 309.
Fitzgerald, M. P. 1970, *Astron. Astrophys.*, **4**, 234.
Flower, P. J. 1996, *Astrophys. J.*, **469**, 355.
Gettel, S. J., Geske, M. T., and McKay, T. A. 2006, *Astron. J.*, **131**, 621.
Hambálek, Ľ., and Pribulla, T. 2013, *Contrib. Astron. Obs. Skalnaté Pleso*, **43**, 27.
Harmanec, P. 1988, *Bull. Astron. Inst. Czechoslovakia*, **39**, 329.
Hoffman, D. I., Harrison, T. E., and McNamara, B. J. 2009, *Astron. J.*, **138**, 466.
Høg, E., *et al.* 2000, *Astron. Astrophys.*, **355**, L27.
Klinglesmith, D. A., and Sobieski, S. 1970, *Astron. J.*, **75**, 175.
Kwee, K. K., and van Woerden, H. 1956, *Bull. Astron. Inst. Netherlands*, **12**, 327.
Linnell, A. P. 1991, *Astrophys. J.*, **374**, 307.
Lucy, L. B. 1967, *Z. Astrophys.*, **65**, 89.
O'Connell, D. J. K. 1951, *Publ. Riverview Coll. Obs.*, **2**, 85.
Prša, A., and Zwitter, T. 2005, *Astrophys. J.*, **628**, 426.
Ruciński, S. M. 1969, *Acta Astron.*, **19**, 245.
Rucinski, S. M. 1993, *Publ. Astron. Soc. Pacific*, **105**, 1433.
Rucinski, S. M., and Duerbeck, H. W. 1997, *Publ. Astron. Soc. Pacific*, **109**, 1340.
Schlafly, E. F., and Finkbeiner, D. P. 2011, *Astrophys. J.*, 737, 103.
Schwarzenberg-Czerny, A. 1996, *Astrophys. J., Lett. Ed.*, **460**, L107.
Skrutskie, M. F., *et al.* 2006, *Astron. J.*, **131**, 1163.
Terrell, D., and Wilson, R. E. 2005, *Astrophys. Space Sci.*, **296**, 221.
van Hamme, W. 1993, *Astron. J.*, **106**, 2096.
Wilson, R. E., and Devinney, E. J. 1971, *Astrophys. J.*, **166**, 605.
Woźniak, P. R., *et al.* 2004, *Astron. J.*, **127**, 2436.

Early Sixty-Day Observations of V5668 Sgr using a DSLR Camera

Shishir Deshmukh
Akash Mitra Mandal (Amateur Astronomers' Organization, Mumbai, India; shishir.supernova@gmail.com

Received July 25, 2015; revised September 28, 2015, accepted October 12, 2015

Abstract Photometric observations of V5668 Sgr (Nova Sagittarii 2015 No.2) were carried out using a consumer-grade DSLR camera. Observations were made under urban sky conditions for 60 days after discovery. The brightness of the nova was monitored with reference to several nearby reference stars using a Canon EOS 600D with CMOS sensor. Estimates were then transformed using a "median" B–V value of 0.28 into standard magnitude. Preliminary plot shows large variations, especially gradual rise and rapid falls.

1. Introduction

A Possible nova in Sagittarius was reported by John Seach, Chatsworth Island, NSW, Australia, on March 15, 2015 (CBAT 2015). The photograph was taken using DSLR and 50-mm f/1.0 lens. The object's estimated magnitude was 6.0 at the time of initial report. There was no object visible down to magnitude 10.5 on the image taken on March 14, 2015.

Follow-up observations taken by John Seach showed a bright H-alpha source visible on six DSLR images taken using a 50-mm f/1.0 lens and H-alpha filter. Subsequent observations were carried out by K. Itagaki and T. Yusa. Further, Ernesto Guido and Nick Howes confirmed the optical counterpart with R-CCD magnitude 5.8 at coordinates R. A. = 18^h 36^m 56.85^s, Dec. = –28° 55' 40.0" (equinox 2000.0; UCAC-4 catalogue reference stars (Zacharias *et al.* 2012)). They also compared their follow-up image taken remotely through a 0.61-m f/6.5 astrograph + CCD of the ITelescope network with the archive POSS2/UKSTU plate (R Filter-1996).

Nova Sgr 2015 No. 2 was subsequently assigned the name V5668 Sgr (Green 2015).

2. DSLR photometry: An overview

The application of consumer grade Digital Single Lens Reflex (DSLR) cameras for astronomical photometry was explored by Hoot (2007), Kloppenborg *et al.* (2012), and others. The variability measurement of variable stars is shown by Loughney (2010) and also by Collins and Prasai (2009).

3. Linearity check

An unmodified Canon EOS 600D camera was used throughout this project. A linearity check was performed so as to ensure that no measured star on the image was ever saturated.

In order to carry out the linearity test, images of an evenly illuminated surface were taken at different exposures, starting from 1/3 of a second to 60 seconds at the same speed at which the science images were taken. Using IRIS freeware (Buil 2015), mean green channel pixel counts were measured. The green channel pixel counts were then plotted against the exposure durations. The resultant plot (Figure 1) shows the response of the detector as a function of exposure duration in terms of pixel counts.

The mean count at which pixels became saturated was found to be a little less than 14,000. Care was taken that no comparison star, check star, or the target was ever saturated during any of the observation sessions of this project.

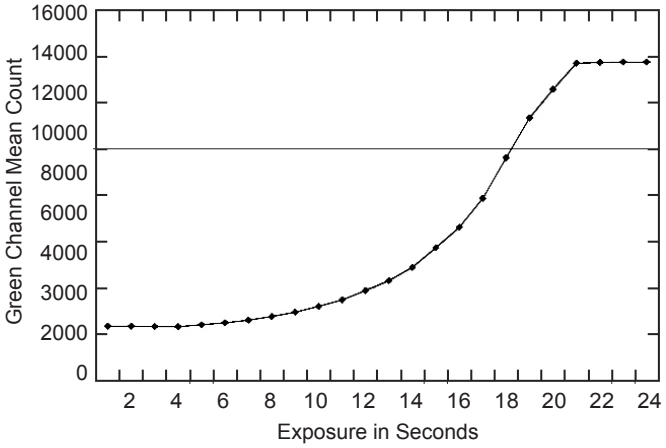

Figure 1. Linearity check plot.

4. Methodology

For photometric observations, a Canon EOS 600D camera was used with a 55- to 250-mm lens; no modifications were made to the camera. Since the images were taken from a light-polluted suburban sky, a suitable wide field focal length was selected to cover the nova and comparison stars in the same frame. Focusing was made manually by taking sample images prior to the science images. With no tracking device, short exposures of five seconds were taken for photometry to minimize the trails.

Exposures were taken at ISO 800 in order to compensate for short exposures. Weather permitting, a minimum of five exposures were taken in order to average out the measurements. Throughout this project, care was taken to have comparison stars, check star, and the target in the same frame. Immediately after the science images, a minimum of eight dark images were taken for each observing session. A minimum of sixteen flat frames taken at the same focal length were used to process the images. Similarly, a bias frame made at the same speed was used to process the images. For image processing, Christian Buil's IRIS software (Buil 2015) was used to de-bayer different channels, such as Red, Green, and Blue.

5. Choice of comparison stars

It has been categorically shown by Hoot (2007) that the DSLR dynamic range of magnitude can cover about 2.5 magnitudes. Outside of this range, errors increase rapidly, thereby reducing the utility of DSLR photometry with a wide magnitude range. Hence, a dynamic range of 2.5 magnitudes limits the choice of comparison stars. Care was taken to select comparison stars having a dynamic range of 2.5 in most cases. However, during the tenure of the observations, the nova remained hovering around magnitude 5.3, hence the selection of comparison stars was limited.

Although the nova was in one of the densest parts of the sky, with a modest limiting magnitude of the sky from the urban area along with a short exposure of five seconds with 154-mm focal length, the faintest star visible on an average image was around magnitude 8.5. Hence there were only a few comparison stars available around the nova. In most cases, a wide field finder chart (Figure 2) available on the American Association of Variable Star Observers website (AAVSO 2015) was used.

Another factor that governed the choice of comparison stars was the color of the stars. Very red stars and very blue stars were both avoided in order to increase the chances of picking up the truly non-variable star with a color (B–V) range of 0.3 and 1.0, and with a mean value of 0.7. Fortunately, the nova appeared in one of the richest parts of the sky; hence there were sufficient ideal comparison star candidates.

As a result, in most cases the comparison stars and check star were selected within the range of this color (B–V = 0.3 to 1.0). Table 1 contains the list of stars selected for photometry in most cases in this project. The adherence to the specified dynamic range of comparison star and the color cut ensures good quality of data. In these sixty days of observation, for almost 87% of the time at least six of the stars in Table 1 were used as comparison and check stars. At times when one or more stars were not visible due to poor seeing conditions, stars with a (B–V) value outside the range of 0.3 to +1.0 were chosen.

However, it should be noted that despite taking care, complete elimination of background starlight was not possible owing to the great density of stars in the region.

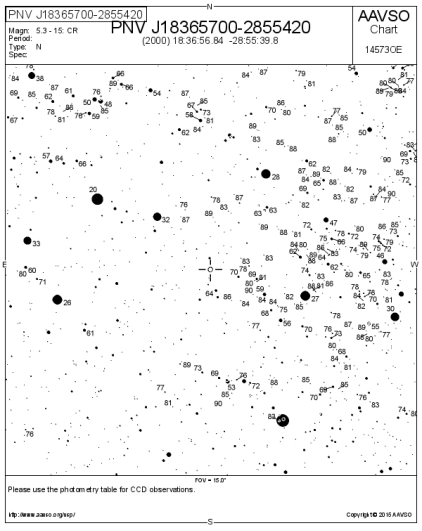

Figure 2. Wide field finder chart for V5668 Sgr (AAVSO 2015).

Table 1. Comparison stars and check star used.

Star (AAVSO Indentifier)	*R. A. (2000)* h m s	*Dec. (2000)* ° ′ ″	*V Mag.*	*(B–V)*
000–BCC–457	18 29 11.93	–29 15 34.3	6.888	0.451
000–BLP–686	18 37 17.21	–29 28 27.5	7.713	0.454
000–BCC–379	18 27 49.48	–29 49 00.7	5.920	0.520
000–BCC–337	18 26 40.81	–30 23 36.0	6.750	0.537
000–BCC–569	18 31 53.35	–28 30 40.4	8.308	0.592
000–BCC–587 = NSV 24489	18 32 14.01	–29 11 24.7	7.035	0.823
000–BLP–685	18 37 03.28	–28 30 47.0	6.782	0.964

6. Data reduction

Images saved in the camera's raw format were converted into "cfa format." After loading the cfa image, a master flat and master dark image were reduced from it apart from a master bias image in the preprocessing phase. The image was then aligned and RGB colors separated (de-bayered). Thus, for each image, there were now three individual images of different colors: red, green, and blue. From each image, the instrumental magnitudes of the objects could be derived. The software offers various display settings that do not alter the image data.

Using the software's "Aperture photometry" option, appropriate radii of different apertures were set depending upon the radii of the objects of interest in the image. Careful readings of the instrumental magnitudes were then taken and noted in a spreadsheet. In most cases, five science images were taken and an average of their instrumental magnitudes were used in the Citizen Sky Intermediate spreadsheet (CSIS; Citizen Sky 2015) for data reduction. The formulae embedded in CSIS accounted for airmass. This spreadsheet has some built-in checks like residuals versus airmass, quality of comparison star fit, and so on. In all cases, six comparison stars and a check star were used to derive DSLR Green magnitude. Since the target star was a nova, an accurate B–V value was not available beforehand; as a result, a B–V value of 0 was taken to keep the reduction effectively non-transformed.

7. Preliminary plot and transformations

A preliminary plot of the reduced Green observations (Figure 3) shows light variations as a function of time. Instrumental Green channel magnitudes were calibrated using nearby six comparison stars after accounting for atmospheric extinction and air mass. These observations are in good agreement with the similar observations submitted to the AAVSO by other observers. The preliminary plot shows large variations, especially a gradual rise and rapid fall. This is very unlike a classical slow nova with a rapid rise and gradual decline.

The transformation of DSLR Tri-G magnitude into standard V magnitude requires an exact color transformation coefficient (B–V value). However, as stated earlier, with the target object being a nova no B–V value was readily available. Non-transformed values can also be reported to the AAVSO using the "Tri-G" magnitude option. Table 2 shows estimated Tri-G values of the nova, along with standard errors that are a simple

Table 2. DSLR observations of V5668 Sgr.

Sl. Number	Julian Day	DSLR Tri-G Magnitude	Average Errors	Standard V Mag. using (B–V) = 0.28	Sl. Number	Julian Day	DSLR Tri-G Magnitude	Average Errors	Standard V Mag. using (B–V) = 0.28
1	2457098.53	6.1	0.028	6.0	31	2457133.49	5.1	0.068	5.2
2	2457099.51	7.1	0.083	7.1	32	2457135.50	4.9	0.084	4.8
3	2457100.52	5.3	0.037	5.3	33	2457136.50	4.8	0.030	4.8
4	2457101.52	4.4	0.089	4.4	34	2457137.50	5.0	0.022	5.0
5	2457102.52	4.9	0.049	4.7	35	2457138.48	4.9	0.053	4.9
6	2457103.52	4.6	0.181	4.6	36	2457139.50	5.0	0.025	5.0
7	2457104.51	4.9	0.086	4.8	37	2457140.49	4.9	0.023	4.9
8	2457105.51	5.5	0.055	5.5	38	2457141.49	5.9	0.074	5.9
9	2457106.50	5.9	0.033	5.9	39	2457142.49	5.7	0.016	5.7
10	2457107.52	5.3	0.609	5.7	40	2457143.49	6.1	0.025	6.0
11	2457112.50	5.0	0.053	5.0	41	2457144.49	5.8	0.060	5.7
12	2457113.51	4.5	0.023	4.5	42	2457145.49	6.2	0.019	6.2
13	2457114.52	4.6	0.049	4.6	43	2457146.49	6.2	0.072	6.2
14	2457115.50	4.2	0.035	4.2	44	2457147.49	5.4	0.044	5.4
15	2457116.50	4.3	0.026	4.4	45	2457149.50	5.2	0.038	5.1
16	2457117.50	4.2	0.126	4.2	46	2457150.46	5.2	0.027	5.1
17	2457119.50	5.0	0.029	4.9	47	2457151.47	5.0	0.083	5.0
18	2457120.51	5.6	0.041	5.6	48	2457152.48	4.8	0.029	4.8
19	2457121.50	5.5	0.054	5.5	49	2457153.47	5.3	0.012	5.3
20	2457122.50	5.8	0.026	5.8	50	2457154.48	5.0	0.055	5.0
21	2457123.50	5.6	0.037	5.6	51	2457155.47	5.3	0.014	5.4
22	2457124.49	4.8	0.066	4.8	52	2457157.46	6.1	0.014	6.1
23	2457125.51	5.1	0.049	5.0	53	2457158.47	5.5	0.045	5.6
24	2457126.50	4.8	0.083	4.8	54	2457159.48	6.3	0.065	6.3
25	2457127.50	5.1	0.035	5.1	55	2457160.45	6.8	0.023	6.7
26	2457128.50	5.0	0.050	5.0	56	2457161.45	6.6	0.034	6.6
27	2457129.51	5.4	0.068	5.3	57	2457162.45	6.5	0.027	6.5
28	2457130.50	5.2	0.050	5.2	58	2457164.46	6.2	0.035	6.1
29	2457131.50	5.1	0.073	5.1	59	2457165.46	6.1	0.036	6.1
30	2457132.50	6.0	0.203	5.7	60	2457166.45	6.1	0.037	6.1

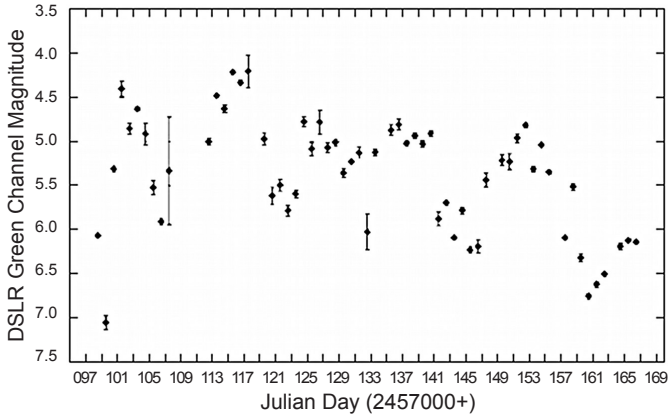

Figure 3. V5668 Sgr DSLR Green magnitude plot.

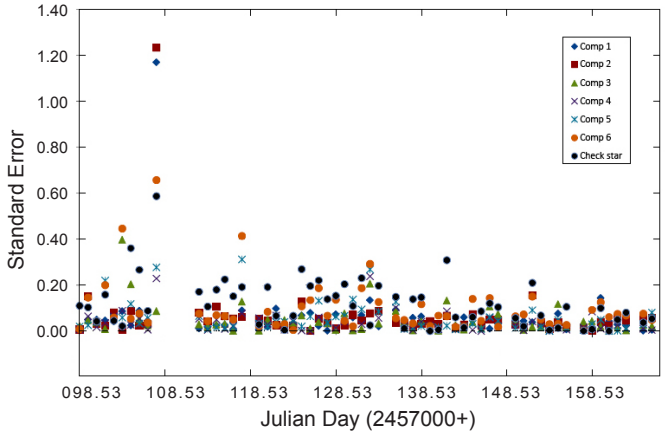

Figure 4. Standard errors of magnitude of comparison stars and check star.

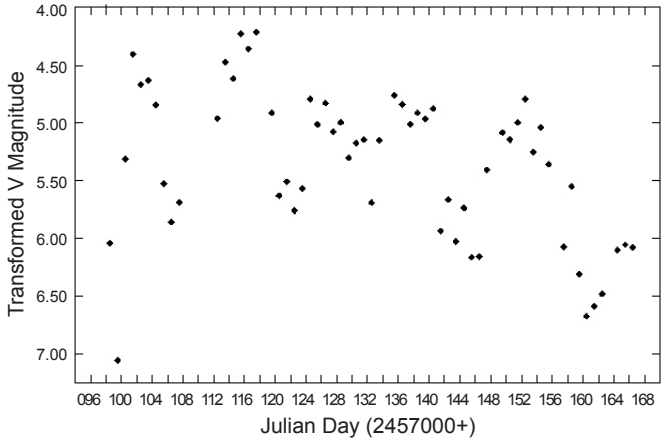

Figure 5. V5668 Sgr transformed V magnitudes.

average of standard errors of all comparison stars used.

A plot of the standard errors of magnitude of the comparison stars and the check star is shown in Figure 4.

The methodology of taking observations was to take five images of the same field with identical camera settings and then average them to reduce the errors in any particular image. However, on some occasions, sky conditions were not quite good and only one or two images were taken. Standard errors were large on such occasions. This is attributed mainly to two important aspects: low signal-to-noise ratio and reduced level of averaging to minimize errors. This is evident in the average of standard errors of all the comparison stars on a few occasions. For example, on March 26, 2015 (JD = 2457107.51736), only

three images were taken and the average of standard errors of all the comparison stars was 0.6.

By the time the observations were compiled, it became evident that the actual color of the nova changed largely over the monitoring period, and the median value B–V = 0.28 was selected as a compromise. Since, CSIS has an in-built mechanism to transform DSLR Green magnitude into Standard V magnitude, all DSLR Green magnitudes were transformed into Standard V magnitude using a B–V value of 0.28. Formulae embedded in CSIS use a least squares fit to compute extinction coefficient, transformation coefficient, and the camera's zero point offset from instrumental magnitude and catalogued (B–V) values of comparison stars after taking atmospheric extinction into account. Then, on the basis of these coefficients, standard V magnitudes were computed. The values of standard magnitudes are also given in Table 2 and shown in Figure 5.

8. Acknowledgements

Image processing and aperture photometry was carried using IRIS (Buil 2015) which is freeware. Thanks to Christian Buil for making this available to the public. The author is also thankful to Mark Blackford and Brian Kloppenborg for their valued input. The author is grateful to members of the AAVSO for their input to the DSLR photometry forum. Members of Akash Mitra, an Amateur Astronomers' Organization, also made valuable suggestions during the course of this project, and the author is also thankful to them.

References

AAVSO. 2015, Variable Star Plotter (VSP; https://www.aavso.org/apps/vsp/).

Buil, C. 2015, IRIS astronomical image processing software (http://www.astrosurf.com/buil/us/iris/iris.htm).

Central Bureau for Astronomical Telegrams. 2015, CBAT Transient object followup reports (http://www.cbat.eps.harvard.edu/unconf/followups/J18365700-2855420.html).

Citizen Sky. 2015, intermediate spreadsheet (CSIS; http://www.citizensky.org/content/calibration-intermediate).

Collins, D., and Prasai, A. 2009, in *The Society for Astronomical Sciences 28th Annual Symposium on Telescope Science. Held May 19–21, 2009 at Big Bear Lake, CA*, The Society for Astronomical Sciences, Rancho Cucamonga, CA, 121.

Green, D. W. E. 2015, *IAU Circ.*, No. 9275, 1.

Hoot, J. E. 2007, in *The Society for Astronomical Sciences 26th Annual Symposium on Telescope Science. Held May 22–24, 2007 at Big Bear, CA*, The Society for Astronomical Sciences, Rancho Cucamonga, CA, 67.

Kloppenborg, B. K., Pieri, R., Eggenstein, H.-B., Maravelias, G., and Pearson, T. 2012, *J. Amer. Assoc. Var. Star Obs.*, **40**, 815.

Loughney, D. 2010, *J. Br. Astron. Assoc.*, **120**, 157.

Zacharias, N., Finch, C. T., Girard, T. M., Henden, A., Bartlett, J. L., Monet, D. G., and Zacharias, M. I. 2012, *The Fourth U.S. Naval Observatory CCD Astrograph Catalog* (UCAC4), VizieR On-line Data Catalog (http://cdsarc.u-strasbg.fr/viz-bin/Cat?I/322).

Studies of RV Tauri and SRD Variables

John R. Percy
Department of Astronomy and Astrophysics and Dunlap Institute for Astronomy and Astrophysics, University of Toronto, 50 St. George Street, Toronto, ON M5S 3H4, Canada; john.percy@utoronto.ca

Received October 14, 2015; revised October 22, 2015; accepted October 26, 2015

Abstract AAVSO visual and Johnson V observations of 42 RV Tauri and 30 yellow semiregular (SRD) variables have been time-series analyzed with the AAVSO VSTAR package. The DCDFT routine was used to determine periods and mean amplitudes, and the WWZ (wavelet) routine was used to study changes in the amplitudes of these stars. For almost half of the stars, improved periods and/or classifications were obtained. For others, existing classifications and periods were confirmed or supported. As was previously found for a subset of RV and SRD stars, the pulsation amplitudes vary by factors of up to 10, on median time scales of about 22 pulsation periods for the RV stars, and about 25 pulsation periods for the SRD stars; these two values are not significantly different. This behavior is consistent with that of pulsating red giants and supergiants. The cause of the pulsation amplitude variations remains unknown.

1. Introduction

RV Tauri (RV) stars are low-mass yellow supergiants which show alternating deep and shallow minima to a greater or lesser extent. RVA stars have constant mean magnitude. RVB stars vary slowly and periodically in mean magnitude; they have a "long secondary period" (LSP). SRD stars are semiregular yellow supergiants. Confusingly, RV stars are clsssified, spectroscopically, as type A (G and K type, probably old Population I), type B (Fp type, with CH and CN bands of normal strength), and type C (Fp type with weak CH and CN bands, Population II) (Preston *et al.* 1963).

This is one in a series of papers which, thanks to AAVSO observations of these stars over many decades, explores the nature of and relation between these classes, and with other pulsating stars such as Type I and II Cepheids, and pulsating red giants: Percy and Mohammed (2004), Percy and Ursprung (2006), and especially Percy and Kim (2014). It also continues our studies of pulsation amplitude variations in these stars.

2. Data and analysis

This study used visual and Johnson V observations from the AAVSO International Database (AID; Kafka 2015) of the RV and SRD stars listed in the tables. See sections 3.5 and 3.6 for remarks on some of these. The stars were chosen from a list, dating back some years, of the stars on the AAVSO visual observing program. The data extend for typically 10,000–30,000 days; not all the stars have the same length of dataset. Percy and Abachi (2013) discussed some of the limitations of visual data which must be kept in mind when time-series analyzing the observations and interpreting the results. In particular, some of the stars have pronounced seasonal gaps in the data, which can produce "alias" periods, and some difficulty in the wavelet analysis.

The data, extending over the range of Julian Date given in the tables, were analyzed with the AAVSO's VSTAR time-series analysis package (Benn 2013), especially the Fourier (DCDFT) analysis and wavelet (WWZ) analysis routines. Periods, and their mean amplitudes, were first determined using the DCDFT routine. The results are given in Tables 1 and 3. The WWZ (wavelet) routine was then used to study the changes in amplitude for the stars with sufficient data. Percy and Kim (2014) have already done this for a subset of the stars in the tables. See that paper for a fuller description of how the analysis was done, and the challenges of doing so. For the wavelet analysis, the default values were used for the decay time c (0.001) and time division t (50 days). The results are sensitive to the former, but not to the latter.

3. Results

See sections 3.5 and 3.6 for notes on individual stars. See the papers by Percy and Abachi (2013) and Percy and Kim (2014) for examples of DCDFT and wavelet plots.

3.1. Periods of RV stars

Table 1 contains the results of the period and mean amplitude determinations for the RV Tauri stars. The columns list the *General Catalogue of Variable Stars* (GCVS; Samus *et al.* 2012)) classification and period P in days, and the periods and amplitudes that were obtained from the AAVSO visual and V observations. If the periods and/or classification differed significantly from the GCVS information, the star name is given in bold face, and the change is noted in section 3.5.

3.2. Amplitude variations in RV stars

Table 2 contains the results of the WWZ amplitude-variability determinations for the RV Tauri stars, for those stars which had sufficient data for wavelet analysis. The columns list the period P used, the range of JD, the range of amplitude, the number N of cycles of amplitude increase and decrease, and the value of L/P where L is the average length of the cycles, and P is the pulsation period. For the stars marked with an asterisk, the results are taken from Percy and Kim (2014). See Percy and Abachi (2013) for a discussion of the determination of N, L, and L/P, and the uncertainties of these. The values of L/P do not depend significantly on the exact value of P used, or whether the "full" period or "half" period is used (Percy and Kim 2014).

Table 1. Period determination for RV Tauri stars.

*Star**	*Type*	*P (d)*	*Filter*	*Period (Amplitude) (days)*
DY Aql	RV	131.42	vis	65.68 (0.33)
EZ Aql	RVA	38.64	vis	19.37 (0.57), 38.73 (0.25)
IS Aur	SR	76.5	V	75.26 (0.80)
TW Cam	RVB	87.22	vis	43.48 (0.08), 669.7 (0.06)
			V	43.25 (0.30)
RX Cap	RV	67.92	vis	140.33 (0.11), 67.93 (0.11)
IW Car	RVB	67.5	vis	36.32: (0.01), 67.55: (0.02), 1433 (0.31)
EQ Cas	RVA	58.34	vis	58.23 (0.16), 29.12 (0.33)
			V	58.21 (0.28), 29.11 (0.45)
RU Cen	—	64.7	vis	32.26 (0.28), 64.7 (0.12)
			V	32.3 (0.41)
SX Cen	RVB	32.9	vis	16.44 (0.29), 31.05 (0.18), 603.2 (0.74)
BI Cep	RVA	212	V	209.8 (0.22)
DF Cyg	RVB	49.808	vis	24.92 (0.21), 50.2 (0.08), 778.4 (1.12)
			V	781.8 (1.31)
GK Cyg	RV	79.75	V	79.25 (0.33), 39.71 (0.34)
V360 Cyg	RVA	70.39	vis	35.18 (0.35), 70.43 (0.09)
SS Gem	RVA	89.31	vis	44.57 (0.21), 89.14 (0.21)
			V	same
SU Gem	RVB	50.0	vis	24.97 (0.24), 50.06: (0.08), 681.66 (0.98)
BG Gem	RV	60	V	91.6 (0.11), 45.73 (0.28)
AC Her	RVA	75.01	vis	75.41 (0.20), 37.70 (0.33)
BT Lac	RVB	40.50	V	79.7 (0.40), 652 (0.89)
EG Lyr	RVB	236	vis	220.61 (0.24)
EP Lyr	RVB	83.34	vis	41.49 (0.22), 82.98 (0.21)
V443 Lyr	RV	—	V	51.2 (0.24) uncertain
U Mon	RVB	91.32	vis	45.73 (0.21), 2427 (0.32)
			V	46.05 (0.24), 91.5 (0.16)
HQ Mon	RV	65	V	25–35 (0.15)
TT Oph	RVA	61.08	vis	30.51 (0.32)
			V	30.50 (0.55), 61.58 (0.19)
TX Oph	RVA	135	vis	134.55 (0.12), 67.62 (0.12)
UZ Oph	RVA	87.44	vis	43.68 (0.36), 88 ± (0.17)
CT Ori	RV	135.52	vis	33.6 (0.14), 67.2 (0.14)
			V	33.59 (0.18), 66.95 (0.12)
DY Ori	RV	60.26	vis	30–40 (0.16)
			V	30.2 (0.16), 60.74 (0.12)
V360 Peg	RV	—		no result
TX Per	RVA	78	vis	76.40 (0.15)
			V	75.7 (0.42)
AR Pup	RVB	74.58	vis	38.35 (0.13), 75.62 (0.03), 1194 (0.31)
TW Ret	RV	—	V	242 (0.80), 121 (0.47)
AR Sgr	RVA	87.87	vis	86.83 (0.18), 43.20 (0.28)
			V	87.93 (0.46), 43.89 (0.46)
AZ Sgr	RVA	113.6	vis	112.82 (0.17), 56.57 (0.19)
R Sge	RVB	70.77	vis	35.39 (0.18), 70.80 (0.10)
			V	35.5 (0.33), 71.0 (0.23)
AI Sco	RVB	71.0		35.82 (0.22), 71± (0.03), 977.6 (0.88)
R Sct	RVA	146.5	vis	143.85 (0.19), 70.93 (0.17)
RV Tau	RVB	78.73	vis	39.24 (0.27), 78.81 (0.08)
			V	39.22 (0.49), 78.32 (0.23)
DZ UMa	RVB:	—	vis	70.52 (0.29), 507.42 (0.19)
CE Vir	RV	67	vis	70 ± (0.11)
			V	70 ± (0.20)
V Vul	RVA	75.7	vis	76.23 (0.17), 38.08 (0.13)
NSV 7378	RV	—	vis:	no result

**If the periods and/or classification differed significantly from the GCVS information, the star name is given in bold face, and the change is noted in section 3.5.*

Table 2. Amplitude variability of RV Tauri stars.

Star	*P (d)*	*JD range*	*A range*	*N*	*L/P*
DY Aql	131.42	2442000–2457250	0.2–0.7	6	19
TW Cam	87.22	2442000–2457250	0.10–0.40	12	15
RX Cap	67.92	2443000–2453000	0.22–0.52	9	16
IW Car*	71.96	2446037–2456646	0.05–0.24	8	18
EQ Cas	58.34	2446000–2457250	0.20–0.55	5.5	35
RU Cen	64.727	2450000–2453250	0.08–0.70	3.5	32
DF Cyg*	24.91	2441000–2456600	0.20–0.86	20	31
GK Cyg	79.75	2445000–2456000	0.2–0.7	7	20
V360 Cyg	70.39	2445000–2457250	0.05–0.40	10	18
SS Gem	89.14	2441000–2457250	0.13–0.35	10	18
SU Gem*	24.98	2446000–2456250	0.00–1.35	15	27
AC Her*	37.69	2435500–2456600	0.28–0.49	12.5	45
EP Lyr	83.34	2445000–2457250	0.11–0.36	7:	21
U Mon	91.32	2433000–2457250	0.05–0.35	13	20
TT Oph	30.51	2427946–2456615	0.25–0.76	39	24
TX Oph	135	2427500–2457250	0.05–0.56	7.75	28
UZ Oph	43.71	2445500–2456626	0.20–0.70	9.5	27
CT Ori	67.29	2446500–2457250	0.06–0.36	9	18
TX Per*	76.38	2427964–2456654	0.12–0.75	7.5	50
AR Pup	74.58	2446000–2457250	0.04–0.22	8	19
AR Sgr	87.87	2449000–2457250	0.12–0.37	7:	13
AZ Sgr	113.6	2451000–2457250	0.13–0.36	1.5	37
R Sge	70.77	2420000–2457250	0.05–0.50	16	35
AI Sco*	35.76	2445000–2455750	0.15–1.10	11	27
R Sct	146.5	2420000–2457259	0.05–0.85	9.5	27
RV Tau	78.73	2435000–2457250	0.03–0.28	17.5	16
V Vul*	76.31	2446000–2456649	0.20–0.35	5.5	22

** See note in section 3.5.*

3.3. Periods of SRD stars

Table 3 contains the results of the period and mean amplitude determination for the SRD stars. If the period and/or classification differ significantly from the GCVS information, the star name is given in bold face, and the differences are noted in section 3.6.

3.4. Amplitude Variations in SRD stars

Table 4 contains the results of the WWZ amplitude-variability determinations for the SRD stars. See section 3.2 for further information.

3.5. Notes on individual RVT stars

These notes are given in the same order as the stars are listed in Table 1. Unless indicated, there is no evidence for an LSP in RV stars which were classified in the GCVS as RVA.

DY Aql: The GCVS period of 131 days is present, but at the noise level; the strongest period is 65.68 days, with an amplitude of 0.33. May not be an RV star.

IS Aur: This star is an M2III SR variable with a period of 75.26 days and a V amplitude of 0.80; not an RV or SRD star.

TW Cam: There is an LSP of 670 days (amplitude 0.06), supporting the RVB classification, but the present analysis does not detect both P and P/2.

RX Cap: The phase curve for 67.93 days has two unequal minima, confirming the RV classification, but there is no LSP, therefore an RVA star.

IW Car: The LSP of 1433 days (amplitude 0.31) confirms the RVB classification.

RU Cen: The data are very sparse. A period of 64.7 days produces a phase curve with two unequal minima, and there is an LSP of 561 days (amplitude 0.19), which supports an RVB classification. This star is a 1489-day binary (Gezer *et al.* 2015); that period is not present in the DCDFT spectrum. The amplitude of the pulsation seems to vary with the LSP.

SX Cen: The LSP of 603 days (amplitude 0.74) confirms the RVB classification. This star is a 600-day binary (Gezer *et al.* 2015).

BI Cep: The visual data are sparse. The (also sparse) V data give a period of 209.8 days, close to the GCVS period of 212 days.

DF Cyg: The LSP of 780 days (amplitude 1.12) confirms the RVB classification.

GK Cyg: The sparse visual data show many peaks of comparable amplitude. The V data show peaks at 79.25 and 39.71 days, both with amplitudes of 0.33; the phase curve for the longer period has two minima with unequal depth, confirming the RV classification, but there is no LSP, therefore the star is RVA.

SU Gem: The LSP of 681.66 days (amplitude 0.98) confirms the RVB classification.

BG Gem: Only V data are available. A period of 91.6 days gives a classic RV phase curve, with two unequal minima, confirming the RV classification. There is no evidence of an LSP so this star is probably RVA.

AC Her: This star is a 1196-day binary (Gezer *et al.* 2015). A period of 1,194 days is present in the DCDFT spectrum, but with an amplitude of only 0.0165 mag.; there are higher long-period peaks in the spectrum.

BT Lac: The LSP of 652 days (amplitude 0.89) confirms the RVB classification. The visual data are sparse. In the V data, the half-period is not resolvable from the noise.

EG Lyr: This star is an SRA/SRB (M-type) star; the (sparse) visual data give a period of 220.61 days, which may be inconsistent with the GCVS period of 236 days.

EP Lyr: Zsoldos (1995) found no periodic variation in mean magnitude; the present data support this conclusion. The star is RVA, not RVB.

V443 Lyr: There are no convincing periods in the AAVSO data.

U Mon: The LSP of 2427 days (amplitude 0.20) confirms the RVB classification. This star is a 2597-day binary (Gezer *et al.* 2015).

CT Ori: The data are rather sparse. A period of 67.29 days produces a phase curve with two unequal minima, and there is no conspicuous LSP, which supports an RVA classification. The GCVS period of 135.52 days is not found.

DY Ori: The data are sparse. In the visual and V data, periods of 60.7 and 30.2 days are present, but not conspicuous. The former period produces a phase curve with two unequal minima, and there is no obvious LSP, which supports an RVA classification.

V360 Peg: There are no convincing periods in the AAVSO data.

TX Per: Only one period (75.7 days) is clearly present, but there is some weak evidence for a 37.5-day period, so the classification of this star is uncertain.

Table 3. Period determination for SRD stars.

*Star**	*Type*	*P (d)*	*Filter*	*Period (Amplitude) (days)*
WY And	SRD	109.65	vis	108.4 (0.33)
			V	108.15 (0.28)
TX Aql	SRD	35	vis	34.75 (0.15)
			V	33.7:
Z Aur	SRD	111.5	vis	110.4 (0.25)
			V	110.2 (0.61)
AG Aur	SRD	99	vis	96.2 (0.30)
			V	96.2 (0.29)
CO Aur	Cep	1.78	vis	1.783027 (0.09)
UY CMa	SRD	114.6	vis	113.9 (0.11)
			V	114.1 (0.36)
RU Cep	SRD	109	vis	108.9 (0.06), 520.8 (0.10)
RX Cep	SRD	55	vis	constant
TZ Cep	SRD	83.0	vis	82.4 (0.48)
RV Col	SRD	105.7	vis	106.1 (0.23)
			V	101.36: (0.21)
AV Cyg	SRD	89.22	vis	88.1 (0.22)
			V	88.14 (0.19)
V395 Cyg	SRD:	40.5	V	40.1 (0.07), 32.8 (0.06) not aliases
VW Dra	SRD:	170	vis	not variable
IS Gem	SRC	47	vis, V	constant
SX Her	SRD	102.9	vis	103.5 (0.17)
			V	102.9 (0.18)
UU Her	SRD	80.1	vis	72.8 (0.02), 44.9 (0.03)
			V	71.2 (0.10), 44.9 (0.10)
DE Her	SRD	165.2	vis	172.76 (0.33)
			V	173.1 (0.57)
V441 Her	SRD	68	vis	68.25/71.8 (0.06)
			V	64.98 (0.02) / 79.04 (0.02) aliases
RS Lac	SRD	237.26	vis	237.74 (0.72)
			V	237.17 (0.45)
SX Lac	SRD	190.0	vis	195.47 (0.10)
AB Leo	SRD	130.2	vis	103.1 (0.16)
			V	103.1 (0.22)
W LMi	SRD	117.2	vis	116.8 (0.80)
			V	116.6 (0.90)
V564 Oph	SRD	70.325	vis	73.1 (0.12)
GT Ori	SRD	86	vis	no periods
TV Per	SRD	358	vis	372.4 (0.48)
RX Ret	SRD	—	vis	74–79 (0.12)
			V	66–69 (0.35)
BM Sco	SRD	815	vis	382 (0.20), alias of LSP?
LR Sco	SRD	104.4	vis (WWZ)	possibly 70, 105, 140
WW Tau	SRD	116.4	vis	114.5 (0.47), 640–690 (0.22)
SV UMa	SRD	76	vis, V:	60–100

**If the periods and/or classification differed significantly from the GCVS information, the star name is given in bold face, and the change is noted in section 3.6.*

AR Pup: The LSP of 1194 days (amplitude 0.31) confirms the RVB classification.

TW Ret: There are no visual data. The V data suggest periods of 242 (amplitude 0.80) and 121 (amplitude 0.47) days, supporting the RV classification. No information about an LSP is found.

R Sge: The LSP of 1125 days (amplitude 0.11) confirms the RVB classification.

AI Sco: The LSP of 977.6 days (amplitude 0.88) confirms the RVB classification.

DZ UMa: The LSP of 507.4 days (amplitude 0.19) confirms the RVB classification; the GCVS classification is RVB:.

CE Vir: The data are sparse. There is a period of about 70 days, but not enough evidence to classify the star as RV or SRD. There are slow variations, but they are not necessarily periodic.

NSV 7378: There are no conspicuous periods in the AAVSO data.

3.6. Notes on individual SRD stars

These are given in the same order as in Table 3. They contain information about e.g. the presence of an LSP, or a proposed change to the GCVS classification.

WY And: There is a large gap in the data; only the most recent data are suitable for wavelet analysis. The periods in the AAVSO data, 108.4 days in the visual data, 108.15 days in the V data, differ slightly from the GCVS period of 109.65 days.

TX Aql: The 34.75-day period in the AAVSO data is consistent with the GCVS period of 35 days.

Z Aur: This well-studied star alternates between periods of

Table 4. Amplitude variability of SRD stars.

Star	*P (d)*	*JD range*	*A range*	*N*	*L/P*
WY And	109.65	2453000–2457250	0.20–0.40	1.5	26
TX Aql	35	2423910–2425568	0.06–0.28	1.5:	32
Z Aur*	110.40	2423000–2456651	0.20–0.76	15	20
AG Aur*	96.13	2441000–2456600	0.15–0.78	11	15
UY CMa	114.6	2435000–2457250	0.03–0.39	8	24
RU Cep	109	2432000–2457250	0.03–0.25	6±	39
TZ Cep*	82.44	2451426–2456635	0.33–0.76	2.2	29
RV Col	105.7	2440000–2457250	0.20–0.45	9:	19
AV Cyg*	87.97	2429012–2456630	0.11–0.57	9	35
SX Her*	103.50	2425000–2456631	0.08–0.44	6	47
UU Her*	44.93	2432000–2456622	0.02–0.18	15	37
DE Her*	173.10	2442000–2456622	0.13–0.64	1.5	56
V441 Her	68	2447000–2457250	0.02–0.07	7.5	20
RS Lac*	237.57	2427592–2456635	0.24–1.02	3.5	35
SX Lac*	195.48	2446000–2456282	0.10–0.17	3.75	14
AB Leo	130.2	2432000–2457250	0.05–0.50	10	25
W LMi	117.2	2440000–2457250	0.73–1.05	7	21
V564 Oph	70.325	2449000–2457250	0.10–0.43	4.5	25
TV Per	358	2437000–2457250	0.08–0.40	2.3	24
RX Ret	(75)	2440000–2457250	0.13–0.70	12	18

** See note in section 3.6.*

110.4 and 133.6 days. It is an M star, and therefore SRA/SRB classification.

AG Aur: The visual and V data support a period of 96.16 days, in agreement with an earlier GCVS period, but not in agreement with the current GCVS period of 99 days.

CO Aur: This star is a Cepheid with a period of 1.783027 days, not an SRD star.

UY CMa: The DCDFT spectrum shows periods of 113.9 (visual) or 114.1 (V) days. There are very slow variations in mean magnitude.

RU Cep: There is a possible LSP of 520.8 days, with visual amplitude 0.06.

RX Cep: There are no peaks higher than 0.02 mag. The GCVS period of 55 days has an amplitude 0.003. Probably not an SRD star.

TZ Cep: There is a large gap in the middle of the dataset.

RV Col: The visual data show possible periods of 106.1 and 149.8 days, with comparable amplitudes; these periods are aliases. The limited V data and the period in the literature support the shorter period.

AV Cyg: The periods (amplitudes) in the AAVSO data are visual: 88.1 (0.22) days, V: 88.14 (0.19) days. Both differ slightly from the GCVS period of 89.22 days.

V395 Cyg: There are peaks at 40.1 and 32.8 days (not aliases) in the V data. No peaks stand out in the visual data. The data are sparse, but the SRD classification is probably correct.

VW Dra: There are no peaks higher than 0.02 mag.

IS Gem: The amplitude is less than 0.01; there is no evidence for the GCVS period of 47 days.

UU Her: This star is well known to switch between periods of about 72 and 45 days. The AAVSO visual data show periods (amplitudes) of 72.8 (0.02) and 44.9 (0.03) days, the V data 71.2 (0.10) and 44.9 (0.10) days, none of them agreeing with the GCVS period of 80.1 days.

DE Her: The periods (amplitudes) in the AAVSO data are visual: 172.76 (0.33) days, V: 173.1 (0.57) days. These are slightly different from the GCVS period of 165.2 days.

V441 Her (89 Her): This photoelectrically-well-studied star shows periods of 64.98 or 79.04 days in the visual data (these periods are aliases) and 71.8 days in the V data, in each case with a small amplitude. The GCVS period is 68 days. Fernie and Seager (1995), from several years of photoelectric data, obtain a period of 63.50 ± 0.48 days. The star is also a 288.4-day binary.

SX Lac: The 195.47-day period in the AAVSO visual data differs slightly from the GCVS period of 190.0 days.

AB Leo: The results support a period of about 103 days, not the GCVS period of 130.2 days.

V564 Oph: The only peak above the noise level is 73.1 days, which is slightly different from the GCVS period of 70.325 days. The data are sparse.

GT Ori: Although the data are plentiful, they show no obvious periods, including the GCVS period of 86 days, which does not produce a significant phase curve. The SRD classification cannot be confirmed.

TV Per: There are very slow variations in mean magnitude.

RX Ret: In addition to the pulsation period of 79.1 days, there is a possible LSP of 736 days, visual amplitude 0.13, but the noise level is high. For the wavelet analysis, we used a period of 75 days, proposed by the RASNZ.

BM Sco: The light curve and DCDFT spectrum shows a time scale of several thousand (nominally 8,000) days, and a 382-day alias of this. There is no evidence for the GCVS period of 815 days. The SRD classification is therefore doubtful.

LR Sco: The DCDFT spectrum does not show any peaks in the visual data greater than the noise level of 0.10, and the phase diagram for the GCVS period of 104.4 days is not convincing. Wavelet analysis suggests that there may be periods of about 70, 105, and 140 days, with variable amplitudes, but the classification is uncertain.

WW Tau: There are possible LSPs of 640–690 days, with visual amplitude 0.22. There is a large gap in the middle of the dataset.

SV UMa: There are several peaks between 60 and 100 days; none stand out, not even the GCVS period of 76 days, so the star's classification is uncertain.

4. Discussion

The classification of low-mass pulsating yellow supergiants is complicated by the fact that the RV phenomenon—alternating deep and shallow minima—is not regular; in fact, there may be a continuous spectrum of behavior from RV to SRD (Percy 1993; Percy and Mohammed 2004). Therefore the classifications in Tables 1 and 3 and in sections 3.5 and 3.6 are uncertain, to a greater or lesser extent. Many previous classifications (and periods) were based on fragmentary data. The systematic, sustained AAVSO data provide an improvement. It would probably require an almost-infinite set of almost-perfect data to make a firm classification. The AAVSO data do make it possible to investigate the long-term changes in pulsation amplitude which were found in the present study and in previous ones.

The cause of these variations is not known, so the results of this paper make a significant contribution to the understanding of stellar pulsation.

As for the nature of RV stars, and the cause of the RVB phenomenon, much has been learned in the last two decades, thanks especially to multi-technique, multi-wavelength studies, notably spectroscopy, and infrared photometry. Van Winckel *et al*. (1999) propose that RVB stars are binaries, with a circumbinary dusty disc. If the disc is seen at high inclination, that is, almost edge-on, then long-period variability will occur because of periodic extinction during the orbital motion. Percy (1993) also proposed a binary model for the RVB phenomenon on the basis of the long-term light curve of U Mon.

Gezer *et al.* (2015) have recently published a comprehensive study of RVA and RVB stars, using new infrared photometry, combined with existing spectroscopic data. They note that (i) all confirmed binary RV stars have infrared properties indicative of a disc, and (ii) all RVB stars in their sample also have infrared properties of a disc. If the long secondary periods of the RVB stars reflect their orbital motion, then the improved photometric periods and classifications in this paper will be useful to spectroscopists; Gezer *et al.* (2015) stress that "more radial velocity monitoring is needed for all RV and RVB objects to test their binary nature." Binaries in our sample include RU Cen (1,489 days), SX Cen (600 days), AC Her (1,196 days), and U Mon (2597 days) (Gezer *et al.* 2015).

In their Tables 4 and 5, Gezer *et al*. (2015) list the spectroscopic types and [Fe/H] metal abundances of the stars in their sample. Of the (photometric) RVA stars, 8/10 are spectroscopic type A. Of the (photometric) RVB stars, 8/12 are spectroscopic type A. These fractions are not significantly different. Only one star—the RVA star V360 Cyg—is spectroscopic type C. The distributions of the [Fe/H] values of the RVA and RVB stars overlap but, on average, are lower for the RVA stars. See Gezer *et al.* (2015) for a detailed discussion of the complex processes which affect the chemical abundances in these stars.

It is heartening to know that there is still science to be extracted from the visual observations in the AAVSO International Database. They are unique in providing a window on the long-term behavior of stars such as RV, SRD (and pulsating red giants).

5. Conclusions

Using AAVSO visual and V observations, it is possible to refine the classifications and periods of many RV and SRD stars, and to confirm or support the classifications and periods of many others. For stars which have sufficiently dense and sustained data, wavelet analysis has been used to show that the pulsation amplitudes of these stars vary by up to a factor of ten, on time scales of 20–25 pulsation periods. Pulsating red giants and supergiants show this same behavior. The cause of these amplitude variations remains unknown.

6. Acknowledgements

This project would not have been possible without the efforts of the hundreds of AAVSO observers who made the observations, the AAVSO staff who processed and archived the observations and made them publicly available, and the team which developed the VSTAR package and made it user-friendly and publicly available. This project made use of the SIMBAD database, which is operated by CDS, Strasbourg, France.

References

Benn, D. 2013, VSTAR data analysis software (http://www.aavso.org/vstar-overview)

Fernie, J. D., and Seager, S. 1995, *Publ. Astron. Soc. Pacific*, **107**, 853.

Gezer, I., Van Winckel, H., Bozkurt, Z., De Smedt, K., Kamath, D., Hillen, M., and Manick, R. 2015, *Mon. Not. Roy. Astron. Soc.*, **453**, 133.

Kafka, S. 2015, observations from the AAVSO International Database (http://www.aavso.org).

Percy, J. R. 1993, *Astrophys. Space Sci.*, **210**, 123.

Percy, J. R., and Abachi, R. 2013, *J. Amer. Assoc. Var. Star Obs.*, **41**, 193.

Percy, J. R., and Kim, R. 2014, *J. Amer. Assoc. Var. Star Obs.*, **42**, 267.

Percy, J. R., and Mohammed, F. 2004, *J. Amer. Assoc. Var. Star Obs.*, **32**, 9.

Percy, J. R., and Ursprung, C. 2006, *J. Amer. Assoc. Var. Star Obs.*, **34**, 125.

Preston, G. W., Krzeminski, W., Smak, J., and Williams, J. A. 1963, *Astrophys. J.*, **137**, 401.

Samus, N. N. *et al*. 2012, *General Catalogue of Variable Stars*, Sternberg Astronomical Institute, Moscow (GCVS database, http://www.sai.msu.su/gcvs/gcvs/index.htm).

Van Winckel, H., Waelkens, C., Fernie, J. D., and Waters, L. B. F. M. 1999, *Astron. Astrophys.*, **343**, 202.

Zsoldos, E. 1995, *Astron. Astrophys.*, **296**, 122.

Recently Refined Periods for the High Amplitude δ Scuti Stars V1338 Centauri, V1430 Scorpii, and V1307 Scorpii

Roy Andrew Axelsen
P.O. Box 706, Kenmore, Queensland 4069, Australia; reaxelsen@gmail.com

Received September 21, 2015; revised October 12 and 22, 2015; accepted October 23, 2015

Abstract Digital Single Lens Reflex (DSLR) photometry of the high amplitude δ Scuti stars V1338 Centauri, V1430 Scorpii, and V1307 Scorpii was taken during the southern autumn and winter of 2015. Fourier analysis revealed pulsation frequencies corresponding to periods very close to those previously reported with significant contributions from harmonics. Only in the case of V1430 Scorpii was another independent frequency detected. The oscillation periods were refined by calculating linear ephemerides based on previously published epochs for each star, and the epochs determined by the author. These periods are: V1338 Centauri, 0.13093808 d; V1430 Scorpii, 0.08377709 d; and V1307 Scorpii, 0.11703066 d.

1. Introduction

The observation of δ Scuti stars by amateur astronomers can yield data not available from professional photometric surveys. Because of their short periods (a few hours), time series photometry by CCD or DSLR photometry can capture a light curve through an entire cycle at least, and sometimes a number of cycles, from a single night's observations. If observations are made for several nights over a period of weeks during one observing season for one star, sufficient data will be obtained for Fourier analysis and for the calculation of the epochs of several times of maximum light (TOM). From the latter, ephemerides can be calculated, and, particularly if historical TOMs are also available, periods can be determined with substantial accuracy.

V1338 Centauri (HD 123460) was first reported to be variable by Strohmeier *et al*. (1968) from photometry of photographic plates, although at that time the type of variability was not stated, nor was an ephemeris reported. The only other reference found is its entry in the *General Catalogue of Variable Stars* (GCVS; Samus *et al*. 2007–2013), where it is classified as a δ Scuti star, with a period of 0.1309382 day, at epoch JD 2453764.8191.

The star now designated as V1430 Sco (GSC 07369 00459) was first identified to be variable by Otero (2007), using the database of the Northern Sky Variability Survey (Wozniak *et al.* 2004) and the ASAS-3 database (Pojmański 2002). It was found to be a high amplitude δ Scuti star (HADS) with the epoch reported by Otero being JD 2453096.878 and the period 0.0837770 day.

The star now designated V1307 Sco (GSC 07892 01411) was recognized as a HADS by Wils *et al*. (2004), using the ASAS-3 database. Its variability was first identified by Strohmeier (1967) from photographic plates, but the type of variability was not stated, and the period was not known at that time. Wils *et al.* reported the epoch HJD 2452057.700 and the period 0.117031 day.

In view of the significant lapse of time since the last reported epochs of these stars (9, 11, and 14 years, respectively), DSLR photometry was taken between April and August 2015, with the aims of confirming and if possible refining their pulsation frequencies.

2. Data and analysis

2.1. Observations

Time series DSLR photometry of V1338 Cen, V1430 Sco, and V1307 Sco was taken between 24 April and 8 August 2015. RAW images were taken with a Canon EOS 500D camera through a Celestron C9.25 Schmidt-Cassegrain telescope on a Losmandy GM-8 German equatorial mount. Exposures of 120 seconds at ISO 800 were taken at intervals of 140 seconds. Dark frames were captured during meridian flips, and flat frames were obtained after dawn with the telescope aimed at the zenith and a white acrylic sheet used as a diffuser placed over the front of the telescope.

Comparison and check stars were chosen with V magnitudes and B–V color indices as close as possible to those of the variables. They are listed in Table 1. The V magnitudes and B–V color indices were obtained from the AAVSO Photometric All-Sky Survey (APASS; Henden *et al.* 2014).

The numbers of usable images for photometry obtained for the three stars were as follows: V1338 Cen, 979 images; V1430 Sco, 898 images; and V1307 Sco, 561 images. V1338 Cen and V1430 Sco were both observed during six nights, while V1307 Sco was observed during four nights. For both V1338 Cen and V1430 Sco, ten peaks of the light curves were obtained for the calculations of linear ephemerides, and four peaks were obtained for V1307 Sco.

Instrumental magnitudes in B and V were calculated after performing aperture photomery on the images from the blue and green channels of the DSLR sensor using the sofware AIP4WIN (Berry and Burnell 2011). Transformed magnitudes in B and V were calculated using transformation coefficients determined from standard stars in the E regions (Menzies *et al.* 1989).

Table 1. The δ Scuti stars and their respective comparison and check stars reported in the present paper.

Variable Star	*Comparison Star*	*Comp. V*	*Comp. B–V*	*Check Star*	*Check V*	*Check B–V*
V1338 Cen	HD 123547	10.417	0.432	HD 123503	10.288	0.554
V1430 Sco	HD 154588	9.905	0.488	HD 319439	9.974	0.463
V1307 Sco	HD 324056	10.129	0.479	HD 324055	10.590	0.483

The time in JD of each magnitude calculation was taken to be the mid point of each DSLR exposure. The heliocentric correction for each night's data was calculated for the mid point in time of the observing run for the night, and the correction applied to all data points for that night.

The time series instrumental magnitude differences between the comparison and check stars for the green channel have standard deviations as follows. For a single night, the standard deviations ranged from 0.006 to 0.009 mag. for V1338 Cen, from 0.005 to 0.008 mag. for V1430 Sco, and from 0.007 to 0.010 mag. for V1307 Sco. The standard deviations of these instrumental magnitude differences for the data from all nights analysed together are 0.008 mag. for V1338 Cen, 0.007 mag. for V1430 Sco, and 0.009 mag. for V1307 Sco.

2.2. Time series analysis

Fourier analysis of the light curves was undertaken with the software PERIOD04 (Lenz and Breger 2004), for which the following settings were used. Frequencies were sought between zero and 50 d^{-1}, using a high step rate (1/20T, where T is the length of the data in days). After each frequency was calculated, the Improve All function was activated, which applies a non-linear least-squares fitting algorithm. After several frequencies were identified, signal/noise ratios for the second and subsequent frequencies were calculated using a box size of $2d^{-1}$. Thus, the range of frequencies across which signal/noise ratios were calculated was (f_n – box size / 2) to (f_n + box size / 2) = (f_n – 1) to (f_n + 1), f_n being the frequency of interest. Frequencies with signal/noise ratios greater than 10 were regarded as being significant. Least squares uncertainties were calculated for each frequency (and for the corresponding semiamplitudes and phases), with the uncertainties for frequency and phase uncorrelated.

The time of each peak in the light curve (TOM) was taken as the time in HJD of the peak value of a 10th order polynomial expression fitted to each peak and its ascending and descending limbs, using the software PERANSO (Vanmunster 2013). A 10th order expression (rather than a lower order) was selected, because the resulting calculated light curve fitted best by eye the sharp peaks of the actual light curves of V1338 Cen and V1307 Sco. With lower order polynomial expressions, the peaks of the fitted curves were shifted in comparison with the actual data. Linear ephemerides were calculated as the least squares linear fit for TOM versus epoch, from the literature and from the new data reported herein.

3. Results

Table 2 lists the frequencies (d^{-1}) together with their errors (least squares uncertainties) and signal/noise ratios (SNRs) for the three target stars. Apart from the dominant frequency (f1) for each of the stars, most of the other frequencies (and in the case of V1307 Sco, all of the other frequencies) are Fourier harmonics, integer multiples of f1. However, in the case of V1430 Sco, f4 at 18.4335 d^{-1} is not a Fourier harmonic. It has a semiamplitude of 0.008 mag. in V, substantially less than the semiamplitude of f1 at 0.15 mag. In the case of V1338 Cen, f5 at 1.020 d^{-1} is not a Fourier harmonic, and is considered to be spurious, for reasons noted in the Discussion. It has a semiamplitude of 0.021 mag., again significantly lower than the semiamplitude of 0.21 mag. for f1.

For the purposes of this paper, frequencies discovered by Fourier analysis were not reported if the signal/noise ratio fell below 10, with the exception of the special case of the frequency of 1.020 d^{-1} for V1338 Cen, mentioned above, with a signal/noise ratio of 9.4. Further frequencies discovered but not reported here had signal/noise ratios that ranged from 2.4 to 6.1. It is possible that frequencies with signal/noise ratios between 4 and 10 could be real. However, a conservative approach has been taken by the author in restricting included frequencies to those with a higher probability of validity, to avoid reporting what may be false frequencies.

Figure 1 illustrates phased light curves for V1338 Cen, V1430 Sco, and V1307 Sco which were created in PERIOD04 using the dominant (f1) frequencies listed for each of these stars in Table 2. For V1338 Cen and V1430 Sco there are subtle shoulders in the descending limbs of the phase plots.

The fits of the data using the reported frequencies leave residual root mean squares for the V magnitude of the variable stars of 0.015 mag. for V1338 Cen, 0.008 mag. for V1430 Sco, and 0.024 mag. for V1307 Sco.

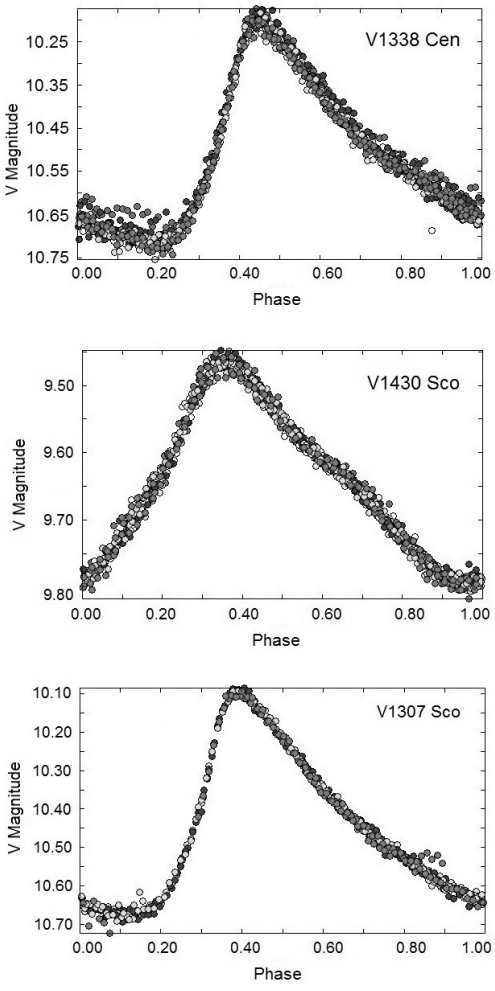

Figure 1. Phased light curves for V1338 Cen, V1430 Sco, and V1307 Sco. A subtle shoulder can be seen in the descending limbs of the curves for V1338 Cen and V1430 Sco.

Table 2. Frequencies of pulsation (d^{-1}), errors of the frequencies, and their signal/noise ratios (SNR) from PERIOD04 Fourier analysis. The error values are least squares uncertainties, with the uncertainties for frequency and phase uncorrelated.

	V1338 Cen			*V1430 Sco*			*V1307 Sco*		
	Frequency	*Error*	*SNR*	*Frequency*	*Error*	*SNR*	*Frequency*	*Error*	*SNR*
f1	7.6372	0.0001	—	11.93629	0.00004	—	8.54475	0.00007	—
f2	15.2739	0.0002	93.8	23.8727	0.0002	60.3	17.0890	0.0002	83.9
f3	22.9112	0.0006	55.0	35.8105	0.0006	26.7	25.6337	0.0004	28.8
f4	30.546	0.001	23.4	18.4335	0.0008	11.7	34.1781	0.0008	16.3
f5	1.020	0.001	9.4	47.7455	0.001	16.4	42.7180	0.002	15.4
f6	38.187	0.002	16.5	—	—	—	—	—	—

Table 3. Times of maximum light (TOM) in heliocentric Julian days (HJD) representing the peaks of the light curves of the target variable stars and the errors of the estimates. The TOMs are the calculated peak values of 10th order polynomial expressions fitted to each light curve segment comprising the ascending limb, peak and descending limb of the curve. The values listed are those output by PERANSO, and are not truncated to the last significant digit.

V1338 Cen		*V1430 Sco*		*V1307 Sco*	
TOM (HJD)	*Error*	*TOM (HJD)*	*Error*	*TOM (HJD)*	*Error*
2457136.997304	0.00080	2457179.002685	0.00103	2457222.028308	0.00053
2457137.128584	0.00069	2457179.170143	0.00090	2457240.052092	0.00067
2457137.258664	0.00084	2457192.993306	0.00076	2457242.041585	0.00072
2457138.044563	0.00075	2457193.160451	0.00072	2457242.977812	0.00065
2457138.175116	0.00082	2457193.999546	0.00066	—	—
2457146.032744	0.00095	2457194.166354	0.00065	—	—
2457146.164086	0.00093	2457206.983177	0.00080	—	—
2457146.949575	0.00100	2457207.905622	0.00074	—	—
2457152.973603	0.00102	2457207.990158	0.00067	—	—
2457154.020365	0.00095	2457209.915224	0.00065	—	—
2457154.150639	0.00086	—	—	—	—

The TOMs for all of the peaks of the light curves for the three variable stars are listed in Table 3, together with the errors of the estimates as calculated by PERANSO. Least squares linear fits for TOMs versus epoch revealed the following ephemerides, where the numbers in brackets represent the error of the last decimal place, and zero epoch is the first peak in the light curve determined by the author from his 2015 observations.

V1338 Cen:

$$T_{max}\ (HJD) = 2457136.9978\ (2) + 0.13093808\ (3)\ E \quad (1)$$

V1430 Sco:

$$T_{max}\ (HJD) = 2457179.0027\ (2) + 0.08377709\ (1)\ E \quad (2)$$

V1307 Sco:

$$T_{max}\ (HJD) = 2457222.0291\ (3) + 0.11703066\ (1)\ E \quad (3)$$

The periods from the above equations are almost identical to those previously published by other authors, namely, 0.1309382 day for V1338 Cen (Samus *et al.* 2007–2013), 0.0837770 day for V1430 Sco (Otero 2007), and 0.117031 day for V1307 Sco (Wils *et al.* 2004).

4. Discussion

Fourier analysis detected harmonics up to 5f1 for V1338 Cen and V1037 Sco, and up to 4f1 for V1430 Sco. They are representations of the extent to which the light curves are skewed from pure sinusoids.

In addition to the Fourier harmonics, special combinations of small instrumental effects and $1 d^{-1}$ aliasing could produce the peak observed at 1.020 d^{-1} in the data for V1338 Cen. Indeed, a single cycle seems systematically shifted in Figure 1 and the six observing nights were clustered into three pairs of consecutive nights (24 and 25 April, 3 and 4 May, and 10 and 11 May). Because of these factors, this peak is not considered to have a stellar origin.

In the case of V1430 Sco, the additional frequency f4 18.4335 d^{-1}, neither a Fourier harmonic nor a combination of other discovered frequencies, has a signal/noise ratio of 11.7 as calculated by PERIOD04, indicating clearly that it should be regarded as a valid pulsation frequency. This frequency has not previously been reported for this star. Its low semiamplitude of 0.008 mag. in comparison with the amplitude of 0.15 mag. for f1 is assumed to be the reason that it was not previously published. The frequency ratio f1/f4 is 0.644, indicating that this is not a fundamental to first overtone ratio, which should lie within the range 0.74 to 0.78 for δ Scuti stars pulsating in the radial mode (Breger 1979). It may therefore represent a non-radial mode, but a detailed consideration of both this possibility and subtle aliasing effects is beyond the resources of the author.

The calculation of linear ephemerides from the previously published TOMs together with the TOMs determined by the author has revealed periods that are essentially identical to those reported by others. The spans of time across which the new ephemerides were calculated, 9 years for V1338 Cen, 11 years for V1430 Sco, and 14 years for V1307 Sco, has allowed the periods of these stars to be reported herein with enhanced

accuracy: 0.13093808 day for V1338 Cen, 0.08377709 day for V1430 Sco, and 0.11703066 day for V1307 Sco.

5. Acknowledgements

The author is grateful to Dr. Simon Murphy, Sydney Institute for Astronomy, University of Sydney, NSW, Australia, for expert assistance in the use of the software PERIOD04.

Part of the work described in this paper was aided by the use of the AAVSO Photometric All-Sky Survey (APASS), funded by the Robert Martin Ayers Sciences Fund.

References

Berry, R., and Burnell, J. 2011, "Astronomical Image Processing for Windows," version 2.4.0, provided with *The Handbook of Astronomical Image Processing*, Willmann-Bell, Richmond, VA.

Breger, M., 1979, *Publ. Astron. Soc. Pacific*, **91**, 5.

Henden, A. A., *et al.* 2014, AAVSO Photometric All-Sky Survey (http://www.aavso.org/apass).

Lenz, P., and Breger, M. 2004, in *The A-Star Puzzle*, eds. J. Zverko, J. Ziznovsky, S. J. Adelman, and W. W. Weiss, IAU Symp., 224. Cambridge University Press, Cambridge, 786.

Menzies, J. W., Cousins, A. W. J., Banfield, R. M., and Laing, J. D. 1989, *S. Afr. Astron. Obs. Circ.*, **13**, 1.

Otero, S. A. 2007, *Open Eur. J. Var. Stars*, **56**, 10.

Pojmański, G. 2002, *Acta Astron.*, **52**, 397.

Samus, N. N., *et al.* 2007–2013, *General Catalogue of Variable Stars*, VizieR On-line Data Catalog (http://cdsarc.u-strasbg.fr/viz-bin/Cat?B/gcvs).

Strohmeier, W. 1967, *Inf. Bull. Var. Stars*, No. 178, 1.

Strohmeier, W., Ott, H., and Schoffel, E. 1968, *Inf. Bull. Var. Stars*, No. 261, 1.

Vanmunster, T. 2013. Light Curve and Period Analysis Software, PERANSO v.2.50 (http//www.peranso.com/).

Wils, P., Greaves, J., and Otero, S. A. 2004, *Inf. Bull. Var. Stars*, No. 5490, 1.

Wozniak, P.R. *et al.* 2004, *Astron. J.*, **127**, 2436.

Multi-Filter Photometric Analysis of Three β Lyrae-type Eclipsing Binary Stars

Tyler Gardner
Gage Hahs
Vayujeet Gokhale
Truman State University, Department of Physics, 100 E. Normal, Kirksville, MO 63501; gokhale@truman.edu

Received September 28, 2015; revised October 9, 2015; accepted November 24, 2015

Abstract We present light curve analysis of three variable stars, ASAS J105855+1722.2, NSVS 5066754, and NSVS 9091101. These objects are selected from a list of β Lyrae candidates published by Hoffman *et al.* (2008). Light curves are generated using data collected at the the 31-inch NURO telescope at the Lowell Observatory in Flagstaff, Arizona, in three filters: Bessell B, V, and R. Additional observations were made using the 14-inch Meade telescope at the Truman State Observatory in Kirksville, Missouri, using Baader R, G, and B filters. In this paper, we present the light curves for these three objects and generate a truncated eight-term Fourier fit to these light curves. We use the Fourier coefficients from this fit to confirm ASAS J105855+1722.2 and NSVS 5066754 as β Lyrae-type systems, and NSVS 9091101 to possibly be a RR Lyrae-type system. We measure the O'Connell effect observed in two of these systems (ASAS J105855+1722.2 and NSVS 5066754), and quantify this effect by calculating the "Light Curve Asymmetry" (LCA) and the "O'Connell Effect Ratio" (OER).

1. Introduction

Eclipsing binary systems are of particular importance to astronomy since they provide a unique opportunity to determine stellar parameters like the mass, radii, and luminosity of each component to a high degree of accuracy. Moreover, once the orbital period, inclination, and radial velocity of the system are determined, the radii of the stars can be determined. Of particular interest are β Lyrae-type systems which exhibit a continuous variation in the light curve, believed to be due to the tidal distortion of the individual components.

We selected three candidate β Lyrae-type systems from Hoffman *et al.* (2008) to determine the exact nature of these systems—whether they are Algols, W UMa-, or β Lyrae-type systems. This project is part of an effort at Truman State University (TSO) to introduce undergraduate students to differential aperture photometry by following three to four eclipsing binary systems per semester with the aim of generating light curves and modeling these systems. Apart from the primary objective of classifying these systems correctly, we are also interested in observing and studying the O'Connell effect (O'Connell 1951), which is the inequality in the out-of-phase maxima in the light curve of eclipsing binaries. The origin of this asymmetry is not well studied or understood, though the most common explanation for this phenomenon is the presence of star spots and/or a hot spot resulting from mass transfer between the components of the binary system (Koju and Beaky 2015).

In the following section, we outline our observational data acquisition and data reduction methods, followed by an analysis of the light curves in section 3. We conclude in section 4 with a discussion on our results and our future plans.

2. Observations

We present BVR photometry of eclipsing variable stars ASAS J105855+1722.2 (period P = 0.38 d), NSVS 5066754 (P = 0.375 d), and NSVS 9091101 (P = 0.25107 d). The data were collected using the 2k × 2k Loral NASACam CCD attached to the 31-inch NURO telescope at Lowell Observatory, Flagstaff, Arizona. The filters used are Bessell BVR. Additional data were obtained (see Table 1) using the SBIG STT-8300 CCD camera attached to the 14-inch LX-200 Meade telescope at the Truman State Observatory at Kirksville, Missouri. The filters used are Baader Planetarium RGB filters. The NURO images are processed by bias subtraction and (sky) flat fielding using the software package MAXIMDL (Diffraction Limited 2012). No dark subtraction was performed since for the nitrogen-cooled camera at NURO, the dark current is negligible. The TSO images are processed by bias and dark subtraction, and (dome) flat fielding using MAXIMDL. Differential photometry is then performed on the target with a suitable comparison and check star, using MAXIMDL and the AAVSO photometry tool VPHOT (Klingenberg and Henden 2013). The aperture size was adjusted to match between 3 to 4 times the full width at half maximum (FWHM) of the brightest object on which photometry was performed for a given target. Similarly, the inner sky annulus was adjusted to about 5 times the FWHM (Beck *et al.* 2015). We searched for any comparison stars from the Tycho (Høg *et al.* 2000) and APASS3 catalogues (Henden *et al.* 2012) that are present in the image frame, and used these stars to determine the B and V magnitudes

Table 1. Observation dates, instrument and filters for the targets.

Target	*Observation Date*	*Telescope*	*Filters*
ASAS J105855+1722.2	03/10/2015	NURO	Bessell BVR
	03/11/2015	NURO	Bessell BVR
	03/20/2015	TSO	Baader RGB
	03/21/2015	TSO	Baader RGB
NSVS 5066754	04/10/2015	TSO	Baader RGB
	10/25/2014	TSO	Baader RGB
	10/28/2014	TSO	Baader RGB
	10/29/2014	TSO	Baader RGB
NSVS 9091101	10/31/2014	TSO	Baader RGB
	11/01/2014	TSO	Baader RGB
	11/24/2014	NURO	Bessell BVR
	11/26/2014	NURO	Bessell BVR

Table 2. Target, comparison, and check star coordinates and comparison star B and V magnitudes.

Star Designation	*Position* R.A. (2000) h m s	Dec. (2000) ° ′ ″	*V*	*B*
Target Stars				
ASAS J105855+1722.2	10 58 55.05	+17 22 12.1	—	—
NSVS 5066754	13 20 57.77	+47 29 29.3	—	—
NSVS 9091101	00 22 43.44	+08 50 05.9	—	—
Comparison Stars				
TYC 1429-165-1	10 58 57.953	+17 25 35.26	12.47	12.30
—	13 20 20.77	+47 33 42.2	12.541	13.388
—	00 22 16.12	+08 47 06.7	13.084	14.179
Check Stars				
—	10 59 01	+17 18 39.97	—	—
—	13 20 51	+47 25 46	—	—
—	00 22 45.9	+08 52 15.43	—	—

of each of the targets. Since we could not find the R magnitude of any of the comparison stars, differential photometry was performed on the R-filter data using instrumental magnitudes. Stars of brightness comparable to the target star were chosen as check stars. Please see Table 2 for details.

3. Analysis and results

For plotting the light curve for each object, the time axis is phase-folded using the period provided by Hoffman *et al.* (2008) and calculating the phase using the equation

$$\Phi = \frac{T - T_0}{P} - \mathrm{Int}\left(\frac{T - T_0}{P}\right), \qquad (1)$$

where P is the period of the system and T_0 is an arbitrarily chosen epoch. The resulting light curve in B and V for each object is shown in Figures 1, 2, and 3. The color B–V is plotted on the bottom panel of each light curve. It is clear from the light curves that ASAS J105855+1722.2 and NSVS 5066754 show two unequal eclipses, whilst only one eclipse is seen in NSVS 9091011. For each object we calculate the average B and V magnitude, and hence the average value of B–V. These values are tabulated in Table 3. Since we have used standard Johnson filters for ASAS J105855+1722.2 and NSVS 9091101, we use the B–V color to calculate an estimate of the temperature using Flower (1996). Unfortunately, we do not have the data to calculate the same for NSVS 5066754 or the NSVS 9091101 data collected at TSO. Nevertheless, the B–V plots for NSVS 5066754 and NSVS 9091011 appear to be more or less flat, which might indicate that the surface temperatures of the two components of the binary are similar. For ASAS J105855+1722.2, a slight "bump" can be seen around the secondary eclipse with a corresponding "dip" around the primary eclipse, which suggests that the hotter star is being eclipsed at primary eclipse, and the cooler component is

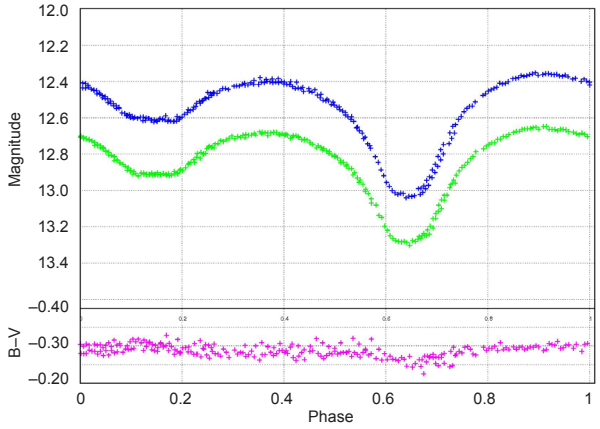

Figure 1. Light curve for ASAS J105855+1722.2, along with the B–V color versus orbital phase. The two colors denote Bessell B and V filters. Note the difference in depth of the two eclipses and the smoothly varying light curve. Also note the difference in the primary and secondary maxima (O'Connell effect).

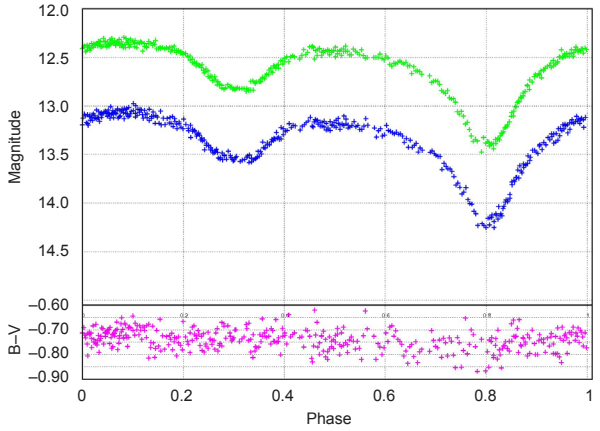

Figure 2. Light curve for NSVS 5066754 in Baader Blue and Green filters and the B–V color versus orbital phase. Note the difference in depth of the two eclipses and the smoothly varying light curve. Also note the difference in the primary and secondary maxima (O'Connell effect).

Table 3. Average B and V magnitudes, B–V color and Temperature estimate.

Target	*Average B*	*Average V*	*Average B–V*	*Temperature K*
ASAS J105855+1722.2	12.563	12.850	–0.287	30789
NSVS 5066754 (Baader filters)	13.349	12.607	0.742	—
NSVS 9091101 (Baader filters)	13.168	12.269	0.899	—
NSVS 9091101	13.008	12.241	0.767	5360

Note: The Baader filter values are "non-standard" and are shown here for completeness.

eclipsed at secondary eclipse. The color temperature of ASAS J105855+1722.2 is quite high, indicating the presence of early-type components.

We converted the differential magnitude measured in each filter to the normalized flux (Warner 2006) by using

$$I(m(\phi)) = I_{max}\ 10^{-0.4 \times (m(\phi) - m(max))} \qquad (2)$$

where m(ϕ) is the magnitude dependent upon phase, m(max) is the maximum magnitude, and the I_{max} value is set to one.

Following Wilsey and Beaky (2009), we perform a Fourier fit analysis on the light curves for each of the objects we studied in each filter. The Fourier coefficients are then used to classify each system as either a β Lyrae, Algol, or WUMa system; and to quantify the O'Connell effect. The Fourier fit is accomplished using VSTAR (Benn 2013) provided by the American Association of Variable Star Observers (AAVSO). The fits are generated after the data for each object were shifted so that the primary eclipse occurred at phase 0. The truncated Fourier fit is given by

$$m(\phi) = \sum_{n=0}^{8} a_n \cos(2\pi n(\phi - \theta)) + b_n \sin(2\pi n(\phi - \theta)) \qquad (3)$$

where a_n and b_n are the Fourier coefficients, ϕ is the phase, and θ is the phase offset to compensate for the unknown time of the maximum/minimum (Hoffman *et al.* 2009).

3.1. Classification of systems

The comparison of the second and fourth cosine coefficients, a_2 and a_4, yields an estimate on the degree of contact of the system (Rucinski 1997). We refer to Rucinski (1973) and Rucinski (1993) for a detailed description of the use of the Fourier coefficients in determining the orbital elements of contact binary stars. For our purposes it is sufficient to appreciate that the a_2 coefficient attempts to quantify the tidal proximity effect in detached systems, whilst a_4 attempts to account for the symmetrical deviations from the exact double cosine term caused by the eclipses. Thus, a_2 is a measure of the global distortion of the contact structure, whilst a_4 represents the more localized eclipse effects. Rucinski (1997) summarizes these effects in terms of the two Fourier coefficients as follows: if $a_4 > a_2(0.125 - a_2)$ then the system can be considered a β Lyrae candidate. Furthermore, if $a_4 < a_2(0.125 - a_2)$ then the system may be considered detached eclipsing binary or Algol. In addition, if $|a_4| < 0.02$, the objects could be either RR Lyr or W UMa variables with periods under 1.2 days (Hoffman *et al.* 2008, 2009). We evaluated these relationships for each of our objects and the results are recorded in Table 4.

It is clear from the results in Table 4 that ASAS J105855 +1722.2 and NSVS 5066754 are β Lyrae-type systems. This is consistent with the fact that the light curves for these objects in each filter is continuously varying; and that the depth of the primary and secondary minima are not similar. Note that the third object, NSVS 9091101, does not show a secondary minima at all and has $|a_4| < 0.02$. Since the object cannot be classified as a W UMa, we classify it as either a β Lyrae or an RR Lyrae system based on the criteria outlined above.

3.2. Quantifying the O'Connell effect

The O'Connell effect is the asymmetry in the heights of the

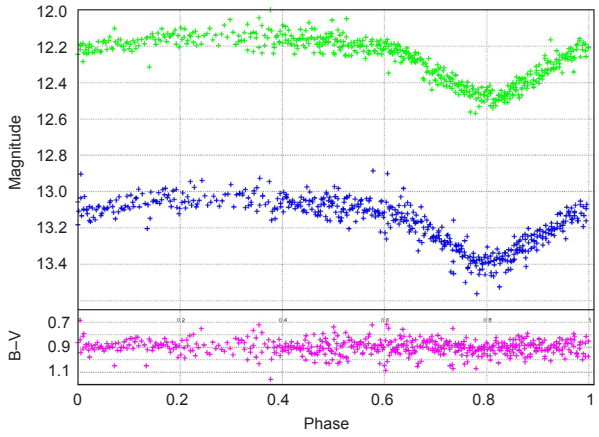

Figure 3. Light curve for NSVS 9091011 in Baader Blue and Green filters and the B–V color versus orbital phase. Note that the light curve varies smoothly, and only one eclipse is observed.

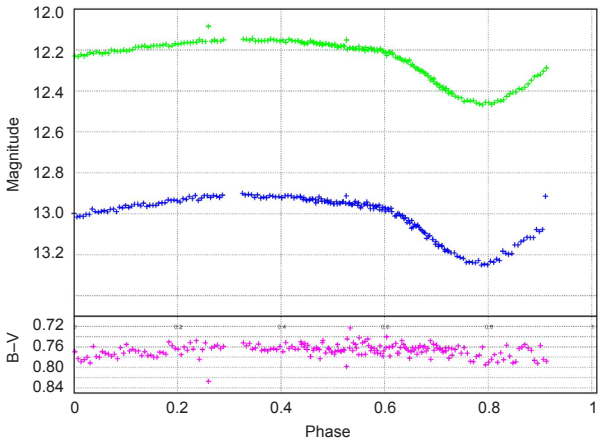

Figure 4. Light curve for NSVS 9091011 in Bessell B and V filters and the B–V color versus orbital phase. Note that the light curve varies smoothly, and only one eclipse is observed. Note that for this set of observations we do not have coverage over the entire phase.

Table 4. Classification of systems based on Fourier coefficients.

Target	*Filter*	a_2	a_4	$a_2(0.125 - a_2)$	*Classification*
ASAS J105855+1722.2	B	–0.15329	–0.03029	–0.04265907	β Lyr
	V	–0.15191	–0.03138	–0.04206368	β Lyr
	R	–0.15199	–0.03246	–0.04210057	β Lyr
NSVS 5066754	B	–0.18786	–0.05218	–0.05877538	β Lyr
	G	–0.19084	–0.05357	–0.06027592	β Lyr
	R	–0.19253	–0.05343	–0.06113507	β Lyr
NSVS 9091101	B	–0.01819	0.006372	–0.0026043	β Lyr/RR Lyr
	V	–0.0048	0.008484	–0.00062277	β Lyr/RR Lyr
	R	–0.01047	0.006927	–0.00141852	β Lyr/RR Lyr
NSVS 9091101 (TSO)	B	–0.038966	–0.005532	–0.0063891	β Lyr/RR Lyr
	G	–0.039086	–0.00707	–0.006413465	β Lyr/RR Lyr
	R	–0.038606	–0.00587	–0.006316173	β Lyr/RR Lyr

maxima observed in the light curves of some eclipsing binaries. A definite explanation for this phenomenon has been somewhat elusive, though the "starspot model" and the "hot spot model" have been suggested as possible explanations for the observed O'Connell effect (Koju and Beaky 2015). The simplest way to quantify the O'Connell effect is to calculate the difference between the primary (m_p) and secondary (m_s) maxima:

$$\Delta m = m_p - m_s \quad (4)$$

A positive Δm means the peak after the primary eclipse is brighter than the peak after the secondary eclipse. A negative Δm implies the opposite. By phase shifting our light curves such that the primary eclipse is set to phase θ = 0.0, we see that the peak magnitudes align approximately at phases θ = 0.25 and θ = 0.75, as shown in Figure 5 and Figure 6.

We use the coefficient of the first sine term in our Fourier fit to approximate Δm. The first sine term has extrema at phases θ = 0.25 and θ = 0.75. This makes it the dominant component accounting for the asymmetry in the peak magnitudes (Wilsey and Beaky 2009). In Figure 5 and Figure 6, we plot the first sine term with the light curve to show how the extremes of the sine wave align with the out-of-eclipse peak magnitudes. The coefficient, b_1, associated with the first sine term is the half-amplitude of the sine wave. This implies that $|2b_1|$ is a close approximation to Δm, and hence, a close approximation to the magnitude of the O'Connell effect. The $|2b_1|$ values for each of our objects are calculated from the Fourier coefficients and recorded in Table 5.

We calculated Δm in two other ways. Firstly, we found the values of the two peak magnitudes of the Fourier fit functions. The difference between the two maxima gives us a measure of the O'Connell effect. These values are presented in Table 5 as "Δm (Fourier)." Secondly, all of the data points within 0.05 phase of each maximum are averaged. The difference between the two average values for the maxima is calculated, yielding another measure of Δm. These values are recorded in Table 5 as "Δm (Average)."

Following Wilsey and Beaky (2009) and McCartney (1999), we quantified the O'Connell effect using two other

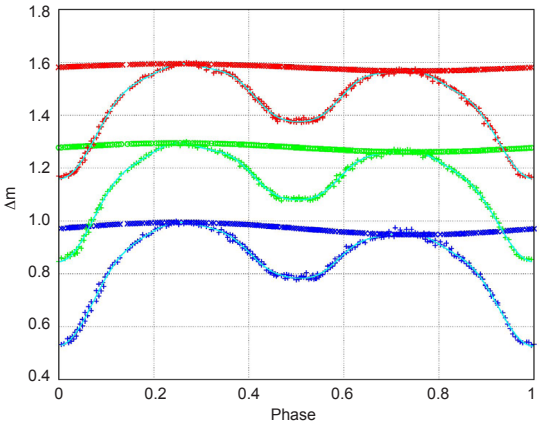

Figure 5. Differential magnitudes ("+" symbols) for ASAS J105855+1722.2. The Fourier fit (continuous curve) and the first sin term of the fit ("×" symbols) are plotted as well. The red, green, and blue curves correspond to RVB filters, respectively.

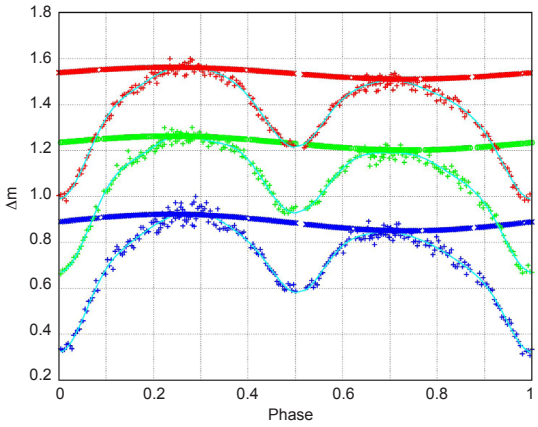

Figure 6. Differential magnitude ("+" symbols) for NSVS 5066754. The Fourier fit (continuous curve) and the first sin term of the fit ("×" symbols) are plotted as well. The red, green, and blue curves correspond to RGB filters, respectively.

Table 5. Quantifying the O'Connell effect in terms of difference in maxima. Please see the text (section 3.2) for details.

Target	*Filter*	$\|2b_1\|$	*Δm (Fourier)*	*Δm (Average)*
ASAS J105855+1722.2	B	0.047	0.037	0.036
	V	0.034	0.030	0.026
	R	0.026	0.027	0.026
NSVS 5066754	B	0.072	0.086	0.083
	G	0.060	0.077	0.070
	R	0.052	0.058	0.059

measures: the O'Connell Effect Ratio (OER) and the Light Curve Asymmetry (LCA). The OER and LCA provide insight into the asymmetries of the light curve regions between the two eclipses.

The OER is simply the ratio of the area under the curves for phases θ = 0.0 to θ = 0.5 and phases θ = 0.5 to θ = 1.0. An OER > 1 implies that the first half of the light curve has more total flux than the second half. There is strong correlation between the OER and Δm, as a positive Δm implies that the peak after the primary eclipse has more flux, which leads to an OER > 1. A negative Δm then implies an OER < 1. The LCA measures the deviance from symmetry of the two halves of the light curve. If both halves are perfectly symmetric, then we would expect the LCA to be zero. The LCA grows as the light curves become less symmetric. It is important to note that the LCA and OER quantify different aspects of the OC effect. For example, an OER equal to 1 does not necessarily imply an LCA equal to 0. The reason for this is that one can imagine a light curve with a tall but narrow peak maximum and short but wide secondary maximum. Although the areas under the curve of each region may be equal, the curves would be very asymmetric.

The Fourier fit (Equation 3) and the calculated relative flux (Equation 1) are used to determine the OER and LCA using

$$\mathrm{OER} = \frac{\int_{0.0}^{0.5} (I(\theta) - I(0.0))d\theta}{\int_{0.5}^{1.0} (I(\theta) - I(0.0))d\theta} \quad (5)$$

and,

$$LCA = \sqrt{\int_{0.0}^{0.5} \frac{(I(\theta) - I(1.0 - \theta))^2}{I(\theta)^2} d\theta} \quad (6)$$

The values for these parameters are tabulated in Table 6.

4. Discussion and future work

We have successfully completed the photometric light curve analysis of ASAS J105855+1722.2, NSVS 5066754, and NSVS 9091101. Based on our light curves and analysis we conclude that the first two systems are β Lyrae systems, while the third system is either a β Lyrae- or RR Lyrae-type system. None of these systems has shown any δ Scuti oscillations (Mkrtichian *et al.* 2004; Tempesti 1971) though the data collected at the Truman Observatory may be too noisy to ascertain any δ Scuti oscillations (which usually are in the millimagnitude range). Both ASAS J105855+1722.2 and NSVS 5066754 show a positive O'Connell effect.

We have tried to model these systems using photometric data alone, but we are not in a position to calculate a unique model. We are in the process of acquiring spectroscopic data (Powell 2015) in order to generate unique and accurate models for these systems. We are particularly interested in understanding the origin of the O'Connell effect based on these models in terms of the "starspot model" and the "hot spot model." To this end, we are in the process of quantifying the O'Connell effect in Kepler EBs using the Kepler Eclipsing Binary Catalogue maintained by Villinova University (Kirk *et al.* 2015). Additionally, we are in the process of acquiring photometric and spectroscopic data on low mass Kepler Eclipsing Binaries (Prša *et al.* 2011) which show the O'Connell effect in order to accurately model these systems and to determine the properties of hotspots and/or starspots (size, lifecycle and so on) in these systems. We believe that this information will be useful to discern the effects of these spots in the detection of exoplanets around low mass (single) stars.

5. Acknowledgements

The authors would like to thank W. Lee Powell for helpful discussions. We have made extensive use of the tools avaliable on the AAVSO website, in particular, the VSP tool to generate star charts, and the VSTAR and VPHOT tools to perform photometry. In addition, we have used the SIMBAD database, operated at CDS, Strasbourg, France and NASA's Astrophysics Data System. We are thankful for the support provided by the Office of Student Research at Truman State University, and to the Missouri Space Grant Consortium. This research was made possible through the use of the AAVSO Photometric All-Sky Survey (APASS), funded by the Robert Martin Ayers Sciences Fund. The authors would also like to thank the anonymous referee for useful comments and suggestions, which greatly improved the manuscript.

Table 6. Quantifying the O'Connell effect in terms of OER and LCA. Please see text (section 3.2) for the definitions of the OER and LCA.

Target	*Filter*	*OER*	*LCA*
ASAS J105855+1722.2	B	1.08629	0.024018
	V	1.06753	0.018802
	R	1.05793	0.014743
NSVS 5066754	B	1.14588	0.054379
	G	1.12555	0.044532
	R	1.11302	0.040538

References

Beck, S., Henden A., and Templeton, M. 2015, *The AAVSO Guide to CCD Photometry*, AAVSO, Cambridge, MA (https://www.aavso.org/ccd-photometry-guide).

Benn, D. 2013, VSTAR data analysis software (http://www.aavso.org/vstar-overview).

Diffraction Limited. 2012, MAXIMDL image processing software (http://www.cyanogen.com).

Flower, P. J. 1996, *Astrophys. J.*, **469**, 355.

Henden, A. A., Levine, S. E., Terrell, D., Smith, T. C., and Welch, D. L. 2012, *J. Amer. Assoc. Var. Star Obs.*, **40**, 430 (https://www.aavso.org/apass).

Hoffman, D. I., Harrison, T. E., Coughlin, J. L., McNamara, B. J., Holtzman, J. A., Taylor, G. E., and Vestrand, W. T. 2008, *Astron. J.*, **136**, 1067.

Hoffman, D. I., Harrison, T. E., and McNamara, B. J. 2009, *Astron. J.*, **138**, 466.

Høg, E., *et al.* 2000, *Astron. Astrophys.*, **355**, L27.

Kirk, J., *et al.* 2015, Kepler Eclipsing Binary Stars (Catalog V3; in preparation; http://keplerebs.villanova.edu/).

Klingenberg, G., and Henden, A. A. 2013 VPHOT photometric analysis tool (http://www.aavso.org/vphot).

Koju, V., and Beaky, M. 2015, *Inf. Bull. Var. Stars*, No. 6127, 1.

McCartney, S. A. 1999, Ph.D. dissertation, University of Oklahoma.

Mkrtichian, D. E., *et al.* 2004, *Astron. Astrophys.*, **419**, 1015.

O'Connell, D. J. K. 1951, *Publ. Riverview Coll. Obs.*, **2**, 85.

Powell, L. 2015, private communication.

Prša, A., *et al.* 2011, *Astron. J.*, **141**, 83.

Ruciński, S. M. 1973, *Acta Astron.*, **23**, 79.

Rucinski, S. M. 1993, *Publ. Astron. Soc. Pacific*, **105**, 1433.

Rucinski, S. M. 1997, *Astron. J.*, **113**, 407.

Tempesti, B. 1971, *Inf. Bull. Var. Stars*, No. 596, 1.

Warner, B. D. 2006, *A Practical Guide to Lightcurve Photometry and Analysis*, Springer-Verlag, New York.

Wilsey, N. J., and Beaky M. M. 2009, in *The Society for Astronomical Sciences 28th Annual Symposium on Telescope Science. Held May 19–21, 2009 at Big Bear Lake, CA, Society for Astronomical Sciences, Rancho Cucamonga, CA, 107.*

Seventeen New Variable Stars Detected in Vulpecula and Perseus

Riccardo Furgoni
Keyhole Observatory MPC K48, Via Fossamana 86, S. Giorgio di Mantova (MN), Italy, and AAMN Gorgo Astronomical Observatory MPC 434, S. Benedetto Po (MN), Italy; riccardo.furgoni@gmail.com

Received July 27, 2015; revised August 14, 2015, September 16, 2015; September 22, 2015; accepted November 24, 2015

Abstract I report the discovery of seventeen new variable stars in the Northern Sky: three eclipsing (GSC 02129-00759; GSC 02129-00947; GSC 02869-02559), one eruptive (GSC 02856-02521), ten pulsating (2MASS J19305329+2558520; GSC 02129-00537; 2MASS J19323543+2524000; 2MASS J19263580+2616428; HD 275169; GSC 02869-00313; GSC 02869-01981; GSC 02856-01391; GSC 02860-01552; GSC 02856-01465) and three rotating (one of which is suspected) (GSC 02142-01107; GSC 02856-00169; GSC 02865-01593).

1. Introduction

Starting in the spring of 2011 the Keyhole Observatory MPC K48, located in S. Giorgio di Mantova (Italy), has been involved in an intense surveying activity mainly focused on new variable star discovery and characterization. Even this year a new observing campaign was conducted in three separate fields located in the constellations of Vulpecula and Perseus for a total of 28 nights, obtaining 2,583 images in the V passband with an overall exposure time of almost 86 hours.

Subsequently, the light curves of all stars in the fields in a magnitude range between 9 V and 14 V have been visually inspected in order to determine the candidate variables, starting with those that have an RMS scatter as function of magnitude higher than normal. When possible the observations were combined with SuperWASP (Butters *et al.* 2010), ASAS-3 (Pojmański 2002), and NSVS (Woźniak *et al.* 2004) datasets to enhance the precision in the determination of the period, magnitude range, and the type of variability.

Considering all the new variables discovered, two are in my opinion the most interesting: GSC 02856-02521, an RS CVn variable with Algol-type eclipses, and GSC 02860-01552, a high-amplitude δ Scuti (HADS) double mode variable.

2. Instrumentation used

The data were obtained with a TS Optics APO906 Carbon, a triplet FPL-53 apochromatic refractor with 90-mm aperture and f/6.6 focal ratio; the telescope was also equipped with a field flattener for pin-point stellar images corner-to-corner.

The telescope was positioned at coordinates 45° 12' 33" N, 10° 50' 20" E (WGS84) at the Keyhole Observatory, a roll-off roof structure managed by the author. The pointing was maintained with a Syntha NEQ6 mount guided via a Baader Vario Finder telescope equipped with a Barlow lens capable of bringing the focal length of the system to 636 mm and focal ratio of f/10.5. The guide camera was a Magzero MZ-5 with Micron MT9M001 monochrome sensor. The CCD camera was a SBIG ST8300m with monochrome sensor Kodak KAF8300. The photometry in the Johnson V passband was performed with an Astrodon Photometrics Johnson-V 50-mm round unmounted filter, equipping a Starlight Xpress USB filterwheel.

The camera is equipped with a 1,000× antiblooming: after exhaustive testing it has been verified that the zone of linear response is between 1,000 and 20,000 ADU, although up to 60,000 ADU the loss of linearity is less than 5%. The CCD is equipped with a single-stage Peltier cell $\Delta T = 35 \pm 0.1°$ C which allows the cooling at a stationary temperature.

3. Data collection

The observed fields are centered, respectively, at coordinates (J2000) R.A. $19^h\ 29^m\ 00^s$, Dec. +25° 50' 00" (Vulpecula), and R.A. $03^h\ 19^m\ 00^s$, Dec. +41° 29' 00" and R.A. $03^h\ 19^m\ 00^s$, Dec. +42° 46' 00" (both in Perseus). For all, the dimensions are 78' × 59' with a position angle of 360°.

These fields were chosen to maximize the possibility of discovering new variable stars. Their determination was made trying to meet the following criteria:

- equatorial coordinates compatible with low air masses for most of the night at the observing site;
- low or no presence of already known variables, where this element has been determined by analyzing the distribution of the variables in the International Variable Star Index operated by the AAVSO (VSX; Watson *et al.* 2014).

The observations were performed with the CCD at a temperature of –10° C (in summer and fall) and –20° C (in winter) in binning 1 × 1. The exposure time was 120 seconds with a delay of 1 second between the images and an average download time of 11 seconds per frame. Once the images were obtained, a full calibration procedure was performed with dark and flat frames. All images were then aligned and an astrometric reduction made to implement the astrometrical WCS coordinate system in the FITS header. All these operations were conducted entirely through the use of software MAXIMDL V5.23 (Diffraction Limited 2012). The complete observing log is reported in Table 1.

4. Methods and procedures

As a continuation of the wider survey activity conducted from the Keyhole Observatory MPC K48 for new variable star discovery, the methods and procedures used will be presented in a very schematic way; in previously published works (Furgoni 2013a, 2013b) more specific details can be found.

Table 1. Observing log.

UT starting time (yyyy/mm/dd hh.mm.ss)	*UT ending time (yyyy/mm/dd hh.mm.ss)*
Vulpecula Field	
R.A. 19h 29m 00s, Dec. +25° 50′ 00″	
(stars described in sections 5.1 through 5.7)	
2014/07/03 20:30:45	2014/07/04 00:05:40
2014/07/15 20:24:53	2014/07/16 01:29:08
2014/07/16 20:19:39	2014/07/17 00:02:07
2014/07/17 20:17:06	2014/07/17 20:58:23
2014/08/07 19:49:18	2014/08/07 22:28:48
2014/08/18 19:27:24	2014/08/18 21:24:43
2014/08/23 21:11:15	2014/08/23 23:34:04
2014/08/28 19:10:18	2014/08/28 23:13:25
2014/09/14 18:32:17	2014/09/14 23:01:44
2014/09/16 18:46:49	2014/09/16 19:58:31
2014/09/22 18:37:41	2014/09/22 20:58:48
2014/09/25 18:13:26	2014/09/25 21:09:26
2014/09/27 18:38:34	2014/09/27 22:37:33
2014/10/24 17:21:46	2014/10/24 21:00:56
2014/10/26 17:20:31	2014/10/26 20:57:32
Perseus 1 Field	
R.A. 03h 19m 00s, Dec. +41° 29′ 00″	
(stars described in sections 5.8 through 5.12)	
2015/01/11 17:28:35	2015/01/11 22:23:41
2015/01/12 17:14:17	2015/01/12 21:23:08
2015/01/26 17:23:42	2015/01/26 19:42:27
2015/01/28 17:23:44	2015/01/28 20:58:01
2015/02/02 17:50:58	2015/02/02 21:54:59
2015/02/09 17:45:05	2015/02/09 21:26:17
Perseus 2 Field	
03h 19m 00s, Dec. +42° 46′ 00″	
(stars described in sections 5.13 through 5.17)	
2015/02/10 17:49:10	*2012/02/10 22:23:19*
2015/02/11 18:17:49	*2015/02/11 22:03:50*
2015/02/17 17:51:46	*2015/02/17 21:28:15*
2015/02/18 17:52:45	*2015/02/18 21:34:48*
2015/03/07 18:16:16	*2015/03/07 21:47:15*
2015/03/08 18:13:56	*2015/03/08 21:37:38*
2015/03/12 18:21:13	*2015/03/12 21:36:25*

The technique used for the determination of the magnitude was differential photometry, ensemble-type in almost all cases. It is necessary to have comparison stars with magnitudes accurately determined in order to obtain reliable measurements and as close as possible to the standard system. Since the entire observational campaign was conducted with the use of the Johnson V filter the comparison star magnitudes were obtained from the APASS (Henden *et al.* 2013) V magnitude data provided by the AAVSO.

The search for new variable stars was performed using the same technique described in Furgoni (2013a, 2013b): the method involves the distinction between discovery nights and follow-up nights. The first is needed to determine if the chosen field contains potential candidate variables through the creation of a magnitude-RMS diagram and the accurate visual inspection of all light curves down to the fourteenth magnitude. If in the discovery night the chosen field does not appear interesting it is discarded without further analysis. The follow-up nights, instead, are necessary for the collection of data concerning variable star candidates. In any case, any follow-up night is checked again by a magnitude-RMS scatter diagram. In this case, however, the light curves of the stars in the field are not inspected visually due to the long time needed for the operation. The combination of these two ways of working ensures a good compromise between the need to maximize the chance of discovery and to obtain the maximum from the data gradually collected.

Before proceeding further in the analysis, the time of the light curves obtained was heliocentrically corrected (HJD) in order to ensure a perfect compatibility of the data with observations carried out even at a considerable distance in time. When necessary, the determination of the period was calculated using the software PERIOD04 (Lenz and Breger 2005), using a Discrete Fourier Transform (DFT). The average zero-point (average magnitude of the object) was subtracted from the dataset to prevent the appearance of artifacts centered at frequency 0.0 of the periodogram. The calculation of the uncertainties was carried out with PERIOD04 using the method described in Breger *et al.* (1999).

To improve the period determination, SWASP, ASAS-3, and NSVS photometric data were used when available. However, due to the high scattering which in some cases affects both, the data with high uncertainties were eliminated. The datasets were also corrected in their zero-point to make them compatible with my V band data. Having the same zero-point is indeed crucial for correct calculation of the Discrete Fourier Transform operated by PERIOD04.

5. New variable stars discovered

In this survey seventeen new variable stars were discovered belonging to a population composed as follows:

- Three eclipsing (two β Lyrae and one β Persei).

- One eruptive (one RS Canum Venaticorum with β Persei eclipses).

- Ten pulsating (six Delta Scuti, one double-mode High Amplitude Delta Scuti, one RR Lyrae Ab-type , one RR Lyrae C-type and one Semi-Regular late-type).

- Three rotating (three rotating ellipsoidal, one of which is suspected).

The coordinates of all new variable stars discovered in this survey are reported as they appear in the UCAC4 catalogue (Zacharias *et al.* 2012) and never differ from the detected positions for a value greater than 1".

5.1. 2MASS J19305329+2558520
Position (UCAC4): R.A. (J2000) = $19^h\ 30^m\ 53.29^s$, Dec. (J2000) = +25° 58' 52.0"
Cross Identification ID: UCAC4 580-084318
Variability Type: RR Lyr Ab
Magnitude: Max. 14.15 V, Min. 14.90 V
Period: 0.47303(2) d
Epoch: 2456898.3480(14) HJD
Rise duration: 19%
Ensemble Comparison Stars: UCAC4 580-083946 (APASS 11.479 V); UCAC4 580-083785 (APASS 11.665 V)
Check Star: UCAC4 580-084083
Notes: Phase plot is shown in Figure 1.

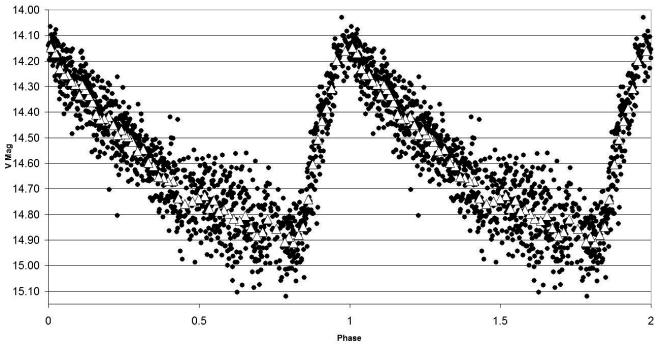

Figure 1. Phase Plot of 2MASS J19305329+2558520. Filled circles denote Furgoni data; open triangles denote Furgoni data (binning 20).

5.2. GSC 02129-00537
Position (UCAC4): R.A. (J2000) = $19^h\ 31^m\ 49.74^s$, Dec, (J2000) = +25° 50' 49.8"
Cross Identification ID: 2MASS J19314974+2550498; UCAC4 580-084953
Variability Type: δ Sct
Magnitude: Max 13.42 V, Min 13.46 V
Period: 0.1039816(38) d
Epoch: 2456854.3844(11) HJD
Ensemble Comparison Stars: UCAC4 580-083946 (APASS 11.479 V); UCAC4 580-083785 (APASS 11.665 V)
Check Star: UCAC4 580-084083
Notes: Low galactic latitude star, probably reddened. Phase plot is shown in Figure 2.

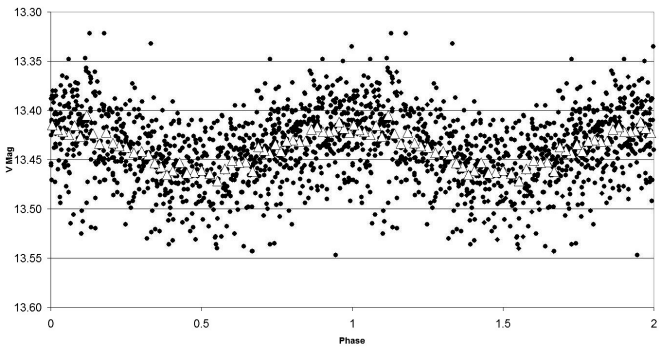

Figure 2. Phase Plot of GSC 02129-00537. Filled circles denote Furgoni data; open triangles denote Furgoni data (binning 20).

5.3. GSC 02142-01107
Position (UCAC4): R.A. (J2000) = $19^h\ 32^m\ 33.71^s$, Dec. (J2000) = +25° 47' 42.7"
Cross Identification ID: 2MASS J19323371+2547427; ASAS J193233+2547.7; UCAC4 579-084405
Variability Type: Rotating ellipsoidal
Magnitude: Max 11.33 V, Min 11.42 V
Period: 1.243460(2) d
Epoch: 2456955.358(3) HJD
Ensemble Comparison Stars: UCAC4 580-083946 (APASS 11.479 V); UCAC4 580-083785 (APASS 11.665 V)
Check Star: UCAC4 580-084083
Notes: Secondary maximum = 11.37 V. Phase plot is shown in Figure 3.

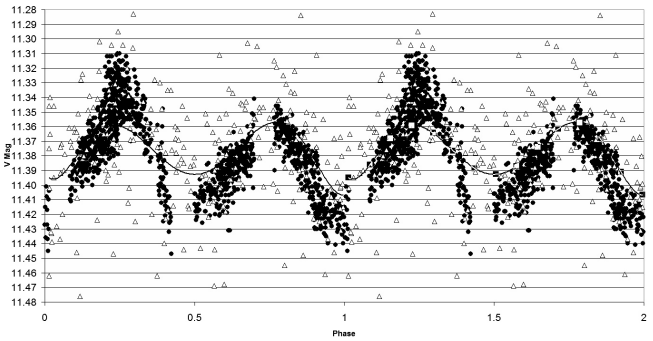

Figure 3. Phase Plot of GSC 02142-01107. Filled circles denote Furgoni data; open triangles denote ASAS3 data (–0.02 mag. offset); line denotes ASAS3 polynomial fitting.

5.4. GSC 02129-00759
Position (UCAC4): R.A. (J2000) = $19^h\ 31^m\ 13.21^s$, Dec. (J2000) = +25° 43' 35.0"
Cross Identification ID: 2MASS J19311321+2543349; NSVS 8365171; UCAC4 579-083612
Variability Type: β Lyr
Magnitude: Max 13.55 V, Min 14.10 V
Period: 0.6647264(2) d
Epoch: 2456854.3911(25) HJD
Ensemble Comparison Stars: UCAC4 579-083181 (APASS 11.595 V); UCAC4 578-089176 (APASS 11.721 V)
Check Star: UCAC4 578-089646
Notes: Secondary minimum = 13.80 V with epoch 2456855.3882(25) HJD. Phase plot is shown in Figure 4.

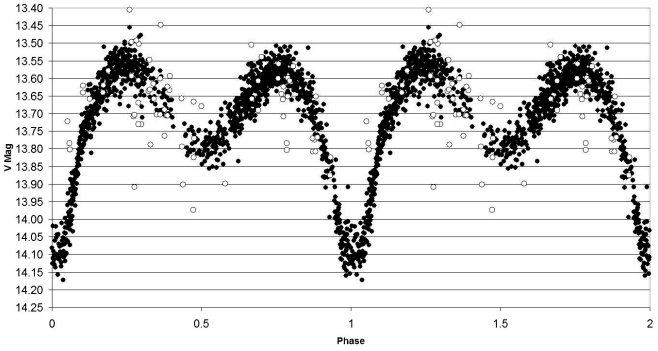

Figure 4. Phase Plot of GSC 02129-00759. Filled circles denote Furgoni data; open circles denote NSVS data (error < 0.3 mag.).

5.5. 2MASS J19323543+2524000
Position (UCAC4): R.A. (J2000) = 19^h 32^m 35.44^s, Dec. (J2000) = +25° 24' 00.1"
Cross Identification ID: UCAC4 578-090607
Variability Type: RR Lyr C
Magnitude: Max 13.67 V, Min 14.15 V
Period: 0.378192(6) d
Epoch: 2456915.330(1) HJD
Rise duration: 40%
Ensemble Comparison Stars: UCAC4 579-083181 (APASS 11.595 V); UCAC4 578-089176 (APASS 11.721 V)
Check Star: UCAC4 578-089646
Notes: Phase plot is shown in Figure 5.

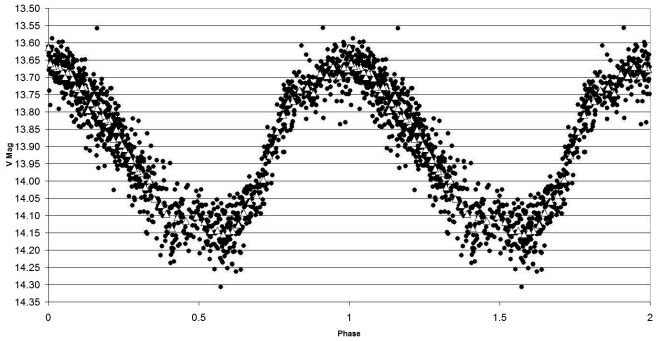

Figure 5. Phase Plot of 2MASS J19323543+2524000. Filled circles denote Furgoni data; open triangles denote Furgoni data (binning 20).

5.6. 2MASS J19263580+2616428
Position (UCAC4): R.A. (J2000) = 19^h 26^m 35.81^s, Dec. (J2000) = +26° 16' 42.8"
Cross Identification ID: UCAC4 582-080882; USNO-B1.0 1162-0380200
Variability Type: δ Sct
Magnitude: Max 13.76 V, Min 13.85 V
Period: 0.182787(7) d
Epoch: 2456854.4373(12) HJD
Ensemble Comparison Stars: UCAC4 580-081384 (APASS 11.856 V); UCAC4 580-082328 (APASS 12.230 V)
Check Star: UCAC4 580-082053
Notes: Phase plot is shown in Figure 6.

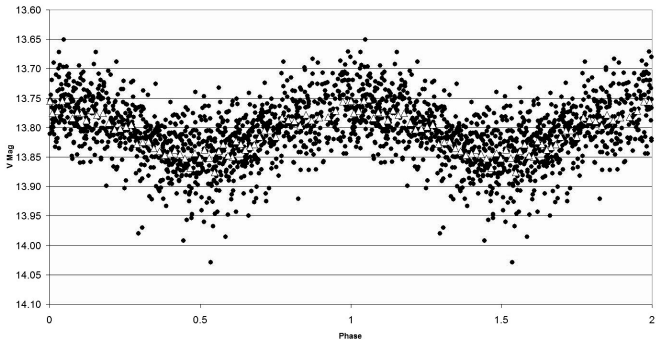

Figure 6. Phase Plot of 2MASS J19263580+2616428. Filled circles denote Furgoni data; open triangles denote Furgoni data (binning 20).

5.7. GSC 02129-00947
Position (UCAC4): R.A. (J2000) = 19^h 26^m 53.10^s, Dec. (J2000) = +25° 52' 00.1"
Cross Identification ID: 2MASS J19265309+2552000; NSVS 8359362; UCAC4 580-081821
Variability Type: β Per
Magnitude: Max 12.90 V, Min 13.30 V
Period: 0.6559882(2) d
Epoch: 2456898.342(2) HJD
Ensemble Comparison Stars: UCAC4 580-081384 (APASS 11.856 V); UCAC4 580-082328 (APASS 12.230 V)
Check Star: UCAC4 580-082053
Notes: Secondary minimum = 13.00 V with epoch 2456855.375(2) HJD. Phase plot is shown in Figure 7.

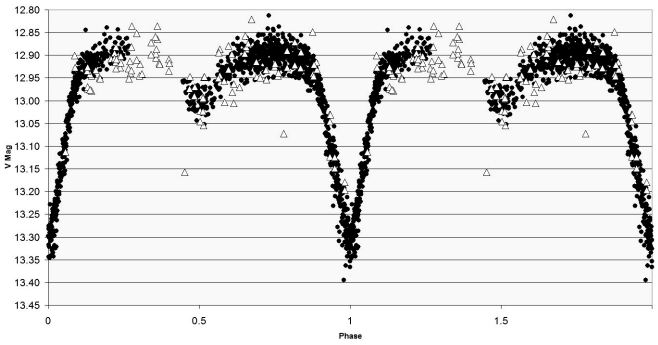

Figure 7. Phase Plot of GSC 02129-00947. Filled circles denote Furgoni data; open triangles denote NSVS data (error < 0.1 mag.; +0.18 mag. offset).

5.8. GSC 02856-02521
Position (UCAC4): R.A. (J2000) = 03^h 19^m 34.83^s , Dec. (J2000) = +41° 56' 04.8"
Cross Identification ID: 1RXH J031934.6+415606; 1SWASP J031934.83+415604.9; 2MASS J03193483+4156048; 3XMM J031934.8+41560; UCAC4 660-015379
Variability Type: RS CVn with β Per eclipses
Magnitude: Max 12.80 V, Min 13.09 V
Period: 3.820158(8) d
Epoch: 2457034.400(2) HJD
Ensemble Comparison Stars: UCAC4 660-015482 (APASS 11.188 V); UCAC4 659-015252 (APASS 11.243 V)
Check Star: UCAC4 660-015415
Notes: Eclipse duration 3%. Min II = 13.03 V. Slightly eccentric system with secondary minimum at phase 0.495 with epoch 2454056.568(2) HJD calculated from SWASP dataset. The system is an X-ray source identified both by the XMM-Newton Serendipitous Source Catalogue 3XMM-DR4 (XMM-Newton Survey Science Centre 2013) and the ROSAT Source Catalog of Pointed Observations with the High Resolution Imager (Rosat Scientific Team 2000) in the 0.2–2 KeV spectrum range. Phase plots are shown in Figures 8a–c; Figures 9a–c show XMM-Newton Source detection, time series, and X-ray spectrum.

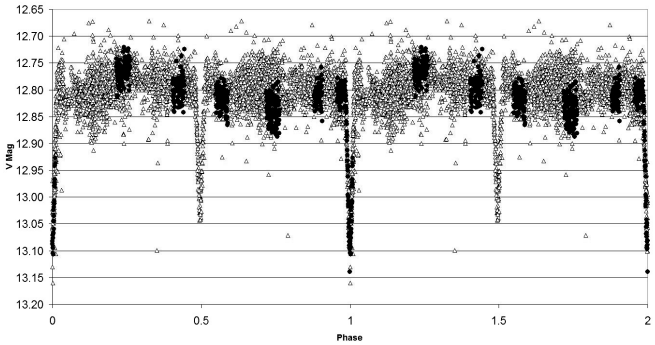

Figure 8a. Phase Plot of GSC 02856-02521. Filled circles denote Furgoni data; open triangles denote SWASP data (camera 142 and 141 with error < 0.03 mag.; +0.07 mag. offset).

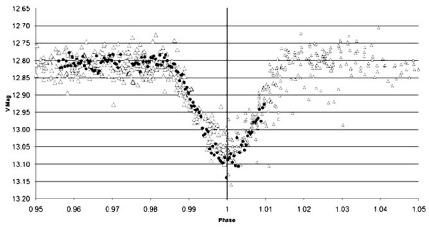

Figure 8b. Phase Plot of GSC 02856-02521. Zoom at phase 1.0.

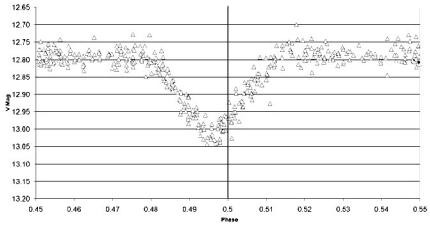

Figure 8c. Phase Plot of GSC 02856-02521. Zoom at phase 0.5.

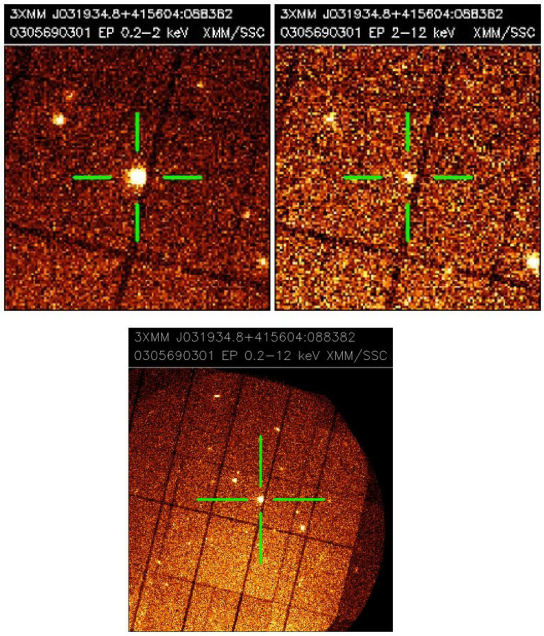

Figure 9a. XMM-Newton source detection of GSC 02856-02521.

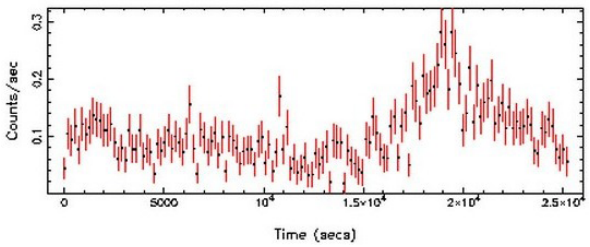

Figure 9b. Background subtracted time series of GSC 02856-02521; mean rate = 0.10366898.

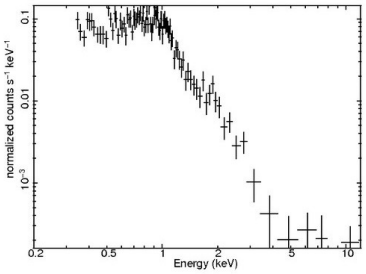

Figure 9c. X-ray spectrum of GSC 02856-02521. Srx 1 minus BGD (P0305690301 PNS003SRSPEC0001).

5.9. GSC 02865-01593

Position (UCAC4): R.A. (J2000) = $03^h\ 23^m\ 07.29^s$, Dec. (J2000) = +41° 14' 41.3"
Cross Identification ID: 2MASS J03230728+4114412; UCAC4 657-015233
Variability Type: Rotating ellipsoidal (suspected)
Magnitude: Max 11.78V, Min 11.80 V
Period: 0.4090484(18) d
Epoch: 2457034.4064(12) HJD
Ensemble Comparison Stars: UCAC4 656-015080 (APASS 11.141 V); UCAC4 656-015057 (APASS 11.740 V)
Check Star: UCAC4 657-015131
Notes: Phase plot is shown in Figure 10.

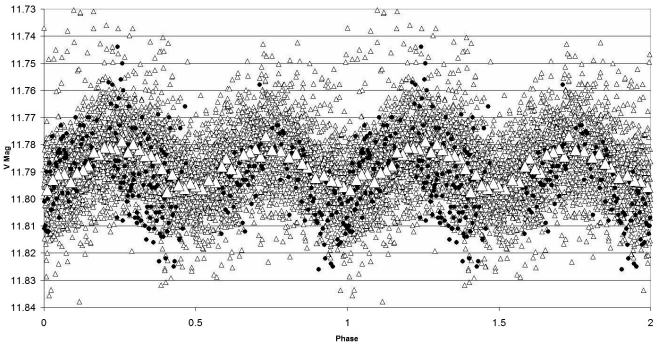

Figure 10. Phase Plot of GSC 02865-01593. Filled circles denote Furgoni data; small open triangles denote SWASP data (camera 148, 142, and 141 with error < 0.02 mag.; +0.26 mag. offset); large open triangles denote SWASP data (binning 40).

5.10. HD 275169
Position (UCAC4): R.A. (J2000) = $03^h\ 21^m\ 12.88^s$, Dec. (J2000) = +40° 56' 45.6"
Cross Identification ID: 1SWASP J032112.86+405645.6; 2MASS J03211287+4056457; BD+40 718; GSC 02865-01872; TYC 2865-1872-1; UCAC4 655-014926
Variability Type: δ Sct
Magnitude: Max 10.61 V, Min 10.65V
Main Period: 0.09041008(6) d
Epoch of the Main Period: 2457034.3456(6) HJD
Ensemble Comparison Stars: UCAC4 656-015080 (APASS 11.141 V); UCAC4 656-015057 (APASS 11.740 V)
Check Star: UCAC4 657-015131
Notes: The star shows a clear variability of the light curve, where at least other two active frequencies were detected with the following elements: HJD 2457034.3442(7) + 0.10055449(8) E with SNR 4.1; HJD 2457034.330(2) + 0.1043577(2)E with SNR 3.0. Spectral type F0 from Nesterov *et al.* (1995). Phase plots and Fourier spectrum plots are shown in Figures 11a–f.

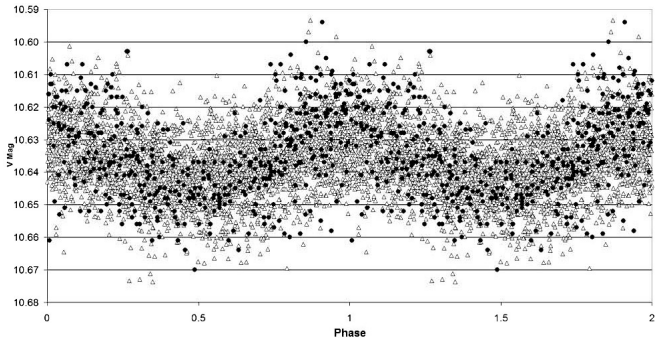

Figure 11a. Main period phase plot of HD 275169; period = 0.09041008(6) d; HDJ_{max} = 2457034.3456(6). Filled circles denote Furgoni data; open triangles denote SWASP data (camera 148, 142, and 141 with error < 0.01 mag.; +0.11 mag. offset).

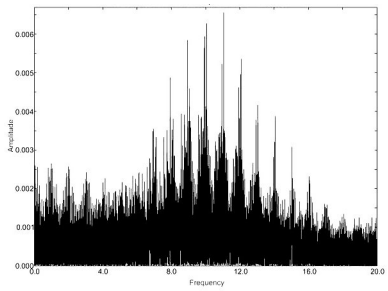

Figure 11b. Fourier spectrum of HD 275169; power spectrum.

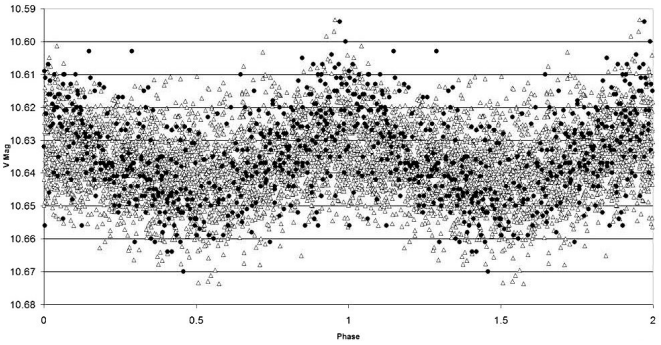

Figure 11c. Second period phase plot of HD 275169; period = 0.10055449(8) d; HDJ_{max} = 2457034.3442(7). Filled circles denote Furgoni data; open triangles denote SWASP data (camera 148, 142, and 141 with error < 0.01 mag.; +0.11 mag. offset).

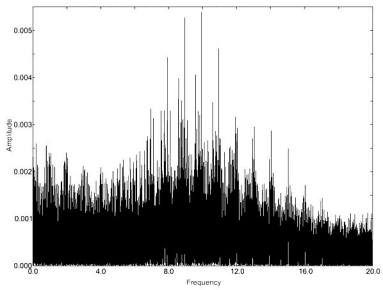

Figure 11d. Fourier spectrum of HD 275169 (after pre-whitening for the 11.060714 c/day frequency).

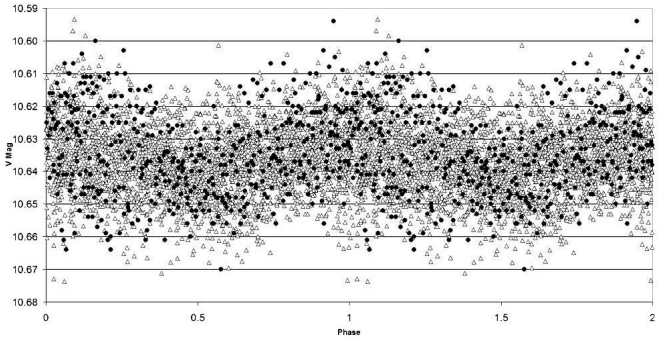

Figure 11e. Third period phase plot of HD 275169; period = 0.1042577(2) d; HDJ_{max} = 2457034.330(2). Filled circles denote Furgoni data; open triangles denote SWASP data (camera 148, 142, and 141 with error < 0.01 mag.; +0.11 mag. offset).

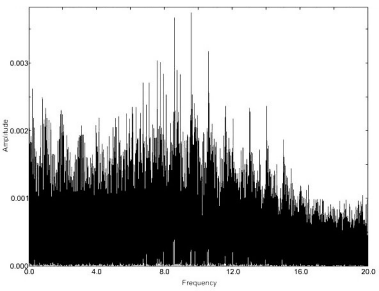

Figure 11f. Fourier spectrum of HD 275169 (after pre-whitening for the 11.060714 c/day 9.944856 c/day frequencies).

5.11. GSC 02869-00313
Position (UCAC4): R.A. (J2000) = $03^h\ 22^m\ 59.17^s$, Dec. (J2000) = +41° 43' 40.5"
Cross Identification ID: 1SWASP J032259.30+414340.9; 2MASS J03225916+4143404; UCAC4 659-015509
Variability Type: δ Sct
Magnitude: Max 11.835 V, Min 11.845V
Period: 0.06505865(6) d
Epoch: 2457034.2432(7) HJD
Ensemble Comparison Stars: UCAC4 659-015465 (APASS 10.949 V); UCAC4 659-015381 (APASS 10.540 V)
Check Star: UCAC4 659-015447
Notes: Phase plot is shown in Figure 12.

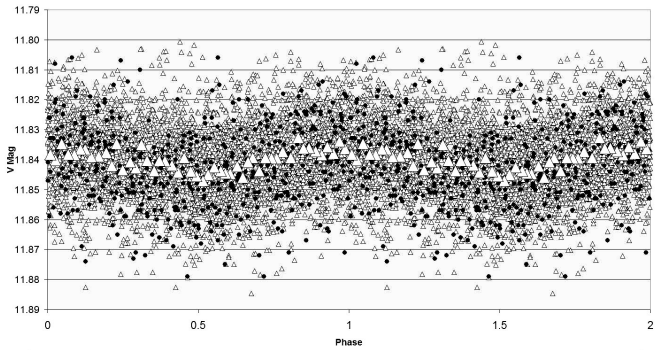

Figure 12. Phase Plot of GSC 02869-00313. Filled circles denote Furgoni data; small open triangles denote SWASP data (camera 141, 142, 144, and 148 with error < 0.02 mag.; –0.25 mag. offset); large open triangles denote SWASP data (binning 40).

5.12. GSC 02869-01981
Position (UCAC4): R.A. (J2000) = $03^h\ 22^m\ 38.08^s$, Dec. (J2000) = +41° 49' 17.4"
Cross Identification ID: 1SWASP J032238.07+414917.5; 2MASS J03223807+4149173; AKARI-IRC-V1 J0322380+414917; TYC 2869-1981-1; UCAC4 660-015709
Variability Type: Semiregular late-type
Magnitude: Max 11.50 V, Min 11.65V
Period: 35.6(1) d
Epoch: 2457040.17(10) HJD
Ensemble Comparison Stars: UCAC4 659-015465 (APASS 10.949 V); UCAC4 659-015381 (APASS 10.540 V)
Check Star: UCAC4 659-015447
Notes: J–K = 1.223. The star is a MID-IR source (CDS catalog II/297/IRC) and probably also identified with the FAR-IR point source PSC 03192-4138 listed in Wise *et al.* (1993). Possibile presence of a secondary period. Phase plot is shown in Figure 13; light curve is shown in Figure 14.

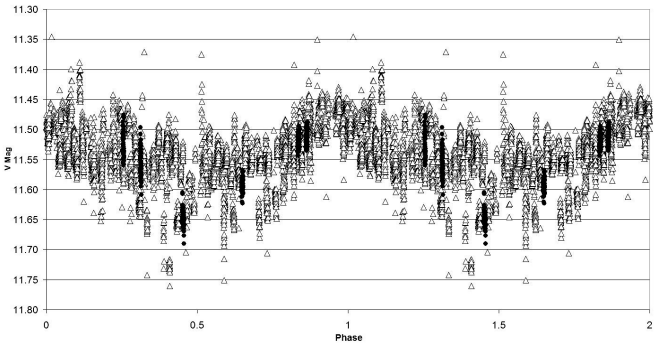

Figure 13. Phase Plot of GSC 02869-01981. Filled circles denote Furgoni data; open triangles denote SWASP data (camera 105, 141, 144, and 148 with error < 0.05 mag.; +0.45 mag. offset).

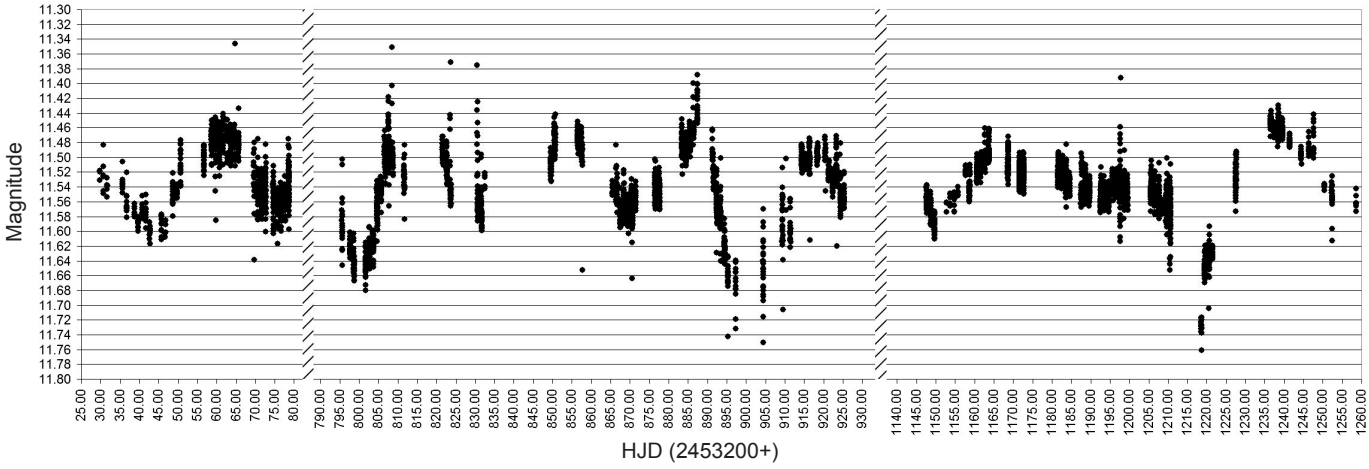

Figure 14. Light Curve of GSC 02869-01981. Y-axis = SWASP magnitude (only datapoint with < 0.05 mag. error and outliers rejected; +0.45 mag. offset); x-axis = HJD from 2453200.0).

5.13. GSC 02856-01391
Position (UCAC4): R.A. (J2000) = $03^h\ 19^m\ 35.51^s$, Dec. (J2000) = +43° 02' 41.3"
Cross Identification ID: 1SWASP J031935.48+430241.4; 2MASS J03193551+4302414; UCAC4 666-016419
Variability Type: δ Sct
Magnitude: Max 13.40 V, Min 13.47 V
Period: 0.1086275(7)
Epoch: 2457064.3295(9) HJD
Ensemble Comparison Stars: UCAC4 666-016582 (APASS 11.679 V); UCAC4 666-016538 (APASS 11.519 V)
Check Star: UCAC4 666-016446
Notes: J–K = 0.23; SWASP magnitudes contaminated by UCAC4 666-016412 (V = 11.500; sep. 24"). SWASP range has been corrected. Phase plot is shown in Figure 15.

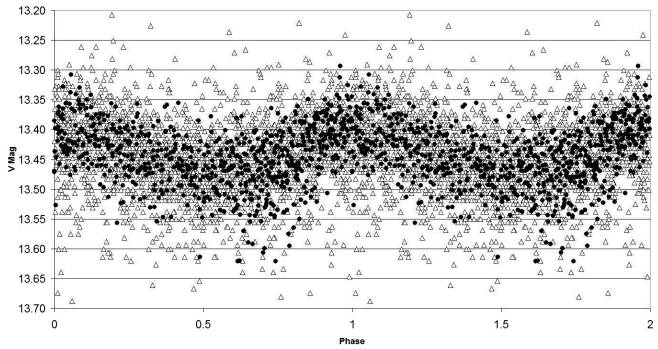

Figure 15. Phase Plot of GSC 02856-01391. Filled circles denote Furgoni data; open triangles denote SWASP data (camera 148, 142, and 141; 0.03 mag. offset and de-blending of UCAC4 666-016412).

5.14. GSC 02869-02559
Position (UCAC4): R.A. (J2000) = $03^h\ 22^m\ 22.08^s$, Dec. (J2000) = +42° 38' 09.7"
Cross Identification ID: 1SWASP J032222.06+423809.7; 2MASS J03222207+4238097; UCAC4 664-016648
Variability Type: β Lyr
Magnitude: Max 12.24 V, Min 12.42 V
Period: 0.8109062(3)
Epoch: 2457072.2259(12) HJD
Ensemble Comparison Stars: UCAC4 664-016588 (APASS 10.948 V); UCAC4 664-016596 (APASS 10.987 V)
Check Star: UCAC4 664-016695
Notes: J–K = 0.25; secondary maximum = 12.27 V; Min II = 12.36 V with epoch 2457065.333(2) HJD from the Furgoni dataset and 2453997.675(2) from the SWASP dataset. Phase plot is shown in Figure 16.

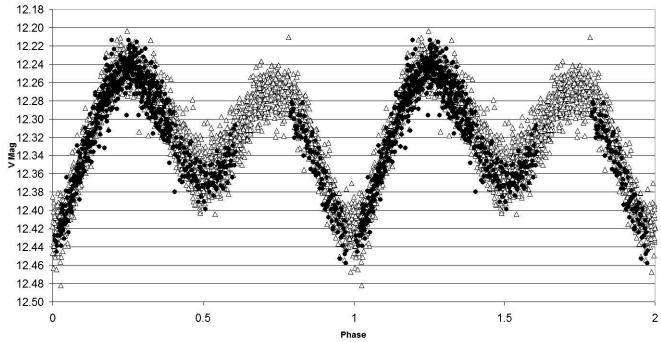

Figure 16. Phase Plot of GSC 02869-02559. Filled circles denote Furgoni data; open triangles denote SWASP data (only camera 142 and 148 with error < 0.02 mag.; –0.23 mag. offset).

5.15. GSC 02860-01552
Position (UCAC4): R.A. (J2000) = $03^h\ 16^m\ 02.70^s$, Dec. (J2000) = +43° 20' 34.3"
Cross Identification ID: 1SWASP J031602.71+432034.4; 2MASS J03160269+4320342; UCAC4 667-016141
Variability Type: HADS Double Mode
Magnitude: Max 12.52 V, Min 13.02 V
Fundamental Period: 0.13831414(4)
Epoch Fundamental Period: 2457064.407(1) HJD
First Overtone Period: 0.10675322(2)
Epoch First Overtone: 2457064.317(1) HJD
Ensemble Comparison Stars: UCAC4 667-016142 (APASS 11.258 V); UCAC4 667-016207 (APASS 11.740 V)
Check Star: UCAC4 666-016112
Notes: The ratio between the fundamental and first overtone modes is 0.7718 and consistent with the Petersen diagram for double mode HADS with P0 close to 0.10 d. The amplitude of the first overtone is higher than that of the fundamental mode. The Fourier spectrum after prewhitening for F0 and F1 shows the existence of the coupling term (F2 = F1 + F0; F3 = F1 – F0; F4 = F2 + F3) (Table 2). Phase plot and Fourier spectrum are shown in Figures 17a–b and Figures 18a–b.

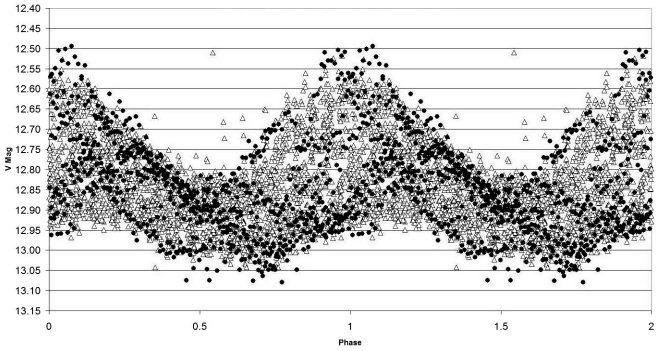

Figure 17a. Fundamental Mode Phase Plot of GSC 02860-01552. Filled circles denote Furgoni data; open triangles denote SWASP data (only camera 142 and 144 with error < 0.02 mag.; flux decontaminated from nearby stars).

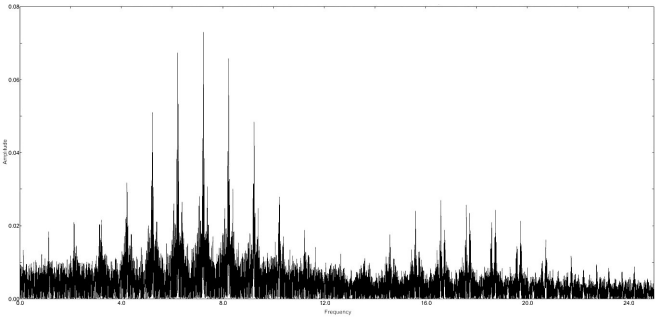

Figure 17b. Fourier Spectrum (after prewhitening for the first overtone frequency) of GSC 02860-01552.

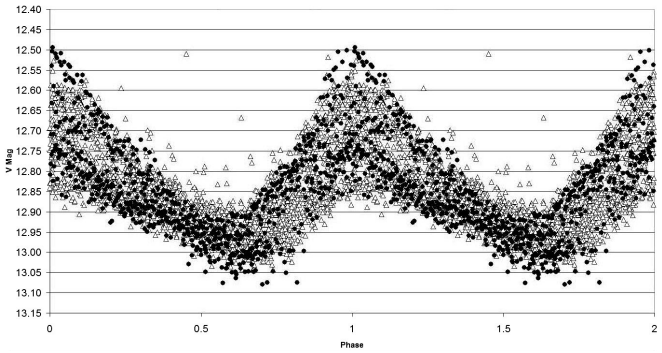

Figure 18a. First Overtone Phase Plot of GSC 02860-01552. Filled circles denote Furgoni data; open triangles denote SWASP data (only camera 142 and 144 with error < 0.02 mag.; lux decontaminated from nearby stars).

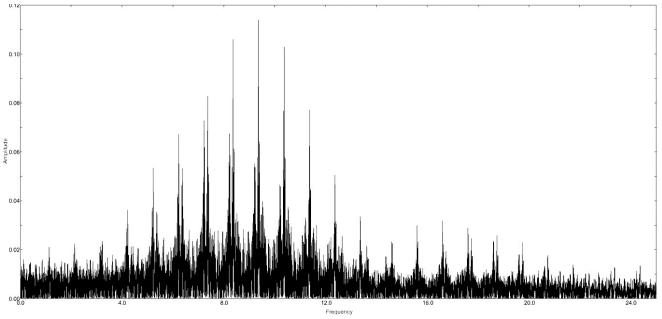

Figure 18b. Fourier Spectrum of GSC 02860-01552.

5.16. GSC 02856-01465

Position (UCAC4): R.A. (J2000) = $03^h\ 16^m\ 37.07^s$, Dec. (J2000) = +42° 40' 19.7"

Cross Identification ID: 1SWASP J031637.07+424019.8; 2MASS J03163707+4240196; UCAC4 664-015911

Variability Type: δ Sct

Magnitude: Max 12.70 V, Min 12.76V

Period: 0.12276888(5)

Epoch: 2457064.3240(3) HJD

Ensemble Comparison Stars: UCAC4 665-016194 (APASS 10.802 V); UCAC4 665-016217 (APASS 11.838 V)

Check Star: UCAC4 664-015818

Notes: The star is a reddened δ Sct: J–K = 0.182 and B–V = 0.269 after extinction correction based on Schlafly and Finkbeiner (2011). Phase plot is shown in Figure 19.

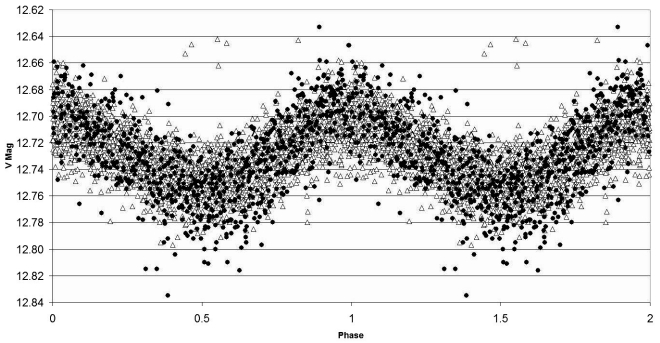

Figure 19. Phase Plot of GSC 02856-01465. Filled circles denote Furgoni data; open triangles denote SWASP data (only camera 142 and 144 with error < 0.02 mag.; +0.14 mag. offset).

Table 2. Coupling term elements for GSC 02860-01552.

Frequency name	*Frequency (c/d)*	*Amplitude*	*SNR*	*Period (d)*	*Err period (d)*	*HJD_{max}*	*HJD_{max} err*
F0	7.22991898	0.074307369	6.39	0.13831414	3.95E-08	2457064.407	1.0E-03
F1	9.36739897	0.115471575	9.86	0.10675322	1.51E-08	2457064.317	1.0E-03
F2 (F1+F0)	16.5973248	0.028539964	4.82	0.06025067	1.95E-08	2457064.416	2.0E-03
F3 (F1-F0)	2.13672248	0.023387893	3.10	0.46800650	1.44E-06	2457064.039	2.0E-03
F4 (F2+F3)	18.7355415	0.022394605	4.57	0.05337449	1.95E-08	2457064.423	3.0E-03

Table 3. Period calculations.

Section (this paper)	*Variable star (HJD)*	*Epoch (d)*	*Period*
5.3	GSC 02142-01107	2456955.354(2)	1.24345(4)
5.4	GSC 02129-00759	2456854.384(1)	0.66471(4)
5.7	GSC 02129-00947	2456898.335(3)	0.65600(3)
5.9	GSC 02865-01593	2457034.39(3)	0.4087(5)
5.10	HD 275169	2457034.345(1) (Main Period)	0.09040(2) (Main Period)
5.11	GSC 02869-00313	2457034.243(3)	0.06509(9)
5.13	GSC 02856-01391	2457064.330(1)	0.10862(1)
5.14	GSC 02869-02559	2457072.224(2)	0.81091(2)
5.15	GSC 02860-01552	2457064.315(3) (First Overtone)	0.106758(6) (First Overtone)
		2457064.406(2) (Fundamental)	0.138301(9) (Fundamental)
5.16	GSC 02856-01465	2457064.324(1)	0.122760(9)
5.17	GSC 02856-00169	2457072.327(1)	0.28391(3)

5.17. GSC 02856-00169
Position (UCAC4): R.A. (J2000) = $03^h\ 16^m\ 24.85^s$, Dec. (J2000) = +42° 42' 55.4"
Cross Identification ID: 1SWASP J031624.90+424254.6; 2MASS J03162484+4242554; UCAC4 664-015890
Variability Type: Rotating Ellipsoidal
Magnitude: Max 13.80 V, Min 13.90 V
Period: 0.2838920(2)
Epoch: 2457072.3274(7) HJD
Ensemble Comparison Stars: UCAC4 665-016194 (APASS 10.802 V); UCAC4 665-016217 (APASS 11.838 V)
Check Star: UCAC4 664-015818
Notes: J–K = 0.553 and B–V = 0.805 after extinction correction based on Schlafly and Finkbeiner (2011). There is a 17.0 V mag. star 7" to the SSE. The magnitudes are for the blend of both stars. If the identification is correct and the variable is not the fainter star (unlikely), the deblended range would be V = 13.86–13.97.

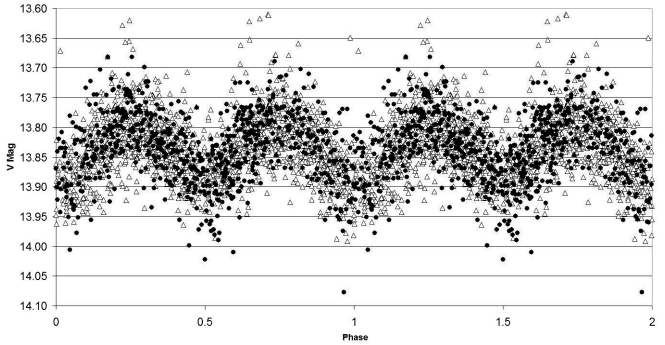

Figure 20. Phase Plot of GSC 02856-00169. Filled circles denote Furgoni data; open triangles denote SWASP data (only camera 142 and 144 with error < 0.04 mag.; –0.10 mag. offset).

6. Ephemeris from Furgoni dataset

Considering that the calculated epoch and period of almost all the variable stars discovered in this campaign are obtained from a combination of my observations and those from other surveys like ASAS, SWASP, and NSVS, it is necessary to point out that this way of work does not necessarily give precise period calculation. In effect almost all the periods are very short, and there are long lasting gaps between my observations and those in the other campaigns or databases. Therefore, in some cases there could be ambiguities in determining the accurate number of cycles that had passed during these gaps. Because of that I want to give for all the short period stars combined with other datasets an additional ephemeris calculated only with my dataset. However, for the stars listed in sections 5.8 and 5.12 I don't provide my own ephemeris because without the other survey datasets it is impossible to make a reasonable period calculation. In addition, for some stars where the cycle count problem is more relevant (sections 5.3, 5.4, 5.7, and 5.9) the period calculation was made weighting the data in relation to the uncertainty: with this approach I try to minimize the effect of most scattered data in the DFT calculation and provide a better period and error calculation. The results are presented in Table 3.

7. Dedication and acknowledgements

I want to dedicate this work to my loved cat Tillo, who passed away this summer, after many years as an irreplaceable companion under the starry sky.

This work has made use of the VizieR catalogue access tool, CDS, Strasbourg, France, and the International Variable Star Index (VSX) operated by the AAVSO, Cambridge, Massachusetts, USA. This work has made use of NASA's Astrophysics Data System and data products from the Two Micron All Sky Survey, which is a joint project of the University of Massachusetts and the Infrared Processing and Analysis Center/California Institute of Technology, funded by the National Aeronautics and Space Administration and the National Science Foundation.

This work has made use of the ASAS3 Public Catalog, NSVS data obtained from the Sky Database for Objects in Time-Domain operated by the Los Alamos National Laboratory, and data obtained from the SuperWASP Public Archive operated by the WASP consortium. This work has made use of observations obtained with XMM-Newton, an ESA science mission with instruments and contributions directly funded by ESA Member States and the USA (NASA).

This work has made use of The Fourth US Naval Observatory CCD Astrograph Catalog (UCAC4).

References

Breger, M., *et al.* 1999, *Astron. Astrophys.*, **349**, 225.
Butters, O. W., *et al.* 2010, *Astron. Astrophys.*, **520**, L10.
Diffraction Limited. 2012, MAXIMDL image processing software (http://www.cyanogen.com).
Henden, A. A., *et al.* 2013, AAVSO Photometric All-Sky Survey, data release 7 (http://www.aavso.org/apass).
Furgoni, R. 2013a, *J. Amer. Assoc. Var. Star Obs.*, **41**, 41.
Furgoni, R. 2013b, *J. Amer. Assoc. Var. Star Obs.*, **41**, 283.
Lenz, P., and Breger, M. 2005, *Commun. Asteroseismology*, **146**, 53.
Nesterov, V. V., Kuzmin, A. V., Ashimbaeva, N. T., Volchkov, A. A., Röser, S., and Bastian, U. 1995, *Astron. Astrophys., Suppl. Ser.*, **110**, 367 (CDS Catalogue III/182).
Pojmański, G. 2002, *Acta Astron.*, **52**, 397.
ROSAT Scientific Team. 2000, VizieR On-line Data Catalog IX/28A (originally published in *Rosat News*, No. 71, ROSAT Consortium, 2000).
Schlafly, E. F., and Finkbeiner, D. P. 2011, *Astrophys. J.*, **737**, 103.
Watson, C., Henden, A. A., and Price, C. A. 2014, AAVSO International Variable Star Index VSX (Watson+, 2006–2014; http://www.aavso.org/vsx).
Wise, M. W., O'Connell, R. W., Bregman, J. N., and Roberts, M. S. 1993, *Astrophys. J.*, **405**, 94.
Wozniak, P. R., *et al.* 2004, *Astron. J.*, **127**, 2436.
XMM-Newton Survey Science Centre, Consortium. 2013, VizieR On-line Data Catalog: IX/44
Zacharias, N., Finch, C., Girard, T., Henden, A., Bartlett, J., Monet, D., and Zacharias, M. 2012, The Fourth US Naval Observatory CCD Astrograph Catalog (UCAC4; http://arxiv.org/abs/1212.6182).

Multiband CCD Photometry of CY Aquarii using the AAVSOnet

David E. Cowall
20361 Nanticoke Drive, Nanticoke, MD 21840; cowall@comcast.net

Presented at the 104th Spring Meeting of the AAVSO, Ball State University, Muncie, IN, June 5, 2015

Received June 17, 2015; revised August 24, 2015, September 9, 2015; September 28, 2015; accepted November 12, 2015

Abstract δ Scuti stars are a class of short-period pulsating variable stars that include CY Aquarii. Multiband CCD photometry was performed on that star using instruments in Massachusetts, New Mexico, and Australia from the AAVSO's global robotic telescope network (AAVSOnet). Rapid cadence, multi-hour time series yielded high precision light curves and 21 new maxima. Data analyses revealed a pulsation pattern consistent with the existing model that describes the origin of SXPHE stars.

1. Introduction

1.1. DSCT

δ Scuti Stars (DSCT) are a diverse class of very short period variables. Some have amplitudes of nearly one magnitude and regular light curves while others have complex light curves with multiple periods and millimagnitude light variations. These stars pulsate radially (and sometimes non-radially) and lie just above or on the main sequence of the Hertzsprung-Russell (H-R) diagram between approximate spectral types A7-F2. The pure non-radial pulsators are called γ Doradus stars and are separate from the DSCTs.

1.2. HADS

The High Amplitude δ Scuti stars (HADS) are a subset of the DSCTs. They are highly evolved pulsating variable stars with amplitudes above 0.1 in V residing well off the main sequence in the sub-giant branch of the H-R diagram. These Population I stars pulsate in a single radial manner and exhibit a period-luminosity relationship (Templeton 2005).

1.3. SXPHE

SX Phoenicis stars (SXPHE), by contrast, are Population II stars which exhibit light curves that closely resemble the HADS. Some SXPHE stars pulsate in one mode and others in two. SXPHE stars tend to be located in globular star clusters or the galactic halo and also exhibit a period-luminosity relationship. Long-term period changes have been noted in these stars which exceed the expected rates from stellar evolution (Handler 2000). The cause of these changes is not generally understood.

Blue straggler stars are believed to increase in mass and luminosity late in life due to interactions with nearby stars in globular clusters or from binary companions. The period ratios of SXPHE stars that pulsate in two modes indicate a greater than expected mass suggestive of a similar mechanism to that which is seen with the blue stragglers (Percy 2007).

1.4. CY Aqr

CY Aquarii (CY Aqr) is an SXPHE star which had the shortest period of any known variable at the time of its discovery by Hoffmeister (1934). The AAVSO's Variable Star Index (VSX; Watson *et al.* 2014) currently lists its period at 0.061038408 day. CY Aqr has a V magnitude of 10.42–11.20 and an epoch 2000 declination of approximately +01^{h} 32^{m}. It is therefore well positioned in the sky for observations done in temperate zones both north and south of the equator using small- aperture instruments. It is not associated with a star cluster and therefore unlikely to be affected by the interactions that are seen with blue stragglers. Observations of this star since 1960 have been recorded in the AAVSO International Database (AID; AAVSO 2015) and are shown in Figure 1.

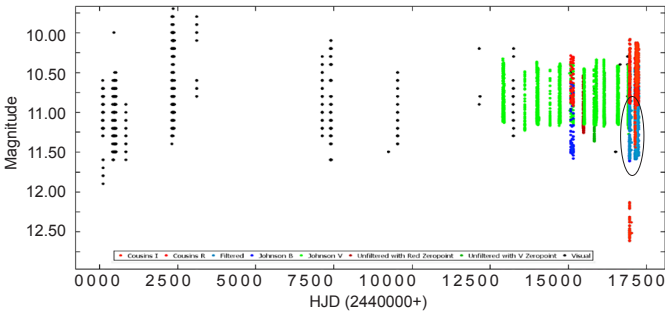

Figure 1. Total AID light curve for CY Aqr. Filtered AAVSOnet data are circled lighter points.

The most recent study of this star (Sterken *et al.* 2011) yielded twenty-nine new maxima based upon more than a dozen partial nights of filterless CCD photometry combined with photomultiplier photometry.

1.5. AAVSOnet

The AAVSO has established a global robotic telescope network. A subgroup of the AAVSOnet instruments are the Bright Star Monitors (BSMs). These are small refractors which provide low resolution but wide field images that are well suited to un-crowded star fields with stars of magnitude 2–12 (Henden 2014). They also work well in light polluted areas. CY Aqr is bright and not in a crowded star field, making it appropriate for study with the BSMs.

2. Methods

2.1. Instrumentation and observations

CCD photometry data were obtained for CY Aqr using the BSM-HQ (Massachusetts), BSM-NM (New Mexico), and BSM-S (Australia). Each instrument performed multi-hour time series with a cadence of approximately six minutes in

four different band passes (Johnson B and V, Cousins R and I) from October 2014 through August 2015. Exposure times were 30s in R and I, 40s in V, and 80s in B. This yielded a total of 1975 usable images over 22 nights. All images were calibrated and air-mass corrected. Due to technical issues with the AAVSOnet's executive software, only some of the data could be transformed. All data were submitted to the AAVSO International Database (AID). Due to the low density of observations (see Figure 3), the times of maximum light and period calculations were determined by visual inspection.

2.2. Mathematical analysis

Epoch: HJD 2454562.14017 analyses were performed using AAVSO's VPHOT (AAVSO 2012) and VSTAR (Benn 2013) software programs.

3. Results

3.1. Light curves

A illustrative image of CY Aqr is shown in Figure 2. The B, V, R, and I light curves from a representative BSM-S time series are provided in Figure 3.

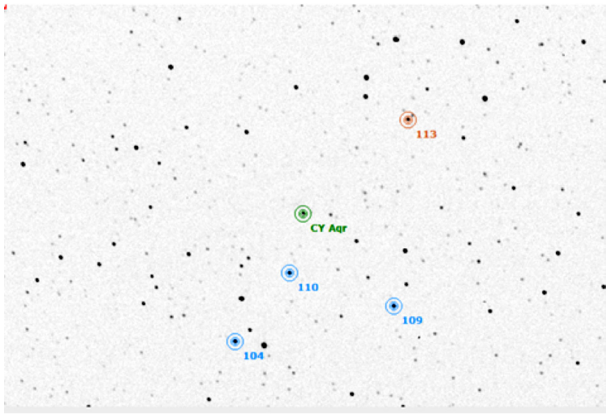

Figure 2. CY Aqr CCD field. South is up and West is left. Field of view 2.40º × 1.30º. Target is CY Aqr; comparison stars are 10.4, 10.9, and 11.0; and check star is 11.3.

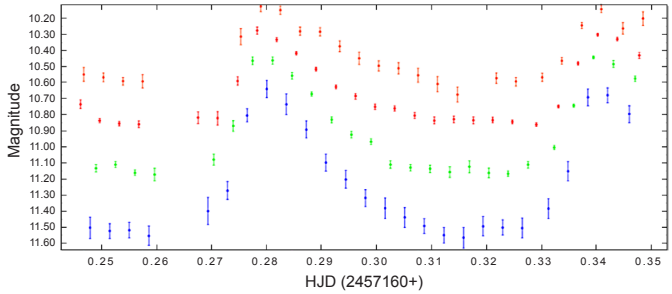

Figure 3. Time Series light curves for CY Aqr showing maxima at HJD 2457160.278 and 2457160.340. Mean Error bars denote 95% confidence intervals (twice Standard Error). Curves are, from top to bottom: Cousins I, Cousins R, Johnson V, Johnson B.

3.2. Phase plot

The phase plot reduced to the sun with Fourier model and residuals for all AAVSOnet V-band data is shown in Figure 4 and is consistent with a single pulsation mode. Higher order

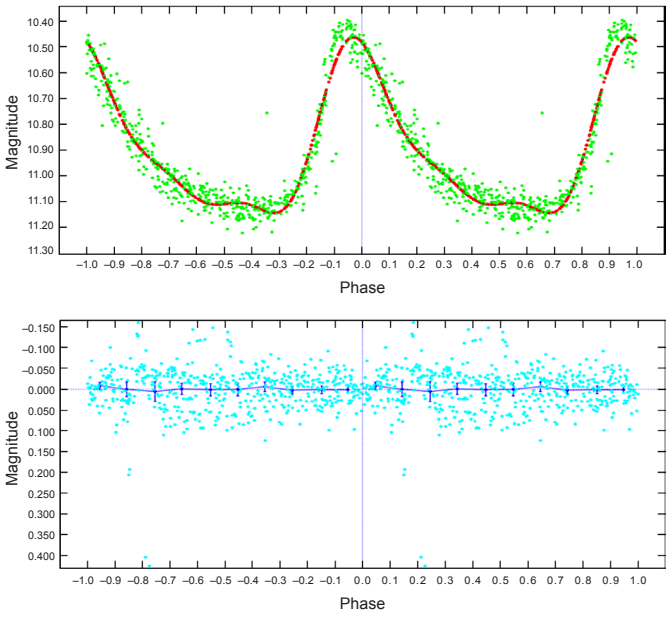

Figure 4. Phase Plot for CY Aqr of all V-Band AAVSOnet data. Period, 0.061038 d; epoch, HJD 2454562.14017. Model (top plot; points are Johnson V, line denotes model) and Residuals (bottom plot; points denote residuals, line with error bars are the means).

harmonics did not improve the model although it imprecisely fits the observations around the time of maximum light.

Based upon the p-value of 0.973829 for the residuals, the null hypothesis is assumed to be true and it is highly unlikely that there is additional periodicity not captured by the model. The Fourier expression is shown in Equation 1.

$$
\begin{aligned}
f(t) &= 11.13841 \\
&+0.315658\times\cos(2\pi1(t-2457134.6))+0.096227\times\sin(2\pi1(t-2457134.6)) \\
&-0.017152\times\cos(2\pi2(t-2457134.6))+0.005503\times\sin(2\pi2(t-2457134.6)) \\
&-0.269837\times\cos(2\pi3(t-2457134.6))-0.180788\times\sin(2\pi3(t-2457134.6)) \\
&-0.253838\times\cos(2\pi4(t-2457134.6))-0.30852\times\sin(2\pi4(t-2457134.6)) \\
&-0.086311\times\cos(2\pi5(t-2457134.6))-0.168185\times\sin(2\pi5(t-2457134.6)) \\
&+0.02972\times\cos(2\pi6(t-2457134.6))+0.085495\times\sin(2\pi6(t-2457134.6)) \\
&-0.016844\times\cos(2\pi7(t-2457134.6))+0.284924\times\sin(2\pi7(t-2457134.6)) \\
&-0.118102\times\cos(2\pi8(t-2457134.6))+0.31447\times\sin(2\pi8(t-2457134.6)) \\
&-0.176364\times\cos(2\pi9(t-2457134.6))+0.214283\times\sin(2\pi9(t-2457134.6)) \\
&-0.081207\times\cos(2\pi10(t-2457134.6))+0.056482\times\sin(2\pi10(t-2457134.6))
\end{aligned}
\qquad (1)
$$

3.3. Ephemeris and period analysis

Twenty-one new maxima were determined from the AAVSOnet data set and are shown in Table 1. The calculated times of maxima were derived from Equation 2 where E is the cycle number. Extrapolating by inspection from the ephemeris of Sterken *et al.* (2011), O–C should be gradually declining from approximately 0.01 to –0.01 between October 2014 and August 2015. The AAVSOnet data set for CY Aqr appears to behave in accordance with that pattern.

$$T_{max} = 2426159.5132 + (0.0610)(E) \qquad (2)$$

For those time series that contained at least two maxima or minima, period calculations were obtained and are displayed

Table 1. Times of Maximum Light (T_{max}) Observed (O), Calculated (C), and cycle number (E) for CY Aqr (HJD 2450000+) from the AAVSOnet data set.

T_{max}(O) (HJD 2450000+)	E	T_{max}(C) (HJD 2450000+)	O–C
6960.933	504941	6960.914	0.019
6960.990	504942	6960.975	0.015
6961.054	504943	6961.036	0.018
7160.278	508209	7160.662	0.016
7160.340	508210	7160.323	0.017
7168.213	508339	7168.192	0.021
7168.278	508340	7168.253	0.025
7168.336	508341	7168.342	–0.006
7188.176	508667	7188.200	–0.024
7188.237	508668	7188.261	–0.024
7195.256	508783	7195.276	–0.020
7195.317	508784	7195.337	–0.020
7211.125	509043	7211.362	–0.237
7211.186	509044	7211.197	–0.011
7221.248	509209	7221.262	–0.014
7222.844	509235	7222.848	–0.004
7222.905	509236	7222.909	–0.004
7223.089	509239	7223.092	–0.003
7223.150	509240	7223.153	–0.003
7223.209	509241	7223.214	–0.005
7223.271	509242	7223.275	–0.004

Table 2. Period analysis for CY Aqr from the AAVSOnet data set.

Interval (HJD 2450000+)	Period (days)
6960.933–6961.054	0.0616
7160.278–7160.340	0.0620
7168.213–7168.336	0.0615
7188.176–7188.237	0.0608
7195.256–7195.317	0.0609
7211.125–7221.248	0.0616
7222.844–7222.905	0.0611
7223.089–7223.271	0.0604

in Table 2. Based principally upon the ephemeris in Table 1, there appears to be no significant changes in the period of this star between October 2014 and August 2015.

4. Discussion

The CY Aqr data provide a striking paradox. HADS, at approximately two solar masses, are sufficiently massive that they should be expected to have remained in the main sequence for only about one billion years. Yet the SXPHE, of similar mass (Andreasen 1983), are Population II stars and therefore about as old as the universe. They should have evolved into white dwarfs and become silent many billions of years ago. However, they clearly continue to pulsate with a primary radial mode closely resembling the HADS.

A binary model with a highly eccentric orbit has been proposed by Fu and Sterken (2003). Thus two ancient Population II white dwarf stars each about as massive as the sun would have merged about one billion years ago. This combination star would have re-ignited and then recently left the main sequence. It now behaves like a typical HADS. This model, however, does not account fully for all data, including the long-term period changes. Further observations to include new times of maxima will be required for a complete solution.

5. Acknowledgements

I acknowledge with thanks the members of the AAVSOnet Telescope Allocation Committee and the site managers of the following BSMs: Arne Henden (HQ), Bill Stein (NM), and Peter Nelson (S) for their hard work and dedication to the AAVSOnet.

References

AAVSO. 2012, VPHOT AAVSO photometric software (http://www.aavso.org/vphot).

Andreasen, G. 1983, *Astron. Astrophys.*, **121**, 250.

Benn, D. 2013, VSTAR data analysis software (http://www.aavso.org/vstar-overview).

Fu, J., and Sterken, C. 2003, *Astron. Astrophys.*, **405**, 685.

Handler, G. 2000, in *Variable Stars as Essential Astrophysical Tools*, ed. C. Ibanoglu, Kluwer Academic Publishers, Boston, 557.

Henden, A. 2014, AAVSOnet (https://www.aavso.org/aavsonet).

Hoffmeister, C. 1934, *Beob.-Zirk. Astron. Nachr.,* **16**, 45.

Kafka, S. 2015, observations from the AAVSO International Database (https://www.aavso.org/aavso-international-database).

Percy, J. 2007, *Understanding Variable Stars*, Cambridge University Press, New York, 186.

Sterken, C., Wiedemair, C., Tuvikene, T., Rigo, J., Munaro, T., and Untergassmair, M. 2011, *J. Astron. Data*, **17**, 2.

Templeton, M. R. 2005, *J. Amer. Assoc. Var. Star Obs.*, **34**, 1.

Watson, C., Henden, A. A., and Price, C. A. 2014, AAVSO International Variable Star Index VSX (Watson+, 2006–2014; http://www.aavso.org/vsx).

Data Mining Analysis for Eclipsing Binary TrES-Cyg3-04450

David H. Hinzel
ETA Virtual Astronomical Observatory, 9315 Argent Court, Fairfax Station, VA 22039; daveeta1@cox.net

Received September 1, 2015; revised September 15, 2015; accepted November 2, 2015

Abstract A data mining algorithm was utilized to analyze Johnson V-band charge-coupled device (CCD) photometric data of an object that were taken during a wide field survey of a region in the constellation Cygnus. That algorithm was the Date Compensated Discrete Fourier Transform (DC DFT) which is part of the AAVSO VSTAR applications software. This analysis clearly indicated that the object under study is a detached eclipsing binary, specifically an EA β Persei-type (Algol) eclipsing system, with an orbital period of 2.0664 days. Neither the type nor period of this eclipsing binary had been characterized up to this point. This object has been given the AAVSO designation TrES-Cyg3-04450 and the AUID 000-BLL-484.

1. Introduction

TrES-Cyg3-04450 is one of 10,000 stars imaged during a wide field survey of a region in the constellation Cygnus. A field of 6° × 6° was centered on R.A. $19^h\ 54^m\ 00^s$, Dec. +37° 00' 00". The survey was conducted by the Transatlantic Exoplanet Survey (TrES; Alonzo *et al.* 2007), which was designed to search for exoplanetary transits using three wide-field optical telescopes of 10-cm diameter located at three different observatories (Lowell Observatory, Palomar Observatory, and the Canary Islands). The array incorporated 10-cm Schmidt telescopes having CCD cameras capable of obtaining precise differential photometry on thousands of stars simultaneously and automated search routines, thereby increasing the light curve coverage in a given observing season by effectively increasing the length of the night as well as improving weather statistics. As the result of the high cadence photometry, several hundred hours of observing time at each target maximized the visibility of an event.

Using the VizieR search engine, it was determined that this object has other catalog names or identifications including: UCAC4 642-085405; 2MASS J20051693+3814518 (J–K = 0.1930 where J = 10.263, K = 10.070); USNO-B1.0 1282-0444845; USNO-A2.0 1275-13314390; NSVS ID 5709370, NSVS ID 8460067, and NSVS ID 8481682. The optical image for TrES-Cyg3-04450 is shown in Figure 1 (directly in the center of the image).

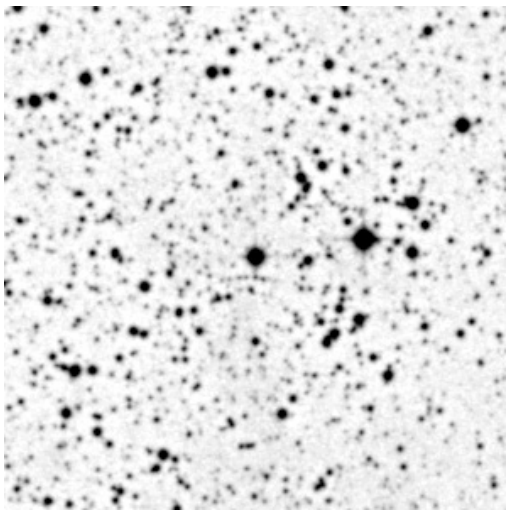

Figure 1. Optical image for TrES-Cyg3-04450 (directly in center of image). Digitized Sky Survey (STScI 1993-1995) UKSTU Red image from VSX (Watson *et al.* 2006–2014).

Table 1. Data for TrES-Cyg3-04450 from TrES database.

Parameter	*Data*
Location	R.A. $20^h\ 05^m\ 17.0^s$, Dec. +38° 14' 52"
Nominal magnitudes	
V	11.530
B–V	0.2470
Magnitude statistics	
Number of measurements	3,890
Mean Magnitude	0.03649
Minimum Magnitude	–0.05931
Maximum Magnitude	0.70207
Magnitude Variance	0.01522
Magnitude Standard Deviation	0.12336
Error statistics	
Mean Error	0.10901
Minimum Error	0.00201
Maximum Error	1.70185
Error Variance	0.02053
Error Standard Deviation	0.14328
Time statistics	
Observation span	2,356 days
Nights observed	120
Maximum nightly observations	76
Minimum nightly observations (> 0)	1
Average nightly observations	32.4

2. Methods

The V data for TrES-Cyg3-04450 obtained by the TrES survey are shown in Table 1.

In addition to the TrES data, survey data from the AAVSO Photometric All Sky Survey (APASS; Henden *et al.* 2014) and the Northern Sky Variability Survey (NSVS; Wozniak *et al.* 2004) sources were incorporated. These additional photometric data improve the estimate of the period and epoch for TrES-Cyg3-04450 as discussed below.

2.1. Analysis method

The 3,890 Johnson V-band CCD photometric data observations of TrES-Cyg3-04450 were downloaded from the "Stellar Photometry Data from TrES" database (Lowell Obs.

2015). Either text or Comma Separated Variable (CSV) format was available. The V data from APASS (Henden *et al.* 2015) and NSVS (Wozniak *et al.* 2004) brought the total number of observations to 4,143. Since the TrES observations are in the Johnson V-band, the zero point was adjusted and calibrated using APASS Johnson V data. NSVS added data points corresponding to TrES data points as well as extending the time baseline. Since the NSVS data also showed several eclipses, they helped to improve the estimation of the period. NSVS data were also shifted to the zero point. Finally, the ascending and descending branches of all eclipses and all data sets were matched such that the epoch of the minimum corresponded exactly to the midpoint of mid-eclipse (Otero 2015).

These combined calibrated data were then input to the Date Compensated Discrete Fourier Transform (DC DFT) algorithm which is part of the AAVSO VSTAR applications software (Benn 2013). The DC DFT algorithm (Ferraz-Mello 1981) yields a power spectrum and a table of "top-hits" given a specified series, frequency (or period) range, and resolution. The "date compensated" part of the name indicates that gaps in the data, common for variable star observations, are compensated for by the algorithm. The light curve for TrES-Cyg3-04450 is shown in Figure 2.

From the raw combined calibrated light curve data as shown in Figure 2, the VSTAR DC DFT algorithm performed the period analysis of TrES-Cyg3-04450 with the power spectrum shown in Figure 3.

2.2. Analysis results

The period computed from the power spectrum analysis in Figure 3 (the strongest signal or "top-hit") is 1.0332 ± 0.045 days. However, this is only one half of the full orbital period since 1.0332 days is the time between two consecutive minima. Since there are two eclipses per orbit the full orbital period is twice as long. Therefore, the full period is 2.0664 days with an epoch (midpoint of mid-eclipse) of HJD 2452121.587 (31 July 2001) as shown below in Figure 4. The magnitude range is 11.33–12.0V and the computed eclipse duration is 9% based on the results shown in Figure 4; TrES, NSVS, and APASS data points are indicated in the composite light curve. The TrES, NSVS, and APASS data are plotted individually in the phase plots, Figures 5, 6, and 7, respectively. It can be seen how these three data sets combine to enhance the estimate of the period and epoch of TrES-Cyg3-04550.

3. Conclusions

This analysis clearly indicated that the object under study is a detached eclipsing binary, specifically an EA β Persei-type (Algol) eclipsing system, with an orbital period of 2.0664 days and with an epoch of HJD 2452121.587 (31 July 2001). The magnitude range is 11.33–12.0V and the computed eclipse duration is 9%. Neither the type nor period of this eclipsing binary had been characterized up to this point. This object has been given the AAVSO designation TrES-Cyg3-04450 and the AUID 000-BLL-484.

4. Acknowledgements

The author would like to thank Sebastian Otero for his expert guidance and incredible patience during the analysis of TrES-Cyg3-04450. Additional thanks goes to the AAVSO for the VSTAR applications software without which this work would not have been possible. Finally the author would like to thank the Transatlantic Exoplanet Survey (TrES) program and the individuals, too numerous to name, that made the raw photometric data available for analysis.

References

Alonso, R., *et al.* 2007, in *Transiting Extrasolar Planets Workshop: Proceedings of the conference held 25–28 September, 2006 at the Max Planck Institute for Astronomy in Heidelberg, Germany*, C. Afonso, D. Weldrake, and Th. Henning, eds.. ASP Conf. Ser. 366, Astronomical Society of the Pacific, San Francisco, 13.

Benn, D. 2013, VSTAR data analysis software (http://www.aavso.org/vstar-overview).

Ferraz-Mello, S. 1981, *Astron. J.*, **86**, 619.

Henden, A. A., *et al.* 2015, AAVSO Photometric All-Sky Survey (https://www.aavso.org/apass).

Lowell Observatory. 2015, "Stellar Photometry from TrES Data" (http://asteroid.lowell.edu/LARI/mgec.html).

Otero, S. 2015, private communications made during data analysis.

Space Telescope Science Institute. 1993–1995, Digitized Sky Survey, STScI, Baltimore.

Watson, C., Henden, A. A., and Price, C. A. 2014, AAVSO International Variable Star Index VSX (Watson+, 2006–2014; https://www.aavso.org/vsx).

Wozniak, P. R., *et al.* 2004, *Astron. J.*, **127**, 2436.

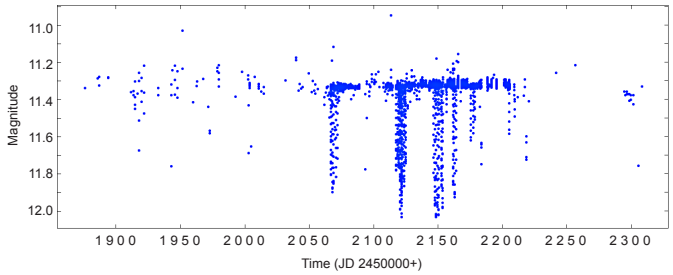

Figure 2. Light curve for TrES-Cyg3-04450.

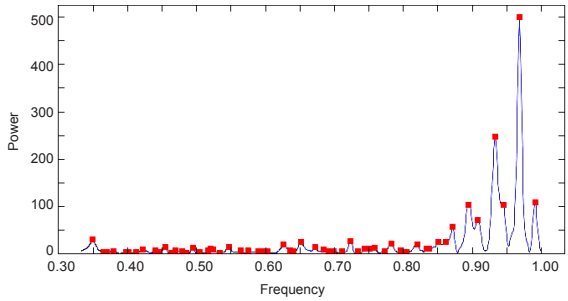

Figure 3. Power spectrum period analysis for TrES-Cyg3-04450.

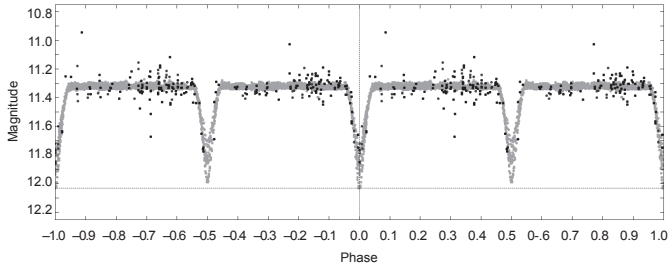

Figure 4. Phase plot for TrES-Cyg3-04450, with NSVS and APASS data superimposed. Period: 2.066486, epoch: 2452121.587.

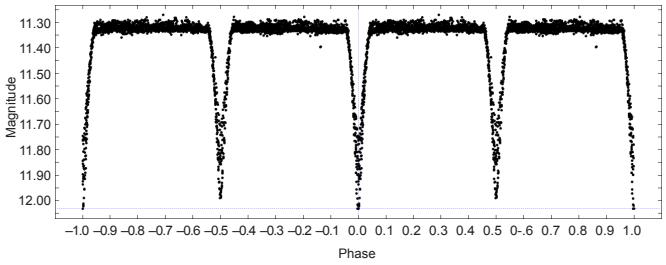

Figure 5. Phase plot for TrES-Cyg3-04450. Period: 2.066486, epoch: 2452121.587.

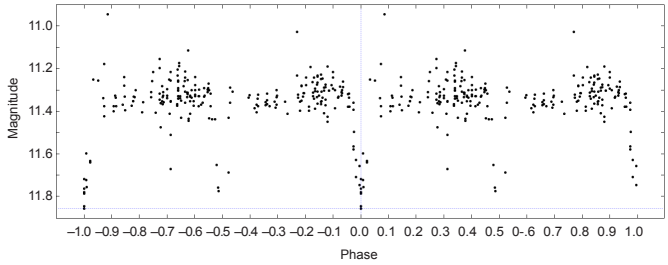

Figure 6. Phase plot for NSVS data. Period: 2.066486, epoch: 2452121.587.

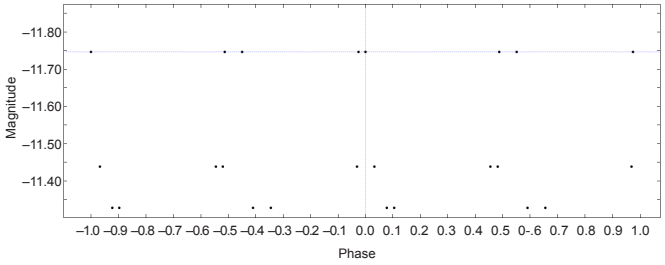

Figure 7. Phase plot for APASS data. Period: 2.066486, epoch: 2452121.587.

New Variable Stars Discovered by Data Mining Images Taken during Recent Asteroid Photometric Observations. Results from the Year 2015

Riccardo Papini
Carpione Observatory (K49), via Potente 52, San Casciano in val di Pesa, Florence, 50026, Italy; riccardo.papini@yahoo.it

Lorenzo Franco
Balzaretto Observatory (A81), Rome, Italy; lor_franco@libero.it

Alessandro Marchini
Astronomical Observatory, DSFTA, University of Siena (K54), via Roma 56, Siena, 53100, Italy; alessandro.marchini@unisi.it

Fabio Salvaggio
Saronno, 21047, Italy; fsalvaggio@gmail.com

Received October 30, 2015; revised November 16, 2015; accepted November 30, 2015

Abstract During the past year the authors observed several asteroids for the purpose of determining the rotational period. Typically, this task requires a time series images acquisition on a single field for all the night, weather permitting, for a few nights although not consecutive. Routinely checking this "goldmine," allowed us to discover 14 variable stars not yet listed in catalogs or databases. While the most of the new variables are eclipsing binaries (GSC 01394-01889, GSC 00853-00371, CSS_J171124.7-004042, GSC05065-00218, UCAC4-386-142199, UCAC4 398-127457, UCAC4 384-148138, UCAC4 398-127590, UCAC4-383-155837, GSC-05752-01113, GSC 05765-01271), a few belong to RR Lyrae class (UCAC4 388-136835, 2MASS J20060657-1230376, UCAC4 386-142583). Since asteroid work is definitely time-consuming, follow-up is quite a difficult task for a small group. Further observations of these new variables are therefore strongly encouraged in order to better characterize these stars, especially RR Lyrae ones whose data combined with those taken during professional surveys seem to suggest the presence of a Blazhko effect.

1. Introduction

Taking CCD images of asteroids for the purpose of plotting their light curves in order to work out their synodic rotational period is always rewarding and very often funny. Although each author has his own targets or program to carry on, very often we collaborate in order to cover gaps due to personal commitments or bad weather, using the advantage of multiple sites. Even if the asteroid is a fast rotator (3–5 hours), it must be followed as long as possible and hopefully all night long on a few consecutive nights to cover all the phased curve. Therefore, each night, one telescope is aimed at the same field for enough hours to work out a light curve variation, if any, for each object in the same field. At the end of each session, all the images are stored on a cloud storage system and shared between the authors who in turn perform the photometric analysis of the asteroid data. Applying this collaboration protocol during the past year, also thanks to the remote control capabilities of the Astronomical Observatory of the University of Siena inside the facilities of the DSFTA (Department of Physical Sciences, Earth and Environment), our group has observed for about 190 nights collecting over 20,000 valid photometric measurements. As a side effect, the group discovered also 14 new variables, specifically, 11 eclipsing binaries and 3 short period pulsators. Indeed, after photometric analysis of the asteroid has been done, data are analyzed again with suitable software packages like C-MUNIPACK (Motl 2011) and MPO CANOPUS (Warner 2012) which highlight all the objects in the images of the series which are not constant over the whole session. Once a new variable has been found, photometric analysis of the object is performed with the software packages MAXIMDL (Diffraction Limited 2012) or MPO CANOPUS (Minor Planet Observer 2010). After adequate zero-point calibration, data have been added to those available from satellite or automated surveys as ASAS-3 (All Sky Automated Survey; Pojmański 2002), CRTS (Catalina Real-Time Transient Survey; Drake 2014) and NSVS (Northern Sky Variability Survey; Wozniak 2004). With these data merged together, a final period analysis is performed with PERANSO software (Vanmunster 2007). In the end, new variable stars were added to the AAVSO Variable Star Index (VSX; Watson, *et al.* 2014), to share them with the larger community of professional and amateur astronomers. Follow up of these stars is encouraged since it is a hard task for a small group of individuals.

2. Instrumentation and methods

The observations were carried out from December 2014 to October 2015. All the observatories involved in this study are located in Italy; one of these is located inside the facilities of the University of Siena, while the others are privately operated. The main features of the equipment used are listed in Table 1.

All the computers' clocks were automatically synchronized via NTP servers. Even considering net delay, the precision on times is less than one second. All the recorded times were UT. Typically, images were taken unfiltered to increase signal intensity. However, at the astronomical observatory of the

Table 1. Observers and main features of the instruments used.

Observer	*Telescope*	*Filter*	*CCD*
Franco (A81)	8" SCT f/5.5	C	SBIG ST7-XME
Marchini (K54)	12" MCT f/5.6	C	SBIG STL-6303e (bin 2 × 2)
Papini (K49)	10" SCT f/10	C	SBIG ST9-XME
Salvaggio	9.25" SCT f/10	C	SBIG ST8-XME (bin 2 × 2)

University of Siena, a parafocal Clear filter which transmits all wavelengths from UV to far IR was used. Exposure times were always between 5 and 8 minutes, depending on the asteroid apparent magnitude. All the images were calibrated with dark and flat-field frames by the same observer who acquired them.

Variable star search in the calibrated images has been performed with the software packages C-MUNIPACK and MPO CANOPUS. They are based on the relation between the standard deviations of the brightness of the stars and their mean brightness. The program reads all photometry files and computes the mean brightness and standard deviations of brightness of all stars. The algorithm automatically removes stars that are missing on the majority of source frames. For stars of lesser magnitude the deviation of brightness exhibits a higher value than the deviation for stars of greater brightness.

Once a new variable has been found, photometric analysis is performed with the software packages MAXIMDL or MPO CANOPUS. Although being equivalent from the point of view of photometry quality, MPO CANOPUS has a few tools for checking comparison stars used for photometry. Bright enough stars in the field of view were chosen for the comparison and check stars. Unfortunately, not so many bright stars were present, so that often color index did not match the color index of the variable as much as desired. Aperture photometry was done on each subset of data using the optimum aperture radius (Howell 1991) in order to maximize the SNR. Magnitude are given as CV, which designates observations made without filter (clear) but using V magnitudes for the comparison stars, the result will be closer to V but will vary depending on the sensitivity of the observer's setup and the star's color.

The overall quality of the photometry, that is its precision, is expressed computing the standard deviation from the mean over the entire night of the difference between the differential magnitude of the Reference star and the Check star. This value is on average about 0.01 magnitude.

Once photometric analysis was completed, a search through the main sky surveys which covered that area was done. The most useful surveys were ASAS-3, CRTS, and NVSV. Since images during these surveys had been taken with different photometric filters, it was mandatory to set a constant zero-point to fit all the available data. Since the main elements presented in this work are independent of absolute magnitude, we decided to shift our data vertically, adding the difference between the average of the survey magnitudes and the average of the differential magnitudes worked out from our images. If data from two or more surveys were available, we used the mean of the larger set.

With all these data merged togheter, PERANSO software was used as the main tool for period analysis using the ANOVA algorithm (Schwarzenberg-Czerny 1996) as well as for period folding. In the end, data for each new variable were added to VSX.

3. Results for individual variables

3.1. GSC 01394-01889

This object was observed unfiltered from December 18, 2014, to January 1, 2015, collecting a total of 272 measurements over 6 nights. Frequency analysis gives an orbital period P = 1.470827 ± 0.00002 days. We show in Figure 1 the light curve folded according to the period found, which clearly reveals the presence of a primary and a secondary minimum with different depths. Data from CRTS were available for this variable and the 689 measurements have been added to the light curve. From its shape, we classified this variable as an eclipsing binary of EA type.

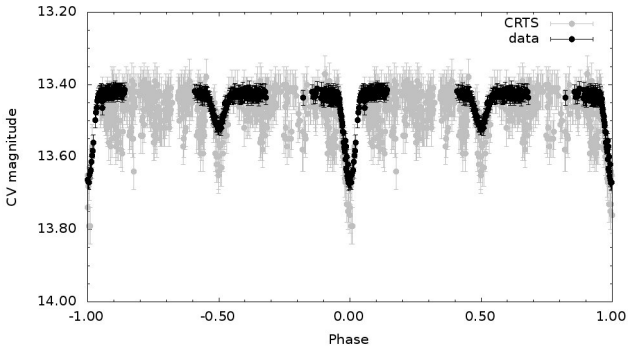

Figure 1. Folded light curve of GSC 01394-01889.

3.2. GSC 00853-00371

This object was observed unfiltered on March 9 and 27, 2015, collecting a total of 122 measurements over 2 nights. Frequency analysis gives an orbital period P = 0.255054 ± 0.00002 day. We show in Figure 2 the light curve folded according to the period found, which clearly reveals the presence of a primary and a secondary minimum with equal depths. Data from CRTS were available for this variable and the 472 measurements have been added to the light curve. From its shape, we classified this variable as an eclipsing binary of EW type.

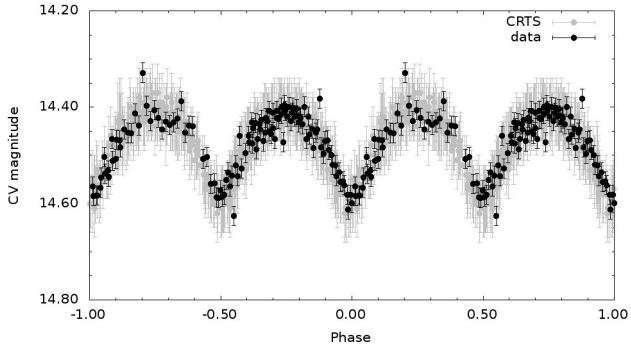

Figure 2. Folded light curve of GSC 00853-00371.

3.3. CSS J171124.7-004042

This object was observed unfiltered from May 28 to June 1, 2015, collecting a total of 314 measurements over 4 nights. Frequency analysis gives an orbital period P = 0.352604 ± 0.00002 day. We show in Figure 3 the light curve folded according to the period found, which clearly reveals the presence of a primary and a secondary minimum with equal depths. Data from CRTS were available for this variable and the 232 measurements have been added to the light curve. From its shape, we classified this variable as an eclipsing binary of EW type.

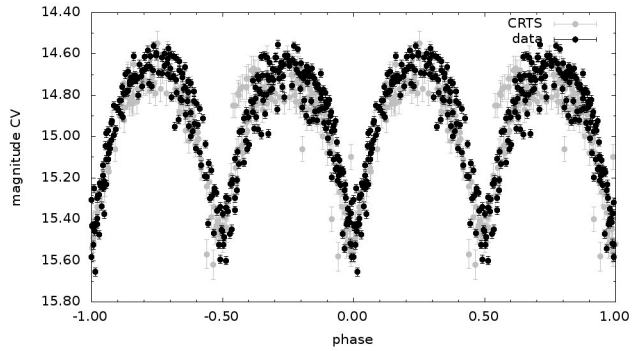

Figure 3. Folded light curve of CSS J171124.7-004042.

3.4. GSC 05065-00218

This object was observed unfiltered from May 12 to June 1, 2015, collecting a total of 596 measurements over 6 nights. Frequency analysis gives an orbital period P = 1.205530 ± 0.00002 days. We show in Figure 4 the light curve folded according to the period found, which clearly reveals the presence of a primary and a secondary minimum with different depths. Data from ASAS-3, CSS, and NSVS were available for this variable and therefore 615 measurements have been added to the light curve. From its shape, we classified this variable as an eclipsing binary of EA type.

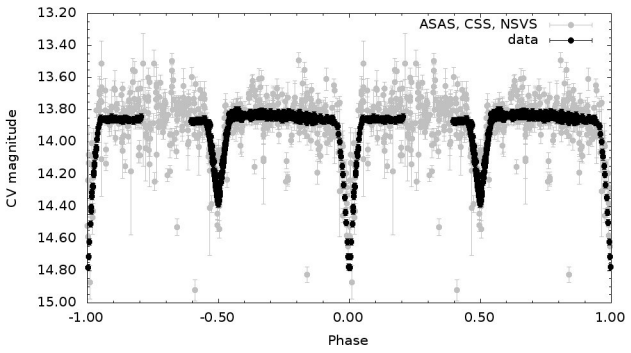

Figure 4. Folded light curve of GSC 05065-00218.

3.5. UCAC4 388-136835

This object was observed unfiltered on July 17, 2015, collecting a total of 51 measurements. Frequency analysis detected a clear sinusoidal-like modulation with a dominant period of 0.465497 ± 0.00002 day. We show in Figure 5 the light curve folded according to the period found. The periodicity and the amplitude of the light curve variations (~1.2 mag. in CV band), as well as its light curve shape, are compatible with those of an RRab, for which the highest frequency represents the principal pulsation mode. Data from CRTS were available for this variable and therefore 81 measurements have been added to the light curve.

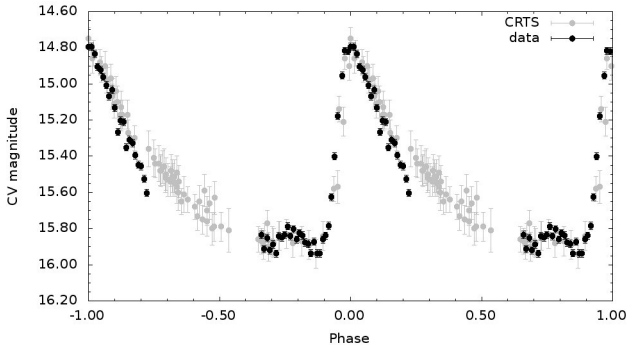

Figure 5. Folded light curve of UCAC4 388-136835.

3.6. UCAC4 386-142199

This object was observed unfiltered on the night of July 14, 2015, for a total of 60 measurements. Frequency analysis gave an orbital period P = 0.319437 ± 0.00002 day. We show in Figure 6 the light curve folded according to the period found, which clearly reveals the presence of a primary and a secondary minimum with equal depths. Data from CRTS are available for this variable and therefore 81 measurements have been added to the light curve. From its shape, we classified this variable as an eclipsing binary of EW type.

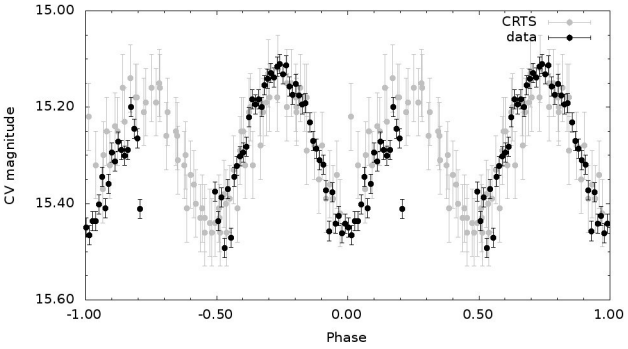

Figure 6. Folded light curve of UCAC4 386-142199.

3.7. 2MASS J20060657-1230376

This object was observed unfiltered on July 14, 2015, collecting a total of 53 measurements. According the 2MASS catalog (Skrutskie *et al.* 2006), this star has J–K = 0.17 (rather blue). From these data, we worked out a color index (V–R) = 0.242 which suggests an F5V spectral type. This is indicative of an RRc variable rather than an EW. Furthermore, the periodicity and the amplitude of the light curve variations (~0.3 mag. in CV band), as well as its light curve shape with shallow minima, are compatible with those of an RRc, for which the highest frequency represents the first overtone pulsation mode. Thus, we can confidently exclude that this object is an eclipsing binary. Frequency analysis detected a clear sinusoidal-like modulation with a dominant period of 0.209923 ± 0.00002 day. We show in Figure 7 the light curve folded according to the period found.

Table 2. Main information and results for the new variables discovered.

Star (VSX identifier)	*R. A. (J2000) h m s*	*Dec. (J2000) ° ′ ″*	*Constellation*	*V*	*Period (days)*	*Epoch (HJD-2455000)*	*Type*
GSC 01394–01889	09 01 35.89	+15 01 59.3	Cnc	13.65–13.89	1.470827 ± 0.000002	2024.5352 ± 0.0001	EA
GSC 00853–00371	10 59 28.58	+14 39 42.5	Leo	14.42–14.61	0.255054 ± 0.000003	2091.3684 ± 0.0001	EW
CSS_J171124.7–004042	17 11 24.62	–00 40 41.5	Oph	14.67–15.51	0.352604 ± 0.000002	2172.4153 ± 0.0001	EW
GSC 05065–00218	17 12 28.99	–00 41 20.0	Oph	13.84–14.77	1.205530 ± 0.000002	2173.5696 ± 0.0001	EA
UCAC4 388–136835	20 01 46.93	–12 25 04.2	Sgr	14.79–15.93	0.465497 ± 0.000002	2221.5128 ± 0.0001	RRab
UCAC4–386–142199	20 04 55.95	–12 54 35.7	Sgr	15.13–15.46	0.319437 ± 0.000003	2218.5527 ± 0.0001	EW
2MASS J20060657–1230376	20 06 06.57	–12 30 37.7	Sgr	16.02–16.36	0.209923 ± 0.000004	2218.5920 ± 0.0001	RRc
UCAC4 386–142583	20 07 58.91	–12 58 04.4	Cap	14.18–15.28	0.674897 ± 0.000002	2216.390 ± 0.001	RRab
UCAC4 398–127457	20 09 51.08	–10 33 59.7	Cap	15.50–15.82	0.291891 ± 0.000004	2210.4150 ± 0.0001	EW
UCAC4 384–148138	20 09 52.43	–13 15 17.8	Cap	14.44–15.12	0.375792 ± 0.000002	2215.5623 ± 0.0001	EW
UCAC4 398–127590	20 10 45.59	–10 27 45.4	Cap	15.12–15.68	0.309689 ± 0.000003	2210.5549 ± 0.0001	EW
UCAC4–383–155837	20 14 23.91	–13 26 57.7	Cap	16.25–16.70	0.437581 ± 0.000002	2202.5222 ± 0.0001	EA
GSC 05752–01113	20 15 50.47	–14 30 57.2	Cap	14.37–14.81	0.332192 ± 0.000002	2199.4786 ± 0.0001	EW
GSC 05765–01271	20 49 33.29	–12 08 51.6	Aqr	12.89–13.09	0.382878 ± 0.000002	2254.5065 ± 0.0001	EW

Data from CRTS were available for this variable and therefore 143 measurements have been added to the light curve.

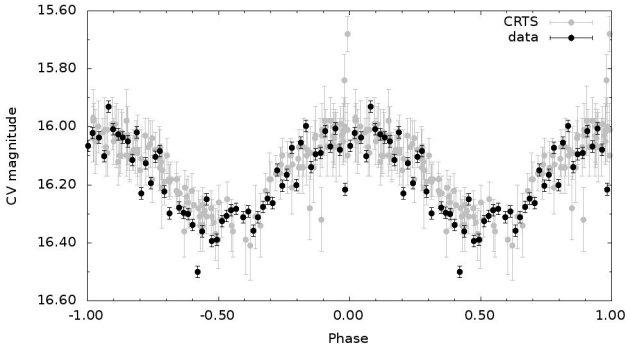

Figure 7. Folded light curve of 2MASS J20060657-1230376.

3.8. UCAC4 386-142583

This object was observed unfiltered on July 12 and 20, 2015, collecting a total of 137 measurements. Frequency analysis detected a clear sinusoidal-like modulation with a dominant period of 0.674897 ± 0.00002 day. We show in Figure 8 the light curve folded according to the period found. The periodicity and the amplitude of the light curve variations (~1.0 mag. in CV band), as well as its light curve shape, are compatible with those of an RRab, for which the highest frequency represents the principal pulsation mode. Data from CRTS were available for this variable and therefore 132 measurements have been added to the light curve. Looking at the survey data, they don't seem to fit exactly with the folded period, suggesting the possible presence of a light curve amplitude distortion which is typically related to the Blazhko effect (Blazhko 1907) in this class of variables.

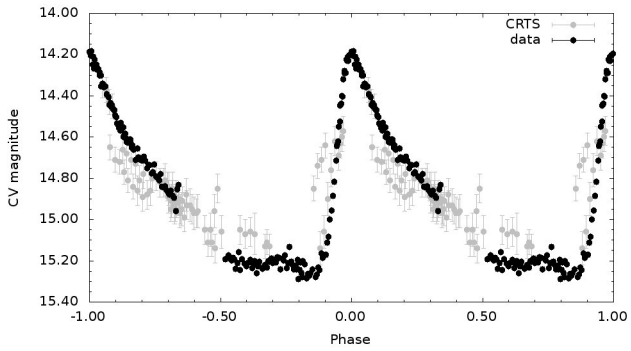

Figure 8. Folded light curve of UCAC4 386-142583.

3.9. UCAC4 398-127457

This object was observed unfiltered on the night of July 7, 2015, for a total of 42 measurements. According to the 2MASS catalog, this star has J–K = 0.55. From these data, we worked out a color index (V–R) = 0.483 which suggests a K0V-K2V spectral type (K0V V–R = 0.45, K2V V–R = 0.52). This is indicative of an EW variable rather than a pulsating one. Frequency analysis gave an orbital period P = 0.319437 ± 0.00002 day. We show in Figure 9 the light curve folded according to the period found, which clearly reveals the presence of a primary and a secondary minimum with equal depths. Data from CRTS are available for this variable and therefore 135 measurements have been added to the light curve.

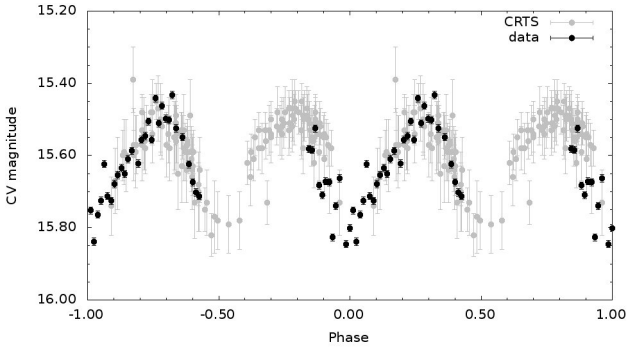

Figure 9. Folded light curve of UCAC4 398-127457.

3.10. UCAC4 384-148138

This object was observed unfiltered on the night of July 11, 2015, for a total of 68 measurements. Frequency analysis gave an orbital period P = 0.375792 ± 0.00002 day. We show in Figure 10 the light curve folded according to the period found, which clearly reveals the presence of a primary and a secondary minimum with equal depths. Data from CRTS are available for this variable and therefore 107 measurements have been added to the light curve. From its shape, we classified this variable as an eclipsing binary of EW type.

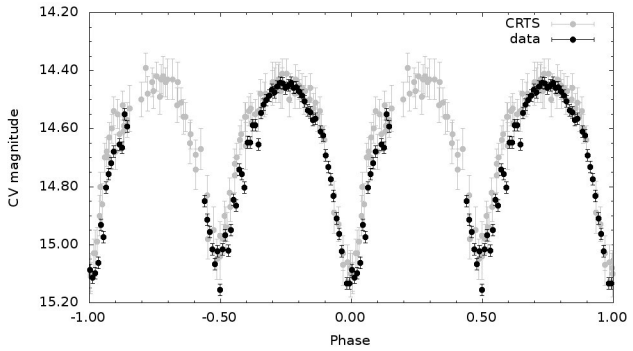

Figure 10. Folded light curve of UCAC4 384-148138.

3.11. UCAC4 398-127590

This object was observed unfiltered on the night of July 7, 2015, for a total of 62 measurements. Frequency analysis gave an orbital period P = 0.309689 ± 0.00002 day. We show in Figure 11 the light curve folded according to the period found, which clearly reveals the presence of a primary and a secondary minimum with equal depths. Data from CRTS are available for this variable and therefore 135 measurements have been added to the light curve. From its shape, we classified this variable as an eclipsing binary of EW type.

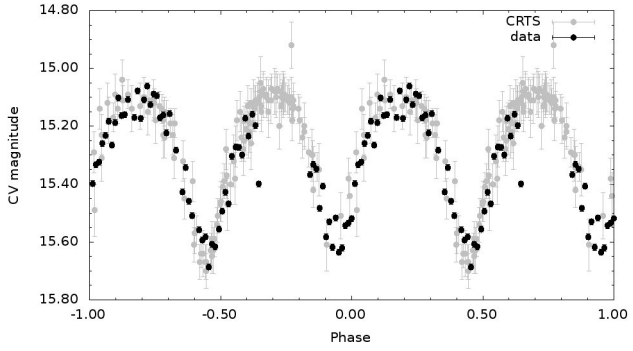

Figure 11. Folded light curve of UCAC4 398-127590.

3.12. UCAC4 383-155837

This object was observed unfiltered from June 28 to July 10, 2015, collecting a total of 139 measurements over 3 nights. Frequency analysis gave an orbital period P = 0.437581 ± 0.00002 day. We show in Figure 12 the light curve folded according to the period found, which clearly reveals the presence of a primary and a secondary minimum with different depths. Data from CRTS were available for this variable and therefore 181 measurements have been added to the light curve. From its shape, we classified this variable as an eclipsing binary of EA type.

3.13. GSC 05752-01113

This object was observed unfiltered on the night of June 25, 2015, for a total of 48 measurements. Frequency analysis gave an orbital period P = 0.332192 ± 0.00002 day. We show in Figure 13 the light curve folded according to the period found, which clearly reveals the presence of a primary and a secondary minimum with equal depths. Data from ASAS and CRTS are available for this variable and therefore 369 measurements have been added to the light curve. From its shape, we classified this variable as an eclipsing binary of EW type.

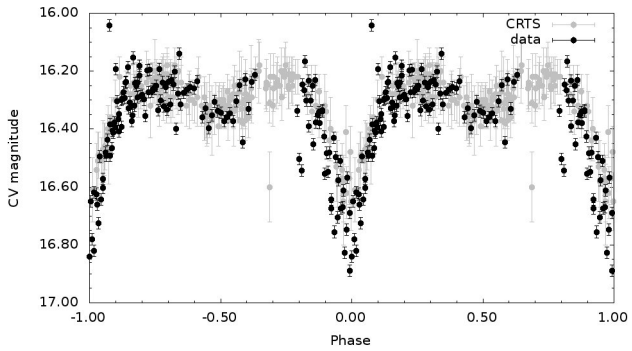

Figure 12. Folded light curve of UCAC4-383-155837.

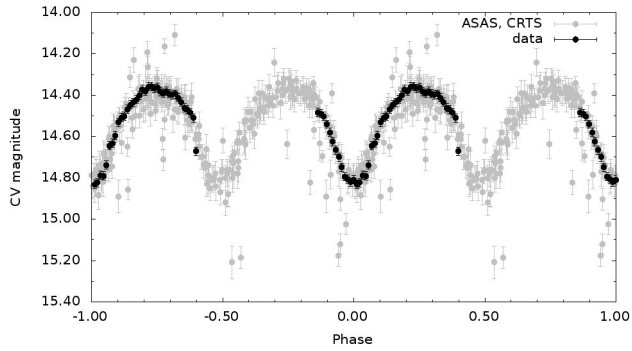

Figure 13. Folded light curve of GSC 05752-01113.

3.14. GSC 05765-01271

This object was observed unfiltered from August 19 to September 9, 2015, for a total of 218 measurements. Frequency analysis gave an orbital period P = 0.382878 ± 0.00002 day. We show in Figure 14 the light curve folded according to the period found, which clearly reveals the presence of a primary and a secondary minimum with equal depths. Data from CRTS are available for this variable and therefore 467 measurements have been added to the light curve. From its shape, we classified this variable as an eclipsing binary of EW type.

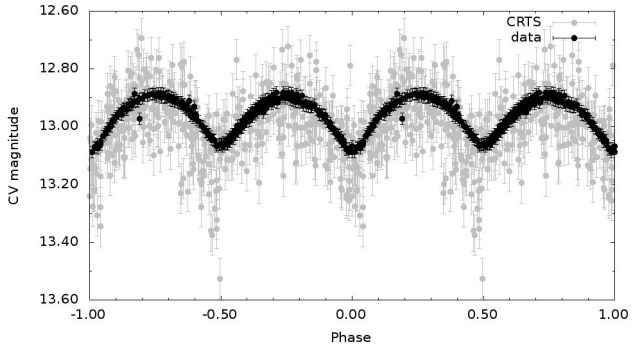

Figure 14. Folded light curve of GSC 05765-01271.

4. Conclusions

After having observed asteroids for about one year for the purpose of doing photometry and plotting their light curves, we have collected thousands images, many of which are centered all night on the same field. Doing a variable star search in these fields allowed us to discover 14 new variable stars—11 eclipsing binaries and 3 short period pulsators of RR Lyrae class. The details of each of the 14 stars are given in Table 2 in order of increasing Right Ascension. Phase plots for all these stars are shown in Figures 1 through 14 in section 3.

5. Acknowledgements

The authors first want to thank Sara Marullo and Jacopo Soldateschi, two students of the course in Physics and Advanced Technologies, who attended several of the observing sessions at the Astronomical Observatory of the University of Siena during their internship activities.

We also want to thank Mike Foylan for his proposal of the target GSC 05065-00218 whose variability he had discovered in 2011 and asked our collaboration for following it up and data analysis. We gladly thank here Brian Warner, Director of the Palmer Divide Observatory, who kindly helped us following up the same star from Colorado.

This work has made use of the VizieR catalog access tool, CDS, Strasbourg, France, the ASAS catalog, the CRTS catalog, the NSVS catalog, and of course the International Variable Star Index (VSX) operated by the AAVSO.

This publication makes use of data products from the Two Micron All Sky Survey, which is a joint project of the University of Massachusetts and the Infrared Processing and Analysis Center/California Institute of Technology, funded by the National Aeronautics and Space Administration and the National Science Foundation.

References

Blazhko, S. 1907, *Astron. Nachr.*, **175**, 325.

Drake, A. J., *et al.* 2014, *Astrophys. J., Suppl. Ser.*, **213**, 9.

Diffraction Limited. 2012, MAXIM DL image processing software (http://www.cyanogen.com).

Howell, S. B. 1991, *J. Amer. Assoc. Var. Star Obs.*, **20**, 134.

Minor Planet Observer. 2010, MPO Software Suite (http://www.minorplanetobserver.com), BDW Publishing, Colorado Springs.

Motl, D., 2011, C-MUNIPACK Software Project (http://c-munipack.sourceforge.net/).

Pojmański, G. 2002, *Acta Astron.*, **52**, 397.

Schwarzenberg-Czerny, A. 1996, *Astrophys. J.*, **460**, L107.

Skrutskie, M. F., *et al.* 2006, *Astron. J.*, **131**, 1163.

Vanmunster, T. 2007, Light Curve and Period Analysis Software PERANSO v.2.50 (http://www.peranso.com).

Warner, B. D. 2012, MPO CANOPUS, BDW Publishing, Colorado Springs, CO (http://minorplanetobserver.com).

Watson, C., Henden, A. A., and Price, C. A. 2014, AAVSO International Variable Star Index VSX (Watson+, 2006–2014; http://www.aavso.org/vsx).

Wozniak, P. R., *et al.* 2004, *Astron. J.*, **127**, 2436.

New Photometric Observations and the 2015 Eclipse of the Symbiotic Nova Candidate ASAS J174600-2321.3

Franz-Josef Hambsch
Oude Bleken 12, B-2400 Mol, Belgium; American Association of Variable Star Observers (AAVSO), Cambridge, MA; Bundesdeutsche Arbeitsgemeinschaft für Veränderliche Sterne e.V. (BAV), Berlin, Germany; and Vereniging Voor Sterrenkunde (VVS), Brugge, Belgium; hambsch@telenet.be

Stefan Hümmerich
Stiftstr. 4, Braubach, D-56338, Germany; American Association of Variable Star Observers (AAVSO), Cambridge, MA; and Bundesdeutsche Arbeitsgemeinschaft für Veränderliche Sterne e.V. (BAV), Berlin, Germany; stefan.huemmerich@gmail.com

Klaus Bernhard
Kafkaweg 5, Linz, 4030, Austria; American Association of Variable Star Observers (AAVSO), Cambridge, MA; and Bundesdeutsche Arbeitsgemeinschaft für Veränderliche Sterne e.V. (BAV), Berlin, Germany

Sebastián Otero
Olazabal 3650-8 C, Buenos Aires, 1430, Argentina; American Association of Variable Star Observers (AAVSO), Cambridge, MA

Received November 9, 2015; accepted December 2, 2015

Abstract The eclipsing binary system ASAS J174600-2321.3, which has shown a conspicuous brightening of ~4 magnitudes (V) in the past, was recently identified as a symbiotic nova candidate. A long-term photometric monitoring program was initiated in July 2014. In its present active stage, the system shows deep eclipses with an amplitude of ~3.5 magnitudes (V) that occur about every 33 months. In order to monitor the eclipse of 2015, *AAVSO Alert Notice 510* was issued. During the ensuing campaign, AAVSO observers obtained 338 measurements in Johnson B, 393 measurements in Johnson V, and 369 measurements in Cousins I, as well as 27 visual observations. The present paper presents and analyzes these data from the AAVSO International Database, along with observations from the aforementioned photometric monitoring program. From these data, we were able to refine the orbital period to P_{orb} = 1012.4 days. Furthermore, the data are suggestive of a slight decrease in mean brightness, which—if proven real—might indicate a decline of the outburst.

1. Introduction

ASAS J174600-2321.3 = EROS2-cg1131n13463 = 2MASS J17460018-2321163, situated in Sagittarius at R. A. (J2000) = 17^h 46^m 00.180^s, Dec. –23° 21' 16.37" (UCAC4; Zacharias *et al.* 2012), is a long-period eclipsing binary system (P_{orb} ~ 33 months). The primary star exhibits the spectral characteristics of a reddened, early F-type supergiant and is likely a white dwarf (WD) currently in outburst. The secondary component is a giant of spectral type late M. The stellar parameters, as derived in Hümmerich *et al.* (2015a; hereafter Paper 1) are given in Table 1. (For more information on the system components, the reader is referred to Paper 1, especially section 3.) The system's photometric variability is characterized by orbital variability (eclipses), semiregular pulsations, and a conspicuous brightening of ~4 magnitudes (V) in the recent past, which has been well documented in available sky survey data (Figure 3 and Paper 1, Figure 1). The outburst has already lasted for more than ~12.8 years and continues to the present day.

Table 1. Stellar parameters and binary separation of ASAS J174600-2321.3, as derived in Paper 1.

Parameter	*Value*
Stellar Parameters	$M_g \approx 1.5\ M_\odot$
(Red Giant)	$R_g \approx 145\ R_\odot$
	$T_{eff} \approx 3{,}130$ K
	Spectral type ~M7
(White Dwarf)	$M_{wd} \approx 0.5\ M_\odot$
Binary Separation	R ≈ 2.5 AU

From the observed characteristics, ASAS J174600-2321.3 was identified as a symbiotic nova candidate (Paper 1). A long-term photometric monitoring program was initiated. Additionally, *AAVSO Alert Notice 510* (AAN 510) was issued in order to get good multicolor coverage of the 2015 eclipse (Hümmerich *et al.* 2015b). The present paper presents and discusses the observations from the aforementioned sources. It is organized as follows: section 2 presents past and present observations of our target, which are analyzed and discussed in section 3. We conclude in section 4.

2. Observations

Before considering the photometric data, it is noteworthy to point out the considerable line-of-sight extinction to ASAS J174600-2321.3. Based on the calculations of Schlafly and Finkbeiner (2011), who employ the colors of stars with spectra in the Sloan Digital Sky Survey and measure reddening as the difference between the measured and predicted colors of a star, we estimate an interstellar extinction of $A_V \approx 2.4$ mag.

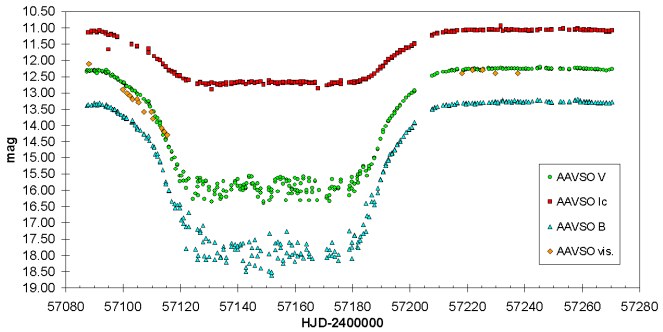

Figure 1. Light curve of ASAS J174600-2321.3, based on data obtained by AAVSO observers during the campaign initiated via *AAVSO Alert Notice 510*. Obvious outliers have been removed by visual inspection.

Table 2. Observers of ASAS J174600-2321.3.

Name	*AAVSO Observer Initials*	*Number of Observations*
Salvador Aguirre	ASA	1
Teofilo Arranz	ATE	7
Alejandra Arranz Lázaro	AALB	2
Lewis Cook	COO	16
Brian Cudnik	CKB	3
Shawn Dvorak	DKS	15
Franz-Josef Hambsch	HMB	912
Michael Heald	HMH	36
Gordon Myers	MGW	70
Peter Robert Nelson	NLX	23
Steve O'Connor	OCN	3
Andrew Pearce	PEX	14
Larry Shotter	SLH	8
Peter John Starr	SPET	18
Robert R. Young	YON	1

and E(B–V) ≈ 0.78 mag. If not indicated otherwise, all light curves illustrated in this and the following sections are based on non-corrected data.

2.1. AAVSO observing campaign

During the observing campaign initiated by *AAN 510*, AAVSO observers obtained 338 measurements in Johnson B, 393 measurements in Johnson V, and 369 measurements in Cousins I (I_C), as well as 27 visual observations (Kafka 2015). A light curve based on these data is shown in Figure 1. In Table 2 we gratefully acknowledge the efforts of the contributing observers.

As the agreement for B and V data between AAVSO observers is very good, we chose to combine the corresponding datasets for the following analyses; some obvious outliers were removed by visual inspection. For I_C data, the situation is more complicated, though. There are significant mean magnitude differences (up to ~0.7 mag.) between several observers' datasets. An investigation of the respective datasets indicates that, most likely, the use of different comparison star sets is responsible for the observed discrepancies. As a solution to this problem, we have chosen to base our analyses on the most comprehensive and homogeneous I_C dataset available. Because of the availability of extensive datasets of CCD photometry, visual observations were not included into the analyses in section 3.

2.2. Photometric monitoring program

In order to study the long-term photometric behavior of the system, a monitoring program was initiated at the Remote Observatory Atacama Desert (ROAD; Hambsch 2012). Starting on July 17, 2014, observations have been taken with an Orion Optics, UK Optimized Dall Kirkham 406/6.8 telescope and a FLI 16803 CCD camera. Images were taken through Astrodon Photometric B, V, and I_C filters. Initially, observations were carried out in V only; with the start of the AAVSO observing campaign, simultaneous observations in B and I_C were added to the observing program. ROAD data taken during the AAVSO campaign (912 observations) are not designated separately but are included with the AAVSO data; they can be identified by the observer code "HMB". A light curve of the observations carried out prior to the start of the AAVSO campaign is shown in Figure 2. Two measurements per night were taken; the plot is based on nightly averages.

2.3. Sky survey data and long-term light curve

In our initial investigation of ASAS J174600-2321.3 (Paper 1), we procured data from the EROS-2 (Renault *et al.* 1998), ASAS-3 (Pojmański 2002), CMC14 (Evans *et al.* 2002), and APASS (Henden *et al.* 2012) archives. EROS-2 B_E and R_E magnitudes were transformed to V and I_C, respectively. Approximate I_C values were derived from APASS r' and i' photometry. The CMC14 observation was transformed to V. Furthermore, obvious outliers with a photometric quality flag

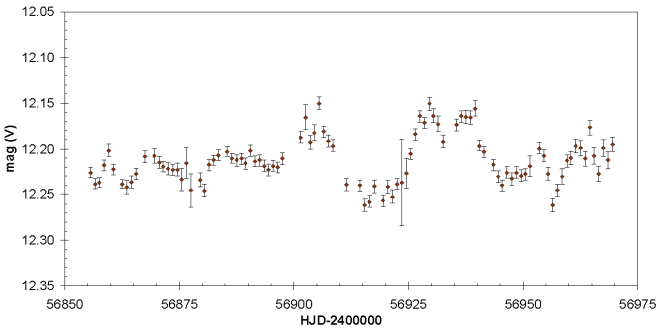

Figure 2. Light curve of ASAS J174600-2321.3, based on ROAD data, which have been acquired during the authors' photometric monitoring program. The plot is based on nightly averages (see text for details).

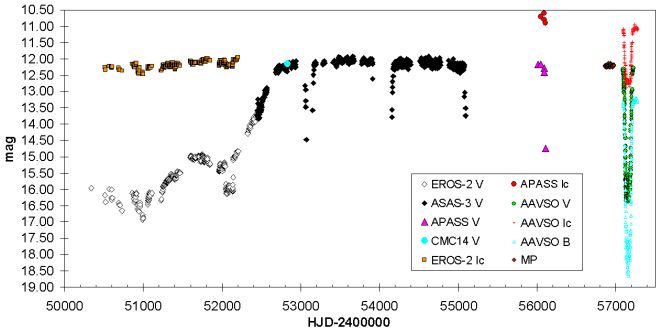

Figure 3. Light curve of ASAS J174600-2321.3, based on various data sources, as indicated in the legend on the right. "MP" designates data from the long-term monitoring program (see section 2.2). Obvious outliers have been removed from AAVSO data by visual inspection.

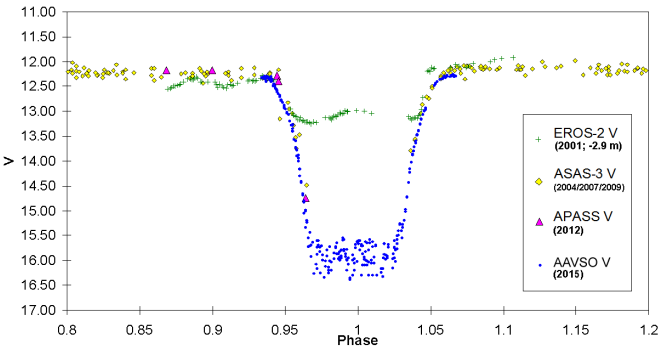

Figure 4. Phase plot of ASAS J174600-2321.3, illustrating all primary eclipses. The plot is based on various data sources, as indicated in the legend on the right, and folded with the elements given in Equation (1).

Table 3. Mean Brightness of ASAS J174600-2321.3 during the total phase of the 2015 eclipse and amplitude of the 2015 eclipse in B, V, and I_C.

Mean Brightness During Totality Phase	*Amplitude of the 2015 Eclipse*
mean B = 17.9 mag.	$\Delta B \approx 4.6$ mag.
mean V = 15.8 mag.	$\Delta V \approx 3.6$ mag.
mean I_C = 12.7 mag.	$\Delta I_C \approx 1.6$ mag.

of D (= "worst data, probably useless") were removed from the ASAS-3 dataset. A detailed description of the various data sources and reduction processes involved can be found in Paper 1, section 2.1.

Figure 3 shows the long-term light curve of ASAS J174600-2321.3, which has been based on sky survey data, the authors' long-term monitoring program (designated as "MP" in the legend), and AAVSO campaign data.

3. Discussion

3.1. Orbital period

In order to fit the new observations, the previously determined orbital period of P_{orb} = 1011.5 days (see Paper 1, section 3.1) had to be adjusted slightly. From an analysis of V-band data for all eclipses, the following improved orbital ephemeris was derived.

$$\text{HJD (Min I)} = 2456142 + 1012.4\ (\pm\ 0.2) \times E \qquad (1)$$

Figure 4 shows the resulting phase plot and illustrates all primary eclipses that have been observed so far. In order to facilitate comparison, EROS-2 V magnitudes have been shifted by the indicated amount to match V magnitudes from ASAS-3, APASS, and AAVSO.

3.2. Eclipse depth

Only rudimentary coverage of the eclipses existed after the onset of activity and the considerable brightening of the system, which has been shown to be restricted to the primary star of the system (the outbursting WD; see Paper 1, section 3.1). In particular, no observations were taken during the total phase of any ensuing eclipse. Thus, for the first time, AAVSO campaign data allow the measurement of the depth of the eclipse in outburst stage. Average values and amplitudes are given in Table 3.

As the seat of the outburst is proposed to be the WD primary component of ASAS J174600-2321.3, and the observed eclipse shows a pronounced phase of totality, in which the red giant passes in front of the WD, it might reasonably be assumed that the system's brightness returns to its pre-outburst value of ~16.5 mag (V) during the total phase of the eclipse. This, however, is obviously not the case—the system's brightness hovers around 15.8 mag. (V) during the total phase of the 2015 eclipse instead (see Table 3). This difference in mean brightness is also reflected in a bluer color index at this phase. Explanations for these interesting phenomena are discussed below in section 3.5.

3.3. Variability during total eclipse

Both components of ASAS J174600-2321.3 were shown to exhibit light variability, which is likely due to pulsations (see Paper 1, section 3.4). The observed semiregular pulsations of the red giant component dominated the light changes of the system before the proposed outburst and the corresponding rise in mean magnitude. They were most obvious in EROS-2 I_C band data, exhibiting a mean amplitude of $\Delta I_C \approx 0.1$ mag. Although the pulsations were rather ill-defined throughout the covered timespan, a dominant signal at P ≈ 56 days was identified (see Paper 1, Figure 14).

Light variability was observed in the form of a rebrightening around the time of mid-eclipse during the total phase of the 2001 eclipse—the only eclipse with good coverage during totality phase in the past. In regard to phase and amplitude, the observed variability was in agreement with the red giant's pulsations and was interpreted in this vein (see Paper 1, section 3.4).

We have searched for variability during the total phase of the 2015 eclipse. As the system gets considerably faint during the phase of totality (B ≈ 17.9 mag.; V ≈ 15.9 mag.; I_C ≈ 12.7 mag.), the measurement errors increase markedly, too, leading to increased scatter during this part of the light curve. These measurement uncertainties are most pronounced in B and V band data, obliterating any trace of variability in B, and rendering detection in the V light curve a borderline case. However, the situation is different in I_C data, which clearly show indications of variability (Figure 5); again, a central rebrightening is observed.

In terms of duration and amplitude, the observed light changes are in agreement with the pulsational variability of the red giant component. However, it seems a curious fact that the pulsations of the red giant should exhibit nearly identical maxima around the time of mid-eclipse during both the 2001 and 2015 totalities. Therefore, it seems worthwhile to consider alternative explanations for the observed phenomenon. Snyder and Lapham (2008) investigated eclipse brightening features in 18 binary systems. Eclipse brightening has been identified throughout a wide range of system configurations, from detached to over-contact binaries and short to very long period systems such as ε Aurigae. Brightenings around mid-eclipse have been described for several objects.

Snyder and Lapham (2008) examined gravitational lensing, microlensing and refracted electromagnetic radiation ("prism effect") as possible causes. In the case of the interacting

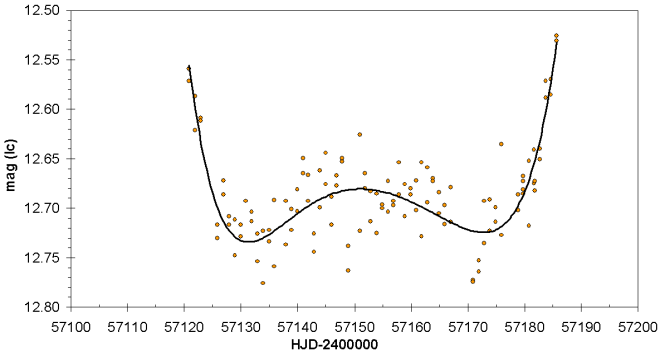

Figure 5. Detailed view of the total phase of the 2015 eclipse, based on AAVSO I_C data. The solid line indicates a 6th order polynomial fit to the data.

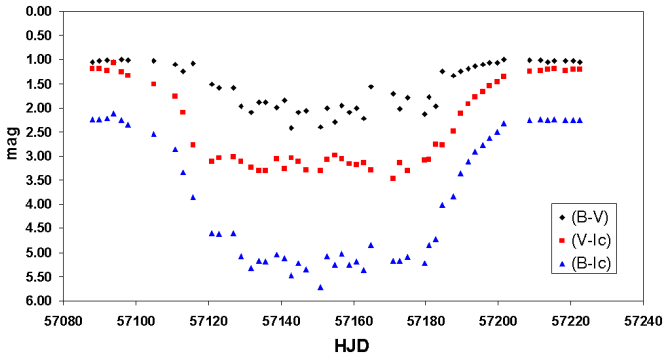

Figure 6. Color curves in (B–V), (V–I_C), and (B–I_C) of ASAS J174600-2321.3, based on two-point averages of nightly mean values of the data obtained by AAVSO observers during the campaign initiated via *AAVSO Alert Notice 510*. Obvious outliers have been removed by visual inspection.

symbiotic binaries with their complex light curves (Skopal 2008, for example) and often variable eclipse shapes (Bruch *et al.* 1994, for example), other scenarios involving mass transfer/mass accretion might be conceivable. However, at this point, we can only speculate on the nature of the observed brightening. Spectroscopic as well as photometric coverage of upcoming eclipses will be necessary to decide on the true nature of the observed phenomenon.

3.4. Variability at maximum visual brightness

After the dramatic rise in brightness, which culminated with reaching ~12.2 mag. (V) at about HJD 2452600, the WD primary component of the system came to dominate the flux at optical wavelengths. Although the light from the WD now effectively swamped the red giant's pulsations in V, there were indications of pulsational-like variability in the ASAS-3 light curve at maximum visual light after the brightening event. The observed variability was rather irregular and poorly defined, although there is indication of a period of about 80–90 days, particularly around HJD 2453500 (see Paper 1, Figure 13).

After the end of ASAS-3 observations, there followed a gap in photometric coverage of about 2,000 days, interrupted only by a few APASS measurements around HJD 2456000. New data were made available with the start of the photometric monitoring program described in section 2.2. Interestingly, the data obtained paint quite a different picture of the variability at maximum visual brightness (Figure 2); the rather slow light changes detected in ASAS-3 data seem to have been substituted by more irregular variability on shorter time-scales. An analysis of the new data with PERIOD04 (Lenz and Breger 2005) and the CLEANest algorithm (Foster 1995) suggests the existence of a weak signal at P ≈ 33 days. However, because of the irregularity of the observed light changes and the short time baseline, the significance of this detection is doubtful. Still, it is intriguing to connect the apparently shortened time-scale of variability at maximum light to a decrease in diameter of the pseudophotosphere of the WD, which would go along well with the apparent slight decrease of the system's mean brightness in recent observations, which is commented on below (see section 3.6).

3.5. Color curves and indices

Average color indices and color curves were constructed from AAVSO campaign data. Because of the faintness of the system during the total phase of the eclipse, a lot of scatter is present during these parts of the light curve, which is attributable to a corresponding increase in measurement errors. In order to augment this situation, we have chosen to use two-point averages based on nightly mean values in the construction of the color curves, which are shown in Figure 6. Average dereddened color indices at maximum light and the middle of total eclipse are presented in Table 4, along with color indices derived from earlier observations in Paper 1.

While the observed dereddened color indices at maximum visual brightness are in accordance with the earlier observations ($(B–V)_0 \approx 0.2$; see Paper 1, Table 4), there is considerable discrepancy between the measured (V–I_C) indices before the onset of activity in the system and during the total phase of the 2015 eclipse (Table 4).

With the red giant component dominating before the brightening event and during the total phase of the eclipse (and the WD's contribution assumed to be negligible during both phases), one would expect the colors to match more closely during these phases. As has been pointed out above, though, the system is also ~0.7 mag. (V) brighter during the total phase of the 2015 eclipse (~15.8 mag. (V)) than at quiescence (~16.5 mag. (V); see section 3.2).

Several mechanisms might contribute to the observed phenomena. For instance, the contribution of the red giant to the total flux of the system might be enhanced, possibly due to the heating of its outer layers by the intense ultraviolet radiation from the WD. On the other hand, there might be a significant flux contribution from the WD even at this phase; for example,

Table 4. Average dereddened color indices at mid-eclipse and maximum visual brightness, as derived from AAVSO campaign data and earlier observations.

Mid-eclipse (2015 eclipse)	*Maximum Visual Brightness*	*Derived from Earlier Observations (Paper 1)*
$(B–V)_0 \approx 1.2$	$(B–V)_0 \approx 0.14$	$(B–V)_0 \approx 0.2$ epoch: HJD 2456008.794 (max. vis. brightness)
$(V–I_C)_0 \approx 2.1$	$(V–I_C)_0 \approx 0.14$	$(V–I_C)_0 \approx 3.0$ mean value at min. vis. brightness (HJD < 2451112.53)
$(B–I_C)_0 \approx 3.3$	$(B–I_C)_0 \approx 0.28$	n/a

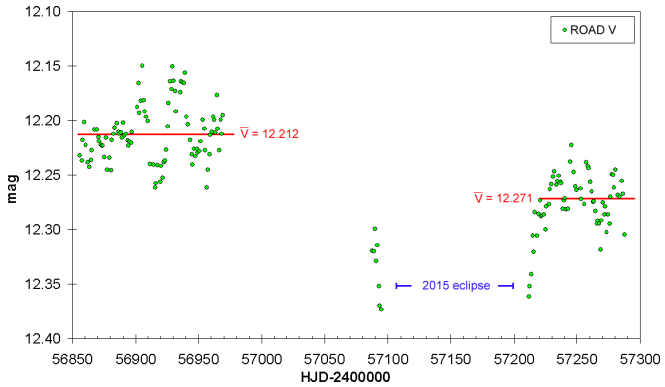

Figure 7. Detailed view of photometric observations taken at ROAD observatory, based on nightly mean values. The solid lines indicate the mean magnitudes of data taken before and after the 2015 eclipse.

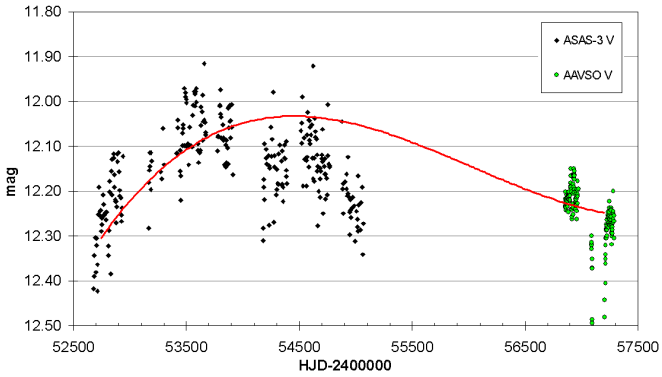

Figure 8. Light curve of ASAS J174600-2321.3, based on ASAS-3 and AAVSO V band data. The solid line represents a polynomial fit to the data.

the light of the WD might permeate the outer layers of the tenuous atmosphere of the red giant.

However, the most significant contribution will likely arise from the huge amount of circumstellar gas ionized by the intense radiation of the outbursting WD. As the volume occupied by the gas will likely exceed the diameter of the cool giant, there will be a significant contribution to the light output of the system even during the total phase of eclipse. This is in accordance with the above mentioned blueward evolution of the system's color indices, which has also been observed in other symbiotic novae (see, for example, Kenyon 1986).

3.6. Mean magnitude trend

Recent data are suggestive of a slight decrease in mean magnitude of the system, especially after the end of the 2015 eclipse. In order to verify its reality, we have investigated this phenomenon in ROAD data, which constitute the most extensive and homogeneous dataset available. No change in instrumental setup was performed at the ROAD observatory during the monitoring program and the AAVSO campaign. As shown in Figure 7, the observed decrease in mean magnitude seems to be real and significant.

We have combined ASAS-3 and AAVSO V-band data to search for overall mean magnitude trends. The data are suggestive of a long-term mean brightness trend, which we have visualized with a polynomial fit to the data in Figure 8. It is tempting to associate the decreasing optical flux output of the system with a possible shrinking of the WD's pseudophotosphere, which might indicate a decline of the outburst.

However, because of the considerable measurement errors of ASAS-3 data and the intrinsic brightness fluctuations of the system, further observations are needed to establish the reality of the proposed long-term mean magnitude trend.

4. Conclusion

We have presented and analyzed observations of the eclipsing symbiotic nova candidate ASAS J174600-2321.3 from our photometric long-term monitoring program and the recent AAVSO observing campaign of the 2015 eclipse, which was initiated via *AAVSO Alert Notice 510*. AAVSO observers obtained 338 measurements in Johnson B, 393 measurements in Johnson V, and 369 measurements in Cousins I, as well as 27 visual observations. These data allowed the measurement of the eclipse depth in outburst stage for the first time ($\Delta B \approx 4.6$ mag; $\Delta V \approx 3.6$ mag; $\Delta I_C \approx 1.6$ mag). By combining all available V-band data, the orbital period could be refined to $P_{orb} = 1012.4$ days. The system is bluer and brighter during the totality phase than before the beginning of the outburst phase and the corresponding rise in magnitude, which is mostly likely due to a significant light contribution by ionized circumstellar gas. Furthermore, recent data are suggestive of a slight decrease in mean brightness, which – if proven real – might indicate a decline of the outburst. Further photometric and spectroscopic studies of this interesting object are encouraged.

5. Acknowledgements

We acknowledge with thanks the variable star observations from the AAVSO International Database contributed by observers worldwide, which have made this research possible. We would also like to thank the anonymous referee for suggestions that helped to improve the paper. This work has made use of the SIMBAD and VizieR databases operated at the Centre de Données Astronomiques (Strasbourg) in France. This research has also made use of EROS-2 data, which were kindly provided by the EROS collaboration. The EROS (Expérience pour la Recherche d'Objets Sombres) project was funded by the CEA and the IN2P3 and INSU CNRS institutes. Furthermore, this research has employed data products from the Two Micron All Sky Survey, which is a joint project of the University of Massachusetts and the Infrared Processing and Analysis Center/California Institute of Technology, funded by the National Aeronautics and Space Administration and the National Science Foundation.

References

Bruch, A., Niehues, M., and Jones, A. F. 1994, *Astron. Astrophys.*, **287**, 829.

Evans, D. W., Irwin, M. J., and Helmer, L. 2002, *Astron. Astrophys.*, **395**, 347.

Foster, G. 1995, *Astron. J.*, **109**, 1889.

Hambsch, F.-J. 2012, *J. Amer. Assoc. Var. Star Obs.*, **40**, 1003.
Henden, A. A., *et al.* 2012, Data Release 3 of the AAVSO All-Sky Photometric Survey (http://www.aavso.org/apass).
Hümmerich, S., Otero, S., Tisserand, P., and Bernhard, K. 2015a, *J. Amer. Assoc. Var. Star Obs.*, **43**, 14.
Hümmerich, S., Otero, S., Tisserand, P., Bernhard, K., and Templeton, M. R. 2015b, *AAVSO Alert Notice 510*, 1.
Kafka, S. 2015, observations from the AAVSO International Database (https://www.aavso.org/aavso-international-database).
Kenyon, S. J. 1986, *The Symbiotic Stars*, Cambridge Univ. Press, Cambridge.
Lenz, P., and Breger, M. 2005, *Commun. Asteroseismology*, **146**, 53.
Pojmański, G. 2002, *Acta Astron.*, **52**, 397.
Renault, C., *et al.* 1998, *Astron. Astrophys.*, **329**, 522.
Schlafly, E. F., and Finkbeiner, D. P. 2011, *Astrophys. J.*, **737**, 103.
Skopal, A. 2008, *J. Amer. Assoc. Var. Star Obs.*, **36**, 9.
Snyder, L. F., and Lapham, J. 2008, in *The Society for Astronomical Sciences 27th Annual Symposium on Telescope Science, held May 20–22, 2008 at Big Bear Lake, CA,* Society for Astronomical Sciences, Rancho Cucamonga, CA, 29.
Zacharias, N., Finch, C. T., Girard, T. M., Henden, A., Bartlett, J. L., Monet, D. G., and Zacharias, M. I. 2012, The Fourth U.S. Naval Observatory CCD Astrograph Catalog (UCAC4), VizieR On-line Data Catalog (http://cdsarc.u-strasbg.fr/viz-bin/Cat?I/322).

High-Cadence B-Band Search for Optical Flares on BY Dra

Gary A. Vander Haagen
Stonegate Observatory, 825 Stonegate Road, Ann Arbor, MI; garyvh2@gmail.com

Received November 2, 2015; revised November 30, 2015; accepted December 1, 2015

Abstract The high-cadence search at 50 and 100 samples/sec of BY Dra revealed very short-duration B-band flares. A statistical criterion was used to isolate the short-duration optical flares from random photon events. Three flares, ranging in duration from 60 to 130 ms, with peaks 0.30–0.43 magnitude above the mean, were detected within the 80.2 hours of periodic monitoring from July 2012 through October 2015. This represents a flare rate of 0.04 flares/hour.

1. Introduction

BY Draconis is a main sequence archetype variable MK-type star whose low-level luminosity variability is due to its rotation coupled to chromospheric surface spots. Movement of these spots produce quasi-periodic variability closely related to its rotational period. Early studies conducted on BY Dra by Cristaldi and Rodono (1970) indicated that the star was also a flare star. Subsequent studies by Cristaldi and Rodono (1973) further supported flaring over a two-year monitoring window. The Cristaldi search was conducted using an S13 spectral response photomultiplier with an electronic equipment time constant of 1 second and recording chart rolling speed of 1 cm per minute, the objective being to capture conventional longer duration flares. While this archetype variable has been widely studied for its surface spots and resultant quasi-periodic variability, Zalinian and Tovmassian (1987) was the only high-cadence search found of BY Dra and recorded two short-duration flares.

The objective of this search was to conduct a high-cadence photometric study to capture conventional longer flares and also any solo or short-duration flares proceeding, during, or after the main outburst. Such data should improve the granularity of knowledge of an outburst event and potentially capture very fast solo events missed by conventional long integration photometry. Vander Haagen (2013) reported such events in RS CVn type star systems. This high-cadence search was conducted principally at sample rates of 50 and 100 samples/sec.

2. Optical system and data collection and analysis pipeline

The optical system consisted of a 43-cm corrected Dall-Kirkham scope, a high-speed silicon photomultiplier (SPM), and a data acquisition system capable of sub-millisecond data collection times. The SPM was chosen for this application because it has comparable sensitivity to a standard single channel vacuum photomultiplier, yet a more robust mechanical and electrical design with the disadvantage of higher dark counts (Vander Haagen 2012). The observations were conducted using an Edmund 500-nm short-pass filter to improve the overall transmission in the UV and blue. When combined with the response of the SPM, the resultant band pass was 380 to 500 nm giving approximately a 20 nm increase in the 3 db down point at the longer blue wavelengths versus a B-band filter. There was very minor UV response improvement due to the SPM's response at shorter wavelengths. This resulted in a non-standard photometric B-band pass.

The optical system is shown is Figure 1. The incoming beam is split approximately 80/4 with the reflected portion passing through the optical filter, an f-stop yielding a 57 arc-second field, and onto the SPM detector. A wide bandwidth pulse amplifier amplifies the SPM signal, producing a 2- to 3-volt pulse of approximately 50 ns for each converted photon. These photon pulses are sent to a PC-based data acquisition system where they are gated and counted based upon the collection rate. A 10 ms gate was used for most of the measurements, generating a 100 Hz data collection rate or 100 samples/second. The balance of the incoming beam passes straight through to a conventional CCD camera used for initial alignment, guiding, and measurement of both the guide star flux and background flux. Referring to Figure 2, the flux value counts from the target data stream along with GPS 1-second time stamps are recorded in the DAQ Log File by the data acquisition system (Vander Haagen and Owings 2014). The CCD Data and Control stream consists of reference and background flux values plus pixel counts for each guide star sample, typically every 5 seconds. These values are stored in the AG (auto-guider) Tracker Log file.

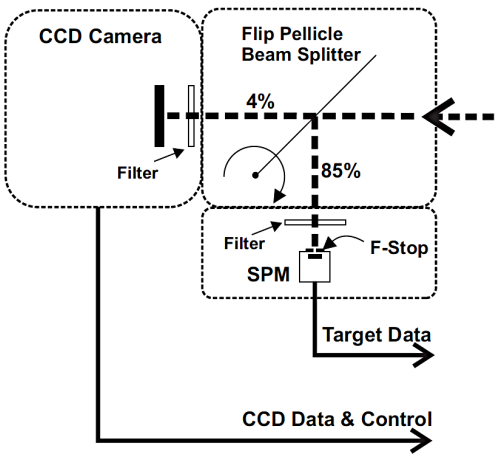

Figure 1. The optical train pictorial shows the pellicle beam splitter with both reflected and pass-through beams. The reflected beam passes through the narrow band filter, aperture, and onto the silicon photomultiplier (SPM). The pellicle can be flipped to allow 100% light transmission for initial target alignment using the CCD camera. The SPM is mounted on an X-Y stage for precise centering of detector to the centerline of the CCD camera. Guiding is provided with pellicle in position shown. The target SPM photon counts and data from the CCD camera are processed and stored as shown in data acquisition pipeline, Figure 2.

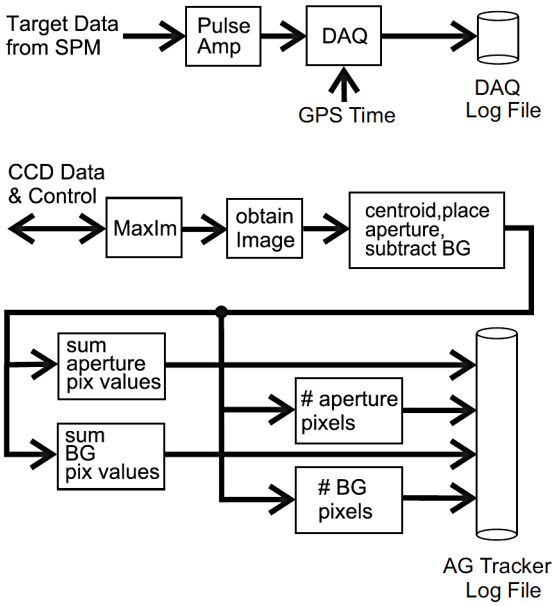

Figure 2. The data acquisition pipeline consists of two streams, the target photon counts and CCD camera image data. The low level SPM photon counts are amplified and counted by the data acquisition system (DAQ) for the period selected (ex. 10 ms) and the data written to the DAQ Log File. A GPS-synced time stamp is added every second to the appropriate data line. The DAQ Log is limited to 1 million data lines per file. The CCD data feed the camera control program that extracts the guide-star image, centroids the image, and extracts both flux and pixel counts for the guide star and background. This occurs at a rate determined by the guide star exposure, typically every five seconds. These data are written to the AG Tracker Log File.

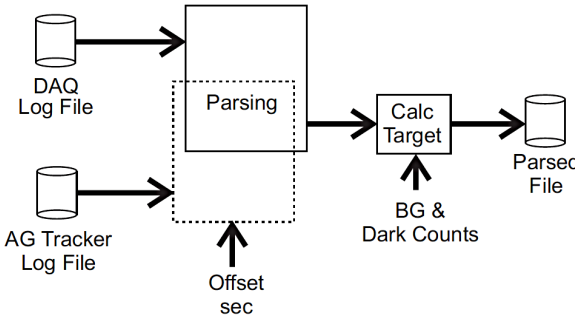

Figure 3. Upon completion of the data collection the DAQ and AG Tracker Log files are merged using a parsing operation. The lower resolution tracker file data are aligned with the DAQ target photon counts; the target counts are reduced using a quadrature calculation to remove the sky background and SPM dark counts thereby producing and integrated file of sample by sample target counts, reference star flux, and sky background all referenced to an accurate UT time stamp in seconds; for example, 5402 sec equals 1:30:02 UT with resolution to the sample period.

Upon completion of the night's search the DAQ Log File and the CCD's AG Tracker Log File are merged as shown in Figure 3. The large DAQ Log File with up to one million data samples is merged with the much slower occurring auto-guider, AG Tracker Log, reference data in a parsing process. Here, every target data point is matched to the time-appropriate Tracker data with the target counts corrected for the SPM dark counts and sky background in a quadrature calculation, and each sample GPS time stamped. This parsing operation results in an integrated file with all constituents ready for analysis, with each file containing up to one million sample lines each containing target, reference, and background data. Files of this size are too large for spreadsheet analysis but are easily analyzed using signal processing software such as SIGVIEW (SignalLab 2015). The files are reviewed and processed using a variety of filters, time domain transforms, and statistical tools.

3. Flare search

The study objective was capturing of high time resolution flaring activity connected with longer-duration conventional flares and short-duration solo flares. Very short flares of 10 to 100 ms duration have been observed unconnected with conventional flaring activity. These very short flares generally consisted of one or more points at 3σ or higher with a peak at 4–10σ. A 50 ms duration flare was reported for EV Lac in the U–B band by Zhilyaev and Romanjuk (1990) and simultaneous U and B-band flares on BY Dra (Zalinian and Tovmassian 1987). Vander Haagen (2013) also reported very short-duration flares on AR Lac, II Peg, and UX Ari of 30 to 85 ms duration with peaks 0.29–0.51 magnitude above the mean.

A criterion was developed to isolate these short-duration flares in very large sample sizes; flares must consist of a minimum of three consecutive data points, two at or above 3σ and one at or above 5σ. Since the minimum number of photons per gate was always 100 or more, normal distribution statistics were used to compute the standard deviation. Statistics were collected 600 seconds prior to the event where possible using digital signal processing software (SignalLab 2015). This process is similar in direction to that followed by flare searches (Byrne *et al.* 1994) and similar as described by Vander Haagen (2013). The probability of this sequence being a random event can be represented by Equation 1, where N is the number of integrations or samples taken during the observing interval and σ is for the positive events only.

$$\Pi_{3,3,5\sigma} = P_r(3\sigma)^2 5\sigma = (1.35 \times 10^{-3})^2 \times (2.9 \times 10^{-7})\,N = 5.2 \times 10^{-13}\,N \quad (1)$$

With N ranging from 1 to 2×10^6 samples during an observing interval the probability of the event sequence being random is appropriately small. This criterion was used for each of the data sets to isolate potential short-duration flares.

4. BY Dra data collection and analysis

Shown in Figure 4, the data collection was conducted over the period July 30, 2012, through October 8, 2015. The majority of the data (82%) were collected between June 2015 and October 2015. The total data collection time was 80.2 hours or 288.8 Ksec, with the first 23.8 Ksec at 200 samples/sec, which was considered oversampled. The next 87.3 Ksec was sampled at 50 samples/sec and after S/N and resolution review was increased to 100 samples/sec, 10 ms gating period, for the remaining 177.7 Ksec of the study. When combined with the response of the SPM the resultant band pass is approximately 380 to 500 nm. This band pass was chosen versus V or R bands due to its generally higher amplitude transmission during flaring conditions. Three short-duration flares were captured,

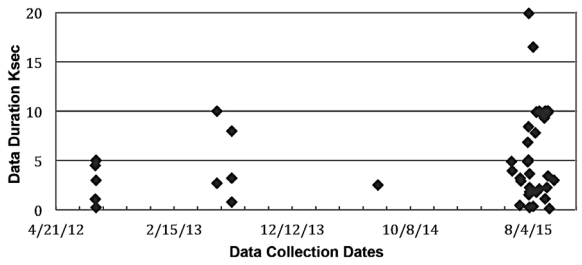

Figure 4. BY Dra data collection over the period July 30, 2012, through October 8, 2015, for a total of 80.2 hours or 288.8 Ksec, with (82%) collected between June 2015 and October 2015.

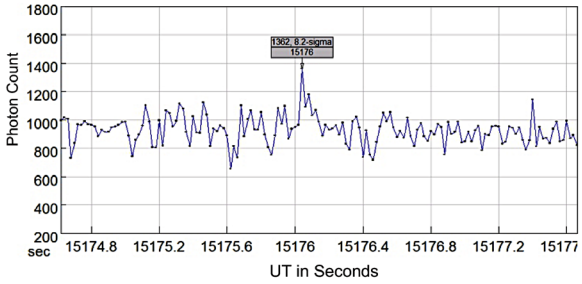

Figure 5. 2015-08-16, BY Dra sampled at 50s/sec (20ms gating period), mean 916, σ 54, data point sequence on peak: 1362 (8.2σ), 1092 (3.3σ), and 1178 (4.8σ). The time axis is in UT (seconds) for the date specified. The 1362 count peak was 0.43 mag. above mean with a flare duration of 120 ms. Annotation box on graph shows peak count and sigma value (top) and time at peak (lower).

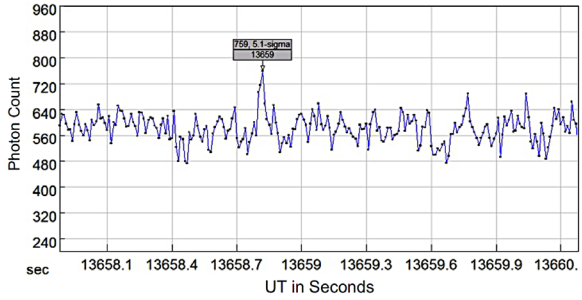

Figure 6. 2015-09-22, BY Dra sampled at 100 s/sec, mean 576, σ 36, data point sequence 694 (3.3σ), 715 (3.9σ), and 759 (5.1σ). The time axis is in UT (seconds) for the date specified. The 5.1σ peak was 0.30 mag. above the mean with a flare duration of 60 ms. Annotation box on graph shows peak count and sigma value (top) and time at peak (lower).

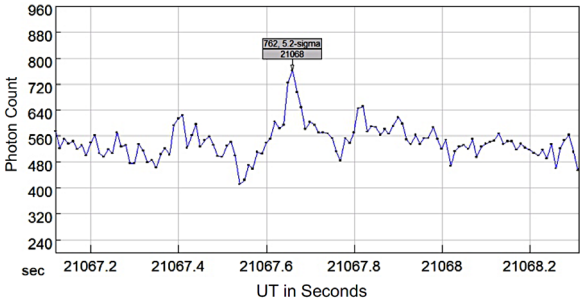

Figure 7. 2015-09-23, BY Dra sampled at 100s/sec, mean 540, σ 43, data point sequence 724 (4.3σ), 762 (5.2σ), and 696 (3.6σ). The time axis is in UT (seconds) for the date specified. The 5.2 σ peak was 0.37 mag. above the mean with a flare duration of 130 ms. Annotation box on graph shows peak count and sigma value (top) and time at peak (lower).

0.04 flare/hour. Two additional flares were captured during the July to October period but narrowly missed at least one of the statistical event criterions. Flare 1 is shown in Figure 5 with an 8.2σ, 0.43 magnitude peak above mean and 120 ms duration. Flare 2 shown in Figure 6 has a 5.1σ, 0.30 magnitude peak above mean and 60 ms duration. Flare 3 shown in Figure 7 has a 5.2σ, 0.37 magnitude peak above mean and 130 ms duration.

5. Discussion and conclusions

Atmospheric scintillation as source or inducer of the short-duration peaks is possible and cannot be ruled out without a simultaneous high-speed reference. Without a substantially more complex optical system the 5-second integration reference star represents a degree of assurance that no major perturbations have occurred.

In addition, Fourier PSD transforms were made of each data set. A wide range of noise amplitude and cutoff frequencies were present across the data sets. Where short-duration peaking occurred, digital band pass filters were employed to isolate the frequency domain signature of the event. No signature that was narrow or consistent enough could be identified. This area of investigation did not prove fruitful. This same issue was noted in Vander Haagen (2013).

The work done by Cristaldi and Rodono (1973) discovered a number of longer duration flares but did not calculate the flare rates. In that study the data collection method consisted of a 1-cm-per-minute chart recorder with an electronic time constant of 1 sec. Five flares of approximately 0.1 magnitude or less were identified within the B band ranging in duration from 1 to slightly over 2 minutes. With the two telescope systems used the flare rates were estimated, from their data, at 0.04 and 0.16 flares per hour. With the systems' slow response, flares of second and sub-second duration could not be identified.

This search did not identify any longer-duration flares. All the data were resampled to a 10-second integration so that the search criterion was appropriate for longer-duration flares. None were found. However, with 82% of the data in this search collected between late June and early October 2015 it is consistent that a period of low activity may have existed.

In conclusion, a statistical criterion was used to isolate short-duration optical flares from random photon events. Three short-duration optical flares were identified in the B band over an 80.2-hour observing period. The three flares ranged in duration from 60 to 130 ms with peaks 0.30–0.43 magnitude above the mean, yielding a flare rate of 0.04 flare/hour. Zalinian and Tovmassian (1987), using an electrophotometer with a 0.1-second time constant, identified two simultaneous BY Dra U- and B-band "spiky flares" exceeding 3σ at less than 0.2 second duration, producing a rate of 0.22 flare/hr. While their acceptance criterion was less stringent, reasonable agreement exists between the searches.

6. Acknowledgements

Thanks are expressed to L. E. Owings for his collaboration on the AG Tracker and Parser data pipeline and writing of

the two software programs. The referee assistance is greatly appreciated for improvement suggestions on several items including the statistical criteria in section 3.

References

Byrne, P. B., Lanzafame, A. C., Sarro, L. M., and Ryans, R. 1994, *Mon. Not. Roy. Astron. Soc.*, **270**, 427.

Cristaldi, S., and Rodono, M. 1970, *Astron. Astrophys. Suppl. Ser.*, **2**, 223.

Cristaldi, S., and Rodono, M. 1973, *Astron. Astrophys., Suppl. Ser.*, **10**, 47.

SignalLab 2015, SIGVIEW 2.7.1 software for DSP applications (http://www.sigview.com/index.htm).

Vander Haagen, G. A. 2012, in *The Society for Astronomical Sciences 31st Annual Symposium on Telescope Science, held May 22-24, 2012 at Big Bear Lake, CA*, ed. B. D. Warner, R. K. Buchleim, J. L. Foote, and D. Mais, Society for Astronomical Sciences, Rancho Cucamonga, CA, 165.

Vander Haagen, G. A. 2013, *J. Amer. Assoc. Var. Star Obs.*, **41**, 114.

Vander Haagen, G. A., and Owings, L. E., 2014, in *The Society for Astronomical Sciences 33rd Annual Symposium on Telescope Science*, Society for Astronomical Sciences, Rancho Cucamonga, CA, 191.

Zalinian, V. P., and Tovmassian, H. M. 1987, *Inf. Bull. Var. Stars*, No. 2992, 1.

Zhilyaev, B. E., and Romanjuk, Ya. O. 1990, in *Flare Stars in Star Clusters, Associations, and the Solar Vicinity. Proceedings of the 137th. Symposium of the International Astronomical Union, held in Byurakan, U. S. S. R., October 23–27, 1989*, ed. L. V. Mirzoyan, B. R. Pettersen, M. K. Tsvetkov, Kluwer Academic, Dordrecht, 35.

Spurious One-Month and One-Year Periods in Visual Observations of Variable Stars

John R. Percy
Department of Astronomy and Astrophysics and Dunlap Institute for Astronomy and Astrophysics, University of Toronto, 50 St. George Street, Toronto, ON M5S 3H4, Canada; john.percy@utoronto.ca

Received November 9, 2015; revised December 1, 2015; accepted December 2, 2015

Abstract Visual observations of variable stars, when time-series analyzed with some algorithms such as DC-DFT in VSTAR, show spurious periods at or close to one synodic month (29.5306 days), and also at about a year, with an amplitude of typically a few hundredths of a magnitude. The one-year periods have been attributed to the Ceraski effect, which was believed to be a physiological effect of the visual observing process. This paper reports on time-series analysis, using DC-DFT in VSTAR, of visual observations (and in some cases, V observations) of a large number of stars in the AAVSO International Database, initially to investigate the one-month periods. The results suggest that both the one-month and one-year periods are actually due to aliasing of the stars' very low-frequency variations, though they do not rule out very low-amplitude signals (typically 0.01 to 0.02 magnitude) which may be due to a different process, such as a physiological one. Most or all of these aliasing effects may be avoided by using a different algorithm, which takes explicit account of the window function of the data, and/or by being fully aware of the possible presence of and aliasing by very low-frequency variations.

1. Introduction

In the course of time-series analyses of AAVSO visual observations of red giants (such as Percy and Long 2010) and T Tauri stars (such as Percy *et al.* 2010), we have found many stars with periods at or close to one year, and occasionally one synodic month (hereinafter "one month"—29.5306 days). We attributed the one-year periods to the Ceraski effect—a physiological effect which is described thus by Gunther and Schweitzer (undated): "when two stars of equal brightness are aligned so that the line-of-stars is perpendicular to the line-of-eyes, an observer may systematically see the 'upper' star brighter than the 'lower' one." Sharonov (1933) carried out an experimental study of the effect, and found that it can be as large as 0.3 magnitude in the most extreme cases.

How might such an effect occur? Here's a simple example. Suppose a northern observer was measuring Betelgeuse every night with the unaided eye, relative to Rigel as a comparison star. At the beginning of the observing season in August, he/she would be observing Orion as it rose, when Betelgeuse and Rigel are at approximately the same altitude, and the line-of-stars is parallel to the line-of-eyes (to use Gunther and Schweitzer's terminology), which we assume to be horizontal. There would be no Ceraski effect. At the end of the observing season, in April, he/she would be observing Orion as it set, when Betelgeuse is at a much higher altitude than Rigel. The line-of-stars is now perpendicular to the line-of-eyes. According to the Ceraski effect, Betelgeuse would be seen artificially brighter than Rigel. In fact, differential extinction might add to the effect. Since this would be a seasonal effect, it would have a one-year period.

I initially hypothesized that the one-month periods were caused by a variant of the Ceraski effect: depending on the position of the moon in the sky, during its monthly cycle, observers will tend to observe a variable in different parts of the sky, with a different orientation of the line-of-stars to the line-of-eyes. A post on the AAVSO Visual Observing forum, asking if this seemed reasonable, resulted in many views but no replies.

In the end, my initial hypothesis about the nature and cause of the one-month periods turned out to be almost certainly incorrect. My efforts also led me to a reconsideration of the nature and cause of the one-year periods, and the Ceraski effect. The pathway to my conclusion was not a direct, linear one; I am "telling it as it was," for the benefit of other users of visual data, and of VSTAR and similar time-series analysis packages.

2. Data and analysis

I used visual observations from the AAVSO International Database (AID; Kafka 2015) of the selected groups of stars described below and the DC-DFT routine in the AAVSO software package VSTAR (Benn 2013). DC-DFT, or date-compensated discrete Fourier transform (Ferraz-Mello 1981) is a common implementation of Fourier analysis, a topic that is discussed in detail in Templeton (2004), a reference which is freely available on the AAVSO website. I occasionally used Johnson V observations from the AID, to compare the results with those from visual observations—for instance, to determine whether "spurious" peaks were solely in the visual data, and therefore possibly due to the visual observing process. I generally scanned periods at a resolution of 0.01 or 0.001 day.

3. Results and discussion

3.1. The incidence of one-month signals

To study the incidence of one-month periods, I initially used visual observations of a sample (Table 1) of 50 carbon and oxygen red giants which Percy and Huang (2015) had been analyzing for other purposes. To avoid confusion, I used only those stars which had pulsation amplitudes less than 0.20

Table 1. One-month periods and their amplitudes in Red Giants.

Star	*P (d)*	Δ*v (mag.)*	*Star*	*P (d)*	Δ*v (mag.)*
RY Cam	29.574	0.025	V UMi	none	≤ 0.008
RY Cnc	29.489	0.037	VY And	29.109	0.059
AA Cas	none	≤ 0.015	AQ And	29.530	0.024
SS Cep	29.502	0.013	V Aql	29.550	0.019
DM Cep	29.490	0.032	U Cam	29.834	0.030
TZ Cyg	29.516	0.015	ST Cam	29.530	0.020
CT Del	29.494	0.042	X Cnc	29.530	0.021
CZ Del	29.483	0.025	Y CVn	29.533	0.018
EU Del	29.527	0.010	WZ Cas	29.473	0.013
S Dra	29.605	0.046	RV Cyg	29.548	0.081
TX Dra	none	≤ 0.010	SV Cyg	29.583	0.043
Y Gem	29.613	0.033	TT Cyg	29.541	0.019
SW Gem	29.548	0.030	AW Cyg	29.481	0.030
X Her	29.519	0.017	V460 Cyg	29.526	0.037
ST Her	29.497	0.034	RY Dra	29.523	0.019
UW Her	none	≤ 0.010	UX Dra	29.526	0.025
g Her	29.525	0.012	U Hya	29.533	0.022
RX Lep	29.526	0.017	Y Hya	29.511	0.033
SV Lyn	29.594	0.026	T Lyr	29.530	0.039
SZ Lyr	29.809	0.033	W Ori	29.536	0.030
SW Mon	none	≤ 0.035	RX Peg	29.552	0.058
V UMa	29.638	≤ 0.020	TX Psc	29.503	≤ 0.015
RY UMa	29.619	0.016	S Sct	29.524	0.026
RZ UMa	29.552	0.041	Y Tau	29.531	0.046
ST UMa	29.574	0.011	VY UMa	29.510	0.009

magnitude (an arbitrary number); most had pulsation amplitudes less than 0.10 magnitude.

In 40 out of 50 stars, there was a peak at or close to a period of one month, or a frequency of 0.03386 cycle/day (c/d). In the other 10 stars, any one-month period was at the noise level, so only an upper limit could be specified. The stars in Table 1 from RY Cam to V UMi are normal M-type giants; those from VY And to VY UMa are carbon stars.

3.2. In search of the cause—alias periods?

In a further effort to understand the nature of the one-month periods, I analyzed visual data on other samples of stars in the AID. R CrB stars had substantial one-month signal amplitudes, here given in magnitudes: U Ant (0.070), S Aps (0.040), U Aqr (0.091), UV Cas (0.011), UW Cen (0.123), DY Cen (0.033), R CrB (0.075), V Cra (0.080), WX Cra (0.053), Y Mus (≤ 0.010), RT Nor (0.037). However, when I analyzed a long stretch of observations of R CrB when it was constant at maximum, the amplitude of the one-month signal was much smaller.

It was at this point that I began to wonder if the one-month signal was a one-month *alias* of very low-frequency (VLF) variability, on a time scale of thousands to tens of thousands of days. One-*year* aliases are well-known. They occur because of the one-year temporal periodicity in the times of observation, that is, the window function of the data. There are times of year when it is difficult or impossible to observe the star, so there are seasonal gaps in the data. The alias frequencies differ from the true frequency by ± N / 365.25 c/d where the strongest alias is normally N = 1. The seasonal gaps are usually quite visible in the light curve, as seen in VSTAR or in the AAVSO Light Curve Generator.

One-*month* aliases might occur for the same reason as one-*year* aliases: there are times of the month when the star might be difficult to observe, due to moonlight, and therefore less likely to be observed, especially if the star is near the ecliptic. These gaps are less obvious in the light curve, but are definitely there. As a check, I looked at the observations of Antares, near the ecliptic. During the 0.15 of the month when the moon was near Antares, only 0.04 of the observations were made.

Indeed, the one-*year* signals might also be alias periods, caused by VLF variations, rather than due to the Ceraski (physiological) effect. We discuss this possibility below.

3.3. Alias periods and the window function

In retrospect: if I had thought about VLF variability in red giants, and/or had been using a different Fourier-analysis routine, I would have been aware of the possibility of one-month and one-year aliases as being part of the *window function* of the dataset (for example, Templeton 2004; Lenz and Breger 2005). The window function, for discretely-sampled data, describes the inherent periodicities in the times of observation, and shows how a true signal at a frequency f "leaks" into other frequencies—the alias frequencies. The window function is centered at f = 0. Often, it is used by being applied to the strongest peak in a Fourier spectrum to determine which weaker peaks are likely to be aliases of it, especially in the case of short-period variables in which there are strong one-*day* aliases. In the present case, we are dealing with an aliased signal with a frequency f which is very close to but not equal to zero. This, in an ideal case, would result in a *pair* of alias periods, separated by 2f. Non-periodic VLF variability would produce more complex aliasing structure (such as in Figure 1).

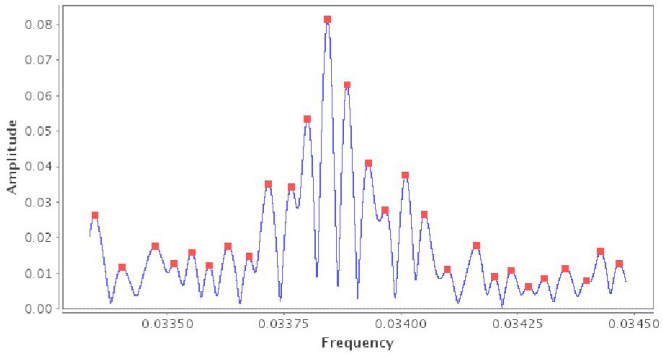

Figure 1. The DC-DFT power spectrum (amplitude in magnitudes versus frequency in c/d) of the pulsating red giant RV Cyg, which shows very slow variations, with a nominal frequency of 0.000027 c/d and an amplitude of 0.36 mag. The spectrum shows a pattern of alias periods around one month, and separated by a frequency of about 0.000027 c/d. The blue curve is the spectrum; the red points are the peaks or "top hits."

The present project began with AAVSO data and specific software (VSTAR) which can be and is used by amateur or professional astronomers or students, and this paper is particularly addressed to these users. VSTAR does not explicitly calculate the window function of the data being analyzed, though the equivalent can be done approximately (as long as VLF variability is present) by calculating the Fourier spectrum from f = 0.00 to f = 0.04 c/d (Figure 2). Also, this project began with a study of what turned out to be the alias periods, rather than with a study of the true VLF peaks, which were not obvious

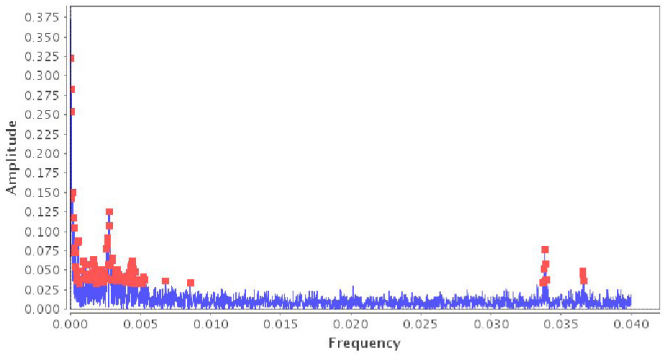

Figure 2. The DC-DFT power spectrum (amplitude in magnitudes versus frequency in c/d) of the pulsating red giant RV Cyg, from f = 0.00 to f = 0.04 c/d. The pattern is approximately equivalent to the window function of the star. See text for further discussion.

to me when I began. In this sense, this project was carried out "in reverse."

3.4. Other results

In the course of arriving at the eventual (probably) correct conclusion about the one-month periods, I carried out several sets of analyses which, in the end, are not directly relevant, but are listed here.

• Stars with long, strong, coherent periods such as S Per (807 days) and VX Sgr (756 days) and AH Sco (738 days) show conspicuous two-peak alias signals at the expected (almost) one-month periods.

• Stars with strong but non-periodic VLF variations, such as R CrB stars, show a more complex aliasing pattern around one month.

• At high resolution, a typical red giant such as RV Cyg shows a complex aliasing pattern around one month (Figure 2).

• Stars near the ecliptic (such as R Cnc, S Vir, T Sgr, and R Gem) show a stronger aliasing amplitude, relative to the amplitude of the aliased signal, than stars further away from the ecliptic (such as R Dra, S UMa, R UMa, and T Cam).

• Stars which are not expected to have VLF variability (such as δ Cep and η Gem) show little or no signal around one month.

• The aliasing effect does not depend, significantly, on the brightness of the star, all other factors being the same.

• Constant stars should not show alias periods around one month. Four stars which were classified as constant in the AAVSO's old Validation File were studied (CI Ori, Z Gem, S Cha, RY Peg); they actually showed VLF signals, and aliases around one month. Compared with the stars in Table 1, RY Peg was an unusual case: the VLF amplitude was 0.29 magnitude and the amplitude of the one-month alias was 0.17 magnitude, which was much larger than usual, relative to the VLF amplitude. I am not sure why.

• Returning to the 50 stars in Table 1, I found that all of these stars showed VLF signals, almost always non-periodic. The aliasing patterns were complex (such as in Figure 1). Whether the VLF variations are real, or due to small changes in the assumed magnitudes of the comparison stars over time, is not clear.

3.5. Is the one-year Ceraski effect due to aliasing?

I re-analyzed the stars which Percy and Long (2010) identified as having a period at or near one year: SV Aur, RT Car, IZ Cas, AD Cen, DM Cep, XY Lyr, T Cyg, SV Cyg, V449 Cyg, CT Del, and WY Gem. In each case, the standard DC-DFT scan showed a peak (or pseudo-peak) at a very low frequency—0.000100 c/d or less. The amplitude of this peak was typically 5 to 10 times that of the peak which was at or near one year. It thus appears probable that the Ceraski effect is not primarily due to a physiological effect, but is partly or wholly due to one-year aliasing of VLF variability of the star. Investigators still need to be aware of these spurious one-year periods, whatever their cause. As Percy and Huang (2015) have shown, they can lead to incorrect conclusions about multiperiodicity in stars, and about the period distribution in the stars under study.

3.6. Final comments

As a test of the hypothesis that the one-month and one-year periods were due to aliasing of VLF variability of the stars, Dr. Matthew Templeton (AAVSO Science Director) kindly analyzed the VX Sgr data using two different methods: DC-DFT as in VSTAR, and a program using the Roberts *et al.* (1987) CLEAN algorithm. The latter takes explicit account of the window function of the data, and is therefore not subject to aliasing. The one-month periods are not present in the latter spectrum, and the one-year periods—if they exist—are close to the noise level. This one example supports the hypothesis that the peaks occur because the DC-DFT program does not take account of the temporal sampling of the data, which can result in aliasing. CLEANest (Foster 1995), an implementation of CLEAN, is available at https://www.aavso.org/software-directory .

I began the study of periods near one month because I thought that they might be analogous to the periods near one year which were thought to be due to a physiological effect of the visual observing process—the Ceraski effect. It now appears that *both* may be primarily or wholly due to aliasing of the star's VLF variability.

If the star has a more moderate period—tens or hundreds of days, for instance—it may still show one-month aliases, whose frequencies are separated from the true frequency by ± N / 29.5306 c/d where N is usually 1. These aliases will not be close to one month but, like one-cycle-per-year aliases, can be confused with true periods. Figure 3 shows the power spectrum of S Aql, with a period of 146 days. There is a complex system of one-month and one-year aliases.

4. Conclusions

Visual observations have been known, for a century, to contain signals at or close to one year. This so-called Ceraski effect was believed to be due to a physiological effect of the visual observing process. AAVSO visual and V data may also contain a signal at a period at or near one month (29.5306 days). Initially, I thought that the one-month signals were also due to a physiological Ceraski effect, but this study suggests that, in most cases, they are primarily or wholly due to one-cycle-per-

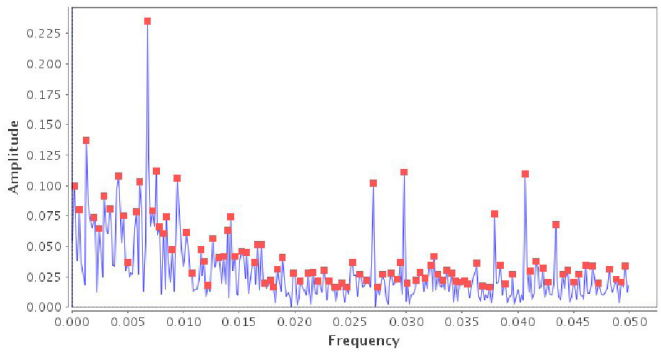

Figure 3. The power spectrum (amplitude in magnitudes versus frequency in c/d) for S Aql, which has a period of 146 days, or a frequency of 0.006849 c/d. There are one-month aliases around 0.027-0.030 and 0.038-0.043 c/d, each with one-year alias peaks.

month aliasing of VLF variability of the star. The amplitudes of the alias peaks are lower, by a factor of 5 to 10, than that of the VLF variability. This study also suggests that, in many or most cases, the one-*year* signals are not due to a physiological effect, but are due to one-cycle-per-year aliasing of VLF variability of the star. A very small (less than 0.02 magnitude) one-month or one-year physiological effect is not ruled out. In any case, these alias or spurious signals must not be confused with true periods in the star. The main goal of this paper is to stress this fact to other users of visual data, especially if using VSTAR.

5. Acknowledgements

I thank the AAVSO observers who made the observations on which this project is based, the AAVSO staff who archived them and made them publicly available, and the developers of the VSTAR package which was used for analysis. I am especially grateful to Dr. Matthew Templeton, at AAVSO HQ, for carrying out the analysis described in section 3.6. This project made use of the SIMBAD database, maintained in Strasbourg, France.

References

Benn, D. 2013, VSTAR data analysis software (https://www.aavso.org/vstar-overview)

Ferraz-Mello, S. 1981, *Astron. J.*, **86**, 619.

Foster, G. 1995, *Astron. J.*, **109**, 1889.

Gunther, J., and Schweitzer, E. undated, (http://cdsarc.u-strasbg.fr/afoev/var/edeb.htx) accessed June 25, 2015.

Kafka, S. 2015, observations from the AAVSO International Database (https://www.aavso.org/aavso-international-database).

Lenz, P., and Breger, M. 2005, *Commun. Asteroseismology*, **146**, 53.

Percy, J. R., Esteves, S., Glasheen, J., Lin, A., Long, J., Mashintsova, M., Terziev, E., and Wu, S. 2010, *J. Amer. Assoc. Var. Star Obs.*, **38**, 151.

Percy, J. R., and Huang, J. D. 2015, *J. Amer. Assoc. Var. Star Obs.*, **43**, in press.

Percy, J. R., and Long, J. 2010, *J. Amer. Assoc. Var. Star Obs.*, **38**, 161.

Roberts, D. H., Lehar, J., and Dreher, J. W. 1987, *Astron. J.*, **93**, 968.

Sharonov, V. V., 1933, *Bull. Tashkent Obs.*, **1**, 4 (This paper is in Russian, with an English summary).

Templeton, M. 2004, *J. Amer. Assoc. Var. Star Obs.*, **32**, 41.

Changing Periods of ST Puppis

Stan Walker
272 Heath Road, Waiharara, Far North 0486, New Zealand; astroman@paradise.net.nz

Neil Butterworth
24 Payne St., Mt. Louisa, Queensland 4814, Australia

Andrew Pearce
35 Viewway, Nedlands WA 6009, Australia

Received November 9, 2015; revised December 7, 2015; accepted December 7, 2015

Abstract ST Puppis is a reasonably bright W Virginis variable star, a Type 2 Cepheid with a record of substantial and erratic period changes—21 during the interval 1900 to 1985 with a range of magnitude from 17.4 to 19.2 days. It was observed as part of Variable Stars South's Cepheid project by Butterworth in 2014 and 2015 using DSLR photometry in BGR passbands and visually by Pearce in 2015. The known period changes are shown graphically and doubtful ones examined and discarded if necessary. With its period and amplitude with a frequently changing period it is a suitable and worthwhile object for visual observing.

1. Introduction

Variable Stars South has a project involving measures of bright southern Cepheids. Details of this may be found at http://www.variablestarssouth.org/BrightCepheidsVisual and http://www.variablestarssouth.org/BrightCepheidsDSLR. It involves fitting of seasonal measures of selected Cepheids to mean light curves to determine annual epochs. At intervals of 5 or 10 years more comprehensive measures will continue to be made to look for shape or color changes in the light curve.

Mean light curves are prepared from high quality data, in the case of ST Pup from Kilkenny *et al.* (1993), and good epochs can be obtained by fitting 15 to 20 DSLR measures in V, or 25 to 35 visual measures made using a very precise comparison sequence.

Our project has mainly been restricted to classical Cepheids but Butterworth decided to measure ST Pup in 2014 as a test of the limits of his system—a Canon 550D DSLR camera using a 135mm f2.0 lens on a Sky-Watcher altazimuth mount producing fully transformed BVR measures.

2. Historical background

Most of these bright Cepheids have a lengthy baseline of measures which is largely part of the reason for observing current behavior. ST Pup, which is a W Virginis star, is no exception and the GCVS (Kholopov *et al.* 1985) lists 21 different periods in the interval ranging back to 1900. The original fit of the DSLR measures was disappointing, but not unexpected given the erratic period and perhaps light curve variations of this Cepheid subtype. Summer of 2015 in Queensland was particularly cloudy and a visual observer, Pearce, was called in to gather enough data to determine a current epoch and period.

We began by collecting as many published measures as we could. UBV measures date from about the year 1954 but many observers made only a few, perhaps 5 to 20 measures in a season, and epochs of maxima are difficult to determine. The main sources were Irwin (1961), Mitchell *et al.* (1964), Eggen (1986), ASAS3 (Pojmański 2002), and Berdnikov (2008). From all of these we produced the O–C diagram of Figure 1.

The cycle numbers are rather uncertain and in many cases were determined from visual measures in the AAVSO

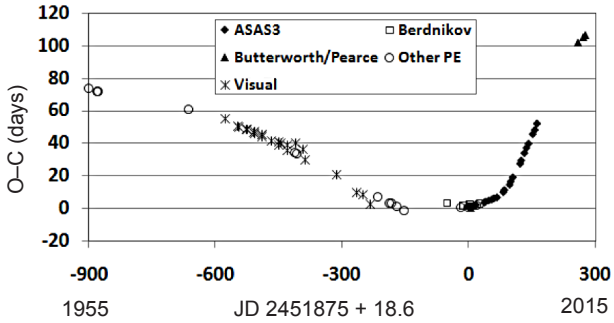

Figure 1. The O–C diagram of ST Puppis since 1955. The vertical scale shows days late (+) or early (–) as compared to the given ephemeris. This clearly shows major changes in period but the uncertainty of the cycle count makes it probably inaccurate for the first 300 cycles. The value of the visual measures from the AAVSO International Database is quite clear, although the accuracy of those epochs is probably ± 2 days at best.

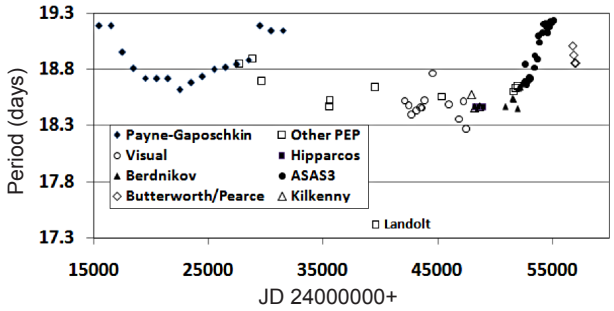

Figure 2. ST Pup periodogram showing the period variations in a more informative manner. The uncertainty of cycle counts is overcome but many photoelectric measures could not be used as they were too few to determine reliable periods. Landolt's measure is separately identified.

International Database (AID; Kafka 2015) using a process of inspection for maxima. Prior to 1955 there are not enough available data. Because of these factors we then produced the periodogram of Figure 2, a better way of tracing and displaying the large period variations of this star.

Periods have been determined by taking two successive epochs of maximum and dividing by the apparent number of cycles between the two. In the case of the periods determined by Payne-Gaposchkin (1950), her values have been accepted and the JD located at the center of each interval. In all cases MJD has been used based on JD –2400000.

This shows some interesting aspects. Three times the period appears to have peaked at ~19.2 days, although that of JD 2430000–2432000 conflicts with other measures. As well, there is a single period derived by Landolt (1971) which does not fit well. We examined these points in detail.

Landolt (1971) discussed the derivation of this period and epoch. It is based upon 21 measures covering 1.3 cycles. Marino (1971), in a discussion of RS Col, compared all-sky measures by Bond and Landolt (1969) to the light curve obtained at Auckland Observatory and estimated their errors at ±0.02 to 0.04 in V. If these uncertainties are similar for ST Pup, the data are far too inaccurate to use the method adopted by Landolt in arriving at his period. In Figure 3 we show that a period of 18.5 days produces a more likely looking light curve for this star. Whilst some data points of the two different cycles coincide better with the shorter period the initial decline is pinched in and abnormal. This period has not been included in Figure 4 as we believe that there are insufficient measures to determine an accurate value.

The other ill-fitting data points were determined by Payne-Gaposhkin (1950) by fitting cycles to 1,000-day intervals. Her data were not published, but presumably they were sparse and photographic in nature. By adding one cycle in each of the last three of the intervals a better fit is obtained. We have no proof that this correction is valid and since this is merely an assumption both sets are included in Figure 4.

This amended periodogram shows an abrupt decline from the originally observed period of ~19.2 days with a slow and erratic decline to ~18.46 days. The visual determinations in this context are low weight. Beginning about 1999 the period began to lengthen quite sharply, reaching a probable peak around 2011 before the present reversal to a shorter period began (Figure 5).

3. Other physical aspects

Gonzalez and Wallerstein (1996) examined ST Pup in detail spectroscopically and concluded that it was a binary system with a period of 410.4±2.9 days. It has some spectral peculiarities. The orbital eccentricity is low, which appears to rule out any possibility of interaction causing the dramatic period changes. But Kiss *et al.* (2007), looking for possible reasons for the very erratic period, suggested a period of 18.4298 days was likely during the period of the Gonzalez and Wallerstein (1996) measures. Kiss *et al.* proposed an orbital period of 25.67 days and some probable interaction. The suggested pulsation period seems strongly based on the Landolt period but periods shown

Table 1. Table of orbital periods of ST Pup during the interval JD 2447362–2449741 obtained by dividing intervals by number of epochs.

Epoch (start-end) JD 2400000+	*Source*	*Orbital Period (d)*
47846–48363	Perryman *et al.* (1997)	18.46107
48456–48696	Perryman *et al.* (1997)	18.46098
48696–49028	Perryman *et al.* (1997)	18.46102
47939–48252	Kilkenny *et al.* (1993)	18.45724
48252–48640	Kilkenny *et al.* (1993)	18.46704
48640–50911	Kilkenny *et al.* (1993) / Berdnikov (2008)	18.46497

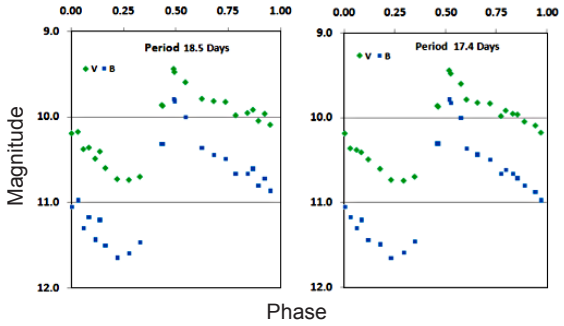

Figure 3. Two treatments of the measures of ST Pup by Landolt (1971). On the right the data are phased using his period of 17.4 days, on the left the same data with a period of 18.5 days, which seems more likely in view of other measures near that time. The left curve looks similar to other measures of this star; that on the right shows a very pinched maximum and a strange step in the early stages of the decline. The decline in other observers' data does have a shoulder but it does not appear like the right-hand graph.

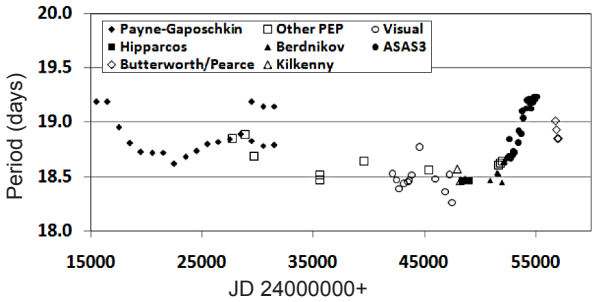

Figure 4. Same data as Figure 2 but with the Landolt epoch omitted and two alternative positions for Payne-Gaposchkin's (1950) last three intervals.

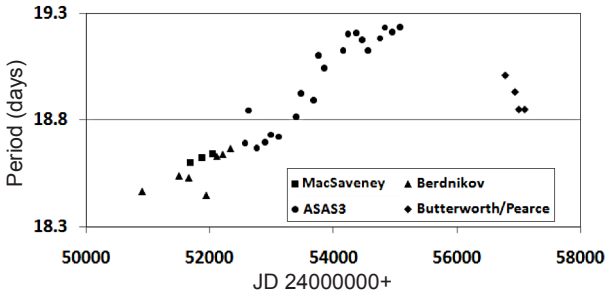

Figure 5. ST Pup period changes since 1999. We hope to add further points over the next year or two.

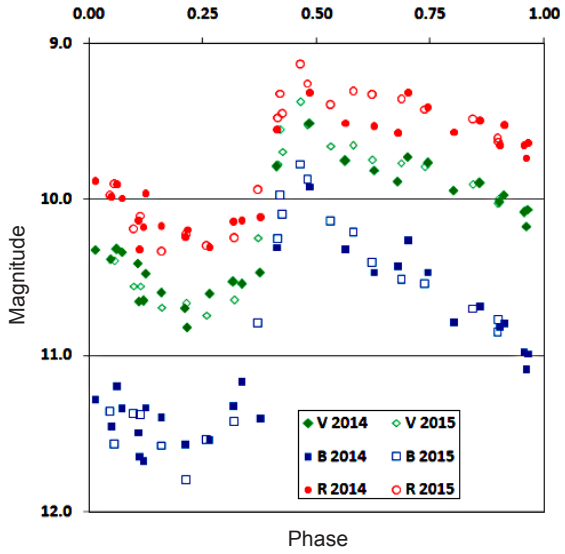

Figure 6. Butterworth DSLR measures of ST Pup for the 2014 and 2015 seasons. Solid points are 2014, open points 2015. This star is rather too faint for the camera set-up described and cycle 7 further complicated by the period change between the two seasons. The phases shown are from two arbitrary epochs offset by ~0.5 cycle.

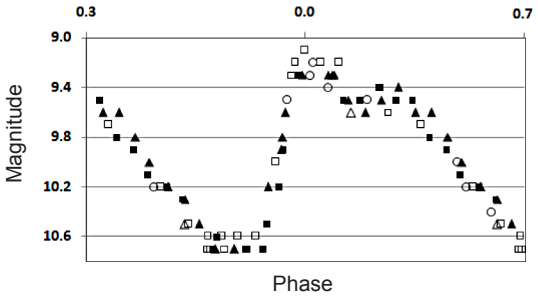

Figure 7. Pearce visual measures of ST Pup over 6 cycles during the 2015 season. The data illustrate that with a large amplitude Cepheid visual measures are quite capable of determining a seasonal epoch. We are now providing visual comparison stars with two decimal accuracy and average sequence steps of 0.2 magnitude.

in Table 1 appear to preclude such an interpolation.

ST Pup is noted by Welch (2012) as one of five known Type 2 Cepheid binaries in the Milky Way Galaxy. It has by far the longest pulsation period of these binary stars and the Gonzalez and Wallerstein orbital period (1996) is also much greater than the others. Eggen (1986) had earlier drawn attention to this star as an important "anomalous" Cepheid. There are, of course, longer period Type 2 Cepheids not in binary systems and our range of targets will be extended to include these.

4. Ongoing measures

In Figures 6 and 7 we present measures made in 2014 and 2015. During this interval the period was changing quite quickly. The two seasons of measures by Butterworth are fitted by a period of 18.905, while the measures in 2015 by Pearce show a best fit of 18.85 days. The measures are listed in Tables 2 and 3.

Table 2. DSLR measures of ST Pup made by Neil Butterworth transformed into V, B–V, V–R, with error values.

HJD 2400000+	*V*	*B–V*	*V–R*	*V Error*	*B–V Error*	*V–R Error*
56663.93741	9.752	0.568	0.242	0.052	0.049	0.031
56702.91874	9.815	0.652	0.285	0.055	0.045	0.035
56703.91879	9.888	0.538	0.315	0.052	0.032	0.048
56710.90736	10.380	1.073	0.400	0.048	0.045	0.041
56730.92974	10.412	1.080	0.280	0.064	0.073	0.067
56731.89251	10.594	0.800	0.425	0.055	0.050	0.046
56732.89412	10.695	0.874	0.456	0.058	0.066	0.041
56733.89003	10.604	0.937	0.302	0.052	0.038	0.047
56734.90317	10.528	0.796	0.388	0.060	0.047	0.043
56749.89053	10.656	0.993	0.339	0.048	0.052	0.057
56751.88007	10.821	1.226	0.627	0.056	0.055	0.049
56754.90878	10.467	0.935	0.355	0.053	0.041	0.048
56761.87745	9.767	0.700	0.359	0.047	0.041	0.044
56764.87466	10.019	0.794	0.368	0.051	0.043	0.038
56765.87718	10.083	0.892	0.431	0.054	0.044	0.037
56767.87732	10.321	0.872	0.419	0.046	0.038	0.032
56775.88248	9.514	0.406	0.202	0.046	0.040	0.059
56781.86953	9.943	0.843	0.374	0.051	0.059	0.030
56784.86954	10.171	0.915	0.438	0.054	0.058	0.038
56785.86669	10.322	0.959	0.443	0.052	0.049	0.055
56787.86479	10.650	1.027	0.477	0.057	0.083	0.049
56798.86831	9.728	0.531	0.412	0.053	0.049	0.059
56801.85731	9.896	0.787	0.401	0.055	0.053	0.031
56802.86197	9.971	0.822	0.450	0.049	0.049	0.037
56803.86318	10.063	0.928	0.424	0.050	0.043	0.023
56805.88077	10.336	1.001	0.343	0.057	0.049	0.048
56806.86364	10.472	0.863	0.513	0.053	0.056	0.035
56810.86080	10.543	0.624	0.410	0.051	0.050	0.052
57095.89551	9.789	0.518	0.239	0.034	0.049	0.014
57096.89665	9.374	0.398	0.234	0.037	0.037	0.015
57099.89717	9.747	0.660	0.414	0.038	0.035	0.015
57107.89168	10.385	0.980	0.409	0.037	0.034	0.017
57108.89140	10.555	0.824	0.360	0.039	0.043	0.024
57111.89848	10.743	0.802	0.441	0.036	0.028	0.022
57114.88384	9.774	0.482	0.290	0.039	0.038	0.024
57133.86952	9.555	0.421	0.233	0.037	0.027	0.017
57136.87180	9.654	0.559	0.346	0.036	0.033	0.020
57138.87561	9.767	0.747	0.405	0.037	0.035	0.022
57139.86880	9.790	0.757	0.369	0.035	0.024	0.025
57141.86835	9.906	0.794	0.417	0.035	0.026	0.030
57142.87511	10.028	0.824	0.418	0.036	0.038	0.028
57145.88177	10.395	1.176	0.491	0.038	0.030	0.025
57147.86441	10.692	0.884	0.356	0.037	0.028	0.020
57148.86540	10.669	1.133	0.439	0.039	0.038	0.020
57150.86718	10.646	0.781	0.397	0.038	0.027	0.024
57151.86392	10.247	0.547	0.304	0.038	0.017	0.017
57152.87494	9.694	0.405	0.238	0.037	0.024	0.017
57153.87241	9.524	0.352	0.267	0.036	0.028	0.024
57154.87649	9.659	0.484	0.264	0.042	0.034	0.019
57161.86713	9.997	0.778	0.367	0.044	0.020	0.016
57165.85940	10.556	0.831	0.452	0.038	0.033	0.019

5. Conclusions

While ST Pup is an interesting star, the period changes show no predictability, and our future observing will be along the lines discussed in the introduction. It is probably too faint for DSLR photometry except through a telescope, but would reward a season's observing at intervals by CCD BVRI photometry. Quite clearly, competent visual observers in the bright Cepheid project are capable of producing good seasonal light curves and epochs of maximum.

Table 3. Visual measures of ST Pup made by Andrew Pearce.

JD	*Magnitude*	*JD*	*Magnitude*
2456976.2694	10.4	2457030.23889	9.8
2456985.2778	9.4	2457031.0938	10.0
2456993.1097	10.0	2457032.2271	10.2
2456999.0986	10.7	2457033.2201	10.3
2457000.0903	10.6	2457034.0924	10.5
2457001.0896	10.2	2457035.0840	10.7
2457002.05000	9.4	2457036.2319	10.7
2457003.0549	9.3	2457038.2500	10.2
2457003.2389	9.2	2457039.0319	9.9
2457005.0632	9.5	2457039.1201	9.8
2457006.0569	9.5	2457039.2917	9.6
2457007.2278	9.4	2457040.2896	9.3
2457007.2611	9.4	2457042.2271	9.3
2457008.2271	9.5	2457043.2424	9.6
2457009.2319	9.5	2457052.0535	10.5
2457010.2563	9.8	2457063.0674	9.5
2457011.2833	9.9	2457069.0632	10.2
2457012.1146	10.1	2457077.0611	9.5
2457013.2458	10.2	2457090.0222	10.5
2457014.2396	10.3	2457091.0792	10.7
2457016.0389	10.7	2457092.0194	10.6
2457016.2660	10.6	2457092.98333	10.6
2457018.0229	10.7	2457094.07639	10.6
2457018.0819	10.7	2457097.02569	9.1
2457019.0507	10.7	2457097.99236	9.2
2457019.2896	10.5	2457099.03264	9.2
2457020.0285	10.2	2457101.9986	9.6
2457020.2986	9.9	2457104.0278	9.7
2457021.2465	9.3	2457109.9806	10.6
2457023.0403	9.3	2457111.0264	10.7
2457023.2660	9.3	2457126.0264	10.2
2457024.2257	9.5	2457128.9667	10.7
2457025.2444	9.6	2457132.9861	10.0
2457026.2243	9.5	2457133.9542	9.3
2457027.26250	9.4	2457134.0819	9.2
2457028.27639	9.6	2457134.9444	9.2
2457029.24931	9.6	2457135.0813	9.2

A strong reason for measuring Cepheids and following period changes is the frequency with which they occur. The classical pulsating targets for visual observers are the large amplitude Mira stars but a perusal of the results suggests that true period changes—such as with R Hya, R Aql, and the dual maxima stars BH Cru and R Cen—occur at a rate of approximately 1% of the target stars per century. Period changes in the longer period Cepheids, >10 days, occur perhaps 10 times more frequently and have amplitudes suited to capable visual observers.

6. Acknowledgements

Several members of the AAVSO contributed visual measures for the old AAVSO Cepheid section, including, Tom Cragg, C. Patrick Mahnkey, Robert B. Ariail, and Paul Goodwin. Their measures filled in a large time gap effectively. The International Database operated by the AAVSO was invaluable there. Our thanks also to Orlon Petterson who searched out MacSaveney's doctoral thesis (2003) and measures. One of us, Walker, also wishes to remember the late Tom Cragg who, in 1984, persuaded a group at Auckland to make UBV measures of these stars but not, unfortunately, ST Pup.

References

Berdnikov, L. N. 2008, VizieR Online Data Catalog: Photoelectric observations of Cepheids in UBV(RI)c (http://vizier.cfa.harvard.edu/viz-bin/VizieR?-source=II/285).

Bond, H. E., and Landolt, A. U. 1969, *Publ. Astron. Soc. Pacific*, **81**, 696.

Eggen, O. J. 1986, *Astron. J.*, **91**, 890.

Gonzalez, G., and Wallerstein, G. 1996, *Mon. Not. Roy. Astron. Soc.*, **280**, 515.

Irwin, J. B. 1961, *Astrophys. J., Suppl. Ser.*, **6**, 253.

Kafka, S. 2015, observations from the AAVSO International Database (https://www.aavso.org/aavso-international-database).

Kholopov, P. N., *et al.* 1985, *General Catalogue of Variable Stars*, 4th ed, Moscow.

Kilkenny, D., van Wyk, F., Marang, F., Roberts, G. D., Laing, J. D., Winkler, H., and Westerhuys, J. E. 1993, *S. Afr. Astron. Obs. Circ.*, **15**, 85.

Kiss, L. L., Derekas, A., Bedding, T. R., and Szabados, L. 2007, *Mon. Not. Roy. Astron. Soc.*, **375**, 1338.

Landolt, A. U. 1971, *Publ. Astron. Soc. Pacific*, **83**, 43.

MacSaveney, J. A. 2003, Ph.D. thesis, University of Canterbury, New Zealand.

Marino, B. F. 1971, *South. Stars*, **24**, 47.

Mitchell, R. I., Iriarte, B., Steinmetz, D., and Johnson, H. L. 1964, *Bol. Obs. Tonantzintla y Tacubaya*, **3**, 153.

Payne-Gaposchkin, C. 1950, *Ann. Harvard Coll. Obs.*, **115**, 205.

Perryman, M. A. C., European Space Agency Space Science Department, and the Hipparcos Science Team. 1997, The Hipparcos and Tycho Catalogues, ESA SP-1200 (VizieR On-line Data Catalog: I/239), ESA Publications Division, Noordwijk, The Netherlands.

Pojmański, G. 2002, *Acta Astron.*, **52**, 397.

Welch, D. L. 2012, *J. Amer. Assoc. Var. Star Obs.*, 40, 492.

A Photometric Study of the Eclipsing Binary Star BN Ari

Edward J. Michaels
Stephen F. Austin State University, Department of Physics and Astronomy, P.O. Box 13044, Nacogdoches, TX 75962; emichaels@sfasu.edu

Received November 3, 2015; revised November 19, 2015; accepted December 8, 2015

Abstract Presented are a set of multi-band light curves, synthetic light curve solutions, and period study for the eclipsing binary star BN Ari. The orbital period was found to be decreasing the past 8 years (~8,200 orbits). The observed light curves were analyzed with the Wilson-Devinney program. The resulting synthetic light curve solution showed the system to be a contact eclipsing binary with total eclipses.

1. Introduction

The variability of BN Ari (GSC 1761-1934, TYC 1761-1934-1) was discovered by Otero *et al.* (2004) in the public data release from the Northern Sky Variability Survey (NSVS) (Wozniak 2004) and in the All-Sky Automated Survey (ASAS) data by Pojmański *et al.* (2005). Otero classified the star as an EW/KW type eclipsing binary system and Pojmański as a contact binary (EC) with a period of P = 0.299377 day. Pojmański gives a V-band magnitude of 10.36 for BN Ari with the amplitude of variation as 0.73. Times of minimum light have been reported by a number of observers and will be discussed in the period analysis section of this paper. In this paper a photometric study of BN Ari is presented. It is organized into sections with the observations and data reduction techniques presented in section 2 and new times of minima and a period study presented in section 3. Light curve analysis using BINARY MAKER 3.0 (BM3) (Bradstreet and Steelman 2002) and the Wilson-Devinney model (WD) (Wilson and Devinney 1971; Wilson 1990, 1994; Van Hamme and Wilson 1998) is presented in section 4. Discussion and conclusions are presented in section 5.

2. Observations

BN Ari was observed in the Johnson B and V and Sloan g', r', and i' filter bands using the 0.31-m Ritchey-Chrétien robotic telescope at the Waffelow Creek Observatory (http://obs.ejmj.net/index.php). Images were acquired with an SBIG-STXL camera with a KAF-6303E CCD (9µm pixels) using 2 × 2 on-chip binning to provide faster readout times and proper sampling. Images were taken in 2014 on October 15, 17, 18, 20, 21, 23, 25, 26, 29, 30, and 31 in 5 passbands: 771 images in B, 1128 in V, 1363 in g', 1,076 in r', and 1,156 in i'. These dates comprise the first data set (DS1) and were analyzed using synthetic light curve modeling in section 4. Additional images were acquired in 2014 on November 8, 9, 18, 19, 23, 25, 26, 27, and more recently in 2015 on September 4, 12, 16. These observations comprise a second data set (DS2) in which only one passband was observed each night to improve cadence. The observations of DS2 were used to determine new times of minima. The total number of observations in both data sets included 1,563 in B, 1,986 in V, 2,858 in g', 2,767 in r', and 1,845 in i'. All images were dark current subtracted using exposures that were equal to the light frame exposures for each filter and flat field corrected. The software package MIRA (Mirametrics 2015) was used for calibration and differential aperture photometry.

The standard magnitudes of the comparison (C*) and check (K*) stars were taken from the AAVSO Photometric All-Sky Survey (APASS; Henden *et al.* 2014) data and are listed in Table 1. Figure 1 shows a finder chart for the stars in this study. The measured instrumental magnitudes for BN Ari (V*) were converted to standard magnitudes using the calibrated magnitudes of the C*. The epoch and orbital period used for all phase (Φ) calculations are 2456989.83596 and 0.29937151 day. All light curve figures are plotted from phase –0.6 to 0.6. A negative orbital phase is defined as Φ – 1. The folded light curves in standard magnitudes for each passband are shown in Figure 2. Also shown in Figure 2 is the V standard magnitude of the K* (bottom panel). The average observed K* magnitudes and errors, over all nights, are listed

Table 1. Variable (V*), comparison (C*), and check (K*) stars in this study.

Star	*R.A. (2000)* *h m s*	*Dec (2000)* ° ′ ″	*B*	*V*	*g′*	*r′*	*i′*	*(B–V)*
BN Ari (V*)	02 09 07.8	+26 29 06.0	11.35	10.54				0.81
[1]GSC1761-2281 (C*)	02 09 28.6	+26 22 32.2	12.062 ± 0.035	11.443 ± 0.055	11.690 ± 0.034	11.270 ± 0.058	11.102 ± 0.020	0.619 ± 0.062
[2]GSC1761-1732 (K*)	02 10 05.9	+26 26 44.3	12.641 ± 0.033	12.142 ± 0.071	12.329 ± 0.022	12.011 ± 0.061	11.879 ± 0.030	0.499 ± 0.078
[3]Observed check star magnitudes			12.644 ± 0.019	12.131 ± 0.016	12.330 ± 0.014	11.997 ± 0.015	11.852 ± 0.019	0.513 ± 0.024

APASS [1]comparison and [2]check star magnitudes and errors. The [3]observed check star magnitudes are the averages over all nights for each passband. The B and V magnitudes and color for BN Ari were taken from the Tycho-2 Catalog (Høg et al. *2000).*

Table 2. Available times of minima and O–C residuals from Equations (2) and (3).

Epoch HJD 2400000+	Error	Cycle	O–C Linear	O–C Quad.	References
54456.2520	0.0070	0.0	–0.0032	0.0028	Paschke 2009
54805.3150	0.0070	1166.0	–0.0073	–0.0042	Paschke 2009
54808.315	0.007	1176.0	–0.0010	0.0020	Paschke 2009
55448.8210	0.0002	3315.5	–0.0002	–0.0008	Nelson 2011
55477.8592	0.0002	3412.5	–0.0010	–0.0017	Diethelm 2011
55478.9091	0.0008	3416.0	0.0011	0.0004	Diethelm 2011
55578.3010	0.003	3748.0	0.0016	0.0006	Paschke 2012
55591.6207	0.0001	3792.5	–0.0007	–0.0018	Nelson 2012
55614.973	—	3870.5	0.0006	–0.0005	Nagai 2012
55836.6580	0.0030	4611.0	0.0011	–0.0006	Paschke 2012
55843.8416	0.0005	4635.0	–0.0002	–0.0019	Diethelm 2012
55843.9922	0.0016	4635.5	0.0007	–0.0010	Diethelm 2012
56153.5438	0.0003	5669.5	0.0022	0.0004	Hoňková *et al.* 2009
56153.5439	0.0003	5669.5	0.0023	0.0005	Hoňková *et al.* 2009
56153.5439	0.0003	5669.5	0.0023	0.0005	Hoňková *et al.* 2009
56157.5880	0.0050	5683.0	0.0049	0.0031	Paschke 2013
56251.2887	0.0001	5996.0	0.0023	0.0005	Hübscher and Lehmann 2013
56226.1419	—	5912.0	0.0027	0.0009	Nagai 2013a
56235.1228	—	5942.0	0.0025	0.0007	Nagai 2013a
56235.2722	—	5942.5	0.0022	0.0004	Nagai 2013a
56575.0589	—	7077.5	0.0023	0.0011	Nagai 2013b
56575.2082	—	7078.0	0.0019	0.0007	Nagai 2013b
56630.2929	0.0012	7262.0	0.0023	0.0012	Hübscher 2014
56630.4432	0.0010	7262.5	0.0029	0.0018	Hübscher 2014
56630.5905	0.0013	7263.0	0.0005	–0.0005	Hübscher 2014
56946.72583	0.00015	8319.0	–0.0004	–0.0002	this paper
56946.87601	0.00015	8319.5	0.0001	0.0003	this paper
56948.82148	0.00017	8326.0	–0.0004	–0.0001	this paper
56948.67210	0.00017	8325.5	–0.0001	0.0002	this paper
56949.71959	0.00010	8329.0	–0.0004	–0.0001	this paper
56949.86961	0.00019	8329.5	–0.0001	0.0002	this paper
56951.81525	0.00014	8336.0	–0.0003	–0.0001	this paper
56951.66573	0.00014	8335.5	–0.0002	0.0001	this paper
56952.71329	0.00012	8339.0	–0.0004	–0.0001	this paper
56952.86328	0.00011	8339.5	–0.0001	0.0002	this paper
56954.80871	0.00010	8346.0	–0.0006	–0.0003	this paper
56954.65938	0.00012	8345.5	–0.0002	0.0000	this paper
56956.60579	0.00021	8352.0	0.0003	0.0005	this paper
56956.90428	0.00013	8353.0	–0.0006	–0.0003	this paper
56956.75511	0.00021	8352.5	–0.0001	0.0002	this paper
56957.80245	0.00014	8356.0	–0.0006	–0.0003	this paper
56957.65326	0.00021	8355.5	–0.0001	0.0002	this paper
56960.79609	0.00008	8366.0	–0.0006	–0.0003	this paper
56960.64678	0.00013	8365.5	–0.0003	0.0000	this paper
56962.59219	0.00013	8372.0	–0.0008	–0.0005	this paper
56962.74228	0.00013	8372.5	–0.0004	–0.0001	this paper
56962.89156	0.00013	8373.0	–0.0008	–0.0005	this paper
56970.67513	0.00007	8399.0	–0.0009	–0.0005	this paper
56970.82509	0.00010	8399.5	–0.0006	–0.0002	this paper
56971.72336	0.00005	8402.5	–0.0004	–0.0001	this paper
56980.85349	0.00010	8433.0	–0.0011	–0.0007	this paper
56980.70501	0.00010	8432.5	0.0001	0.0005	this paper
56981.60284	0.00010	8435.5	–0.0002	0.0002	this paper
56985.64357	0.00006	8449.0	–0.0010	–0.0006	this paper
56985.79356	0.00006	8449.5	–0.0007	–0.0003	this paper
56987.58979	0.00010	8455.5	–0.0007	–0.0002	this paper
56988.63706	0.00010	8459.0	–0.0012	–0.0008	this paper
56988.78722	0.00010	8459.5	–0.0007	–0.0003	this paper
56989.83464	0.00004	8463.0	–0.0011	–0.0007	this paper
57270.79407	0.00006	9401.5	–0.0018	0.0003	this paper
57278.72655	0.00006	9428.0	–0.0027	–0.0005	this paper

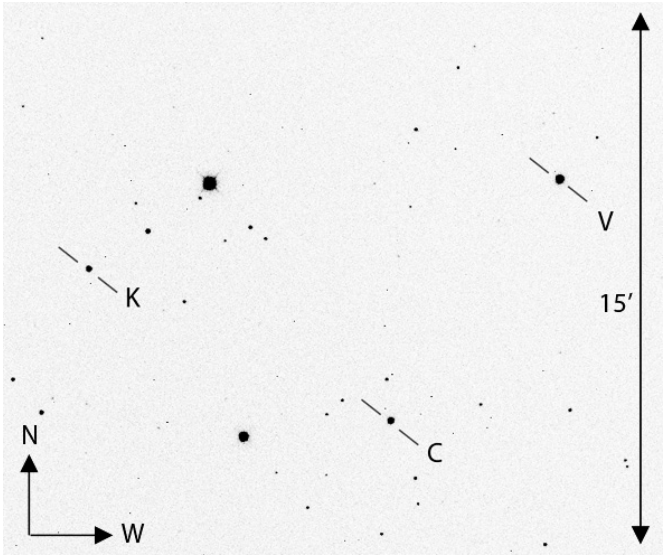

Figure 1. Finder chart for BN Ari (V), comparison (C), and check (K) stars.

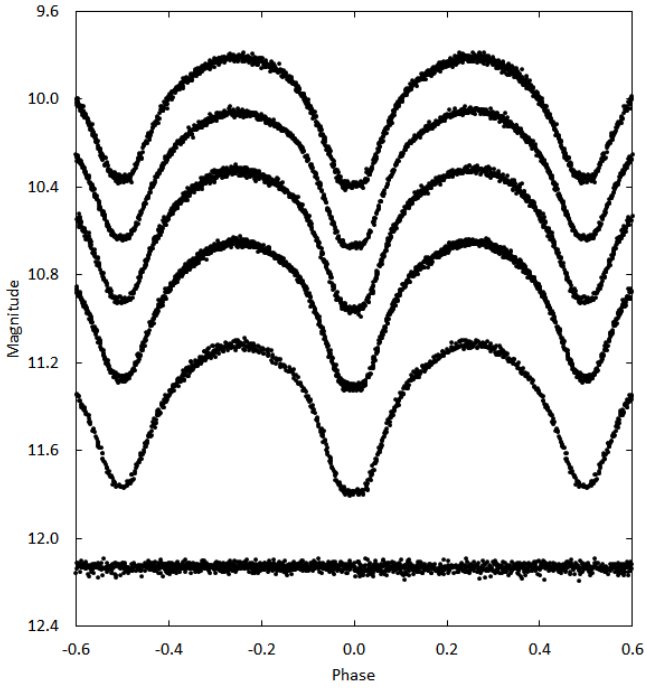

Figure 2. Folded light curves for each observed passband. The differential magnitudes of the variable were converted to standard magnitudes using the comparison star's calibrated magnitudes. From top to bottom the light curve passbands are Sloan i', Sloan r', Johnson V, Sloan g', and Johnson B. The bottom panel shows the standard V magnitudes of the check star. The standard deviations of the check star magnitudes (all nights) are shown in Table 1. Error bars are not shown for clarity.

in Table 1. These magnitudes compare well with the APASS all-sky photometry. Inspection of the K* light curves for each bandpass showed no significant variability over the two months of observation. All the observations in this study can be accessed from the AAVSO International Database (Kafka 2015).

3. Analysis

3.1. Period analysis and ephemerides

Heliocentric Julian Dates (HJD) of the new times of minima were calculated from the observations using the Kwee and van Woerden (1956) method. Time of minima from differing passbands on the same dates were compared and no significant offsets were observed. For each data set the times of minimum from DS1 were formed by averaging together the times from each passband. The new time of minima and errors are reported in Table 2 along with all available minima from other observers. The initial linear ephemeris used in this period study was taken from Paschke (2009) and is given by

$$\text{HJD Min I} = 2451525.671 + 0.299375\ E. \quad (1)$$

The O–C residuals from Equation 1 were used to calculate an improved linear ephemeris by least-squares solution and is given by

$$\text{HJD Min I} = 2456989.83596(73) + 0.29937145(10)\ E. \quad (2)$$

Figure 3 shows the residuals from Equation 1 and the best-fit linear line (solid line on figure) of Equation 2. The O–C diagram from Equation 2 is shown in Figure 4. The general trend of the O–C data indicates the period of BN Ari is continuously decreasing. A least-squares solution of the residuals from Equation 2 yields the following quadratic ephemeris:

$$\text{HJD Min I} = 2457278.77826(73) + 0.29937396(28)\ E - 1.73(16) \times 10^{-9}\ E^2. \quad (3)$$

From this solution the rate of period change was determined to be $dP/dt = -6.20\ (0.70) \times 10^{-7}$ d yr^{-1}. As can be seen in Figure 4, this ephemeris describes the data reasonably well (solid line in the figure).

3.2. Temperature, spectral type

No spectroscopic data were available for BN Ari, therefore the effective temperature and spectral type were estimated from the (B–V) color index. All DS1 B and V observations were binned with a phase width of 0.005. Both phase and magnitude were averaged in each bin interval. The binned V magnitudes were subtracted from the linearly interpolated binned B magnitudes at quadrature ($\Phi = \pm 0.25$), which gave a (B–V) value of 0.816 ± 0.005. Figure 5 shows the binned V-magnitude light curve and the bottom panel the color index. The color index at primary eclipse ($\Phi = \pm 0.025$) was also determined, giving a value of 0.832 ± 0.013. This value was corrected for interstellar extinction using galactic coordinates and a map of dust reddening (Schlafly *et al.* 2014; http://faun.rc.fas.harvard.edu/eschlafly/2dmap/querymap.php). The color

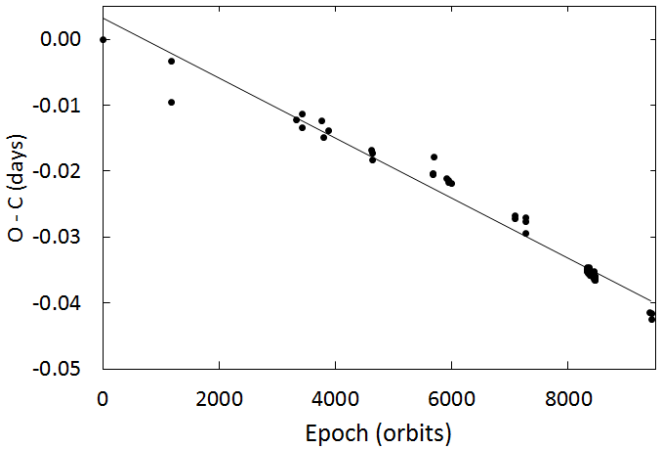

Figure 3. O–C residuals from Equation 1 with the solid line the linear ephemeris fit of Equation 2.

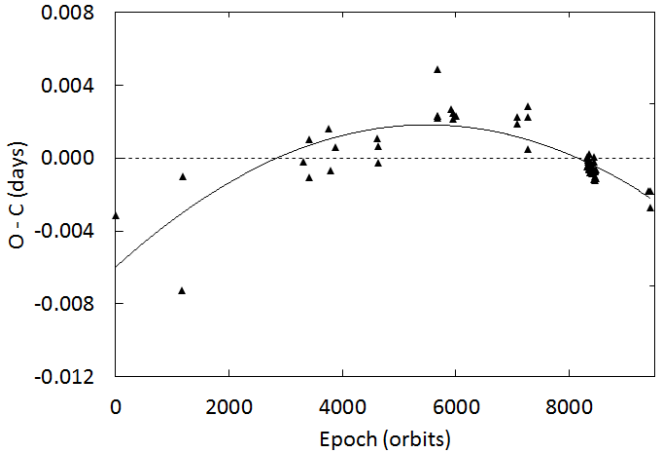

Figure 4. O–C residuals from Equation 2 with the solid line the quadric ephemeris fit of Equation 3.

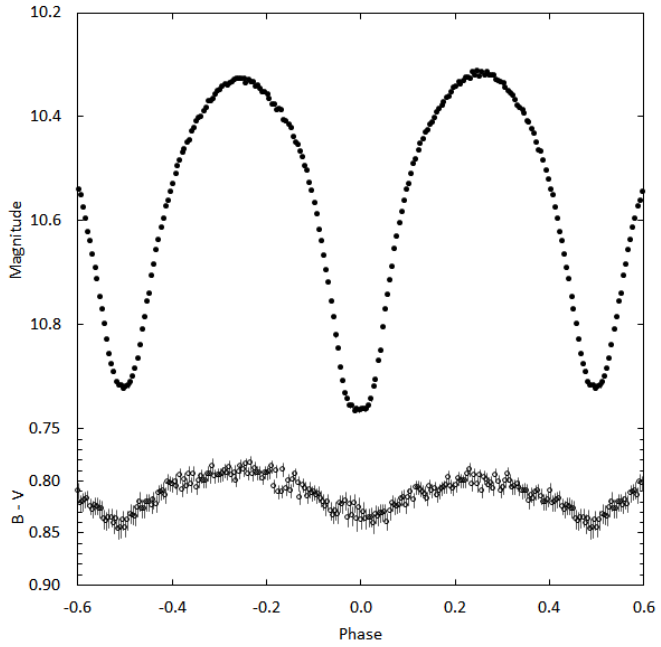

Figure 5. Light curve of all V-band observations in standard magnitudes (top panel). The observations were binned with a phase width of 0.005. The errors for each binned point are smaller than the plotted points. The B-V colors were calculated by subtracting the binned V magnitudes from the linearly interpolated binned B magnitudes.

excess is E(B–V) = 0.115 ± 0.032. The intrinsic color of the larger cooler star is thus $(B–V)_o = 0.715 \pm 0.082$. Using Table 5 of Pecaut and Mamajek (2013) gives an effective temperature of $T_{eff} = 5527 \pm 217$K and a spectral type of G7. This value was used for the effective temperature of the secondary component in the light curve analysis of section 3.3.

3.3. Synthetic light curve modeling

For light curve modeling only DS1 observations were used. These data were binned in both phase and magnitude with a phase interval of 0.01. The average number of observations per bin was 11. The binned magnitudes were converted to relative flux for modeling. For preliminary solutions BM3 was used to fit each curve individually. Standard convective parameters and limb darkening coefficients from Van Hamme's (1993) tabular values for the spectral type were used. The BM3 light curve fits for each color were consistent. The values from the V light curve fit were used as the initial input parameters for computation of a simultaneous five-color light curve solution with the WD program. In this analysis Mode 3 (the contact configuration) was used assuming a common convective envelope in direct thermal contact. The Method of Multiple Subsets (MMS) (Wilson and Biermann 1976) was employed to minimize strong correlations of the parameters. A Kurucz stellar atmosphere model was applied and the fixed inputs included standard convective parameters: gravity darkening, g1 = g2 = 0.32 (Lucy 1968), and albedo value A1 = A2 = 0.5 (Ruciński 1969). The temperature of the cooler star, T_2, was fixed at the value determined in section 3.2, 5527K. Linear limb darkening coefficients were calculated by the program from tabulated values using the method of Van Hamme (1993). A q-search was not necessary given the total eclipses provide the necessary constraints for determining the mass ratio (q). No third light was noted when included in the adjustable parameters. Only negligible small values resulted, indicating no appreciable contribution to the system's light. The solution's adjustable parameters include the inclination (i), mass ratio ($q = M_2 / M_1$), potential (Ω), temperature of the primary star (T_1), and the normalized flux for each wavelength (L). The best-fit solution parameters with errors are shown in column 3 of Table 3. The fill-out parameter was computed using a modification of the parameter defined by Lucy and Wilson (1979) and is given by

$$f = \frac{(\Omega_{inner} - \Omega)}{(\Omega_{inner} - \Omega_{outer})}, \quad (4)$$

where Ω_{inner} and Ω_{outer} are the inner and outer critical equipotential surfaces that pass through the Lagrangian points L1 and L2 and Ω is the equipotential surface which describes the stellar surface. For this solution $\Omega_{inner} = 6.214$, $\Omega_{outer} = 5.600$, and $\Omega = 6.120$ gives a fill-out value of f = 0.15. The best-fit solution with this fill-out value is consistent with a contact binary. Figure 6 shows the normalized light curves for each passband, overlaid by the synthetic solution curves. The residuals for each passband are shown in Figure 7.

Table 3. BN Ari synthetic light curve solutions.

Parameter	*Symbol*	*Solution (no spots)*	*Solution (with spots)*
Gravity Darkening	$g_1 = g_2$	0.32	0.32
Bolometric Albedo	$A_1 = A_2$	0.5	0.5
Inclination(°)	(°)	82.41 ± 0.11	82.23 ± 0.10
Effective Temperature	T_1, T_2 (K)	5731 ± 3, 5527	5728 ± 3, 5527
Surface Potential	$\Omega_1 = \Omega_2$	6.120 ± 0.006	6.114 ± 0.004
Mass Ratio	$q(M_2 / M_1)$	2.699 ± 0.004	2.685 ± 0.002
Fill-outs	$F_1 = F_2$	0.15	0.13
Luminosity	$L_1/(L_1 + L_2)B$	0.3449 ± 0.0005	0.3454 ± 0.0006
	$L_1/(L_1 + L_2)V$	0.3314 ± 0.0004	0.3312 ± 0.0004
	$L_1/(L_1 + L_2)g'$	0.3395 ± 0.0005	0.3391 ± 0.0005
	$L_1/(L_1 + L_2)r'$	0.3252 ± 0.0004	0.3251 ± 0.0004
	$L_1/(L_1 + L_2)I'$	0.3200 ± 0.0003	0.3200 ± 0.0003
Limb Darkening	x_{1B}, x_{2B}	0.813, 0.839	0.813, 0.839
	x_{1V}, x_{2V}	0.674, 0.700	0.674, 0.700
	$x_{1g'}$, $x_{2g'}$	0.763, 0.790	0.763, 0.789'
	$x_{1r'}$, $x_{2r'}$	0.603, 0.630	0.603, 0.630
	$x_{1i'}$, $x_{2i'}$	0.508, 0.532	0.509, 0.532
	$\sum res^2$	0.01416	0.00627
Spot 1 on Star 1			*Hot Spot*
Colatitude	(°)		92 ± 19
Longitude	(°)		9 ± 8
Spot Radius	(°)		15 ± 6
Spot T-factor	(T_{spot} / T_{eff})		1.11 ± 0.05
Spot 2 on Star 2			*Cool Spot*
Colatitude	(°)		39 ± 9
Longitude	(°)		299 ± 4
Spot Radius	(°)		18 ± 9
Spot T-factor	(T_{spot} / T_{eff})		0.95 ± 0.06

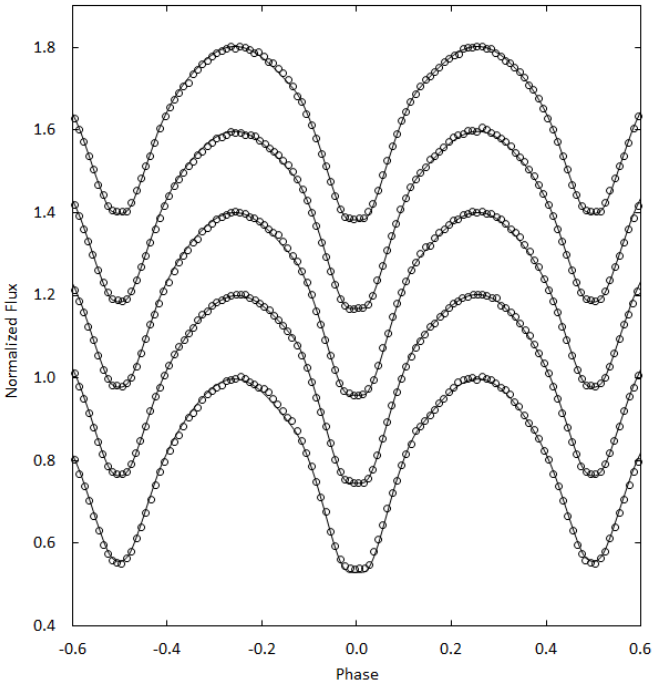

Figure 6. The WD model fit (solid curve) to the observed normalized flux curves for each passband (model without spots). From top to bottom the passbands are Sloan i', Sloan r', Johnson V, Sloan g', and Johnson B. Each curve is offset by 0.2 for this combined plot. The best-fit parameters are given in column 3 of Table 3. Error bars are omitted from the points for clarity.

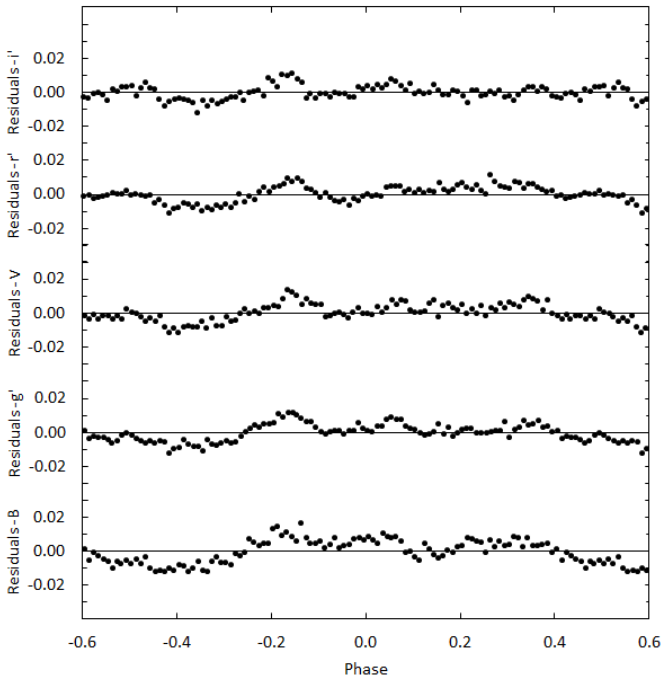

Figure 7. The residuals for the best-fit WD model without spots. Error bars are omitted from the points for clarity.

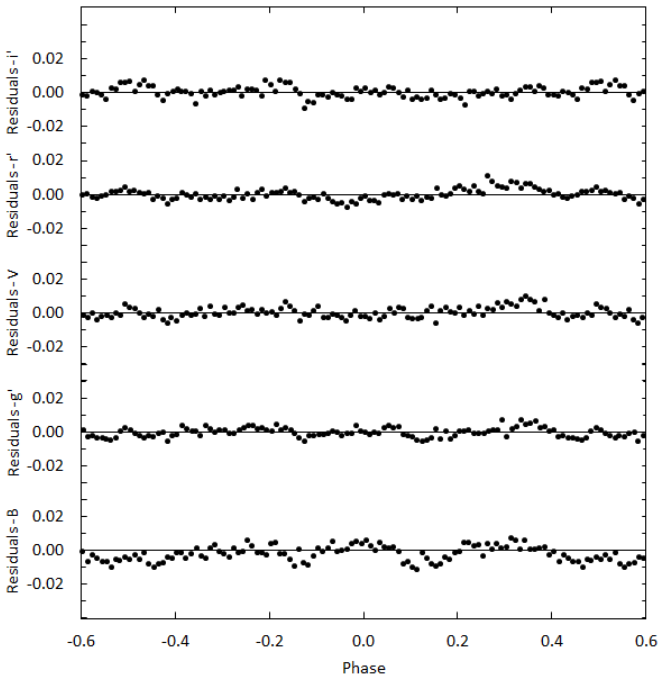

Figure 9. The residuals for the best-fit WD model with spots. Error bars are omitted from the points for clarity.

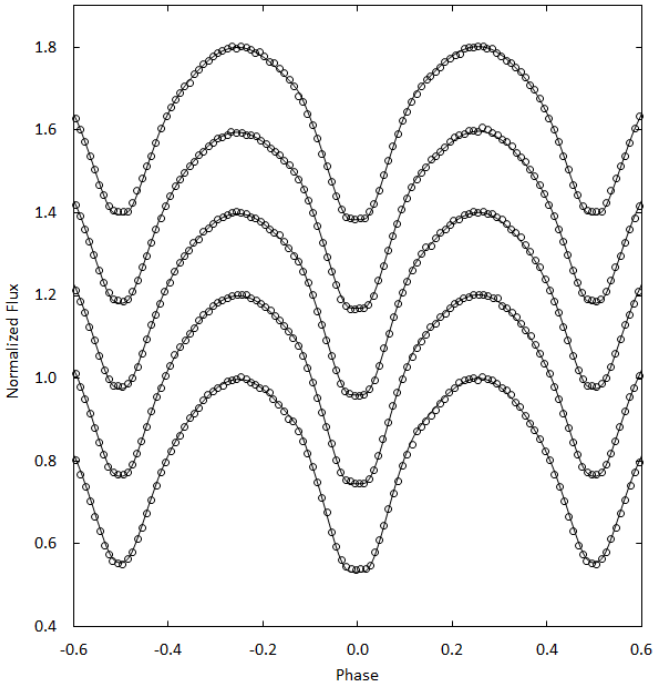

Figure 8. The WD model fit (solid curve) to the observed normalized flux curves for each passband (model with spots). From top to bottom the passbands are Sloan i', Sloan r', Johnson V, Sloan g', and Johnson B. Each curve is offset by 0.2 for this combined plot. The best-fit parameters are given in column 4 of Table 3. Error bars are omitted from the points for clarity.

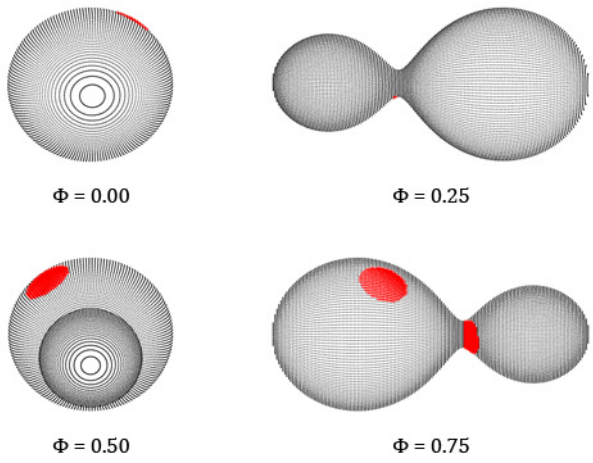

Figure 10. Roche Lobe surfaces of the best-fit WD spot model of BN Ari (orbital phase shown below each diagram).

3.4. Spot model

Figures 6 and 7 show the model light curves do not accurately reproduce the observed light curves in the phase range of 0.40 to 0.90. To improve the fit it was necessary to incorporate two star spots into the model. BM3 was used initially to manually adjust the latitude, longitude, size, and temperature of each spot until a reasonable fit was made between the synthetic and observed curves. The resulting spot parameters were then included in the first best-fit model and a new solution was attempted using the WD program. The stellar parameters were held fixed with only the spot parameters adjusted until the solution converged. Following that convergence the spot parameters were held fixed and the stellar parameters were adjusted. This was repeated until the model converged to a final solution. Column 4 in Table 3 shows the final best-fit stellar model with spots. Figure 8 shows the final model fit (solid line) to the observed light curve for each passband and Figure 9 shows the residuals for the spotted model. The sum of the residuals squared was 0.00627 for the spotted model and 0.01416 for the unspotted model (2.26 times

Table 4. Absolute parameters for BN Ari.

Parameter	*Symbol*	*Value*
Stellar masses	M_1 ($M_\odot$)	0.36
	M_2 ($M_\odot$)	0.98
Stellar radii	R_1 ($R_\odot$)	0.64
	R_2 ($R_\odot$)	0.99
Bolometric magnitude	$M_{bol,1}$	5.76
	$M_{bol,2}$	4.96
Semi-major axis	a ($R_\odot$)	2.08

larger). A graphical representation of this solution is shown in Figure 10.

4. Discussion and conclusions

Spectroscopic data are not available for this system but the absolute mass of the more massive secondary star can be estimated (M2 in this study) using the orbital period. From a statistical study of contact systems Qian (2003) found the mass is given by

$$M_2 = 0.391(\pm 0.059) + 1.96(\pm 0.17)P. \quad (5)$$

Using Equation 5 gives a mass of $M_2 = 0.98 \pm 0.08\ M_\odot$ for the secondary star and this value combined with the mass ratio (q) gives a mass of $M_1 = 0.36 \pm 0.08\ M_\odot$ for the primary component. Applying Kepler's Third Law gives the distance between the stars mass centers of $2.08 \pm 0.01\ R_\odot$. These values, stellar radii, and bolometric magnitudes are collected in Table 4.

A distance estimate to BN Ari can be found using an empirical formula derived by Ruciński and Duerbeck (1997) based on a luminosity calibration for contact binaries (using HIPPARCOS parallaxes). The absolute visual magnitude with an accuracy of ±0.22 is given by

$$M_v = -4.44 \log_{10}(P) + 3.02\,(B-V)_o + 0.12. \quad (6)$$

Using Equation 6 gives a distance modulus of (m–M) = 5.99 ± 0.25 after accounting for the extinction ($A_v = 0.358$) from the color excess found in section 3.2. This distance modulus gives a value of 158 ± 19 pc for the distance. An additional determination of distance can be made using the bolometric magnitudes in Table 4 combined with the bolometric corrections from Pecaut and Mamajek (2013). The correction for the primary star is $BC_1 = -0.12$ and $BC_2 = -0.16$ for the secondary star. The calculated magnitude for the system is $M_v = 4.69$, giving a distance of 152 pc. The two distance determinations differ by less than 5%.

The orbital period of this system appears to be changing rapidly. Magnetic braking could explain a decreasing orbital period for this pair of solar type stars but the rapid period change combined with the contact configuration may indicate conservative mass exchange. In this case the decreasing orbital period would result from mass transfer from the larger more massive star to its smaller hotter companion. The mass transfer rate can be calculated using the rate of period change and the estimated stellar masses using the following equation:

$$\frac{dM}{dt} = \frac{\dot{P} M_1 M_2}{3P(M_1 - M_2)}, \quad (7)$$

This gives a value of $1.01(0.06) \times 10^{-9}\ M_\odot$/day. There is another possible cause for the observed period change that should be considered. Light time effects caused by orbital motion around a third body may be causing an apparent orbital period change. The observed period change curve in Figure 4 may only be a small part of a sinusoidally varying ephemeris. Due to the limited number of cycles observed this model cannot be confirmed at this time. Additional observations by dedicated observers over many years may be necessary to confirm the changing period presented here and its cause.

BN Ari is a W UMa system with total eclipses and a spectral type of approximately G7. The surface temperatures of the component stars differ by 201K, which may indicate poor thermal contact. The fill-out factor of F = 0.13 indicates a contact system. A spectroscopic study of this system would be invaluable in constraining the stellar masses and spectral types.

5. Acknowledgements

The author wishes to thank Dr. Norman Markworth for the many discussions and guidance in the use of the WD program. This research was made possible through the use of the AAVSO Photometric All-Sky Survey (APASS), funded by the Robert Martin Ayers Sciences Fund.

References

Bradstreet, D. H., and Steelman, D. P. 2002, *Bull. Amer. Astron. Soc.*, **34**, 1224.

Diethelm, R. 2011, *Inf. Bull. Var. Stars*, No. 5960, 1.

Diethelm, R. 2012, *Inf. Bull. Var. Stars*, No. 6011, 1.

Henden, A. A., *et al.* 2014, AAVSO Photometric All-Sky Survey, data release 8 (http://www.aavso.org/apass).

Høg, E., *et al.* 2000, The Tycho-2 Catalogue of the 2.5 Million Brightest Stars, *Astron. Astrophys.*, **355**, L27.

Hoňková, K., *et al.* 2009, *Open Eur. J. Var. Stars*, No. 160 (*B.R.N.O. Contributions*, No.38; http://var.astro.cz/oejv/oejv.php?oejv=160).

Hübscher, J. 2014, *Inf. Bull. Var. Stars*, No. 6118, 1.

Hübscher, J., and Lehmann, P. B. 2013, *Inf. Bull. Var. Stars*, No. 6070, 1.

Kafka, S. 2015, observations from the AAVSO International Database (https://www.aavso.org/aavso-international-database).

Kwee, K. K., and van Woerden, H. 1956, *Bull. Astron. Inst. Netherland*s, **12**, 327.

Lucy, L. B. 1968, *Astrophys. J.,* **151**, 1123.

Lucy, L. B., and Wilson, R. E. 1979, *Astrophys. J.*, **231**, 502.

Mirametrics. 2015, Image Processing, Visualization, Data Analysis (http://www.mirametrics.com).

Nagai, K. 2012, *Var. Star Obs. League*, No. 53, 1.

Nagai, K. 2013a, *Var. Star Obs. League*, No. 55, 1.

Nagai, K. 2013b, *Var. Star Obs. League*, No. 56, 1.

Nelson, R. H. 2011, *Inf. Bull. Var. Stars*, No. 5966, 1.

Nelson, R. H. 2012, *Inf. Bull. Var. Stars*, No. 6018, 1.

Otero, S. A., Wils, P., and Dubovsky, P. A. 2004, *Inf. Bull. Var. Stars*, No. 5570, 1.
Paschke, A. 2009, *Open Eur. J. Var. Stars*, No. 116, 1.
Paschke, A. 2012, *Open Eur. J. Var. Stars*, No. 142, 1.
Paschke, A. 2013, *Open Eur. J. Var. Stars*, No. 155, 1.
Pecaut, M. J., and Mamajek, E. E. 2013, *Astrophys. J., Suppl. Ser.*, **208**, 9.
Pojmański, G., Pilecki, B., and Szczygiel, D. 2005, *Acta Astron.*, **55**, 275.
Qian, S. 2003, *Mon. Not. Roy. Astron. Soc.*, **342**, 1260.
Ruciński, S. M. 1969, *Acta Astron.*, **19**, 245.
Ruciński, S. M., and Duerbeck, H. W. 1997, *Publ. Astron. Soc. Pacific*, **109**, 1340.
Schlafly, E. F., *et al.* 2014, *Astrophys. J.*, **789**, 15.
Van Hamme, W. 1993, *Astron. J.*, **106**, 2096.
Van Hamme, W., and Wilson, R. E. 1998, *Bull. Amer. Astron. Soc.*, 30, 1402.
Wilson, R. E. 1990, *Astrophys. J.*, **356**, 613.
Wilson, R. E. 1994, *Publ. Astron. Soc. Pacific*, **106**, 921.
Wilson, R. E., and Biermann, P. 1976, *Astron. Astrophys.*, **48**, 349.
Wilson, R. E., and Devinney, E. J. 1971, *Astrophys. J.*, **166**, 605.
Wozniak, P. R., *et al.* 2004, *Astron. J.*, **127**, 2436.

Recent Minima of 171 Eclipsing Binary Stars

Gerard Samolyk
P.O. Box 20677, Greenfield, WI 53220; gsamolyk@wi.rr.com

Received November 2, 2015; accepted November 3, 2015

Abstract This paper continues the publication of times of minima for 171 eclipsing binary stars from observations reported to the AAVSO Eclipsing Binary section. Times of minima from CCD observations received by the author from March 2015 through October 2015 are presented.

1. Recent observations

The accompanying list contains times of minima calculated from recent CCD observations made by participants in the AAVSO's eclipsing binary program. This list will be web-archived and made available through the AAVSO ftp site at ftp://ftp.aavso.org/public/datasets/gsamoj432.txt. This list, along with the eclipsing binary data from earlier AAVSO publications, is also included in the Lichtenknecker database (Kreiner 2011) administrated by the Bundesdeutsche Arbeitsgemeinschaft für Veranderliche Sterne e. V. (BAV) at: http://www.bav-astro.de/LkDB/index.php?lang=en. These observations were reduced by the observers or the writer using the method of Kwee and Van Woerden (1956). The standard error is included when available. Column F indicates the filter used. A "C" indicates a clear filter.

The linear elements in the *General Catalogue of Variable Stars* (GCVS: Kholopov *et al.* 1985) were used to compute the O–C values for most stars. For a few exceptions where the GCVS elements are missing or are in significant error, light elements from another source are used: CW Cas (Samolyk 1992), DV Cep (Frank and Lichtenknecker 1987), DK Hya (Samolyk 1990), GU Ori (Samolyk 1985). The light elements used for QX And, LR Com, V1193 Cyg, and 1901 Cyg, are from (Kreiner 2004). The light elements used for PU Boo and BG Vul are from Paschke (2014). O–C values listed in this paper can be directly compared with values published in the AAVSO EB monographs.

References

Frank, P., and Lichtenknecker, D. 1987, *BAV Mitt.*, No. 47, 1.
Kholopov, P. N., *et al.* 1985, *General Catalogue of Variable Stars*, 4th ed., Moscow.
Kreiner, J. M. 2004, "Up-to-date linear elements of eclipsing binaries," *Acta Astron.*, **54**, 207 (http://www.as.up.krakow.pl/ephem/).
Kreiner, J. M. 2011, Lichtenknecker-Database of the BAV (http://www.bavdata-astro.de/~tl/cgi-bin/varstars_cgi).
Kwee, K. K., and van Woerden, H. 1956, *Bull. Astron. Inst. Netherlands*, **12**, 327.
Paschke, A. 2014, "O–C Gateway" (http://var.astro.cz/ocgate/).
Samolyk, G. 1985, *J. Amer. Assoc. Var. Star Obs.*, **14**, 12.
Samolyk, G. 1990, *J. Amer. Assoc. Var. Star Obs.*, **19**, 5.
Samolyk, G. 1992, *J. Amer. Assoc. Var. Star Obs.*, **21**, 34.

Table 1. Recent times of minima of stars in the AAVSO eclipsing binary program.

Star	*JD (min) Hel. 2400000 +*	*Cycle*	*O–C (day)*	*F*	*Observer*	*Error (day)*	*Star*	*JD (min) Hel. 2400000 +*	*Cycle*	*O–C (day)*	*F*	*Observer*	*Error (day)*
RT And	57258.8250	25626	–0.0117	V	G. Samolyk	0.0001	QX And	57307.5986	11664	0.0004	V	G. Samolyk	0.0004
RT And	57277.6933	25656	–0.0113	V	S. Cook	0.0004	QX And	57307.8045	11664.5	0.0002	V	G. Samolyk	0.0003
RT And	57313.5423	25713	–0.0113	V	N. Simmons	0.0001	QX And	57307.8050	11664.5	0.0007	V	K. Menzies	0.0002
UU And	57223.8281	10478	0.0786	V	G. Samolyk	0.0002	QX And	57310.8953	11672	–0.0003	V	K. Menzies	0.0003
UU And	57278.8219	10515	0.0795	V	G. Samolyk	0.0002	CX Aqr	57250.7889	37406	0.0141	V	G. Samolyk	0.0001
WZ And	57257.8805	23554	0.0714	V	R. Sabo	0.0002	CZ Aqr	57235.8667	16070	–0.0591	V	G. Samolyk	0.0001
XZ And	57321.6194	24567	0.1793	V	G. Samolyk	0.0001	XZ Aql	57258.6784	7178	0.1762	V	G. Samolyk	0.0001
AB And	57221.8655	63612	–0.0372	V	G. Samolyk	0.0001	KO Aql	57221.7220	5354	0.0991	V	N. Simmons	0.0002
AB And	57245.4301	63683	–0.0370	V	L. Corp	0.0002	KP Aql	57255.7583	5006.5	–0.0195	V	G. Samolyk	0.0001
AB And	57245.5943	63683.5	–0.0387	V	L. Corp	0.0002	OO Aql	57214.4472	36704	0.0606	V	L. Corp	0.0002
AB And	57258.7055	63723	–0.0373	V	N. Simmons	0.0001	OO Aql	57221.7967	36718.5	0.0617	V	G. Samolyk	0.0002
AB And	57273.6404	63768	–0.0375	V	K. Menzies	0.0001	OO Aql	57247.6421	36769.5	0.0609	V	N. Simmons	0.0002
AD And	57222.8785	18475.5	–0.0336	V	G. Samolyk	0.0002	OO Aql	57255.7496	36785.5	0.0598	V	S. Cook	0.0003
BD And	57307.6353	48272	0.0155	V	G. Samolyk	0.0003	V343 Aql	57222.8714	15602	–0.0416	V	G. Samolyk	0.0003
BX And	57270.7894	33997	–0.0795	V	K. Menzies	0.0001	SS Ari	57285.9852	44971	–0.3480	V	R. Sabo	0.0001
BX And	57297.6329	34041	–0.0811	V	N. Simmons	0.0002	SX Aur	57312.8208	14173	0.0186	V	N. Simmons	0.0001
BX And	57322.6459	34082	–0.0828	V	S. Cook	0.0006	TT Aur	57320.7240	27071	–0.0016	V	G. Samolyk	0.0002
DS And	57270.8405	20908.5	0.0030	V	K. Menzies	0.0002	EM Aur	57278.8541	14428	–1.1050	V	G. Samolyk	0.0004
DS And	57271.8512	20909.5	0.0032	V	K. Menzies	0.0003	HP Aur	57321.7537	10237	0.0675	V	N. Simmons	0.0001
DS And	57307.7237	20945	0.0022	V	G. Samolyk	0.0002	TY Boo	57139.7531	71447	0.0764	V	G. Samolyk	0.0001

Table continued on following pages

Table 1. Recent times of minima of stars in the AAVSO eclipsing binary program, cont.

Star	*JD (min) Hel. 2400000 +*	*Cycle*	*O–C (day)*	*F*	*Observer*	*Error (day)*
TY Boo	57139.9120	71447.5	0.0767	V	G. Samolyk	0.0001
TY Boo	57150.6950	71481.5	0.0767	V	K. Menzies	0.0001
TZ Boo	57140.6495	58916.5	0.0627	V	G. Samolyk	0.0001
TZ Boo	57140.7982	58917	0.0628	V	G. Samolyk	0.0002
TZ Boo	57145.7015	58933.5	0.0630	V	K. Menzies	0.0004
TZ Boo	57150.6047	58950	0.0630	V	K. Menzies	0.0001
UW Boo	57131.7649	14658	0.0010	V	K. Menzies	0.0001
VW Boo	57168.6623	75938	–0.2423	V	N. Simmons	0.0002
AD Boo	57197.7228	15239	0.0319	R	S. Cook	0.0006
CK Boo	57152.4916	40139.5	0.0682	V	L. Corp	0.0003
CK Boo	57179.4800	40215.5	0.0652	V	L. Corp	0.0003
PU Boo	57166.2840	11966	–0.0019	V	Y. Ogmen	0.0001
TY Cap	57258.6882	8757	0.0863	V	G. Samolyk	0.0001
RZ Cas	57312.6617	11807	0.0741	V	G. Samolyk	0.0001
ZZ Cas	57279.6544	19173	0.0162	V	N. Simmons	0.0001
AB Cas	57278.6332	10655	0.1302	V	G. Samolyk	0.0001
CW Cas	57235.8691	48935.5	–0.0901	V	G. Samolyk	0.0002
CW Cas	57310.6392	49170	–0.0936	V	N. Simmons	0.0001
CW Cas	57313.6692	49179.5	–0.0928	V	N. Simmons	0.0001
CW Cas	57314.6254	49182.5	–0.0932	V	G. Samolyk	0.0001
CW Cas	57314.7855	49183	–0.0925	V	G. Samolyk	0.0001
DZ Cas	57320.7236	36803	–0.1980	V	G. Samolyk	0.0001
GT Cas	57236.6792	9999	0.2040	V	G. Samolyk	0.0002
IR Cas	57280.6052	21914	0.0113	V	G. Samolyk	0.0002
IR Cas	57310.5543	21958	0.0103	V	N. Simmons	0.0001
IS Cas	57321.6157	15501	0.0690	V	G. Samolyk	0.0001
IT Cas	57297.5814	7323	0.0673	V	G. Samolyk	0.0001
OR Cas	57317.7379	10522	–0.0286	V	G. Samolyk	0.0002
PV Cas	57236.6853	9717	–0.0347	V	N. Simmons	0.0001
U Cep	57278.7816	5109	0.1988	V	N. Simmons	0.0001
SU Cep	57279.5854	34340	0.0066	V	G. Samolyk	0.0001
WW Cep	57313.6525	21051	0.3439	V	G. Samolyk	0.0002
WZ Cep	57226.6360	69916	–0.1514	V	G. Samolyk	0.0002
WZ Cep	57226.8428	69916.5	–0.1534	V	G. Samolyk	0.0002
WZ Cep	57278.6055	70040.5	–0.1541	V	N. Simmons	0.0001
XX Cep	57255.6913	5312	0.0102	V	N. Simmons	0.0001
DK Cep	57225.7270	23973	0.0299	V	G. Samolyk	0.0001
DL Cep	57221.7892	14275	0.0649	V	G. Samolyk	0.0003
DV Cep	57246.6840	9022	–0.0056	V	N. Simmons	0.0001
EE Cep	56893.96	11	3.13	B	G. Samolyk	0.03
EE Cep	56894.05	11	3.22	V	G. Samolyk	0.04
EE Cep	56894.32	11	3.49	R	G. Samolyk	0.03
EE Cep	56894.34	11	3.51	I	G. Samolyk	0.04
EG Cep	57214.7673	26845	0.0118	V	G. Samolyk	0.0002
EG Cep	57215.8572	26847	0.0124	V	B. Harris	0.0001
EG Cep	57225.6607	26865	0.0127	V	N. Simmons	0.0001
GK Cep	57246.6615	19817	0.1319	V	N. Simmons	0.0003
RW Com	57157.6070	72195	0.0034	V	K. Menzies	0.0001
RZ Com	57128.7686	65852	0.0491	V	K. Menzies	0.0001
SS Com	57139.6292	77851	0.8570	V	N. Simmons	0.0001
SS Com	57140.6619	77853.5	0.8577	V	N. Simmons	0.0001
CC Com	57116.7393	79675	–0.0231	V	G. Samolyk	0.0001
CC Com	57116.8510	79675.5	–0.0217	V	G. Samolyk	0.0002
LR Com	57126.5591	5161	0.0113	V	L. Corp	0.0001
U CrB	57138.8546	11700	0.1272	V	G. Samolyk	0.0001
RW CrB	57128.6753	22545	0.0001	V	K. Menzies	0.0001
RV Crv	57139.6721	21559.5	–0.0935	V	G. Samolyk	0.0002
Y Cyg	57214.8163	15940	–0.1477	V	G. Samolyk	0.0001
Y Cyg	57226.8014	15944	–0.1480	V	G. Samolyk	0.0001
Y Cyg	57256.7719	15954	–0.1408	V	S. Cook	0.0006
SW Cyg	57205.7558	3354	–0.3533	V	G. Samolyk	0.0001
WW Cyg	57195.7851	5069	0.1280	V	G. Samolyk	0.0001
ZZ Cyg	57150.8169	19329	–0.0673	V	K. Menzies	0.0001
ZZ Cyg	57281.5681	19537	–0.0683	V	K. Menzies	0.0001
AE Cyg	57211.8266	13027	–0.0038	V	G. Samolyk	0.0003
BR Cyg	57235.7399	11779	0.0014	V	G. Samolyk	0.0002
CG Cyg	57227.7903	28207	0.0740	V	G. Samolyk	0.0001
CG Cyg	57236.6257	28221	0.0734	V	G. Samolyk	0.0001
DK Cyg	57222.6950	40840	0.1091	V	G. Samolyk	0.0002
DK Cyg	57272.5908	40946	0.1117	V	K. Menzies	0.0001
DO Cyg	57156.8023	7409	–0.0321	V	B. Harris	0.0003
KR Cyg	57201.8101	33243	0.0191	V	N. Simmons	0.0001
KR Cyg	57267.7314	33321	0.0186	V	S. Cook	0.0007
KV Cyg	57236.6450	9781	0.0596	V	G. Samolyk	0.0002
MY Cyg	57197.8534	5830	0.0044	V	G. Samolyk	0.0002
V346 Cyg	57317.7125	7885	0.1839	V	G. Samolyk	0.0002
V387 Cyg	57221.6616	45639	0.0215	V	G. Samolyk	0.0003
V387 Cyg	57280.5960	45731	0.0210	V	N. Simmons	0.0001
V387 Cyg	57305.5785	45770	0.0203	V	G. Samolyk	0.0001
V388 Cyg	57222.6128	17775	–0.1107	V	G. Samolyk	0.0003
V388 Cyg	57227.7655	17781	–0.1123	V	N. Simmons	0.0002
V401 Cyg	57208.8101	22950	0.0812	V	G. Samolyk	0.0002
V401 Cyg	57319.5242	23140	0.0781	V	K. Menzies	0.0002
V456 Cyg	57201.8354	13791	0.0508	V	G. Samolyk	0.0001
V456 Cyg	57285.6080	13885	0.0513	V	G. Samolyk	0.0001
V466 Cyg	57197.8332	20425.5	0.0069	V	G. Samolyk	0.0001
V466 Cyg	57200.6163	20427.5	0.0069	V	K. Menzies	0.0001
V477 Cyg	57233.8043	5558	–0.0334	V	G. Samolyk	0.0001
V548 Cyg	57255.6222	7090	0.0244	V	G. Samolyk	0.0003
V704 Cyg	57213.8308	33773	0.0356	V	G. Samolyk	0.0002
V1034 Cyg	57255.3910	14655	0.0082	V	L. Corp	0.0004
V1193 Cyg	57192.2812	9314	0.0072	C	Y. Ogmen	0.0001
V1315 Cyg	57233.3598	44194	0.0214	C	Y. Ogmen	0.0001
V1901 Cyg	56915.2817	5458	0.0172	C	Y. Ogmen	0.0001
V2311 Cyg	57233.2990	44194	–0.0394	C	Y. Ogmen	0.0001
W Del	57227.8222	2892	0.0315	V	G. Samolyk	0.0001
W Del	57256.6583	2898	0.0310	V	N. Simmons	0.0001
TT Del	57250.8099	4186	–0.1132	V	G. Samolyk	0.0002
TY Del	57250.6519	11998	0.0665	V	G. Samolyk	0.0001
YY Del	57256.5955	18027	0.0104	V	G. Samolyk	0.0002
YY Del	57279.5947	18056	0.0099	V	G. Samolyk	0.0001
YY Del	57283.5606	18061	0.0104	V	K. Menzies	0.0001
FZ Del	57222.7931	33067	–0.0269	V	G. Samolyk	0.0001
RZ Dra	57221.7595	23679	0.0633	V	G. Samolyk	0.0002
TW Dra	57193.7353	4652	–0.0119	V	G. Samolyk	0.0002
AI Dra	57208.6988	11609	0.0331	V	G. Samolyk	0.0001
CM Dra	57174.7349	11259	0.0034	V	B. Harris	0.0002
S Equ	57241.4561	4262	0.0676	V	L. Corp	0.0002
S Equ	57313.6146	4283	0.0681	V	G. Samolyk	0.0001
WW Gem	57326.9051	25321	0.0358	V	K. Menzies	0.0002
AF Gem	57320.9298	24253	–0.0696	V	G. Samolyk	0.0001
Z Her	57214.8254	11052	–0.0198	V	S. Cook	0.0007
RX Her	57257.6040	13543	0.0000	V	G. Samolyk	0.0002
SZ Her	57221.6186	18772	–0.0275	V	G. Samolyk	0.0001
TT Her	57208.6401	18872	0.0440	V	G. Samolyk	0.0002
TT Her	57271.5745	18941	0.0452	V	K. Menzies	0.0003
TU Her	57225.6993	5807	–0.2346	V	G. Samolyk	0.0001
AK Her	57227.4387	35682.5	0.0195	V	L. Corp	0.0002
CC Her	57197.6793	10109	0.2727	V	G. Samolyk	0.0001
CT Her	57140.8490	8183	0.0120	V	G. Samolyk	0.0001
CT Her	57251.6051	8245	0.0129	V	K. Menzies	0.0002
V718 Her	57187.2973	33959	–0.0199	C	Y. Ogmen	0.0002
AV Hya	57140.5975	29949	–0.1108	V	G. Samolyk	0.0002
DK Hya	57116.6859	27347	0.0025	V	G. Samolyk	0.0001
SW Lac	57255.6272	37354.5	–0.0894	V	G. Samolyk	0.0001
SW Lac	57255.7890	37355	–0.0879	V	G. Samolyk	0.0001
SW Lac	57256.4313	37357	–0.0871	V	L. Corp	0.0001
SW Lac	57256.5903	37357.5	–0.0884	V	L. Corp	0.0002
SW Lac	57270.8634	37402	–0.0874	V	K. Menzies	0.0001
SW Lac	57286.5788	37451	–0.0873	V	K. Menzies	0.0001
SW Lac	57312.3951	37531.5	–0.0891	V	L. Corp	0.0002
VX Lac	57233.7866	11145	0.0827	V	G. Samolyk	0.0001

Table continued on next page

Table 1. Recent times of minima of stars in the AAVSO eclipsing binary program, cont.

Star	JD (min) Hel. 2400000 +	Cycle	O–C (day)	F	Observer	Error (day)	Star	JD (min) Hel. 2400000 +	Cycle	O–C (day)	F	Observer	Error (day)
AR Lac	57278.7270	7909	–0.0511	V	N. Simmons	0.0002	ST Per	57317.7023	5619	0.3123	V	G. Samolyk	0.0001
AW Lac	57251.6578	26799	0.2040	V	N. Simmons	0.0002	IU Per	57261.8442	13594	0.0090	V	N. Simmons	0.0002
CO Lac	57213.8617	19245	0.0056	V	G. Samolyk	0.0002	KW Per	57258.8571	15951	0.0153	V	G. Samolyk	0.0001
CO Lac	57234.6656	19258.5	–0.0103	V	G. Samolyk	0.0001	V432 Per	57278.7460	66573	0.0188	V	G. Samolyk	0.0001
CO Lac	57261.6699	19276	0.0053	V	N. Simmons	0.0003	V876 Per	56984.2090	17213.5	0.0135	C	Y. Ogmen	0.0001
XY Leo	57145.6201	42489	0.1363	V	K. Menzies	0.0003	V876 Per	56984.3684	17214	0.0130	C	Y. Ogmen	0.0001
XZ Leo	57128.5702	24815	0.0657	V	K. Menzies	0.0001	RV Psc	57280.7574	59386	–0.0588	V	G. Samolyk	0.0002
RR Lep	57320.9128	29433	–0.0415	V	G. Samolyk	0.0002	U Sge	57234.7021	11863	0.0036	V	G. Samolyk	0.0001
UZ Lyr	57227.6347	7158	–0.0368	V	N. Simmons	0.0001	U Sge	57234.7025	11863	0.0040	V	N. Simmons	0.0001
UZ Lyr	57227.6356	7158	–0.0359	V	G. Samolyk	0.0002	RS Ser	57224.7494	37287	0.0515	V	S. Cook	0.0002
EW Lyr	57256.6587	15783	0.2666	V	G. Samolyk	0.0002	AO Ser	57213.6847	26247	–0.0118	V	G. Samolyk	0.0001
FL Lyr	57234.6606	8729	–0.0017	V	G. Samolyk	0.0001	CC Ser	57221.6740	38253.5	1.0608	V	G. Samolyk	0.0001
U Oph	57197.7539	7620	–0.0103	V	G. Samolyk	0.0003	RW Tau	57326.8920	4205	–0.2657	V	K. Menzies	0.0001
SX Oph	57197.7003	11534	–0.0027	V	G. Samolyk	0.0001	TY Tau	57295.9212	33511	0.2660	V	R. Sabo	0.0002
V508 Oph	57213.6839	35184	–0.0254	V	G. Samolyk	0.0001	WY Tau	57310.8106	28738	0.0617	V	N. Simmons	0.0001
V508 Oph	57217.4774	35195	–0.0246	V	L. Corp	0.0002	WY Tau	57310.8111	28738	0.0622	V	K. Menzies	0.0002
V508 Oph	57273.3342	35357	–0.0241	V	L. Corp	0.0004	CT Tau	57313.8851	17860	–0.0631	V	N. Simmons	0.0001
V508 Oph	57294.3650	35418	–0.0256	V	L. Corp	0.0002	EQ Tau	57294.8832	50041.5	–0.0318	V	R. Sabo	0.0001
V839 Oph	57139.8049	40810	0.2930	V	G. Samolyk	0.0001	EQ Tau	57326.7989	50135	–0.0321	V	K. Menzies	0.0001
V839 Oph	57223.6495	41015	0.2936	V	G. Samolyk	0.0001	V Tri	57307.8501	56106	–0.0059	V	G. Samolyk	0.0002
V839 Oph	57273.5492	41137	0.2958	V	K. Menzies	0.0001	X Tri	57308.8304	15240	–0.0870	V	S. Cook	0.0005
V1010 Oph	57220.7364	27642	–0.1737	V	S. Cook	0.0005	RS Tri	57319.8183	10152	–0.0621	V	K. Menzies	0.0002
V1010 Oph	57226.6890	27651	–0.1739	V	G. Samolyk	0.0001	RV Tri	57256.8691	14892	–0.0401	V	N. Simmons	0.0001
ER Ori	57309.8619	37041.5	0.1240	V	R. Sabo	0.0001	W UMi	57205.7397	13828	–0.1906	V	G. Samolyk	0.0002
ER Ori	57314.9436	37053.5	0.1249	V	G. Samolyk	0.0001	VV Vir	57195.6435	58221	–0.0452	V	G. Samolyk	0.0003
FZ Ori	56620.7879	31492	–0.0484	V	N. Simmons	0.0001	AG Vir	57152.4274	18237	–0.0089	V	L. Corp	0.0004
FZ Ori	57314.9707	33227.5	–0.0424	V	G. Samolyk	0.0003	AH Vir	57134.3681	27777	0.2723	V	L. Corp	0.0004
GU Ori	57316.8890	30269	–0.0572	V	R. Sabo	0.0006	NY Vir	57126.4386	68336.5	–0.0020	R	L. Corp	0.0003
GU Ori	57320.8881	30277.5	–0.0589	V	G. Samolyk	0.0003	AW Vul	57280.6003	13634	–0.0232	V	G. Samolyk	0.0001
U Peg	56620.6018	53655.5	–0.1519	V	N. Simmons	0.0001	AW Vul	57322.5361	13686	–0.0229	V	K. Menzies	0.0001
U Peg	57234.8621	55294.5	–0.1584	V	G. Samolyk	0.0001	AY Vul	57222.6541	6026	–0.1273	V	G. Samolyk	0.0002
U Peg	57305.5067	55483	–0.1601	V	L. Corp	0.0002	AY Vul	57280.5514	6050	–0.1287	V	K. Menzies	0.0001
BB Peg	57246.8984	37296	–0.0173	V	R. Sabo	0.0002	BE Vul	57250.7013	11043	0.0984	V	G. Samolyk	0.0002
BB Peg	57279.6150	37386.5	–0.0167	V	G. Samolyk	0.0002	BE Vul	57278.6389	11061	0.0992	V	G. Samolyk	0.0001
BB Peg	57279.7936	37387	–0.0188	V	G. Samolyk	0.0002	BG Vul	56885.3419	79650	0.0219	C	Y. Ogmen	0.0001
BB Peg	57281.6022	37392	–0.0177	V	N. Simmons	0.0001	BO Vul	57224.6740	10913	–0.0254	V	G. Samolyk	0.0001
BB Peg	57310.7025	37472.5	–0.0183	V	S. Cook	0.0004	BS Vul	57224.6505	29315	–0.0311	V	G. Samolyk	0.0001
BG Peg	57279.8135	6017	–2.2207	V	G. Samolyk	0.0002	BS Vul	57314.6086	29504	–0.0317	V	G. Samolyk	0.0002
BX Peg	57234.8262	46500	–0.1181	V	G. Samolyk	0.0001	BT Vul	57227.6348	19125	0.0048	V	G. Samolyk	0.0001
BX Peg	57326.5230	46827	–0.1189	V	K. Menzies	0.0001	BT Vul	57307.5185	19195	0.0045	V	K. Menzies	0.0001
DI Peg	57251.8222	16936	0.0049	V	K. Menzies	0.0001	BU Vul	57224.8574	41637	0.0129	V	B. Harris	0.0001
GP Peg	57309.6288	16473	–0.0529	V	N. Simmons	0.0001	BU Vul	57235.6691	41656	0.0137	V	G. Samolyk	0.0001
Z Per	57312.6515	3813	–0.2906	V	G. Samolyk	0.0001	BU Vul	57244.7735	41672	0.0142	V	B. Harris	0.0001
RT Per	57246.8540	28103	0.0985	V	N. Simmons	0.0001	CD Vul	57233.6378	15993	–0.0010	V	G. Samolyk	0.0001
RT Per	57314.8077	28183	0.1002	V	G. Samolyk	0.0002	CD Vul	57285.6025	16069	–0.0009	V	G. Samolyk	0.0002
RV Per	57313.8542	7736	0.0022	V	G. Samolyk	0.0002	ER Vul	57317.6989	24546	0.0193	V	R. Sabo	0.0004

Simultaneous Collocated Photometry

Tom Calderwood
1184 NW Mt. Washington Drive, Bend, OR 97703; tjc@cantordust.net

Evan Getz
Tom McBratney
Oregon Episcopal School, Portland, OR 97223

Eric Holcomb
Bend, OR 97701

Received October 29, 2015; revised November 11, 2015; accepted November 30, 2015

Abstract Two telescopes equipped with single channel photometers are operated side-by-side, observing the same stars, to evaluate the consistency of their results. In fifteen paired V band observations, we find that the median absolute difference between the two systems is 6 mmag, and that they always agree within 2σ errors.

1. Background

During the observing of the outburst of Nova Delphini 2013, substantial discrepancies were noted among the photometry of AAVSO observers, and a major effort was undertaken to improve data quality (Henden 2013). This work continues, and it invites the question of how much agreement can be achieved among disparate observers. The exercise here described is an effort to provide a baseline answer to that question. We conceived to operate two nearly identical photometric instruments at the same location at the same time, and compare their results. The project was planned as part of the 2015 astronomy workshop for high school students at Pine Mountain Observatory (PMO) in central Oregon. PMO, a research facility of the University of Oregon, is located at an altitude of 6,300 feet in a desert environment. The systems consisted of Optec SSP3 photoelectric photometers (Optec 1997) with Johnson V filters, mated to 10- and 9.25-inch schmidt-cassegrain telescopes. For historical reasons, the two photometers are known as "Boris" and "Carlo." During the July workshop, observations were made of λ And and V642 Her. Those data were supplemented by observations of DM Cep in September. The three stars, all in the AAVSO Photoelectric Photometry (PEP) observing program (AAVSO 2015a), served as increasingly challenging targets as shown in Table 1. DM Cep, besides being dimmest and having the widest color contrast vis-a-vis its comparison star, was observed in a part of the sky subject to light pollution. The three stars vary slowly, so intrinsic brightness changes would be expected to be on the order of only 1 mmag. during a single observation (Watson *et al.* 2014). However, over the course of a night's series of observations, and certainly over successive nights, the variation could be much larger. Hence, we compare the agreement of each star's observations pairwise, rather than in aggregate.

Table 1. Stars in program.

Star	*No. Obs.*	*V Approx.*	*Comparison Star*	*Comparison Star V*	*Δ (B-V)*
λ And	4	3.8	HD 223047	4.99	–0.102
V642 Her	5	6.5	HD 159353	5.69	0.59
DM Cep	6	6.9	HD 211867	7.22	0.91

All data were reduced by the same software, written by one of us. Since the two telescopes would make their paired observations at the same airmass, no corrections were applied for differential extinction between the variables and their comparison stars. The magnitudes were transformed, however, to account for different spectral sensitivity of the two instruments. Transformation coefficients for AAVSO PEP systems are usually determined by observing a color-contrasting pair of stars (AAVSO 2015b). Boris and Carlo were calibrated on the same night in May 2015, using a star pair in Serpens (HD 140573, HD 140775). Table 2 shows the transformation values.

Table 2. Transformation data.

Photometer	*Telescope*	*eV*	*λ And V xform*	*V642 Her V xform*	*DM Cep V xform*
Boris	10"	–0.035	0.004	–0.021	–0.032
Carlo	9.25"	–0.027	0.003	–0.016	–0.025

2. PEP observations

The program and comparison stars were observed in the standard PEP observing sequence (AAVSO 2015c). In short, the variable is sampled three times, bracketed by four samples of the comparison. Each sample consists of three ten-second integrations of the star, followed by three integrations of the sky near the star. The star and sky counts are each averaged, and the latter subtracted from the former. Three differential magnitudes are computed for the variable, which are averaged for a final value. The error associated with this magnitude is computed as the standard deviation of the mean of the three values. The photometers are manually operated, so perfect synchronization between corresponding samples by Boris and Carlo was not

Table 3. Photometry summary.

I.D. of Observation from Figure 1	*Star*	*MJD*	*X*	*Boris V*	*err*	*Carlo V*	*err*	*ΔV*	*within 1σ*	*2σ*
A	λ And	57218.85	1.27	3.762	0.005	3.761	0.005	0.001	Yes	Yes
B	λ And	57218.87	1.20	3.760	0.003	3.764	0.001	-0.004	Yes	Yes
C	λ And	57219.83	1.37	3.784	0.015	3.763	0.002	0.021	No	Yes
D	λ And	57219.84	1.31	3.766	0.001	3.763	0.002	0.003	No	Yes
E	V642 Her	57218.76	1.14	6.477*	0.005	6.471	0.004	0.006	Yes	Yes
F	V642 Her	57218.78	1.15	6.486	0.005	6.480	0.003	0.006	Yes	Yes
G	V642 Her	57219.80	1.18	6.488	0.005	6.485	0.006	0.003	Yes	Yes
H	V642 Her	57219.81	1.21	6.482	0.002	6.479	0.004	0.003	Yes	Yes
I	V642 Her	57219.83	1.25	6.490	0.001	6.492	0.009	-0.002	Yes	Yes
J	DM Cep	57284.80	1.15	6.932	0.006	6.924	0.009	0.009	Yes	Yes
K	DM Cep	57284.82	1.16	6.923	0.003	6.933	0.006	-0.010	No	Yes
L	DM Cep	57284.83	1.17	6.926	0.002	6.933	0.005	-0.006	Yes	Yes
M	DM Cep	57284.85	1.18	6.922	0.002	6.929	0.002	-0.006	No	Yes
N	DM Cep	57284.86	1.20	6.925	0.006	6.927	0.001	-0.002	Yes	Yes
O	DM Cep	57284.88	1.21	6.920	0.011	6.934	0.004	-0.014	Yes	Yes

** See section 4.2.*

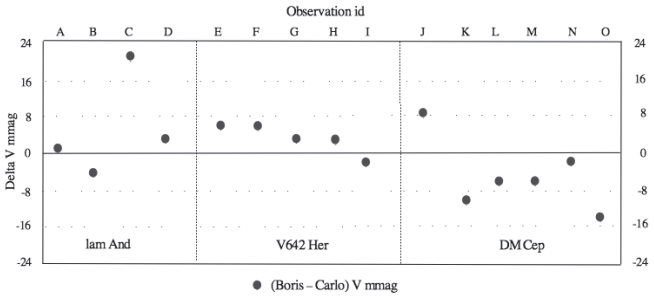

Figure 1. Delta V.

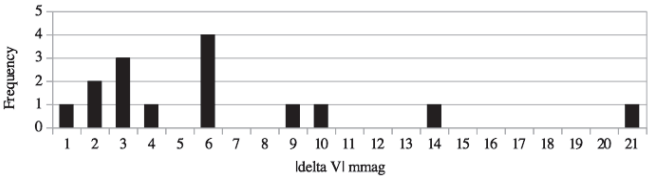

Figure 2. Histogram of |Delta V|.

possible, but we strove to keep them within 1 to 2 minutes of each other. There was an anomaly in the first Boris observation of V642 Her, which is discussed below. Table 3 summarizes the magnitudes and errors of the observations, and indicates if the 1σ error bars overlapped. Airmasses are given in column X. All observations overlapped at 2σ. Figure 1 shows the magnitude differences.

3. Results

The differences between magnitudes ran from –0.014 to +0.020, the bulk falling in a band from –0.006 to +0.006, the median absolute difference being 0.006 (Figure 2). The median 1σ errors for all observations by Boris and Carlo were 0.005 and 0.004, respectively. Eleven of the fifteen pairs of magnitudes agreed within 1σ errors, close to the ten pairs one would theoretically expect. Boris yielded mostly dimmer magnitudes than Carlo for λ And and V642 Her, while the reverse was true for DM Cep.

Conducting the experiment was a logistical challenge, hence the limited amount of data. A single observation takes at least fifteen minutes. Neither of the telescopes were permanently mounted, so all the equipment had to be set up and torn down for observing sessions, and observer schedules had to be coordinated. While all data were collected in the absence of moonlight, we did not have the luxury of choosing the best photometric nights.

Photoelectric equipment was used for this study, both because it was readily available, and because PEP calibration, operation, and data reduction are simpler than for CCD systems. The lower sensitivity of the SSP3 restricted us to brighter stars. Note that if the very bright star λ And were to be excluded from the analysis, the median difference between Boris and Carlo would still be 6 mmag. It would be very interesting to see this experiment repeated with CCDs.

4. Notes

4.1. Magnitudes

Reference magnitudes used in this study came from the *General Catalog of Photometric Data* (GCPD) database (Mermilliod *et al.* 1997), mean UBV system values. The GCPD lists two different "standard" V magnitudes for calibration star HD 140573, 2.66 and 2.65, which differ from the mean, 2.638, with corresponding B–V indexes of 1.165 and 1.168. If the average of the two standards is used in the analysis, eV values for Boris and Carlo become –0.013 and –0.005, respectively. The median absolute difference between Boris and Carlo magnitudes remains 6 mmag, and 1σ and 2σ agreements still hold.

4.2. Boris V642 Her anomaly

Table 4 shows all nine star integrations for the MJD 57218.76 observation of V642 Her by Boris. Integration number one of sample three is clearly discordant with the others, and this is almost certainly due to "cockpit error." Carlo was operated by an experienced PEP observer, but Boris was run by a rotation of

Table 4. Anomalous Boris V642 Her integration.

Sample	*Integration 1*	*Integration 2*	*Integration 3*
1	400	405	402
2	402	397	400
3	375*	400	400

observers who had had only a familiarization session beforehand. The Optec photometers have a flip mirror that directs light either to the sensor or to an eyepiece with a target reticle. A sample is taken by centering the star in the eyepiece, then flipping the mirror and collecting three integrations. The integration circuitry, however, is not synchronized to the mirror movement. The integrator runs in continuous ten second cycles, latching and displaying the value of the previous count during the current integration. When the mirror is moved, the operator must be careful to discard the integration in progress. If the flip is completed very shortly after the start of an integration, it can appear, from the large subsequent count, that the mirror moved just at the end of the prior integration, and that the new count represents a full integration. Upon seeing the next integration, an experienced observer will recognize what happened and discard the partial count. It seems likely that the Boris operator did not do this. The 375 integration, was, therefore, excluded from the analysis, and a value of 400 used as the average integration for sample three. If the suspect integration were to be kept, the results of the observation would be V = 6.486 and σ = 0.012, which still puts it within 1σ agreement with Carlo, and the median absolute difference between all Boris and Carlo magnitudes would remain 6 mmag.

References

AAVSO. 2015a, Photoelectric Photometry Program (https://ww.aavso.org/content/aavso-photoelectric-photometry-pep-program).

AAVSO. 2015b. Obtaining your PEP epsilon(V) coefficient (https://www.aavso.org/obtaining-your-pep-epsilon-coefficient).

AAVSO. 2015c, The Photoelectric Photometry (PEP) Observing Program of the AAVSO: An Introduction (https://www.aavso.org/photoelectric-photometry-pep-observing-program-aavso-introduction).

Henden, A. A. 2013, "Nova Del Photometry" (https://www.aavso.org/nova-del-2013-photometry).

Mermilliod, J.-C., Mermilliod, M., and Hauck, B. 1997, *Astron. Astrophys. Suppl. Ser.*, **124**, 349.

Optec. 1997, Model SSP-3 Solid-State Stellar Photometer (https://archive.org/details/OptecSsp-3PhotometerManual).

Watson, C., Henden, A. A., and Price, C. A. 2014, AAVSO International Variable Star Index VSX (Watson+, 2006–2014; https://www.aavso.org/vsx).

As International as They Would Let Us Be

Virginia Trimble
Department of Physics and Astronomy, University of California, Irvine, CA 92697-4575; vtrimble@uci.edu

Received July 15, 2015; accepted August 28, 2015

Abstract Astronomy has always crossed borders, continents, and oceans. AAVSO itself has roughly half its membership residing outside the USA. In this excessively long paper, I look briefly at ancient and medieval beginnings and more extensively at the 18th and 19th centuries, plunge into the tragedies associated with World War I, and then try to say something relatively cheerful about subsequent events. Most of the people mentioned here you will have heard of before (Eratosthenes, Copernicus, Kepler, Olbers, Lockyer, Eddington…), others, just as important, perhaps not (von Zach, Gould, Argelander, Freundlich…). Division into heroes and villains is neither necessary nor possible, though some of the stories are tragic. In the end, all one can really say about astronomers' efforts to keep open channels of communication that others wanted to choke off is, "the best we can do is the best we can do."

1. Introduction

Astronomy has always been among the most international of sciences. Some of the reasons are obvious. You cannot observe the whole sky continuously from any one place. Attempts to measure geocentric parallax and to observe solar eclipses have required going to the ends (or anyhow the middles) of the earth. Even now, when satellites at L2 can watch nearly the whole sky nearly continuously and heliocentric parallax has replaced geocentric as the more interesting, we are still sufficiently thin on the ground that somebody must cross mountains, oceans, and borders to assemble a critical mass of folks who are wise enough to be interested in the topics you are interested in. How thin? The total number of astronomers in the world has not been counted, but two or three times the membership of the International Astronomical Union or the American Astronomical Society (one-third of everything expensive happens in the U.S., it used to be one-half) suggests 25–30 thousand. A quick look around confirms that physicists and chemists, not to mention microbiologists, greatly outnumber us. On the other hand, we have, uniquely, the IAU, which, unlike the other 30 international scientific unions that are part of ICSU (International Council for Science, formerly International Council of Scientific Unions), has individual, and not just national or societal, members. This means that a typical IAU Symposium attracts two or three hundred participants (not all members) from two or three dozen countries. So, how did we get here; what have some of the obstacles been; and what sorts of international collaborations are with us for the present and future?

2. Before and after the Treaty of Westphalia

Was Eratosthenes the first astronomer with an international collaborator? (Carman and Evans 2015) Not really, for his 2nd century BCE measurement of the circumference of the earth was carried out when Alexandria and Syene (now Aswan) were both part of a sizeable Ptolemaic Egypt. Cyrene, where he was born, is in Libya today, and yes, those we think of as "the Greeks" worked in lands now part of Turkey, Egypt, Italy, and other places, as well as Greece. Similarly, one gets the impression from comprehensive histories of astronomy (North 2008; Hoskin 1997) that the golden age of Arabic/Moslem astronomy (though some of the practitioners were actually Christian and Jewish) coincided with the largest extents of regions governed by caliphates and other Moslem empire-like structures. In addition, Arabic astronomy also drew on earlier Greek, Persian, and Indian writings.

In contrast, the Europe of the 16th century, across which Copernicus and his first adherent, Rheticus, wandered, had nothing quite like modern boundaries to be crossed, though it was certainly possible for astronomer-astrologers to get into trouble away from home, or even close to where they had been

Figure 1. Central Europe during the life of Rheticus. The rivers, seas, and cities haven't moved very much, but the national and other political boundaries are a different story. (From Danielson 2006, with permission of the author).

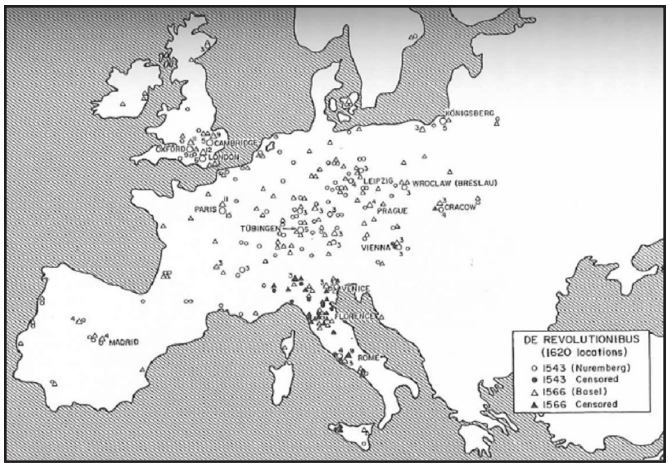

Figure 2. Locations of the censored (filled symbols) and uncensored (open symbols) copies of *De Revolutionibus* in 1620. Circles are the first edition (Nuremberg 1543) and triangles the second edition (Basel 1566). Also during the 15th and early 16th centuries, Jesuits traveled to India, China, and Japan. Their purposes were primarily apostolic rather than astronomical, but they brought with them some astronomical instruments and tables that permitted more accurate calculations of planetary motions than those then in use in the east. These were typically based on Tycho's rather than Copernicus's picture of the solar system. North (2008, p.151) says that "the long-term effect of the work of the Jesuits was great, even though between 1600 and 1640 every missionary in Japan was put to death or deported, while a similar fate met missionaries in China in 1665." (From Gingerich 2004, with permission of the author).

born (Danielson 2006; Ferguson 2002). On a map of the period (Figure 1) we recognize most of the city names but have to draw in modern national boundaries for ourselves. Copies of *De Revolutionibus* had diffused over much of the same territory by 1620 (Figure 2). Nearly all of the censored copies were in Italy, though France, Spain, Vienna, and Poland were also Catholic. They seem to have regarded the censorship as part of an internal Italian dispute (Gingerich 2015). Pan-European book fairs were also part of this pattern (Gingerich 2004). Kepler had just participated in one in Leipzig when he rode on to Regensburg and died in 1630.

It is relevant to subsequent astronomical history that the potential importance of astronomical observations and tables for navigation became clear at a time when England and France were largely unified countries, while what we now think of as Germany and Italy were patchworks of territories answerable to princes and prelates, dukes and doges, not to mention electors (of the Holy Roman Emperors). Thus the first two each had a single major observatory at Greenwich and Paris (and also single scientific societies and journals established in the 1660s) while the latter two gave birth to multiple observatories in multiple states, universities, and all.

The Treaty and Peace of Westphalia in 1648 ended the Thirty Years' War and is said to have established modern nation-states. England, Poland, Moscow, and Turkey were the only European powers not represented, while representatives from Spain, the Low Countries, the Holy Roman Empire, France, Sweden, other German entities, and the Pope were there. Sweden (which was much bigger then), France, Brandenberg, and Bavaria were confirmed in their sovereignty over their territories. The Netherlands and Switzerland were recognized as independent republics, and the member states of the Holy Roman Empire were given full territorial sovereignty over their own territories, greatly weakening the Empire (neither Holy, nor Roman, nor an Empire, as you don't need me to tell you).

The Thirty Years' War had killed a quarter to a third of the population of the German states that came to Westphalia. The underlying disputes about national territory and about heliocentric cosmologies affect what we call things to this day. Riccioli, who named most of the lunar features in 1651, gave more visible, bigger craters to the good guys and the little ones to the bad guys, so Ptolemy and Tycho are large and in regions where shadows away from full moon make them easily visible, while Copernicus and Kepler are "tossed on the Sea of Storms" (Livingston 2015). Kepler himself led a sufficiently storm-tossed life, and, in due course, his grave was destroyed by the Swedes in the sack of Regensburg (Livingston 2015) or perhaps just lost (Ferguson 2002).

While Kepler is with us, let's not suppose that relations among him and his contemporaries elsewhere were always sunny. Galileo sent telescopes to distinguished men throughout Europe, but refused Kepler's request for one (Bucciantini *et al.* 2015). Claude Mellan's 1634 map of the moon, for instance, came from a telescope with parts provided by Galileo.

Kepler had predicted the 1631 transits of Mercury and Venus, but did not live to see them, either with or without a telescope. The Mercurial was seen from Paris by Gassendi; Venus in 1631 took place during European night; but 1639 was recalculated and observed in England by Jeremiah Horrocks and William Crabtree (J. P. Luminet in Hockey *et al.* 2014 [BEAII hereafter], p. 478). William Gascoigne, another of their collaborators, was killed fighting on the royalist side in the English Civil Wars (1644), though Kepler had dedicated his *Harmonice Mundi* to James I.

Tycho and his contemporaries were able to show that the great comet of 1577 was outside the orbit of the moon using observations made just within Europe (Leverington 2013). But to measure an accurate distance for the earth-sun separation (the Astronomical Unit) using transits of Venus required a longer baseline. Edmund Halley put forward the idea in 1716 in the same time period when he organized simultaneous observations of a lunar eclipse between St. Andres and Paris to get an accurate measure of their difference in longitude. James Gregory had suggested using transits of Venus around 1670 (T. A. Dobbins in BEAII, p. 850–851). Halley himself had seen a transit of Mercury from St. Helena in 1670, when he was mapping the southern sky (Hirschfield 2001; K. K. Yeomans in BEAII, p. 891–894).

Another generic reminder: the colonial empires of Spain, Portugal, England, and France were gradually spreading outwards, and Halley at St. Helena was not on foreign soil. It was a coaling station for the East India Company by then. Napoleon at St. Helena is a different story (as well as a very elaborate solitaire game, requiring two decks of cards).

On the other hand, Nicolas-Louis de La Caille from the Paris Observatory, working at the then-Dutch Cape of Good Hope from 1750 to 1754, was an international astronomer (cataloguing southern stars and recording 42 nebulae and star clusters), the more so as he coordinated simultaneous observations by

Joseph Lalande from Berlin of positions of the moon, Venus, and Mars, aiming to measure geocentric parallaxes (M. Murarain in BEAII, p. 536–537). Lalande was, of course, French, but was "well received by Frederik II" in Berlin (S. Dumont in BEAII, p. 1264–1265). He was also part of an observing campaign for the 1753 transit of Mercury, but from nearer home in Meudon. That campaign was organized by Joseph-Nicolas Delisle, who was back home from spending 1725–1747 in Russia, where he established the St. Petersburg observatory for Peter the Great.

This brings us to the Venus transits of 1761 and 1769, which seem to have involved every living astronomer of the period of whom you have heard, and some you have not, from eight different countries, going to many more sites expected to be under friendly control. Astronomer Royal Nevil Maskelyne went to St. Helena, Charles Green to Tahiti, and Charles Mason and Jeremiah Dixon were in South Africa for both events, taking time in between to survey the line that bears their name (between Pennsylvania and Maryland). Saddest is the case of Guillaume Le Gentil, who headed for the French colony at Pondicherry to find it had just fallen to the British. Rather than make two trips, he stayed there for 1769, only to be clouded out. Returning to France, he found his job and possessions in other hands and himself officially dead (Hirshfield 2001, p. 64).

While transits were important for measuring the earth-sun distance and timing of eclipses for pinning down the theory of the moon's motion, measuring the lengths of arcs of the meridian in far away places was needed to settle whether the earth was an oblate or prolate spheroid, which sent Louis Godin from France to Peru in 1736 and de Maupertuis to Lapland. It is oblate, like Newton said.

3. The long nineteenth century

We know when it ended—August 1914. But when did it begin? Historians have suggested 1789 (U.S. Constitution and French Revolution). The routing of Napoleon would seem an alternative. For our purposes, however, any date between 1769 (the end of Le Gentil's miserable experiences with the transit of Venus) and 1798–1799 will do. The latter saw what was arguably the first international conference, the International Commission on the Metric System in Paris (Mechain and Delambres are names to look up in BEAII). Push back a decade if you wish to take in the vertical circle made by Ramsden (England) for Piazzi (Italy) with which the latter found the first asteroid in 1800. Fraunhofer in Munich made the large reflector for Dorpat, and William Herschel's reflectors were also sold all over the place, in years around 1800. North (2008, chapters 14 and 15) has a good deal more on who built what for whom, which were the biggest 19th century telescopes, and so forth. For instance, the Clark (U.S.) 30-inch mounted by Repsold (Germany) for Pulkova (Russia) was briefly the world's largest refractor.

Technological advances came not just to telescopes, but, vitally for eclipse expeditions, transits of Venus, and other long-range collaborations, to transport by land (the railways) and sea (steamships). Never again would there be anything quite like Le Gentil's Pondicherry adventure or Captain W. S. Jacob's 1862, 100-day voyage back to Madras, which ended with his death soon after, surely at least in part as a result of the very limited diet enroute. His daughters' diary of the voyage can be accessed from a Jacob family genealogy site.

Table 1. Nationalities of astronomers who met at Lilienthal in 1800.

Name	*Nationality or Location*
Bode, Johann Elert	German
Brugge, Thomas	Danish
Burckhardt, Johann Karl to Jean Charles	German to French in 1799
Bürg, Joseph T. or Johann Tobias	Austrian
Gildemeister, Johann	German
Harding, Karl Ludwig	German
Herschel, Wilhelm or William	German to English
Huth, Prof.	Frankfurt am Oder, German
Klügel, Georg Simon	German
Koch, Dr.	Danzig, German
Maskelyne, Nevil	English
Mechain, Pierre	French
Melanderhielm, Prof.	Stockholm, Swedish
Messier, Charles	French
Olbers, Wilhelm	German
Oriani, Barnaba	Italian
Piazzi, Joseph (Guiseppe)	Swiss to Italian
Rollegienrath, Schubert	Petersburg, Russian (?)
Schröter, Johann Heironymus	German
Sniadecki, Jan	Krakow, Polish-Lithuanian
Svanberg, Prof.	Uppsala, Swedish
Thulis, Jacques	Marseilles
von Ende, Ferdinand (Adolf)	German
von Zach, Franz	Hungarian
Wurm, Johann Friedrich	Stuttgart, German

The first international scientific meeting was conceivably the International Commission on the Metric System in Paris in 1798–1799, one of whose participants, Brugge, appears in Table 1. Our hero, however, is Janos Ferenc (Franz) von Zach, whose career swept across Europe (Hungary, Vienna, Lemberg, Paris, London, Seeberg Observatory near Gotha, by increments to Geneva, Naples, and back to Paris, L. Szabados in BEAII, p. 2369). In 1798 he brought together an international group at Seeberg to think about the planet that, according to Bode's Law (not a law and not due to Bode, of course), should orbit between Mars and Jupiter.

The organization was fully established in 1800 at Lilienthal, under the presidency of its director, Johann Schröter. Table 1 lists the members, a list generously provided by Gudrun Wolfschmidt (2015). At least 12 of the 25 were pretty much German, and most of the others would have had German as a strong second language. Piazzi actually found the first asteroid (Ceres) on 1 January 1800, shortly before the coordinated observations were to begin. I have always wondered whether it was in the zone he was supposed to "police," the group having been variously called the Vereinigen Astronomischen Gesellschaft, Astronomischen Gesellschaft Heimatverein, celestial police, and Himmelspolizei.

The principal was sound; Olbers doing his detective job found (2) Pallas in 1802, followed by (3) Juno in 1804, and (4) Vesta in 1807, found by Schröter's assistant Harding (Wolfschmidt 2001; Gerdes 1990). But in April 1813, the Lilienthal Observatory was heavily damaged by French soldiers retreating from Moscow, its records and equipment taken or

destroyed (C. J. Cunninghan in BEAII, p. 1953). The next asteroid was not found until 1845 by Karl Hencke. It was (5) Astra, and he had been working for 15 years from his own observatory at Driesen to find it. He also served in the Prussian military against Napoleon in 1813–1815. The last asteroid I've heard about being named for a colleague (Robert B. Brownlee) has a five-digit number, 15970.

Progressing through the century we find some well-known star catalogues (BD, CD, AGK) with input from observatories in more than one country, leading up to the *Carte du Ciel*. Those D's mean Durchmusterung, and it was Argelander of Bonn who proposed to the new Astronomische Gesellschaft that 17 observatories (many German) should produce a catalogue of all the stars down to 9th magnitude with accurate positions (Hoskin 1997, p. 259). The lagging project was overtaken by the application of photography to positional astronomy, and Admiral Mouchez, director at Paris, prompted by suggestions from Prosper and Paul Henry, convened 56 scientists from 19 nations to produce both a photographic atlas of the sky (the *Carte du Ciel*) and a catalogue with positions of all the stars down to 11th magnitude in 1887 (Hoskin 1997, p. 259; North 2008, p. 519).

All the observatories were supposed to use identical astrograph telescopes and agreed-upon methods of photography and imaging. The Permanent International Committee of the *Carte du Ciel* was an important entity from then until World War I, though no American observatory was involved. The exclusion of Germany from post-war scientific organizations (next section) required much rearrangement of the zones, and the initial IAU Commission *Carte du Ciel* (23) had H. H. Turner of England for its president. The last parts of the catalogue were published in 1964 (North 2008; Hoskin 1997; Blaauw 1994). Commission 23 was still *Carte du Ciel* in 1970, but then merged itself into Commission 24 (stellar parallax and proper motion), though some of the astrographs were still in use, and some of the plates began to be applied to proper motion studies (Dieckvoss 1970). Hale's International Union for Solar Research founded in 1907 was the other major astronomical organization in 1914. At the 1910 meeting in Pasadena, Karl Schwarzschild suggested that its remit should expand to take in all of astrophysics, and there seemed to be no objection. But at the time of the last, 1913, meeting in Bonn, it was still just the Solar Union.

As transport became faster and more reliable through the century, solar eclipse expeditions and the 1874 and 1882 transits of Venus established the custom of astronomers from many places going to many other places, most often North American and the colonies of European powers, but the long lists of eclipses attended by Lockyer (founder of *Nature*), Copeland (Astronomer Royal for Scotland), Maunder (of the minimum), Dyson (Astronomer Royal for England), and many others also took in Japan, Peru, Lapland, Sicily, and other unlikely places (see articles about them in BEAII and the Exploratorium website under solar eclipses.)

The 1868 solar eclipse as seen from India was particularly important in revealing to a Frenchman (Jules Jenssen) and an Englishman (Norman Lockyer) that you could use a spectroscope to separate out the light from the chromosphere, and that it could be done even without the eclipse (Nath 2013). The discovery of helium, however, belonged to Lockyer alone. And, looking ahead to the end of the next section, we can see that, of the astronomers who went to Sobral and Principe to test General Relativity, Eddington himself was the only chap attending his first eclipse.

The 1911 founding of the AAVSO of course belongs to the end of this (relatively) peaceful long 19th century. Variable star observing in the U.S. goes back considerably further (Saladyga 1999, who indicates that more detail is to be found in Williams and Saladyga 2011), but was initially hampered relative to European work by the non-availability of Argelander's *Uranometria Nova* (a catalogue of 3,500 northern stars from his own observations). While we have Argelander with us, it should be mentioned that he was a founder of the modern version of the Astronomische Gesellschaft in 1863 and organized 13 observatories in multiple European nations to get precise positions of all northern stars down to the 9th magnitude in his *Bonner Durchmusterung*. Completion of the 15-volume resulting AGK (*Katalog der Astronomischen Gesellschaft)* came in 1910.

Meanwhile, as it were, Benjamin Apthorp Gould, the first American astronomer trained in Europe, had visited Paris and London, picked up a doctoral degree in Göttingen, and visited Altona, home of Heinrich Schumacher, founder of *Astronomische Nachrichten*. Gould brought that idea back home as well as some star catalogues, founded *The Astronomical Journal* in 1849, got into a frightful mess in connection with Dudley Observatory, and went off to Argentina from 1870 to 1885, bringing back the plates whose eventual measurement led to the *Cordoba Durchmusterung* (T. E. Bell in BEAII, p. 833). His long-term indirect influence on Seth Chandler (who also visited Argelander in Germany), E. C. Pickering, and William Tyler Olcott also fed into the founding of the AAVSO by the third of these.

A mostly national rather than international organization, the AAVSO happily survived the organizational massacre of 1914–1919 under Olcott's secretaryship, holding its first regular meeting at Harvard College Observatory in 1915 and being incorporated in 1918 (M. Saladyga in BEAII, p. 1608). About half the Association's members are now resident outside the U.S., according to the AAVSO website.

Indeed it seemed that internationalism experienced a major growth spurt as the long century drew to a close. After meeting in Rome in 1884, the International Geodetic Association held its Washington Conference in 1885 establishing time zones (essential for railways!) with longitude 0º at Greenwich (A. R. Christie the Astronomer Royal at the time thought it best not to go to the latter meeting). According to Emerson (2013) there were, between 1900 and 1913, 426 international meetings in Paris, 168 in Brussels, 141 in London, 96 in Berlin, and a mere 14 in New York. All this came to a precipitous end with the guns of August. Astronomers were far from the only scientific sufferers. The international Association of Chemical Societies first met in Paris in 1911 and gave high priority to rationalizing the names of organic compounds and producing a fourth edition of Beilstein's catalogue. Paul Jacobson, former professor at Heidelberg, had just established a commission to get to work in the summer of 1914. When the International Union of Pure

and Applied Chemistry took over the tasks in 1919, Germans were not permitted, so Jacobson was lost to the projects, and Freidrich Beilstein would not have been allowed to work on his own catalogue if he had still been alive (Heppler-Smith 2015).

4. A deep relative minimum: 1914–1919

For astronomers, The Great War to end all Wars began with the capture of an Observatory of Berlin solar eclipse expedition under Erwin Freundlich to the Crimea in August 1914. The expedition was partly financed by the Krupp family, and the primary goal was to look for bending of starlight by the sun. They had been urged to do this by Albert Einstein (Halpern 2015) who was then expecting a value near 0.8" at the solar limb, as you can calculate for yourself, using Newtonian mechanics and a particle theory of light. Although Freundlich himself was quickly traded for a Russian prisoner of war held by the Germans, August Kühl (1916) was held for more than a year, and the equipment was never recovered. Halpern has speculated on the possible outcome if the measurement had been made, because they would presumably have found about twice the value they were expecting. Freundlich participated in other eclipse expeditions later, found a value larger than the general relativistic prediction of 1.86" at the limb, and remained somewhat out of step with the rest of the astronomical community the rest of his life (H. Kragh in BEAII, p. 757) Alan Batten, who knows a great deal about binary and variable stars, was a student in some of Frendlich's classes as an undergraduate at St. Andrews.

A very large number of physicists, astronomers, and other scientists served in a wide variety of capacities through World War I. My list of just astronomers and those in closely related sciences is three single-spaced pages, mostly survivors like Erwin Schrödinger and Rudolph Minkowski on the Austrian-Italian and German-Russian fronts, respectively. I knew only the latter, who refereed, gently and helpfully, the second paper that came out of my Ph.D. dissertation. Those killed were mostly too young to have made their reputations. But we remember Karl Schwarzschild, an over-age volunteer, who died of pemphigus (an autoimmune disorder) very soon after he wrote his famous paper on the "black hole" solution of Einstein's equations, and also Henry Moseley, of atomic weights (a young volunteer), and the younger son, Robert, a budding geologist, of Sir William H. Bragg the 1915 Nobelist. The latter two were among the 44,000 U.K., Australian, and New Zealand troops killed at Gallipoli. The Ottoman casualties were nearly double that at 84,000 and must surely also have included potential future outstanding scientists. According to a recent advertisement, Gallipoli is now a tourist destination.

The end came in 1919, with eclipse expeditions to Principe and Sobral, once again intended to look for bending of light, this time at the modern GR level, and they found it. Primary credit is generally given to Arthur Eddington, who went to Principe and whose "war work" had been planning the expedition, though the Astronomer Royal, Frank Watson Dyson, had also been involved. Himself born in 1868, Dyson remained at Greenwich through the war, continuing work on almanacs and ephemerides, but 36 members of his staff went off to war, not all to return,

ARTICLE 131.

Germany undertakes to restore to China within twelve months from the coming into force of the present Treaty all the astronomical instruments which her troops in 1900-1901 carried away from China, and to defray all expenses which may be incurred in effecting such restoration, including the expenses of dismounting, packing, transporting, insurance and installation in Peking.

Figure 3. Article 131 from the *Traité de Paix*.

and were replaced by conscientious objectors, retirees, Belgian refugees, and women (J. Tenn in BEAII, p. 629). Charles Davis and Andrew Crommelin (b. 1875 and 1864, respectively) were the actual observers at Sobral, Brazil. The two eclipses, 1914 and 1919, form symmetric bookends to the war.

But we are not yet back on peaceful soil. The year 1919 also saw the founding of the International Astronomical Union under the International Research Council, both with significant input from George Ellery Hale, whose solar Union had been abolished under the treaty of Versailles. The rules were that only "allied countries" and their scientists (the winners) could join in the first instance; neutrals later; and Germany did not adhere to the IAU until after WWII, though by the 1930s the primary barriers were financial. There was much bitterness over these restrictions in the (neutral) Netherlands, especially from Kapteyn, and obviously in Germany, where the astronomers felt that their own Astronomische Gesellschaft, with half its pre-war members non-German, was the appropriate international organization (Blaauw 1994).

The previous paragraph requires some clarification. Astronomy is mentioned in the *Traité de Paix*, an authentic, first-edition copy of which purchased recently at auction now lies on my desk, but only in Article 131 (Figure 3). Article 282 provides a list of 26 previously-existing "multilateral treaties, conventions, and agreements of an economic or technical character" allowed to survive. Hale's International Union for Solar Research is not there, though the International Agricultural Institute at Rome is. Many of the rest deal with health and safety issues, standardization (including concert pitch), and the metric system. They date from between 1857 and 1910.

The words I was looking for, however, come from Article I of the resolutions adopted at the Conference of London, October 1918, and are duplicated in the statutes of the International Astronomical Union, and quoted in Chapter I of Blaauw (1994):

> That it is desirable that the nations at war with the Central Powers withdraw from the existing conventions relating to International Scientific Associations in accordance with the Statutes or Regulations of such Conventions respectively, as soon as circumstances permit. (and)
>
> That new associations, deemed to be useful to the progress of science and its applications, be established without delay by the nations at war with the Central Powers, with the eventual cooperation of neutral nations.

Figure 3 shows Article 131 of the 1919 Treaty of Versailles, in which Germany agrees to restore to China (transport and

installation paid) all the astronomical instruments removed by her troops in 1900–1901. I rather doubt that this ever happened! (Xerocopied from a copy of the *Treaty of Peace*, purchased at auction in 2015, which once belonged to Frank W. Mason. The English text appears on the right hand, odd-numbered pages, and the French text on the left hand, even-numbered pages.) This is the only mention of astronomy in the 428-page volume. The Americans signed first, led by Woodrow Wilson, the British second, led by David Lloyd George, the French third, led by G. Clemenceau, J. van den Heuvel for Belgium (no, I don't know if the astronomer is a relative or descendent), I. J. Paderewski for Poland, and Eduard Benes for Czheco-Slovokia. The Germans were Hermann Muller and Dr. Bell, and Hedjz and Liberia were among the others. Germany was still, just, an Empire, and there were more kings and other titled folk than you would find mentioned today on any hypothetical similar treaty. The United States of America also leads the list of founding members of the League of Nations, though, in the absence of Senate approval, we were never a member. Some of the pages in my copy had not been cut, particularly in the section defining the new boundaries of Germany.

Blaauw tells much more of the story. The last (so far) entanglement of the IAU with political issues was the membership of Taiwan and China from 1959 to 1979, resolved with a decision to have one adhering nation represented by two adhering organizations, one initially located in the People's Republic of China at Purple Mountain Observatory, and one in Taiwan, ratified at the Patras IAU in 1982. Similar history, with the dissolution of the International Association of Chemical Societies in 1919 and the establishment of the International Union of Pure and Applied Chemistry, but with more rapid German consultation, is outlined by Hepler-Smith (2015). They, the International Union of Biochemists, and others welcomed one China with two adhering organizations at about the same time as did the IAU.

On the whole, the purely scientific events gradually improved, though consult Blaauw once more (pp. 12–13 and 16–17) to see that the participants at the Bonn 1913 meeting of the Solar Union look a good deal more cheerful than those at the second IAU General Assembly in Rome in 1922.

5. From war to war

Here it is necessary to distinguish between the winners and the losers. German astronomers gradually took back some of their old tasks of maintaining databases for variable stars and minor planets and the enormously valuable, *Astronomische Jahrsberichte*, but the Central Telegram Bureau remained in Copenhagen and time in Paris. But you can walk along the shelves of any library that still keeps paper copies of journals (if you can find one!) and see that their publication rate was climbing back only very slowly (in physics and chemistry, as well as astronomy) even before the depression hit everyone, but Germany and Austria harder than most.

Meanwhile there is a definite exuberance to the state of astronomy (as well as many other things) in the United States (see Trimble 1995 on the cultural background of the Curtis-Shapley debate). Dorrit Hoffleit (2002), because of her German parents and names, was considered a natural enemy of her playmates in 1917–1918, but firmly advanced to be paid half as much as the men (40 cents/hour) at Harvard College Observatory during the Depression, onward to war work at Aberdeen Proving Ground, partly under Edwin Hubble, and through many triumphs and occasional vicissitudes to have her autobiography published by the AAVSO, of which she had been president in 1961–1963.

Hubble? Didn't we leave him enroute to Europe as a volunteer when the U.S. entered WWI? Yes, and Shapley the same year took up an appointment at Mt. Wilson, carrying out with the 60-inch telescope some of the things that Hubble later said he had planned to do. They would probably not have been bosom buddies in any case (Sandage 2004), but competition for photons did not improve the situation. They diverged also in the second war, Shapley staying put at Harvard and Hubble heading to Aberdeen, Maryland, to work in the ballistic missile laboratory. Of the other stars of the 1920 debate, Hale spent the years 1916–1918 establishing the National Research Council, while Heber Curtis taught navigation and worked in the optical section of the National Bureau of Standards. Harvard under Shapley produced one third of the American Astronomy Ph.D.'s from 1930 to 1940 (Sandage 2004). Caltech produced two (Josef Johnson and Olin C. Wilson), and they were not Hubble's students. Indeed Hubble had none, though Sandage as a Caltech graduate student and George Abell as an undergrad worked with him.

Meanwhile the IAU had grown from 207 members and 19 countries at the Rome General Assembly (1922) to 554 members and 26 countries at the Stockholm General Assembly (1938). But national affairs were beginning to affect international collaborations. The Stalinist purges beginning in 1936–1937 led to the loss of about nine IAU members (Blaauw 1994), of whom the best-known in Europe and America (which is what got him into trouble) was Boris Gerasimovich (K. Haramundanis in BEAII, p. 796).

In the same time frame, astronomers and many others began leaving Germany and, later, Austria because they were Jewish, had Jewish family, or were otherwise displeasing to the authorities. Einstein was the best known (and among the first to leave), Baade moved voluntarily from Hamburg to Mt. Wilson in 1931, and Minkowski (with a Jewish father-in-law) lost his professorship in 1935 and made it to Mt. Wilson soon after (I. T. Dunham in BEAII, p. 1391). Martin Schwarzschild, whose father you met in section 4, despite being the son of a war hero (with a non-Jewish mother), thought it wisest to finish up his Göttingen Ph.D. very quickly in 1935, moving on via Leiden, Oslo (as a Nansen fellow), the U.K., and on to the U.S. in 1937 (Trimble 1997). A number of future astronomers and physicists were among the nearly 10,000 children ages 3–16 who left Germany, Austria, and Czechoslovakia via the Netherlands for Britain in 1938–1939 as part of the Kindertransport. The number indeed seems large compared to the number of physical scientists among the population of any country then or now, so I suppose it must have been some sort of a class distinction that carried over to the next generation.

6. The Second World War and immediate aftermath

Some cultures are said to distinguish three classes of people: the living (whom one insults at one's peril), the far dead (like Tycho, Kepler, and Galileo, about whom you may say what you please, at risk only of your academic reputation), and the near dead (who are still remembered with friendship, blood ties, admiration, or hatred by folks still living, and so about whom you speak or write with caution). The people and events of the Second World War still, just, belong to this precarious near-dead category. I am the widow of a 1940 graduate of the U.S. Naval Academy who was on USS *Lexington* when she steamed out of Pearl Harbor on the 6th of December 1941, had her sunk out from under him at the Battle of the Coral Sea, went on to skipper a submarine chaser back and forth across the Atlantic a number of times, and participated in the Sicilian landing. But he later had close scientific collaborations with Japanese and Italian colleagues and somewhat more cautious ones with German physicists and astronomers.

That being said, the main cause of World War II was World War I and the incredible provisions of the Treaty signed at Versailles on June 28, 1919, by 60 men from five Allied Countries, 22 Associated Countries, and Germany. The required "reparations" exceeded the income of Germany by some sizable factor, and she was expected to get permission from Allied Commissions to repair her railroads, dredge her canals, and even less seemingly-other-regarding activities. There were also consequences for Austria, Hungary, Italy, Turkey, and Denmark, though they were not signatories but were covered by other, later treaties.

The sum total of slaughter and suffering was, as during the first war, beyond description, though again the "horror weapon" (atomic bomb) was not the main killer, as poison gas had not been in the first war. Book-length treatments (Hastings 2015; Beevor 2015) continue to appear, which you can peruse for accounts of cannibalism and all the rest (though little mention of science per se except as a weapon in the form of radar, rockets, and bombs). On a personal level, Blaauw (2004) noted that, of his group of six close friends at Leiden Observatory, two became famous (Blaauw himself and Wesselink of the Baade-Wesselink method for measuring Cepheid distances), one spent the war as a high school teacher, and three died in Indonesia as Japanese prisoners of war.

As for the IAU, battle lines quickly separated the British president (Eddington, who was to die in 1944), the Dutch secretary (Oort), and vice presidents in Italy, Poland, Sweden, France, Switzerland, and the United States. Walter S. Adams at Mt. Wilson became the secretary. Remarkably, the collection of national dues and support of ongoing projects continued to take place separately in the blocks of countries held by Germany and by the opposition ("allies" at this point is an excessively charged word!)

In some ways, at least, the war-engendered ruptures healed faster than after the first war. The surviving members of the IAU executive committee and other distinguished astronomers met in Copenhagen in March 1946 at the invitation of Ellis and Bengt Strömgren (father and son). The obvious winners, plus Czechoslovakia, Poland, and Russia were represented; Germany and Japan were not, and the initial proposals for new commission members included no one from those two major losers. Abetti from Florence, Italy, however retained his vice-presidency. An exceedingly large number of issues were discussed informally over the next two years and ratified at the 1948 General Assembly in Zurich (Blaauw 1994).

Some of the specifically international items were: (1) establishment of new commissions on international observatories and exchange of astronomers (among member nations). (2) Prager had died in 1945, and the Belin-Babelsburg Observatory was not in a position to continue cataloguing, naming, and collecting data on variable stars, so the task was handed over to B. V. Kukarkin and P. P. Parenago in Moscow. (3) Many other tasks that had been historically German were spread out among Potsdam (East Germany/DDR), Heidelberg (West Germany/DBR), Cincinnati, and Leningrad. (4) The enormously valuable *Jaharesberichte*, suspended after 1940 but with supplemental efforts in France, also ended up in Heidelberg, with publication shifting to Springer Verlag in 1969 under the title *Astronomy and Astrophysics Abstracts*, only recently discontinued. (5) And yes, Germany was admitted and Japan (a 1919 founding member) readmitted to Union membership at the 1952 General Assembly at Rome (the same one where Baade cut Hubble's constant in half and so doubled the length scale and age of the universe). That 1952 General Assembly replaced one previously scheduled for 1951 in Leningrad, a victim of the gradually-rising tensions of what was soon named the Cold War, though Americans went to Moscow in 1958 and Russians to Berkeley in 1961. 1964 was held in Heidelberg, recognizing the healing of that rift, at least for people too young to remember.

But let us end this section on a note of at least moderate astronomical cheer. The United Nations has never drawn unqualified praise (though more than the League of Nations, whose charge is part of the 1919 Peace Treaty). But UNESCO (the United Nations Educational, Scientific, and Cultural Organization into which Shapley is said to have inserted the S) became a supporter of the IAU projects to the tune of $49,884 over 1948–1951, nearly equal to the sum of national contributions through the same period. The money paid for many projects of the individual Commissions and the central Bureau, which in those days moved after each General Assembly to the home of the new General Secretary.

At least three other (mostly) good things came out of the war: (1) engineers (etc.) with radar dishes pointed them up and became radio astronomers (some German dishes having been moved to England and Holland for the purpose); (2) captured V-2 rockets and rocketeers began carrying UV and X-ray detectors above the atmosphere, seeing, first the sun (Hufbauer 1991), and, in modified form, Sco X-I and the Crab Nebula; and (3) people, both those forced immigrants of 1933–1945 and after, and those honed in the Manhattan Project, turned much of their attention to fundamental problems in physics and astronomy. Development of computers (now meaning machines rather than women paid at most 40 cents per hour!) should probably also be counted among the pluses.

Widespread destruction in Europe, Japan, China, and elsewhere, coupled with outstanding observing sites in the United States and rapidly-developing computational equipment

and skills at Los Alamos, Lawrence Radiation Lab, and elsewhere, meant that post-war leadership in astronomy moved firmly to the United States. The rest of the world has at least caught up since then.

7. Now and into the future

It is somehow fitting that, since both World Wars started as European disputes, Europe has moved furthest toward integrating many things today. The first large pan-European organization was CERN (The European Organization for Nuclear Research), established with help from UNESCO. Its structural plan was sound enough that many aspects of the European Southern Observatory were modeled on it (Blaauw 2004; Woltjer 2006), though it all took some time. Discussions started in 1953, the requisite treaties were signed in 1962, and "first light" at La Silla came in 1966 with a 1-meter reflector. The situation has since improved enormously. The five founding partners, Belgium, France, Germany, the Netherlands, and Sweden, have expanded to 17, including Brazil and covering the map of western Europe with little holes for Ireland, Norway, and Luxemburg. The merging of a handful of national journals into *Astronomy and Astrophysics* in 1969 has been almost as successful, and now involves a larger number of countries, paper being cheaper than optical-quality glass.

Other ongoing successes have included the European Very Long Baseline (radio) Interferometer (which now extends Eastward to China) and the European Space Agency (ESA), a yet slightly different partnership that began life as ESRO (European Space Research Organization) with an Austrian-English Jewish director, Sir Hermann Bondi.

Space and even ground-based facilities have become so expensive that many of the most productive now and in the future will extend past these "small" international collaborations to take in all of Europe, much of Asia, the United States, Australia, and Canada, and non-governmental partners, universities, foundations, and commercial organizations. The Hubble Space Telescope, an early ESA-NASA partnership, has set a standard for this sort of thing. ALMA, the now-nearly-complete Atacama Large Millimeter Array, involves Europe, the U.S., Canada, Japan, and, of course, Chile, where it is located. The 20–40-meter class optical telescopes planned for the next decade—E-ELT (European Extremely Large Telescope), TMT (Thirty Meter Telescope), GMT (Giant Magellan Telescope), and the radio SKA (Square Kilometer Array) will bring in many countries, including China, that have not previously been partners in world-wide astronomy. I find particularly hopeful plans for an East Asian telescope involving China, Japan, Taiwan, and South Korea, with some input from Chinese-American astronomer Ron Taam (2015). Parts of SKA will also involve South Africa and Australia, and H.E.S.S. (High Energy Stereoscopic System—a high energy gamma-ray detector) is in Namibia.

The U.S. attitude could still use a little fine tuning. A prepublication copy of *New Worlds, New Horizons* (National Research Council 2010) says (p. 3–4) "nearly all of this report's ranked recommended projects have opportunities for contributions—often substantial—by foreign partners." The very long lead times, costs, and disagreements on priorities are tempting ESA and NASA to try once more to go it alone, with unavoidable loss of capabilities of the missions.

There is now so much going on that everything you pick up is likely to have an item relevant to international astronomy successes (or failures), or light as a symbol of something good or as a pollutant for astronomy as well as wildlife. Here are a very few to check and decide for yourself whether they belong on the plus or minus side.

• Li *et al.* (2015) on magnetic fields in star forming regions has authors from Hong Kong, Beijing, Taipei, Nanjing, and Harvard.

• SESAME, a synchrotron light source being constructed in Lebanon, is a collaboration involving the Palestinian Authority, Israel, and about a dozen other Middle Eastern nations (Winnick 2015).

• Construction of the Large Synoptic Survey Telescope has been in happy partnership with Chile, its host; the construction of the Thirty Meter Telescope on Maunakea has been interrupted (at best) by lack of agreement between the many partners (Americans and international) and the descendants of the citizens of the former nation hosting it. By the way, Mauna Kea is "a white mountain," while Maunakea is "the white mountain," and is the form preferred by the locals.

• The European Association for Chemical and Molecular Sciences organized a 3-day conference on the 22 April 2015 (centenary of the first extensive use of chemical weapons) to discuss how to improve international laws to prevent the future use of such weapons. Where was the conference? Ypres, Belgium, of course.

• A spread on "The Next Great Exoplanet Hunt" (Heng and Winn 2015) characterizes 4 prospective missions as pure ESA (CHEOPS, PLATO) or pure NASA (TESS, Kepler2). Don't try to remember the names; they will all have changed many tines before anything flies. The article is also wrong about the main reason that apparently bright stars are much less common than apparently faint stars.

• A Swedish colleague has just called my attention to a published use of the phrase "dunkle materie" by Knut Lundmark (1931) with a fairly good estimate of the amount in a couple of galaxies. Notice that 1931 is before 1933, and yet Fritz Zwicky is virtually always given credit for the German phrase, because search engines do not easily find the Swedish paper.

• The next few space detectors for gamma-rays will come neither from ESA nor from NASA but from approved Chinese (2) and Russian (1) planned launches for about 2020 (Bergstrom 2015).

• The Nuclear Science Advisory Committee (advisory to the

U.S. Department of Energy) has put as its first priority either turning the Relativistic Heavy Ion Collider (Brookhaven National Laboratory, Upton, New York) or the Continuous Electron Beam Accelerator Facility (Newport News, Virginia) into an electron-ion collider to maintain an American "world leadership position." But folks not on the committee say it cannot be done without international buy-in, as has also turned out to be necessary for the Long Baseline Neutrino Experiment. Each of them, when/if, will yield results useful for astrophysics and cosmology.

• The International Dark Sky Association has found a few places to declare successfully dark sites, and not just because of tanking economies (the surest way to darken skies). But I think probably that even the U.S. can learn to become as international as Schröter's and von Zach's "celestial police" and as international as world conditions will let us be.

8. Acknowledgements

I am indebted to AAVSO Director Stella Kafka and *JAAVSO* Editor John Percy for the invitation to assemble this oddly-motivated assortment of items from the history of astronomy and related fields; to Dennis Danielson and Owen Gingerich for permission to use maps from their books; to Robert Cumming of the Onsala Space Observatory for transmission of the Bergstrom presentation and the Lundmark paper (in proper German); to editor Michael Saladyga for fine-tuning the text and references; to the late Frank W. Mason, the original owner of my copy of the 1919 *Traite de Paix*; and especially to Alison Lara for her, as always, excellent transformation of a typed original into a submittable keyboarded script.

References

Beevor, A. 2015, *The Second World War*, Little, Brown, and Co., Boston.

Bergstrom, L. 2015, presentation on dark matter at Onsala, 17 April 2015.

Blaauw, A. 1994, *History of the IAU: The Birth and First Half-Century of the International Astronomical Union*, Kluwer Academic Publishers, Dordrecht.

Blaauw, A. 2004, *Ann. Rev. Astron. Astrophys.*, **42**, 1.

Bucciantini, M., Camerota, M., and Giudice, F. 2015, *Galileo's Telescope: A European Story*, Harvard Univ. Press, Cambridge, MA.

Carman, C. C., and Evans, J. 2015, *Isis*, **106**, 1.

Danielson, D. 2006, *The First Copernican: Georg Joachim Rheticus and the Rise of the Copernican Revolution*, Walker & Co., New York.

Dieckvoss, W. 1970, in C. de Jager ed. *Transactions of the IAU Reports on Astronomy Vol. XIVA*, Reidel, Dordrecht, 225.

Emmerson, C. 2013, *1913: In Search of the World Before the Great War*, Public Affairs, New York.

Ferguson, K. 2002, *Tycho and Kepler: The Unlikely Partnership That Forever Changed Our Understanding of the Heavens*, Walker & Co., New York.

Gerdes, D. 1990, *Die Geschichte der Astronomischen Gesellschaft gegründet in Lilienthal am 20. September 1800. Die ersten 63 Jahre ihres Bestehens von 1800 bis 1863*, Heimatverein, Lilienthal, Germany, 28 ff.

Gingerich, O. 2004, *The Book Nobody Read: Chasing the Revolutions of Nicolaus Copernicus*, Walker & Co., New York.

Gingerich, O. 2015, private communication.

Halpern, P. 2015, *Einstein's Dice and Schroedinger's Cat: How Two Great Minds Battled Quantum Randomness to Create a Unified Theory of Physics*, Basic Books, New York.

Hastings, M. 2015, *All Hell Let Loose: the World at War 1939–45*, Harper Press, London.

Heng, K., and Winn, J. 2015, *Amer. Scientist*, **103**, 196.

Hepler-Smith, E. 2015, *Chem. Int.: News Magazine of IUPAC*, **37**, No. 2, 10.

Hirshfield, A. 2001, *Parallax*, W. H. Freeman, New York, esp. pp. 64-65.

Hockey, T., Trimble, V., Williams, T. R., Bracher, K., Jarrell, R., Marché, J. D., Palmeri, J., and Green, D., eds. 2014, *The Biographical Encyclopedia of Astronomers*, 2nd ed., Springer, Berlin.

Hoffleit, D. 2002, *Misfortunes as Blessings in Disguise: The Story of My Life*, AAVSO, Cambridge, MA.

Hoskin, M., ed. 1997, *Cambridge Illustrated History of Astronomy*, Cambridge Univ. Press., Cambridge.

Hufbauer, K. 1991, *Exploring the Sun: Solar Science Since Galileo*, Johns Hopkins Univ. Press, Baltimore.

Kühl, A. 1916, *Sirius*, January, p. 19 (in 3 parts).

Leverington, D. 2003, *Babylon to Voyager and Beyond: A History of Planetary Astronomy*, Cambridge Univ. Press, 141–142.

Li, H.-B., *et al.* 2015, *Nature*, **520**, 518.

Livingston, A. 2015, *Sky & Telescope*, **129**, No. 5 (May), 26.

Lundmark, K. 1931, *Lund Medd.*, No. 125, 1.

Nath, B. B. 2013, *The Story of Helium and the Birth of Astrophysics*, Springer, Berlin.

National Research Council (Committee for a Decadal Survey of Astronomy and Astrophysics, Board on Physics and Astronomy, Space Studies Board, Division on Engineering and Physical Sciences, and National Research Council). 2010, *New Worlds, New Horizons in Astronomy and Astrophysics*, National Research Council, Washington, DC (the 2010 Decadal Review, often called the Blandford Report).

North, J. 2008, *Cosmos: An Illustrated History of Astronomy and Cosmology*, Univ. Chicago Press, Chicago.

Saladyga, M. 1999, *J. Amer. Assoc. Var. Star Obs.*, **27**, 154.

Sandage, A. 2004, *Centennial History of the Carnegie Institute of Washington, Vol. I: The Mt. Wilson Observatory*, Cambridge Univ. Press, Cambridge.

Schwarzschild, Nationale Entwicklungen und Internationale Beziehunger im 10 Jahrhunderst, Harri Deutsch, Frankfurt am Main (*Acta Historia Astronomicae* **14**, 182.

Taam, R. 2015, private communication.

Trimble, V. 1995, *Publ. Astron. Soc. Pacific*, **107**, 1133.

Trimble, V. 1997, *Publ. Astron. Soc. Pacific*, **109**, 1289.

Williams, T. R., and Saladyga, M. 2011, *Advancing Variable Star Astronomy, the Centennial History of the American Association of Variable Star Observers*, Cambridge Univ. Press, Cambridge.

Winnick, H. 2015, private communication.
Wolfschmidt, G. 2001, "Internationalität von VAG (1800) bis zur Astronomischen Gesellschaft," in Dick, S., Wolfgan, R., and Hamel, J. eds., Astronomice von Olbers bis Schwarzschild, Nationale Entwicklungen und Internationale Beziehunger im 10 Jahrhunderst, Harri Deutsch, Frankfurt am Main (*Acta Hist. Astron.*, **14**, 182).
Wolfschmidt, G. 2015, private communication.
Woltjer, L. 2006, *Europe's Quest for the Universe*, EDP Sciences, Les Lilis, France.

Letter to the Editor

The End of an Era

James W. Hanner
18 Alyssum Drive, Amherst, MA 01002; msh_jwh@yahoo.com

Received August 31, 2015; accepted September 10, 2015

Your readers may be interested in this follow-up to my article on Margaret Harwood, the first—and longest serving—Director of the Maria Mitchell Observatory (Hanner 2015).

At Maria Mitchell Observatory on Nantucket Island, a 45-year era ended on June 1, 1957. The moment of transition was recorded in a letter which came to light in, of all places, Hawaii.

One evening in 1991, during a conversation with astronomer Dr. George Herbig at the University of Hawaii, the subject of Maria Mitchell Observatory arose. Professor Herbig asked if I would be interested in correspondence between Margaret Harwood and himself. The letter (now in my possession) was interesting, then became compelling when one date caught my eye. George Herbig had asked Margaret Harwood to observe the variable star CM Aquilae. The Harwood letter discusses the night's observations and notes the CM Aql magnitude to be fainter than 16.4.

Margaret Harwood had continued interest in this "peculiar" variable. It was discovered at MMO on May 19, 1925, by Margaret Walton (then Miss Harwood's assistant, later to become Director of the American Association of Variable Star Observers, Margaret Walton Mayall. In her publication "The Variable Stars in the Scutum Cloud" Harwood (1962) refers to the star as a "nova-like variable" and lists 5 maxima between 1914 and 1951 (p. 405). The final and largest of the 165 identification charts is of CM Aql (p. 464). In her announcement of the discovery, Harwood noted the similarity in spectrum to the variable Z Andromedae (Harwood 1925). Recent publications describe CM Aql as a symbiotic variable with a long period of 1,058 days. The object is both a variable and a binary in an orbit bringing the two stars close enough to interact. One star is a red giant transferring material to a hot blue star or possibly a white dwarf.

And so, an era ended. When she opened the dome the evening of May 31, 1957, to observe CM Aql, Margaret Harwood was Director of Maria Mitchell Observatory. At dawn on June 1, 1957, she closed the dome as retired Director.

References

Hanner, J. W. 2015, *J. Amer. Assoc. Var. Star Obs.*, **43**, 84.
Harwood, M. 1925, *Bull. Harvard Coll. Obs.*, No. 826, 3.
Harwood, M. 1962, *Ann. Leiden Obs.*, **21**, 387.

Abstracts of Papers and Posters Presented at the 104th Spring Meeting of the AAVSO, Held in Muncie, Indiana, June 4–6, 2015

General Paper Session Part I

Light Curves and Period Changes for Type II Cepheids in the Globular Cluster M13

Horace A. Smith
Michigan State University, Department of Physics and Astronomy, Bio-Physical Sciences Building, 567 Wilson Road, East Lansing, MI 48824; smith@pa.msu.edu

Mary Anderson
P. O. Box 300, North Highlands, CA 95660; address email to H. A. Smith, smith@pa.msu.edu

Wayne Osborn
Central Michigan University and Yerkes Observatory, 118 Eagle Pointe Drive, Unit C, Delevan, WI 53115; wayne.osborn@cmich.edu

Andrew Layden
Bowling Green State University, Department of Physics and Astronomy, 104 Overman Hall, Bowling Green, OH 43403; laydena@bgsu.edu

Grzegorz Kopacki
Instytut Astronomiczny, Uniwersytet Wrocławski, Kopernika 11, 51-622Wrocław, Poland; kopacki@astro.uni.wroc.pl

Barton Pritzl
Department of Physics and Astronomy, University of Wisconsin Oshkosh, Oshkosh, WI 54901; pritzlb@uwosh.edu

Andrew Kelley
Bowling Green State University, Department of Physics and Astronomy, 104 Overman Hall, Bowling Green, OH 43403

Keith McBride
Bowling Green State University, Department of Physics and Astronomy, 104 Overman Hall, Bowling Green, OH 43403

Michael Alexander
Lehigh University, Department of Physics, 16 Memorial Drive E., Bethlehem, PA 18015; mia313@lehigh.edu

Charles Kuehn
University of Sydney, 44 Rosehill Street, Redfern, NSW 2042, Australia; kuehn@physics.usyd.edu.au

Aron Kilian
Department of Physics and Astronomy, Michigan State University, East Lansing, MI 48824

Eric King
Department of Physics and Astronomy, Michigan State University, East Lansing, MI 48824

David Carbajal
Department of Physics and Astronomy, Michigan State University, East Lansing, MI 48824

R. Lustig
Department of Physics and Astronomy, Macalester College, Saint Paul, MN 55105

Nathan De Lee
University of Nebraska at Kearney, 2401 11th Avenue, Kearney, NE 68849

Abstract B, V, and Cousins I-band light curves have been observed for the type II Cepheids V1, V2, and V6 in the globular cluster M13. These are relatively short period, BL Her-type Cepheids, with periods of 1.5, 5.1, and 2.1 days, respectively. Additional observations of V2 have been obtained from early photographic plates in the Yerkes Observatory archive. Long term period changes of these Cepheids have been determined by combining recent photometry with earlier observations that now extend back for more than a century. The observed period changes for V1, V2, and V6 are compared with the predictions of stellar evolution theory, under the assumption that the progenitors of the Cepheids were stars that at one time were on the blue horizontal branch.

The BSU Short Period Variable Stars Progam (poster)

Robert Berrington
Ball State University, Dept. of Physics and Astronomy, Muncie, IN 47306; rberring@bsu.edu

Thomas Jordan
Ball State University, Department of Physics and Astronomy, Muncie, IN 47306

Erin Tuhey
Ball State University, Department of Physics and Astronomy, Muncie, IN 47306; emtuhey@bsu.edu

Abstract Recent large area sky surveys like the Northern Variability Sky Survey (NSVS), and the All Sky Automated Survey (ASAS) have discovered numerous variable stars in the magnitude range $8 < V < 15$. While these surveys will extend our knowledge of luminosity variability to much fainter systems ($V < 15$) their large area coverage prevents the systematic temporal coverage or accurate photometric coverage needed to accurately study these systems. We have begun a program to obtain

accurate photometric measurements of select variable stars detected with both the NSVS and ASAS for further study. All photometric measurements are obtained by the Cooper Science Rooftop observatory located on the BSU campus in Muncie, Indiana, the SARA-KP 1-meter or the SARA-CT 0.6-meter telescopes at Kitt peak and Cerro Tololo. The naturally modular nature of the study makes this program ideal for students. I will summarize the work that has been done to date with both students and faculty at BSU.

Adventures in Transformations: TG, TA, Oh My! (poster)

Marco Ciocca
Department of Physics and Astronomy, Eastern Kentucky University, 521 Lancaster Avenue, Moore 351, Richmond, KY 40475; marco.ciocca@eku.edu

Abstract AAVSO made available, through the great volunteer work of Gordon Myers and George Silvis, two very useful tools, Transform Generator and Transform Applier (TG and TA) for transforming instrumental magnitudes to the standard system. I will juxtapose the steps necessary to obtain transformation parameters "the old fashion way" and how can the same result be achieved with these two tools. I will present transformation parameters for the Eastern Kentucky University (EKU) telescope obtained with the standard field M67. These parameters were applied to photometric results for AE UMa, a short-period, high-amplitude δ Scuti star (Period ~ 0.086 d).

Sunlight in the Spotlight in the International Year of Light (poster)

Kristine Larsen
Department of Physics and Earth Sciences, Central Connecticut State University, 1615 Stanley Street, New Britain, CT 06053; Larsen@ccsu.edu

Abstract One of the main focuses of the International Year of Light (IYL) is interdisciplinary education and outreach. While variable stars in general provide myriad opportunities to accomplish this, one variable star in particular—our sun—offers unique opportunities in this vein. From conducting ground-based safe solar observations with white light and hydrogen alpha filters, to highlighting satellite observations at other wavelengths and spectroscopy, observing our nearest star provides a solid basis from which to explore the electromagnetic spectrum (and the relevant technologies used to study it). The IYL highlights cultural astronomy, the history of science, and the important role women have played in our understanding of the natural world. Not only was the primary deity in many cultures the sun god or goddess, but the motions of the sun across the heavens were carefully studied using sundials, astrolabes, and monolithic structures (including Stonehenge). Sunspots were discovered long before the invention of the telescope, and their occurrences carefully recorded. Today, these records (along with records of another important way the sun interacts with our planet, namely the creation of aurorae) extend our understanding of the solar cycle backwards in time across the centuries to before the time of Galileo. Women have played an important role in our observation and understanding of the sun, including Annie Maunder at the Royal Greenwich Observatory and Elizabeth Brown, Solar Section Director of the British Astronomical Association. The sun also played a central role in verifying Einstein's General Theory of Relativity (itself celebrating its centenary during the IYL). This poster will provide examples of sun-centered projects and activities that can be used during the IYL and beyond to educate and interest citizens young and old about our nearest star, with an eye to especially highlighting the importance of the ongoing work of the Solar Section of the AAVSO.

Variable Star Projects—A Southern Perspective (poster)

Andrew Pearce
35 Viewway, Nedlands, WA 6009, Australia; andrew.pearce@woodside.com.au

Stan Walker
P. O. Box 173, Awanui, Northland 0451, New Zealand; astroman@paradise.net.nz

Abstract The group Variable Stars South is based on the concept of projects in different fields of variable star astronomy which are expected to provide useful information about a star or stars on a time scale of a year to a decade—there are a few exceptions. This poster covers projects and results for binary stars, Cepheids, Mira stars, and some others, and also the techniques in use—visual observing, CCD and DSLR photometry, and some spectroscopy. We also look at some of the problems associated with a lack of adequate longitude coverage in a very watery hemisphere!

The SIDdatagrabber (poster)

George Silvis
194 Clipper Road, Bourne, MA 02532; gasilvis@gmail.com

Abstract The Stanford/SARA SuperSid project offers an opportunity for adding data to the AAVSO Sudden Ionospheric Disturbance (SID) Monitoring project. You can now build a SID antenna and monitoring setup for about $150. With the SIDdatagrabber application you can easily re-purpose the data collected for the AAVSO.

Transforms Explained (poster)

George Silvis
194 Clipper Road, Bourne, MA 02532; gasilvis@gmail.com

Abstract This presentation gives a review of why and how transforms are applied to your photometric data and a visualization of what happens to your data when they are transformed.

General Paper Session Part II

Double Trouble

Mike Simonsen
AAVSO Headquarters, 49 Bay State Road, Cambridge, MA 02138; msimonsen@aavso.org

Abstract Variable stars with close companions can be difficult to accurately measure and characterize. The companions can create misidentifications, which in turn can affect the perceived magnitudes, amplitudes, periods, and colors of the variable stars. We will show examples of these Double Trouble stars and the impact their close companions have had on our understanding of some of these variable stars.

Standard Stars for the BYU H-α Photometric System

Michael Joner
Brigham Young University, Department of Physics and Astronomy, N488 ESC, Provo, UT 84602; xxcygni@gmail.com

Eric Hintz
Brigham Young University, Department of Physics and Astronomy, N480 ESC, Provo, UT 84602; hintz@physics.byu.edu

Abstract We present primary standard stars for the Brigham Young University (BYU) H-alpha photometric system. This system is similar to the H-beta photometric system that is often used with the intermediate band uvby system. Both systems use the difference between magnitudes measured in a wide (15–20-nm) and narrow (3-nm) bandpass centered on one of the strong Balmer lines of hydrogen to establish a color index. Line indices formed in this manner are independent of atmospheric extinction and interstellar reddening. These indices provide intrinsic measures of effective temperature for stars with spectral types between B and G.

The present primary standard stars for the BYU system is established using spectroscopic observations that cover the region between the H-alpha and H-beta lines. The indices were formed using synthetic photometry reductions to convolve ideal filter profiles with the observed spectra. The number of observations per star is generally in excess of 25. Some stars have been observed more than 100 times over a period of 7 years. The typical error per observation for these stars is on the order of 1–3 mmag. In addition to the standard field stars, we present H-alpha and H-beta observations of individual stars that are members of selected open clusters. These include the Hyades, Pleiades, Coma Berenices, and NGC 752 clusters. Additional stars that exhibit varying degrees of hydrogen emission are easily distinguished in a plot of the alpha-beta plane. We have found that candidates for emission line objects, high mass x-ray binaries, and young stellar objects are readily identified in our alpha-beta plots.

We acknowledge continued support from the BYU College of Physical and Mathematical Sciences as well as support from NSF Grant AST #0618209. We also thank the Dominion Astrophysical Observatory for continued allocation of robotic observing time for spectroscopy on the 1.2-m telescope.

Roll-Off Roof Observatory Construction

Joseph H. Ulowetz
855 Fair Lane, Northbrook, IL 60062; joe700a@gmail.com

Abstract This presentation discusses lessons learned about building an observatory by someone with limited construction experience, and the advantages of having a observatory roll-off roof for imaging and variable star studies. Sample results shown of composite light curves for cataclysmic variables UX UMa and V1101 Aql with data from my observatory combined with data from others around the world.

General Paper Session Part III

Thomas Cragg Proves to Be a Good Observer

Rodney Howe
3343 Riva Ridge Drive, Fort Collins, CO 80526; ahowe@frii.com

Frédéric Clette
World Wide Data Center SILSO, Royal Observatory of Belgium, Av. Circulaire, 3-B-1180 Brussels, Belgium; frederic.clette@oma.be

(presented by Roger Kolman and Kristine Larsen)

Abstract Longtime AAVSO member and observer Thomas A. Cragg proves to be a good solar observer, good enough to be included in the club of 21 long-duration stations without major stability problems over the interval 1945–2015. However, his sunspot counts seem to make a slight downward jump in 1983, and there is a sharp decline in the last two years of his observing career (due to aging?). Cragg's observations will be used for the equivalent comparison with the new reconstructed sunspot number that is produced from the 21 stations showing the same features in the past six solar cycles. This reconstructed number is fully independent from the original Zürich sunspot number. It actually confirms the corrections being applied to the original sunspot number series (a more simple approach simply multiplying the original series by the correction factor established for the Locarno Observatory's drift), as published in the 2014 paper by Frédéric Clette et al. (Space Sci. Rev., 186, 1–4, pp. 35–103).

Searching for Motion within the Solar Atmosphere

Susan N. Oatney
9516 West Morgan Avenue, Partridge, KS 67566; susanoatney@emypeople.net

Abstract The mystery of heat transfer within the solar atmosphere has long been a subject of study and debate. Not unlike large solar observatories that are funded by public monies, amateur solar observers also have a keen interest in

this subject, and are able to creatively employ tools at hand such as a two-slit interferometer used to create interference lines in an attempt to measure motion (interference patterns: http://en.wikipedia.org/wiki/Double-slit_experiment). With a 6-inch equatorially pier-mounted refractor focused just above the visible disk of the sun, images were taken with a Meade Lunar Planetary Imager video LPI CMOS camera at ~30 Hz sample rates and stored as FITS files. A variety of photometry, unrated color, and full-aperture solar filters were combined with and without a two-slit interferometer placed at the focus of the telescope. These images, explored through the NASA FITS viewer (http://heasarc.gsfc.nasa.gov/docs/software/ftools/fv/), were applied to show logarithmic color contours. Selected fv images were placed consecutively in a movie format that shows some cyclical motion around and between the contours, mostly of the solar corona.

Study of Eclipsing Binary Systems NSVS 7322420 and NSVS 5726288

Matthew Knote
Department of Physics and Astronomy, Ball State University, Cooper Physical Science Building, room 101, Muncie, IN 47306; physics@bsu.edu

Abstract In this paper, I present photometric data collected on two β Lyrae-type eclipsing binary systems: NSVS 7322420 and NSVS 5726288. I also present the results of the analysis of the data. This was done by modeling the systems using the Wilson-Devinney code to determine the characteristics of the stellar components. The analysis indicates that NSVS 7322420 is a semi-detached system while NSVS 5726288 is a detached system.

A Search for Exoplanets in Short-Period Eclipsing Binary Star Systems

Ronald Kaitchuck
Ball State University Department of Physics and Astronomy, Muncie, IN 47306; rkaitchu@bsu.edu

Garrison Turner
Big Sandy Community and Technical College, Prestonsburg, KY 41653; gturner0040@kctcs.edu

Joseph Childers
Address correspondence to R. Kaitchuck, Ball State University Department of Physics and Astronomy, Muncie, IN 47306; rkaitchu@bsu.edu

Abstract In recent years over 1,900 exoplanets have been discovered. Far fewer have been found in binary star systems. Exoplanets can either orbit both stars at a very great distance (p-type) or they can orbit one star of a widely separated stellar pair (s-type). For the s-type situation, how close can the stars be before planetary formation and stability are no longer possible? Can exoplanets be found in short period (<20 days) binaries? The existence or non-existence of exoplanets can place constraints on the theory of both planetary and binary star formation. An on-going program to detect planetary transits in close binary star systems will be discussed. The stellar selection criteria and the unique problems and advantages of searching for exoplanets in eclipsing binary stars will be presented.

Stellar Presentations

Donna Young
AAVSO Headquarters, 49 Bay State Road, Cambridge, MA 02138; donna@aavso.org

Abstract The AAVSO is in the process of expanding its education, outreach, and speakers bureau program. POWERPOINT presentations prepared for specific target audiences such as AAVSO members, educators, students, the general public, and Science Olympiad teams, coaches, event supervisors, and state directors will be available online for members to use. The presentations range from specific and general content relating to stellar evolution and variable stars to specific activities for a workshop environment. A presentation—even with a general topic—that works for high school students will not work for educators, Science Olympiad teams, or the general public. Each audience is unique and requires a different approach.

The current environment necessitates presentations that are captivating for a younger generation that is embedded in a highly visual and sound-bite world of social media, Twitter, and YouTube, and mobile devices. For educators, presentations and workshops for themselves and their students must support the Next Generation Science Standards (NGSS), the Common Core Content Standards, and the Science Technology, Engineering and Mathematics (STEM) initiative.

Current best practices for developing relevant and engaging POWERPOINT presentations to deliver information to a variety of targeted audiences will be presented along with several examples.

General Paper Session Part IV

The Nature of Z Cam Standstills

Mike Simonsen
AAVSO Headquarters, 49 Bay State Road, Cambridge, MA 02138; msimonsen@aavso.org

Abstract Because the standstills in Z Cam light curves are the defining characteristic of Z Cam dwarf novae, it would be helpful to better define what constitutes a standstill. The author will attempt to clarify the definition of standstills to aid in the classification of Z Cams. We will also examine some of the interesting features of standstills and Z Cam behavior before and after standstills.

The Lyncis Two for One Special

Michael Joner
Brigham Young University, Department of Physics and Astronomy, N488 ESC, Provo, UT 84602; xxcygni@gmail.com

Eric Hintz
Brigham Young University, Department of Physics and Astronomy, N480 ESC, Provo, UT 84602; hintz@physics.byu.edu

Abstract The pulsating δ Scuti star AN Lyn and the near contact binary UU Lyn are conveniently located at high declination in the northern constellation of Lynx. These variable stars are about 15 arc minutes apart in the sky and differ in average brightness by roughly one magnitude. This combination makes it fairly straightforward to secure photometric data on both stars at the same time using a common set of comparison stars. We present observations made at the BYU West Mountain Observatory during the spring of 2015 and outline some preliminary conclusions that can be drawn about these distinctly different variable stars.

Automated Supernova Discovery

Richard S. Post
33 Fairbanks Road, Lexington, MA 02421; rspost@comcast.net

Abstract We are developing a system of robotic telescopes for automatic recognition of Supernovae as well as other transient events in collaboration with the Puckett Supernova Search Team. At the SAS2014 meeting, the discovery program, SNARE, was first described. Since then, it has been continuously improved to handle searches under a wide variety of atmospheric conditions. Currently, two telescopes are used to build a reference library while searching for possible supernovae (PSN) with a partial library. Since data are taken every night without clouds, we must deal with varying atmospheric and high background illumination from the moon. Software is configured to identify a PSN, then reshoot for verification with options to change the run plan to acquire photometric or spectrographic data. The telescopes are 24-inch CDK24, with Alta U230 cameras, one in CA and one in NM. Images and run plans are sent between sites so the CA telescope can search while photometry is done in NM. Our goal is to find bright PSNs with magnitude 17.5 or brighter, the limit of our planned spectroscopy. We present results from our first automated PSN discoveries and plans for PSN data acquisition.

General Paper Session Part V

IM Normae: A Second T Pyx?

Joe Patterson
Center for Backyard Astrophysics, 25 Claremont Avenue, Apt. 7C, New York, NY 10027; jop@astro.columbia.edu

Berto Monard
CBA (Pretoria), P. O. Box 281, Calitzdorp 6661, Western Cape, South Africa

Paul Warhurst
address correspondence to J. Patterson, Center for Backyard Astrophysics, 25 Claremont Avenue, Apt. 7C, New York, NY 10027; jop@astro.columbia.edu

Gordon Myers
5 Inverness Way, Hillsborough, CA 94010; GordonMyers@hotmail.com

Abstract T Pyx is the Galaxy's most famous recurrent nova, erupting to magnitude 6 about every 20 years. For nova hunters and variable-star observers generally, it should be quite easy to discover stars with similar properties. There are probably half a million CVs out to the distance of T Pyx, and most have an underlying structure similar to that of T Pyx: low-mass secondary, fairly massive white dwarf, short orbital period. But of these half million stars, there is no second T Pyx. The star is unique in another way: its orbital period is increasing on a timescale of 300,000 years. Like the proverbial bat out of hell.

A 2002 nova eruption nominated a second star for this elite club: IM Nor, a short-orbital-period (2.5 hours) star which previously erupted in 1920. We began a program of time-series photometry to track the shallow eclipses—to test for orbital period change, the other signature of T Pyx resemblance. By 2015 we found this effect: P_{orb} increases on a timescale of 2 million years.

Thus, the two stars appear to be blowing themselves apart on a timescale of roughly a million years. This could explain why the stars are so rare: because they are rapidly self-immolating. And that could happen because the classical-nova outburst overwhelms the low-mass secondaries that live in short-period CVs—leading to unstable mass transfer which quickly evaporates the secondary. This implies that all short-P_{orb} classical novae should be "recurrent" (erupting on a timescale of decades). Greater attention to CP Pup (1942), RW UMi (1956), GQ Mus (1983), and V Per (1887) is definitely warranted.

Globular Cluster Variable Stars—Atlas and Coordinate Improvement using AAVSOnet Telescopes

Doug Welch
Department of Physics and Astronomy, McMaster University, Hamilton, ON L8S 4M1, Canada; welch@physics.mcmaster.ca

Arne Henden
106 Hawkins Pond Road, Center Harbor, NH 03226; arne@aavso.org

Taylor Bell
Saskatoon, SK, Canada; taylor.bell@usask.ca

Cissy Suen
Ian Fare
Alison Sills
Address correspondence to D. Welch, Department of Physics and Astronomy, McMaster University, Hamilton, ON L8S 4M1, Canada; welch@physics.mcmaster.ca

Abstract The variable stars of globular clusters have played and continue to play a significant role in our understanding of certain classes of variable stars. Since all stars associated with a cluster have the same age, metallicity, distance, and usually very similar (if not identical) reddenings, such variables can produce uniquely powerful constraints on where certain types of pulsation behaviors are excited.

Advanced amateur astronomers are increasingly well-positioned to provide long-term CCD monitoring of globular cluster variable stars but are hampered by a long history of poor or inaccessible finder charts and coordinates. Many of variable-rich clusters have published photographic finder charts taken in relatively poor seeing with blue-sensitive photographic plates. While useful signal-to-noise ratios are relatively straightforward to achieve for RR Lyrae, Type 2 Cepheids, and red giant variables, correct identification remains a difficult issue—particularly when images are taken at V or longer wavelengths.

We describe the project and report its progress using the OC61, TMO61, and SRO telescopes of AAVSOnet after the first year of image acquisition, and demonstrate several of the data products being developed for globular cluster variables.

A LARI Experience

Michael Cook
Newcastle Observatory, 9 Laking Drive, Newcastle ON L1B 1M5, Canada; michaeljcook@rogers.com

Abstract In 2012, Lowell Observatory launched The Lowell Amateur Research Initiative (LARI) to formally involve amateur astronomers in scientific research by bringing them to the attention of and helping professional astronomers with their astronomical research. One of the LARI projects is the BVRI photometric monitoring of Young Stellar Objects (YSOs), wherein amateurs obtain observations to search for new outburst events and characterize the colour evolution of previously identified outbursters. A summary of the scientific and organizational aspects of this LARI project, including its goals and science motivation, the process for getting involved with the project, a description of the team members, their equipment and methods of collaboration, and an overview of the programme stars, preliminary findings, and lessons learned is presented.

Index to Volume 43

Author

Subject

PHOTOELECTRIC PHOTOMETRY
[See PHOTOMETRY, PHOTOELECTRIC]

PHOTOMETRY

PHOTOMETRY, CCD

VARIABLE STARS (GENERAL)

VARIABLE STARS (INDIVIDUAL); OBSERVING TARGETS

NOTES